Msc Thesis

Stability of rocks on mild slopes

T. Venrooy 4442849

Msc Thesis
CIE 5060
2020-2021

TU Delft Delft University of Technology
Deltares Enabling Delta Life
de Vries & van de Wiel Dredging & Environmental Solutions

Hydraulic Engineering

December 16, 2021

MSC THESIS

Stability of rocks on mild slopes

by

T. Venrooy 4442849

Hydraulic Engineering

Faculty Civil Engineering and Geosciences
Technical University Delft

Thesis Committee

Chair	Dr. ir. B. Hofland	Delft University of Technology
	Ing. C. Kuiper	Delft University of Technology
	Dr. R. C. Lindenbergh	Delft University of Technology
	Prof. Dr. ir. M.R.A. van Gent	Deltares & Delft University of Technology
	Ir. H.D. Jumelet	De Vries & van de Wiel - DEME Group
	Ir. E.A.F. Wendt	De Vries & van de Wiel - DEME Group

December 16, 2021

TU Delft Delft University of Technology

Preface

This thesis project is the final marking to fulfil my Master of Science degree Hydraulic Engineering at TU Delft. This project has been a collaboration between the Technical University of Delft, Deltares and de Vries & van de Wiel. After my bachelor's degree in Civil Engineering at TU Delft, my love for Water Management and Hydraulic Engineering arose during an internship at the start-up Fleet Cleaner.

The fact that I have been able to combine science with practice during for my graduation project has given me great satisfaction. Being able to perform physical model tests in the Deltares laboratory and get started with data and software to substantiate hydraulic engineering theories. Together with working with the wonderful people at Deltares, I could not have wished for a better graduation project. These tests are carried out with the help of the laboratory technicians Wesley, Danny, Pim, Richard and Peter, for which I am immeasurably grateful.

With the help of a great coaching team, also called graduation committee, this project has been taken to a higher level. I am amazed at the willingness and patience to help me day and night as well as during the week and on weekends. Thank you Daan and Emiel for the general guidance during all phases of the project. Roderik helped me a lot regarding the improved measurement method. Marcel guided me to find in-depth theoretical as well as practical solutions. Coen shows his critical view by aiming on hydraulic engineering practice to improve my design method. Bas for performing the role of chairman and everything that comes with it.

I would like to thank my dear family, friends, roommates and fellow students for their moral, practical, emotional and informative support.

Finally, special thanks to my grandfather Dick, without his help I would not have been able to give this meaning to my time as a student. Thanks to my aunt Pieternel and uncle Maikel, I had the best possible working environment to write my thesis. I will never forget this hospitality during a period that was very important to me as a person.

Tom Venrooy
Amsterdam, December 2021

Abstract

Since the behaviour of damage formation on steep slopes varies from mild slopes, a comprehensive definition of damage needs to be established for different situations. Knowledge about the transition of rock stability between steep and mild slopes is lacking. This study presents a reliable and efficient design method. The goal of this study is to describe the stability of rock slopes (1:6 - 1:10). Insight into governing processes and quantified damage characteristics are gained by analyzing wave attack in the transition zone of mild and steep slopes.

The method is based on physical model test series with deep water wave conditions and perpendicular wave attack, which were performed to understand the stability of slope 1:6. The slopes were measured with stereophotogrammetry and processed in a 3D model with Agisoft Metashape software. Before wave attack, an initial profile is retrieved which can be compared with cumulative damaged profiles. Automatically detectable Ground Control Points are used as reference to assign scaling information and location recognition. The quantity and location of normative damage on mild slopes are identified for six damage parameters, based on different relations regarding erosion area and depth.

The tests results have led to a number of key findings. Damage formations are developed by dominant downward (bar profile) or upward transport (berm profile). In general, a thicker layer and a milder slope give more upward transport. Besides the change in transportation direction, no significant differences in stability numbers were observed for various layer thicknesses with similar wave characteristics. For an increasing slope angle, the influence on stability significantly decreases between various wave steepnesses, due to the impact of a higher amount of more damaging plunging waves. The definition of initial, intermediate and failure damage limits are specified and the test profiles are matched per limit. Initial and intermediate damage are found at a constant value of $E_{3D,3}$ for a varying layer thickness and slope angle based on the definition and matching profile analysis. Failure of the slope is defined by the event in which the impermeable layer or filter layer becomes visible, which occurs for a layer thickness of $2.5d_{n50}$ at a damage level of $E_{3D,3} = 1.5$. Research at 1:6 slope shows that a higher failure limit is observed for layer thickness $5d_{n50}$. Due to the lack of test results of other slopes (1:8 - 1:10), specific values cannot yet be indicated for the range 1:6 - 1:10. The lack of testing is also due to limits of the flume and wave machine. In order to remain at least $1d_{n50}$ over the slope, an acceptable damage limit for a design with a layer thickness of $2.5d_{n50}$ is found at $E_{3D,3} = 0.9$. For a layer thickness of $5d_{n50}$, an acceptable value of $E_{3D,3} = 1.5$ holds a remaining layer of $2.5d_{n50}$ due to the increase of bed mobility for higher damage numbers.

The design formula of mild slopes is based on $E_{3D,3}$ because this gives the lowest bias error, variability and measurement errors. The design formula for mild slopes is used to estimate stability, nominal rock diameter and acceptable damage for conditions within the applicability range of performed tests. This new method for mild slope design indicates that a higher allowable stability can be used compared to the previously used (extrapolated) method of Van der Meer (1988).

A displacement is not necessarily linked to erosion due to alternating upward and downward transport on mild slopes. It can be discussed to what extent a rock, after displacement, contributes to the stability of the design. This can be investigated by the ratio of mobility and erosion over the entire slope. This study has shown that the damage parameters, based on displacements, are larger than the width-averaged erosion parameters. This appears to be a useful ratio for distinguishing mild slopes from steep slopes. In the latter these parameters are considered equal. Requirements for mild slope stability can also be imposed on the basis of the ratio between mobility and erosion as described in this research.

Table of content

1 Introduction

First, chapter 1 provides relevant background information about the research topic, which is discussed in section 1.1. Here, the definition of a mild and steep slope is introduced. Steep slopes are defined in the Rock Manual as the range of validated structure slopes in the deep water formulae by Van der Meer (1988)[b]. Consequently, mild slopes are defined as a structure slopes more gentle than 1:6. The stability of rock on mild slopes is influenced by other processes and mechanisms compared to steep slopes. In section 1.2, a problem analysis is conducted from which the research objective is determined in section 1.3.

1.1 Background information

1.1.1 Stability of rock slopes on coastal protection structures

Worldwide, people are working on the protection of coastal areas with the use of stability calculations. Nearly 2.4 billion people (about 40 per cent of the world's population) live within 100 km of the coast following Ocean Conference (2017). The efficiency of these coastal protection structures depends on the reliability of these so-called design formulas which determine the required size of rock material under wave attack. There are different methods available to determine the stone size as well as multiple parameters that can influence the design.

The design formulas determined by scientists and researchers are often only valid for the tested range of conditions under which they conducted their research. In the case of a design outside the validity interval, extrapolating the method already used can provide an estimate for an application. The conditions for the design are in reality subject to many complicated processes and variable influences, therefore research is important to develop an optimal design method for coastal protection structures.

In the last 80 years there have been a number of decisive studies with regard to the empirical approach of the required stone size of rock material, which provided stability formulas for mild and steep slopes as well as for permeable, homogeneous and impermeable structures. Examples are the stability formulas under irregular and regular wave attack are described by Iribarren (1938) and (1953), Hudson (1953) and (1959), Thompson and Shuttler (1975), Van der Meer (1988), Shiereck et al. (1994). Also, a modification of the formulae by Van der Meer (1988) as proposed in Van Gent et al. (2003) and the formula by Van Gent et al. (2003).

Within the framework of research on mild slopes, multiple master thesis projects have already been carried out over the past 5 years. At the start of this research, numerical model XBeach-G was used by Wit (2015) and Postma (2016). Simulations of the model showed that the damage limit could be higher for mild slopes than for more steeper slopes, based on experiments with a homogeneous slope structure. In this research series, Kramer (2016) used physical model tests to show a positive correlation of wave attack, erosion of the armour layer and structure slope for increasing slope angle $\cot \alpha$ (based on 1:5, 1:10 and 1:15 slopes). Wendt (2017) focused, in addition to comparisons with the numerical model, on the development of a design method for static stability of rocks on mild slopes based on the

test results of Kramer (2016). Mossinkhof (2019) and Van Wijland (2020) presented design formulas for respectively structure slope 1:10 and 1:8, based on permissible damage described by Hofland et al. (2011). Estimation of the required size of rock material is a major task in the design of coastal structures under wave loading and there is a need for detailed knowledge on the governing processes, which could lead to more accurate stability formulas on mild slopes.

1.1.2 Physical model tests

Physical modelling is an established technique for research in the field of hydraulic engineering to deliver an empirical method. According to Mossinkoff (2019) , physical model tests are the preferred approach to investigate the stability of rock slopes under wave attack. With the principle of physical modelling, for these design formulas a smaller copy of an object (e.g. dike revetment or shore protection) is used. Additional scale effects could be noticed for low Reynolds number (Re), which is further discussed in subsection 3.1.4.

Especially for large and complex hydraulic engineering projects, physical modeling is used to achieve an efficient design, because in such a project often the design conditions deviate too much to design with numerical models or simplified analytical methods.

1.1.3 Involvement & current activities

De Vries & Van de Wiel is a player in the field of hydraulic engineering and operational contracting. As part of DEME-group, which is globally known as a company specialised in many different engineering disciplines. With a capacity of more than 5000 colleagues with almost 80 nationalities, it is possible to deliver contributions to efficient engineering solutions.

During constructions at the Eastern Scheldt in 2015 it was found that use was made of stone size of rock material that was too large and therefore an inefficient design was delivered. At the time of this project, the method of extrapolation of the Van der Meer (1998) formula, which is based on structure slopes between 1:1.5 and 1:6, was the most commonly used method for contractors for these slopes.

De Vries & Van de Wiel noticed that the design could be improved by conducting research for the design of rocks on mild slopes. In cooperation with Msc students and professors of TU Delft a research project was started in combination with research institute Deltares, which has testing facilities to perform the physical model tests.

1.2 Problem analysis

A recurring problem in the most recent studies of Van Wijland (2020), Mossinkoff (2019), Wendt (2017) and Kramer (2016) is that the transition of the formulas between mild and steep slopes have not yet been optimized and validated for efficient design methods. The deep water Van der Meer (1988) formula is based on tests with a structure slope steeper than 1:6, this validated range is considered as steep slopes. Outside this range, more gentler than slope 1:6, the concept of extrapolation was used in the field. Extrapolation of the Van der Meer (1988) formula leads to conservative rock sizes for the design of mild structure slopes, which is concluded based on physical model tests performed by Mossinkoff (2019) and Van Wijland (2020).

Van der Meer (1988) designed a method with two design formulae for each surging and plunging breaker wave types. The Van der Meer (1988) formula, which is used today for designing mild slopes, only considers plunging waves. In the range of mild slopes there is a transition zone between plunging and spilling waves, which are both representing different processes and mechanisms. The breaker types are described with the dimensionless Iribarren number (ξ) which includes slope angle, wave height and wave length (formula 2.20). For mild slopes, the distribution from just plunging waves changes to a situation with both plunging and spilling waves. As shown in figure 2.6, Mossinkoff (2019) found

for the lowest tested Irribarren number a ratio of approximately 50/50 for slope 1:10. Following this approach, Van Wijland (2020) observed approximately 70% plunging waves for slope 1:8. Based on their observations, there are expected to be about 90% plunging waves for slope 1:6. So for the design of mild slopes, both breaker types are needed to consider: plunging and spilling waves (figure 2.5). One of the essential differences between these two breaker types is the damage impact of wave energy dissipation on the layer composition of the structure slope, which is naturally higher for plunging waves.

As an additive for determining rock size on mild slopes, more insight into the characteristics of damage is also important for the development of an efficient design method. The behavior of how the rocks move under wave attack is different on mild and steep slopes and this changes the formation of damage on the slope and therefore influence stability of the structure. As observed during physical model tests of Kramer (2016), a difference in damage profile may occur, such as a berm damage profile on a mild slope of 1:10 and a bar profile on a steep slope of 1:5 (figure 2.8). The concept of damage could be described as many different types of damage parameters, but in the most recent research series two parameters S (formula 2.24) and $E_{3D,m}$ (formula 2.28) are often used. The advantage of using $E_{3D,m}$ was given by Kramer (2016) because it would describe the concept of damage more precisely and locally than S. A disadvantage is that the use of damage parameter $E_{3D,m}$ is still very limited in contrast to more widely used damage parameter S, which is for instance used by Van der Meer (1988).

Complete datasets of physical modelling described with damage parameter E_{3D} are presented by Van Wijland (2020) and Mossinkoff (2019) for respectively slope 1:8 and slope 1:10. These datasets are not yet easy to compare with the data from the tested range (1:1.5 - 1:6) of Van der Meer (1988), due to inconsistent use of damage parameters.

Van der Meer (1988) concluded from his tests that damage is negligible after 15000 waves by considering only plunging waves on steep slopes (1:1.5 - 1:6) described with damage parameter S. The tests results (figure 2.1) for slope 1:8 (Van Wijland, 2020) and 1:10 (Mossinkoff, 2019) show contrary outcome with respect to the statement of predicted constant damage Van der Meer (1988). Even after more than 15000 waves, a clear linear trend is observed for damage parameters S. Damage parameter $E_{3D,3}$ shows a more constant progress for an increasing number of waves.

The failure limits for different damage parameters are divided in three categories: initial damage, intermediate damage and failure damage (table 2.5). Van der Meer (1988) did not specify the range of intermediate damage for damage parameter S on steep slopes. With respect to failure damage on a slope 1:8, Van Wijland (2020) made an assumption of $E_{3D,3}$ equal to 1.5 but mentioned this value was maybe too conservative. Another possible value for the failure limit equals 2.0 (Van Wijland, 2020), but this value is based on observed restorative effects and temporary failures. Therefore, a possibility is present to increase this failure damage limit which could result in more efficient designs.

With respect to the permeability of the structure, Van der Meer (1988) has only varied the permeability, i.e. a homogeneous or permeable core, on test series with slope 1:1.5 - 1:3. A clear difference regarding the stability can be observed from the results of Van der Meer (1988) for different cores (figure 2.3). To this end, Van der Meer (1988) extrapolated the results found to his total range of structure slopes of 1:1.5 to 1:6. So there are not tests conducted yet for a slope 1:6 with a more permeable layer composition other than an impermeable core.

Mossinkoff (2019) and Van Wijland (2020) have conducted tests with varying armour thickness in order to simulate a change in the permeability of the structure. This doubling in armour layer thickness from $2.5 * d_{n50}$ to $5.0 * d_{n50}$ did not result in a significant change in stability for slopes 1:8 and 1:10. Both have used the method of Eldrup and Andersen (2019) to estimate the notional permeability of their layer compositions, which has not yet been validated for application on mild structure slopes.

In previous studies, many damage tests of rocks on mild and steep slopes have been done and useful results have emerged. In order to fully understand these results, this research will focus on the fundamentals. From this analysis, one could define the problem in one phrase as:

'For a reliable and efficient design method, knowledge of the transition of rock stability between steep and mild slopes is lacking and can be examined by conducting physical scale model tests to investigate processes with respect to hydraulic properties, structural parameters and damage characteristics.'

1.3 Research objective and sub-questions

The objective of this research, based on the identified problems in section 1.2, is here presented by means of a main research objective. On the basis of a number of sub-questions, from which each partly contributes to achieve the stated objective of this research. This research is a continuation of series of previous studies, but will focus more in detail on the transition of rock stability between mild and steep slopes. The objective is to fill the knowledge gap between steep slopes (1:1.5 - 1:6) and the tested mild slopes (1:6 - 1:10) in order to create a efficient design method for mild slopes. This is translated in the following research objective:

'Describe the stability of rock slopes under wave attack in the transition zone of breaking waves between mild and steep slopes to provide insights into governing processes and quantified damage characteristics in order to contribute to an efficient design method.'

The following sub-questions are extracted from the main research objective:

1. How do the governing hydraulic and structural parameters influence the damage on mild slopes?
2. How do the influences of the changing distribution of plunging and spilling waves on mild slopes evolve based on the Iribarren number?
3. How are the damage characteristics on mild slopes quantified and on the basis of which processes and mechanisms does this occur?
4. What is an efficient design method for stability of rocks on mild slopes?
5. How is the design method for mild slopes related to the steep slopes test series of Van der Meer (1988)?

1.4 Scope

This section contains the explanation of the specific that is being analyzed in this research. The limitations in this thesis are given and explained as follows:

1. The uniform structure slope 1:6 is used for physical model tests. No tests with a sloping foreshore are conducted in this research.
2. JONSWAP energy spectrum for a young sea state in deep water with irregular waves is considered as the governing wave spectrum.
3. Deep water wave conditions at the toe of the structure are considered such that the waves break on the slope. Therefore, a Rayleigh distribution of the wave height is assumed. Wave propagation in shallow water involves various processes including refraction, diffraction, shoaling, bottom friction dissipation and breaking waves on the foreshore. In this research only energy dissipation due to wave breaking on the slope is taken into account. Only the deformation of the wave is considered and the run-up, run-down, reflection and overtopping are not the main topics to support.
4. Perpendicular wave attack is considered the lower limit of rock stability on slopes. If the angle of wave attack differs from perpendicular, the rock slope will show the same or better stability (Van der Meer, 1988). This research only conducted tests with perpendicular wave attack.
5. The considered range of damage is the range from start of displacement of single armour units (static stability) to quantified erosion of armour layer which presents failure of the structure. For instance when the filter layer is visible for a certain area.

1.5 Outline of report

A concise preliminary outline of the report is given in this section 1.5. In chapter 1, a clear analysis of the problem is performed and relevance is shown by earlier presented background information. Consequently, the problems are translated to a research objective with supportive sub-questions. Chapter 2 shows a brief overview and understanding of the current literature of this research field. Simultaneously, the literature review also provides a representation of the knowledge gaps from the problem analysis that have been addressed earlier in this thesis. To provide information for the main objective, a research methodology is developed and described in in chapter 3. The approach to answer the formulated research objective and sub-question is elaborated by the use of physical model tests with slope 1:6. The model set-up, test procedure damage characteristics are discussed. In chapter 4, the results are presented and validated in the form of a design formula and from there the discussions starts. Eventually, conclusions and recommendations regarding the research objectives and sub-questions are presented in 5. A mindmap is presented in figure 1.1.

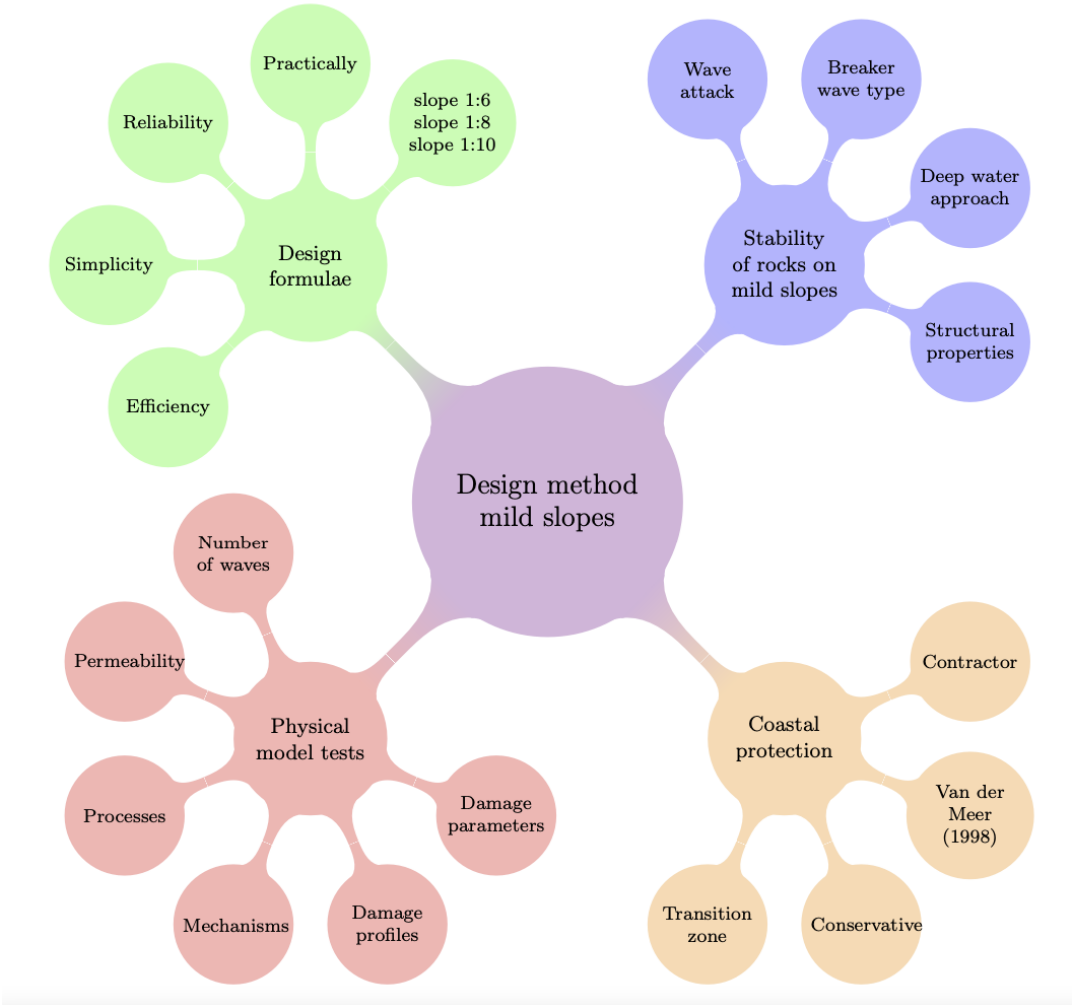

Figure 1.1: Mind map mild slope research series.

2 Literature study

2.1 Governing parameters

A distinction is made between the main governing parameters in the form of hydraulic and structural parameters. The hydraulic parameters are mainly related to the incoming wave conditions and the structural parameters represent the main properties of the coastal protection structure. A selection of main governing parameters is made based on the researches described in section 1.1.1

Table 2.1: Main governing hydraulic and structural parameters.

Hydraulic parameters			Structural parameters		
Symbol	**Description**	**Unit**	**Symbol**	**Description**	**Unit**
H_s	Significant wave height	m	d_{n50}	Nominal stone diameter	m
T_p	Peak wave period	s	Δ	Relative mass density	-
$s_{o,p}$	Wave steepness	-	$\cot \alpha$	Slope angle	-
N	Number of waves	-	t_a	Armour layer thickness	m
h	Water depth	m	P	Notional permeability	-

2.1.1 Hydraulic parameters

Understanding the impact of water waves is crucial for the design of slope structures. This section describes hydraulic variables and conditions that influence stability and damage characteristics.

- **Significant wave height**

  The significant wave height H_s can be interpreted in three different ways as respectively time measured $H_{1/3}$, visually observed H_v and spectral obtained H_{m0} significant wave height respectively. These are each explained in this subsection.

  By using measuring equipment such as wave gauges and buoys, the vertical wave motion of the surface can be recorded in time at a certain location. To eventually determine the significant wave height $H_{1/3}$ from this time records, one should first determine the zero level of the records and remove any linear trend in time in order to obtain a record with a mean surface elevation of zero (Holthuijsen, 2007). Second, one should identify all individual waves with their corresponding wave height. Following Buckley et al. (1984) and Goda (1986), an individual wave is here defined as the profile of the surface elevation between two successive downward zero-crossings of the elevation. The main reason that the zero-down crossing method will be used in this study is because breaking waves are investigated. These waves have the property of not being symmetrical due to a steep front. The wave height H is defined as the difference between the lowest and the highest level per wave. By ranking all these wave heights and select the mean of the highest one-third of the waves gives the significant wave height H_s of the wave record as in equation 2.2 (Holthuijsen, 2007):

$$H_s = H_{1/3} = \frac{1}{N/3} \sum_{j=1}^{N/3} H_j \tag{2.1}$$

where:

N = number of waves
j = rank number of the wave based on wave height

Two points of interest regarding wave characterization based on equation 2.2 is that the wave record has a finite time duration D, which must be short enough to be stationary but also long enough to provide enough data to give reliable wave height averages (Holthuijsen, 2007). In addition, measurement errors may occur due to possible processing errors. Therefore it can be useful as a control mechanism to make use of a visually estimated significant wave height H_v, defined by the WMO as the the average height of 15 to 20 well defined, higher waves of a number of wave groups. Battjes (1974) investigated the relationship of instrumental measurements and visual observations as $H_{1/3} = 1.67H_v^{0.77}$ and thus $H_{1/3} \approx H_v$.

It is stated de Almeida et al. (2019) that the spectral obtained significant wave height ($H_s = H_{m0} = 4\sqrt{m_0}$) is a better parameter than the significant wave height from the time domain ($H_s = H_{1/3}$) for shallow water wave conditions because of effects of nonlinear phenomena such as bottom dissipation and triad wave-wave interaction, which are not considered in this research. Instead, a deep water approach is followed. Wave heights in a random sea state in deep water can be described by the Rayleigh probability distribution. Where m_0 of the H_{m0} is the zeroth moment of the wave energy density spectrum. An advantage of this method is that with one significant value of a wave height the probability of exceedance of other values can be calculated.

Assuming a Rayleigh distribution in deep water, the 98th percentile of the wave height is formulated as $H_{2\%}$ and the relation with respect to $H_{1/3}$ is given as $H_{1/3} = 0.72H_{2\%}$ (Holthuijsen, 2007).

Table 2.2: Interpretations of various (significant) wave heights.

Symbol	**Description**	**Relation**
$H_{1/3}$	Time record measured	$H_s = H_{1/3}$
H_v	Visually observed	$H_{1/3} = 1.67H_v^{0.77}$ (Battjes, 1984)
H_{m0}	Obtained from spectrum	$H_{1/3} = 0.95H_{m0}$ (Goda, 1988a)
$H_{2\%}$	Percentile 98th	$H_{1/3} = 0.72H_{2\%}$

- **Wave period**

  In this section different characteristic wave periods are discussed. The choice of the wave period has a possible influence on the stability.

  The wave period $T_{1/3}$ in equation 2.2)is also measured from a time record and is defined as the mean period of the highest one-third of the waves:

$$T_{1/3} = \frac{1}{N/3} \sum_{j=1}^{N/3} T_j \tag{2.2}$$

  where:

  N = number of waves
  j = rank number of the wave based on wave height

The mean wave period could be interpreted as the mean zero-crossing wave period $\bar{T}_0$ for a time record or the spectral mean period (T_{m02}). Van der Meer (1988) used T_m in his analysis for rocks on steep slopes, without substantiation this choice. This thesis uses T_{m02} as T_m. The spectral mean period T_{m02} is calculated from the spectrum by use of equation:

$$T_{m02} = T_m = \frac{m_0}{m_2} \tag{2.3}$$

where:

m_0 = zero-order spectral moment
m_2 = second-order spectral moment

The moment m_n of an variance density spectrum $E(f)$ could be expressed based on the assumption that the surface elevation is a stationary, Gaussian distributed process as following:

$$m_n = \int_0^\infty f^n E(f) df \tag{2.4}$$

A disadvantage of using m_2 in a test analysis is the relative high sensitivity of small errors or variations in the high-frequency range of the spectrum, because higher-order moments are larger influenced by noise in this range. Therefore the mean periods ($\bar{T}_0$ and T_{m02}) are considered as not the most practical and reliable estimates for the characteristic wave length.

According to Van Gent et al. (2003), the wave period can be better characterized by the spectral mean energy period $T_{m-1,0}$ in shallow water conditions for rock stability. When using a different wave period in a design method, fitting coefficients must be re-calibrated. The spectral mean energy period is given as $T_{m-1,0} = m_{-1}/m_0$, obtained with n=1 for equation 2.4 and is also used to describe the modified Van der Meer (1988) formulae.

The peak frequency T_p is defined as the frequency for which the variance density spectrum $E(f)$ shows a maximum. Following (Van Gent et al., 2003), the relation between $T_{m-1,0}$ and T_p can be approximated as $T_p = 1.1T_{m-1,0}$ when using JONSWAP.

An overview of the described characteristic wave periods is given in table 2.3.

Table 2.3: Characteristic wave periods.

Type	Symbol	Description	Formula	Relation
Time record measured or visually observed	$T_{1/3}$	Significant wave period	$\frac{1}{N/3}\sum_{j=1}^{N/3} T_{0,j}$	$T_s = T_{1/3}$
	$\bar{T}_0$	Mean zero-crossing wave period	$\frac{1}{N}\sum_{i=1}^{N} T_{0,i}$	$\bar{T}_0 = T_m$
	T_v	Visually significant wave period	-	$T_{1/3} = 2.83T_v^{0.44}$
Spectral obtained (JONSWAP)	T_p	Spectral peak period	$1/f_{peak}$	$T_{1/3} \approx 0.95T_{peak}$
	T_m	Spectral mean period	$\sqrt{m_0/m_2}(= f_{mean}^{-1})$	$T_m = \bar{T}_0$
	$T_{m-1,0}$	Spectral mean energy period	m_{-1}/m_0	$T_p = 1.1T_{m-1,0}$

- **Wave spectra**

  In this section the two most widely used one-dimensional wave spectra are discussed. The first wave spectrum is observed by Pierson and Moskowitz (1964) and will be abbreviated as the PM-spectrum. The second wave spectrum is obtained by the Joint North Sea Wave Project, also named JONSWAP. The spectra gives information about e.g. the variance of the sea surface elevation, governing frequencies and wave breaking processes.

  PM-spectrum represents a fully developed sea state and is used with the tests of Van der Meer (1988). As this distance travelled by the water (fetch) is so long it is assumed that the peak

frequency can depend only on the wind speed (Holthuijsen, 2007). The obtained PM-spectrum is given in equation 2.5 as:

$$E_{PM}(f) = \alpha_{PM} g^2 (2\pi)^{-4} f^{-5} \exp[-\frac{5}{4}(\frac{f}{f_{PM}})^{-4}] \tag{2.5}$$

where:

α_{PM} = energy scale [−]
f_{PM} = peak frequency [s^{-1}]

The JONSWAP-spectrum represents fetch-limited and arbitrary wind-conditions (e.g. storms, hurricanes) in deep water wave conditions. The spectrum is well applicable to relatively steeper waves and not to swell waves. Waves are propagating at different speed, this phenomenon is called frequency dispersion. For example, a storm in the open ocean generates a large range of frequencies from what the waves with the lowest frequency arrive first at the coast, these waves are called swell waves. The JONSWAP spectrum does not apply to swell because the wave steepness of swell is too low and the shape-stabilising capacity of the quadruplet wave–wave interactions is therefore weaker or practically absent. This shape-stability effect is one of the main reasons why JONSWAP is widely accepted (Holthuijsen, 2007).

Since in the design of coastal structures in The Netherlands the fetch-limited and arbitrary wind-conditions with are normative. Van Gent et al. (2003), Mossinkoff (2019) and Van Wijland (2020) considered JONSWAP as design spectrum for their physical model tests.

During experiments with idealised wave generation, it is found that the peak period T_p shifts to a lower frequency because of involved energy processes in the spectrum (Hasselmann et al., 1973). Interestingly, similarities in the shape at the high-frequency tails of JONSWAP and Pierson and Moskowitz (1964) were found. During the tests a sharper peak was observed and to still make use of the corresponding shape of the tail, use was made normalizing the spectrum and eventually derive a peak-enhancement function G(f) to enhance the peak and shape:

$$G(f) = \gamma^{\exp[-\frac{1}{2}(\frac{f/f_{peak}-1}{\sigma})^2]} \tag{2.6}$$

A combination of equation 2.5 and 2.6 provides the complete expression of the JONSWAP-spectrum in equation 2.7

$$E_{JONSWAP}(f) = \alpha g^2 (2\pi)^{-4} f^{-5} \exp[-\frac{5}{4}(\frac{f}{f_{peak}})^{-4}] \gamma^{\exp[-\frac{1}{2}(\frac{f/f_{peak}-1}{\sigma})^2]} \tag{2.7}$$

- **Wave steepness**

  The wave steepness depends on the ratio between wave height H and wavelength L and thus the wave period T is involved. For deep water wave conditions the relation of the wave length and the wave period is given as $L_0 = \frac{gT^2}{2\pi} \approx 1.56T^2$. It is possible to interpret the wave steepness based on different wave height and period characteristics.

  Van der Meer (1988) performed tests with a wave steepness s_m based on the spectral mean period T_m and de Almeida et al. (2019) used wave steepness $s_{0,m-1,0}$ based on the peak energy period $T_{m-1,0}$ both for deep water conditions. Mossinkoff (2019) and Van Wijland (2020) used the peak period T_p, this provides the following equations for T_p (equation 2.8), T_m (equation 2.9) and $T_{m-1,0}$ (equation 2.10):

$$s_{0,p} = \frac{H_s}{L_0} \approx \frac{H_s}{1.56T_p^2} \quad (2.8) \qquad s_{0,m} \approx \frac{H_s}{1.56T_m^2} \quad (2.9) \qquad s_{0,m-1,0} \approx \frac{H_s}{1.56T_{m-1,0}^2} \quad (2.10)$$

where:

$s_{0,p}$ = Iribarren number based in spectral peak period T_p
$s_{0,m}$ = Iribarren number based on mean period T_m
$s_{0,m-1,0}$ = Iribarren number based in spectral mean period $T_{m-1,0}$

Mossinkoff (2019) and Van Wijland (2020) both performed tests with a range of s_{op} between 0.01 and 0.05. To give an indication of the range of wave steepnesses in the North Sea, Reijmerink et al. (2020) provides measurements of a wave steepness s_p between 0.01 and 0.04 for shallow water wave conditions.

- **Number of waves**

  The storm duration can determine the design of coastal protection and during physical model tests this is simulated as the number of waves.

  Van der Meer (1988) performed physical model tests with a number of waves N in range 1000 to 3000 and also conducted a re-analysis of the test results of Thompson and Shuttler (1975). The range of tested structure slopes are 1:1.5 to 1:6. In this tests a linear relation is present between the damage level S and the first 500 waves, then this relationship changes into a squared root relation, $S \sim \sqrt{N}$, with a range of 500 waves until the approximated upper limit of 8500 waves for application. From his tests he concluded that marginal damage is negligible after 15000 waves. After reaching this number, an equilibrium should be reached. The influence of storm duration on the stability can be described according to equation 2.11 for the whole range of N:

  $$f(S) = a[1 - exp(-bN)] \quad (2.11)$$

  Where a and b are curve-fitting coefficient based of the data of the specific test.

  Van Wijland (2020) investigated a linear relationship between the number of waves N and the damage parameters $E_{3D,m}$ from an initial point of damage. Contrary to the findings of Van der Meer (1988), there is an indication that for mild slopes (1:8 and 1:10) even after 15600 waves damage would still increase (Van Wijland, 2020). But Van der Meer (1988) made his conclusions based on plunging waves on steep slopes (1.1.5 - 1:6) described with damage parameter S. The number of waves N are tested by Van Wijland (2020) for a broader range of 250 to 15600 waves. The results of Mossinkoff (2019) and Van Wijland (2020) shows a clear linear trend for the 2D damage parameters S, S_{all} and E_{2D} and after more than 15000 waves the trend is still increase linearly. The $E_{3D,3}$ parameter seems to become relative more constant for increasing number of waves. To give an indication of these trends, damage parameter S and E_{3D} with respect to the number of waves N are shown in figure 2.1:

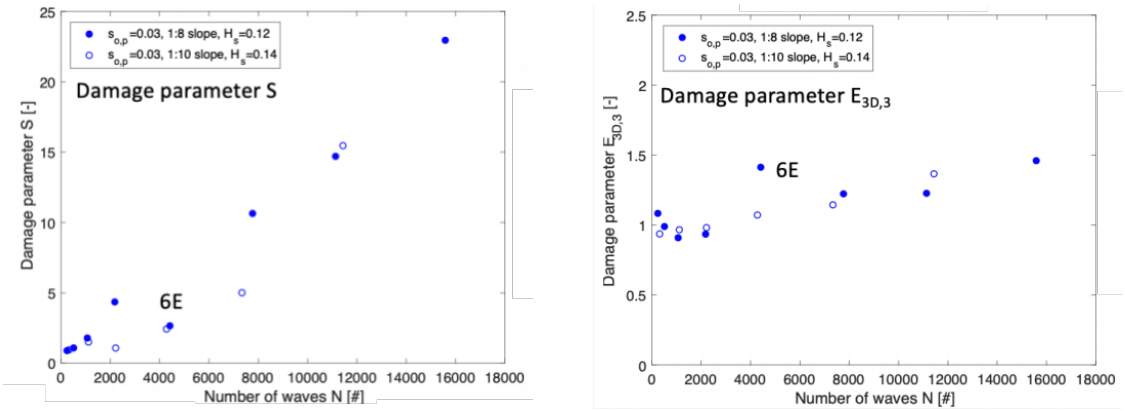

(a) Damage parameter S

(b) Damage parameter $E_{3D,3}$

Figure 2.1: Damage parameters a) S and b) $E_{3D,3}$ with respect to number of waves N for slope 1:8 (Van Wijland, 2020) and slope 1:10 (Mossinkoff, 2019).

- **Water depth**

  Water depth could be defined as h(x,t) as a function of time (tide) and space (sloping foreshore). As this research is not considering these effects we use a water depth h that is only affected by the incoming wave motion.

  de Almeida et al. (2019) investigated that for structures with a shallow foreshore, increasing water levels can increase the damage to rock armour slopes. In the performed tests, the increasing water levels caused increased wave loading and therefore an increase of the damage with a factor 2 (for $E_{3D,1}$) to 44 (for S) while the wave conditions in deep water were equal (de Almeida et al., 2019). The quantified relationship between water level and damage depends on which damage parameters are used. More explanation about use of different damage parameters will be given in section 2.2.1.

- **Scale effects and Reynolds number**

  To be able to make an assumption about scale effects for the interest of this test series, several studies describing these effects for an armour layer with incoming irregular waves. As stated in Van der Meer (1988), armour stability on a rock slope could be influenced for Reynolds numbers outside range $1 * 10^4$ and $4 * 10^4$ for tests with irregular waves. Tests by Thompson and Shuttler (1975) showed no clear dependence of erosion for tests with irregular waves and stones in the range of $20 - 40mm$ (DELOS, 2000). Jensen and Klinting (1983) argued from theoretical considerations that the critical Reynolds number must be larger than $0.7 * 10^4$. Based on the Reynolds number of the performed tests, information can be given about the possible significant influence of scale effects on the stability. When the translation is made between small scale models to larger designs, scale relations are need to take into account.

  The Reynolds number ($Re = \sqrt{(U * D)/\nu}$) can be useful in research with a scale model. The characteristic flow velocity (U) is often taken as $\sqrt{g * H_s}$ (DELOS, 2000). If during the physical model tests it is assumed that (viscous) scale effects do not play a role, then the following condition must be met:

$$Re = \frac{gH_s d_{n50}}{\nu} > Re_{crit} \tag{2.12}$$

  where:

  ν = kinematic viscosity of the flowing medium $\quad [m^2/s]$

For water with a temperature of 20 $^{\circ}C$ the kinematic viscosity is considered as $\nu = 1 * 10^{-6}$.

- **Deep and shallow water wave conditions**

  The distinction between deep and shallow water waves is not directly linked with the absolute water depth h. Instead, whether the depth is considered as 'deep water' is determined when the ratio of water depth to wavelength of the wave exceeds 0.5. This gives the deep water condition $h/L > 1/2$.

  This deep water wave approach is also used with the stability formulae of Iribarren (1938), Hudson (1953) and Van der Meer (1988), Van Wijland (2020). This research also uses a deep water approach, but this is not the only possible method for the design of coastal structures. Care must be taken to avoid inconsistent use of the deep and shallow water wave conditions.

  Frostick et al. (2011) concluded that the deep water section should fulfill the condition that the water depth must be three times larger than the significant wave height ($h/H_s > 3$) in order to comply with the deep water approach of physical model tests.

2.1.2 Structural parameters

Understanding the main aspects of the structure is crucial for the design of rock on coastal structure slopes. This section describes structural variables and relations that influence stability and damage characteristics.

- **Nominal stone diameter**

  The diameter of stones defines the behavior of the structure. Very large stone sizes are related to statically stable structures such as breakwater. Smaller diameters are more common for dynamically stable structures as rock and gravel beaches (Van der Meer, 1988). In devising an efficient and reliable design method it is important that the stone size can be quantified based on the design specifications.

  The nominal stone diameter d_{n50} is related to the median weight M_{50} and the stone density ρ_s and is expressed in equation 2.13 :

$$d_{n50} = \sqrt[3]{\frac{M_{50}}{\rho_s}} \tag{2.13}$$

  The median weight M_{50} can be obtained by the 50 % weighted percentile of the stone particles as described in the Rock Manual (CIRIA, 2007). Rock sizes will always have an uncertainty as not every rock is exactly the same and therefore comes within standard gradings. It is important to perform measurements to obtain information about the rock prior to construction.

- **Relative mass density**

  Relative density, or specific gravity, is the ratio of the density (mass of a unit volume) of a substance to the density of a given reference material.

  The relative mass density Δ is used to quantify the submerged weight of the particles with respect to their reference material and is denoted in equation 2.14:

$$\Delta = \frac{\rho_s - \rho_w}{\rho_w} \tag{2.14}$$

  For the same stone, the value of Δ is the same for both fresh water and seawater.

- **Permeability**

  An important difference in the stability is the permeability of an entire coastal structure. For instance, breakwaters usually have a permeable core, while in dike revetments the core is made from sand or clay, considered as impermeable. The permeability of the design has a significant influence on the stability of the protecting armour layer (Schiereck, 2016).

  Imagine that a homogeneous mass of stones reacts differently from a cover layer on stones on an impermeable core. In the first case, a lot of wave energy is dissipated in the core of structure, while for the latter situation the pressure could build-up under the cover layer (Schiereck, 2016) Therefore, the permeability can be related to the volume of water that is stored (dissipated) in the core of the structure but also in the voids of the cover layer.

  If the core of the structure has a higher dissipating energy capability (buffer capacity) and thus a higher permeability P, the stability of the structure is likely to increase. The permeability P also depends on the different layer designs of the structure (Kik et al., 2012). For example the value differs when geotextile filter layers are applied or when ratio of armour and filter layer vary.

  Van der Meer (1988) empirically derived the notional permeability parameter P to ensure that the effect of permeability was taken into account for his design method. Please note that the notional permeability parameter is not equal to the permeability of the structure, but it is a fitted parameter related to phenomena as run-up and porous flow resistance. A homogeneous structure consisting only of armour stones is considered as upper boundary (P = 0.6), regarding permeability. An impermeable core can be regarded as the lower boundary of permeability (P=0.1) (Van der Meer, 1988).

  For different armour layer thicknesses t_a and filters on an impermeable core, research of Eldrup and Andersen (2019) showed that the notional permeability P could vary in a range of 0.1 to 0.38. In appendix B, the fitted notional permeability factor P of different layer compositions are shown.

  Mossinkoff (2019) and Van Wijland (2020) performed tests on an impermeable core and used the notional permeability is given by the 'New Method for the Estimation of the Notional Permeability Factor' of Eldrup and Andersen (2019). They assumed this method to be valid to empirically determine the notional permeability P of the tested rock armour layer composition. Eldrup and Andersen (2019) have shown that this method is reliable by correlating their calculated P-values of with the P-values of Van der Meer (1988) with a typical deviation of ±0.03. The empirical method of Eldrup and Andersen (2019) is based on a total of 13 layer compositions with permeable and impermeable core for slopes 1:1.5 - 1:6. Eldrup and Andersen (2019) concluded that the impact of the armour layer thickness on the notional permeability P was largest for an impermeable core and smallest for a permeable core. Also, for finer core material, the influence of the armour layer thickness was found to be higher compared to a coarse material (Eldrup & Andersen, 2019).

  A re-calculation of the notional permeability with the method of Eldrup and Andersen (2019) is performed for the tested layer compositions of Van Wijland (2020). To calculate the notional permeability P of a layer composition, first a closed form integration function k is calculated with 2.15:

$$k = \sum_{i=1}^{N} 0.79 - 0.79exp(-4.1\frac{d_{n50,i}}{d_{n50_{armour}}})(\frac{exp(-0.62z_1^*) - exp(-0.62z_2^*)}{0.62}) \tag{2.15}$$

  where:

  N = number of layers
  i = rank number of the layer
  d_{n50} = nominal diameter
  z^* = relative layer depth

  The definition of relative layer depth z^* is defined in figure 2.2. The value for z_2^* should always stop at the impermeable core or at a maximum value of 13 (Eldrup & Andersen, 2019).

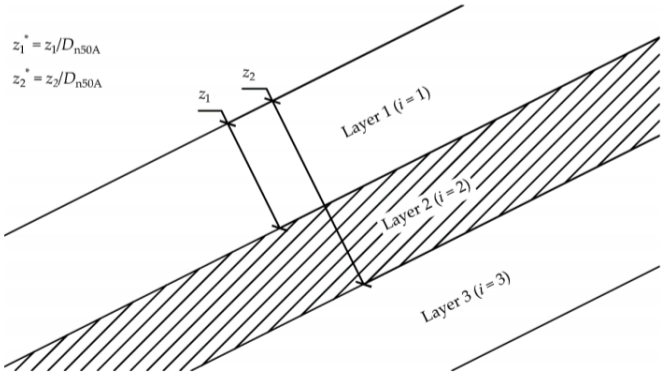

Figure 2.2: Example of the definition of the relative layer depth z^* of equation 2.15 with D_{n50A} as nominal diameter of the armour layer (Eldrup & Andersen, 2019).

Based on equation 2.15 and figure 2.2, an estimation for the notional permeability of the Eldrup and Andersen (2019) method is depicted as:

$$P = max \begin{cases} 0.1 \\ 1.72k - 1.58 \end{cases} \tag{2.16}$$

The estimation of the notional permeability on the tests of Van Wijland (2020) are given in table:

Table 2.4: Estimation of notional permeability factor for test conditions Van Wijland (2020) following the method of Eldrup and Andersen (2019)

			Impermeable core					
			One rock layer armour ($2.5D_{n50}$)			One rock layer armour ($5D_{n50}$)		
Description	**Symbol**	**Unity**	**Armour**	**Filter**	**Core**	**Armour**	**Filter**	**Core**
Density of the stone	ρ_s	$[kg/m^3]$	2944	-	-	2944	-	-
Nominal rock size	d_{n50}	[m]	0.0148	-	-	0.0148	-	-
Layer thickness	t	[m]	0.037	-	-	0.074		
Relative layer depth	z_1^*	-	0	2.5	2.5	0	5	5
	z_2^*	-	2.5	2.5	13	5	5	13
Integration function	k	-	0.99	0	0	1.2		
Notional permeability	P	-	0.12			0.48		

The notional permeability is not influenced by the slope angle as this is included in the stability formula by Van der Meer (1998). The most gentle slope Van der Meer (1998) tested was a 1:6 slope, therefore it is not known if the stability method of Eldrup and Andersen (2019) works for mild slopes. In addition, the test procedure of Eldrup and Andersen (2019) differed in a number of key aspects from that of Van der Meer (1988). Two main differences are that Van der Meer (1988) did not measure accumulated damage and he used the significant wave height as $H_{1/3}$ where Eldrup and Andersen (2019) expressed the waves in the tests with wave height $H_{2\%}$. The ratio between $H_{1/3}$ and $H_{2\%}$ is explained in 2.1.1 and shown in table 2.2. A conversion from accumulated damage to non-accumulated damage by use of formulas 2.17 is made to comply with the basis of the Van der Meer (1998) formulas (equations 2.30 and 2.31) .

$$\frac{H_{2\%,i}}{\Delta D_{n50,A}} = A(\frac{S_{d,i}}{\sqrt{N_i}})^{0.2} \quad ; \quad N_{extra,i} = \frac{A^{10}(S_{d,i-1}^2)}{\frac{H_{2\%,i}}{\Delta D_{n50,A}}^{10}} \quad ; \quad N_{total,i} = N_i + N_{extra,i} \tag{2.17}$$

The conversion in the method of Eldrup and Andersen (2019) is based on the relations found by Van der Meer (1988) between wave height, number of waves and damage. This relation is described as A which is the slope of a continuous linear function ($y = A \cdot x$) with $y = \frac{H_{2\%,i}}{\Delta D_{n50,A}}$ and $x = (\frac{S_{d,i}}{\sqrt{N_{total,i}}})^{0.2}$, as displayed in figure B.2 of appendix B. Regarding the notional permeability parameter P, Van der Meer (1988) only considered tests with a more permeable layer than an impermeable layer composition ($P = 0.1$) for slopes 1:1.5 - 1:3. A clear difference in stability number N_s can be excluded from the results of Van der Meer (1988) shown in figure 2.3:

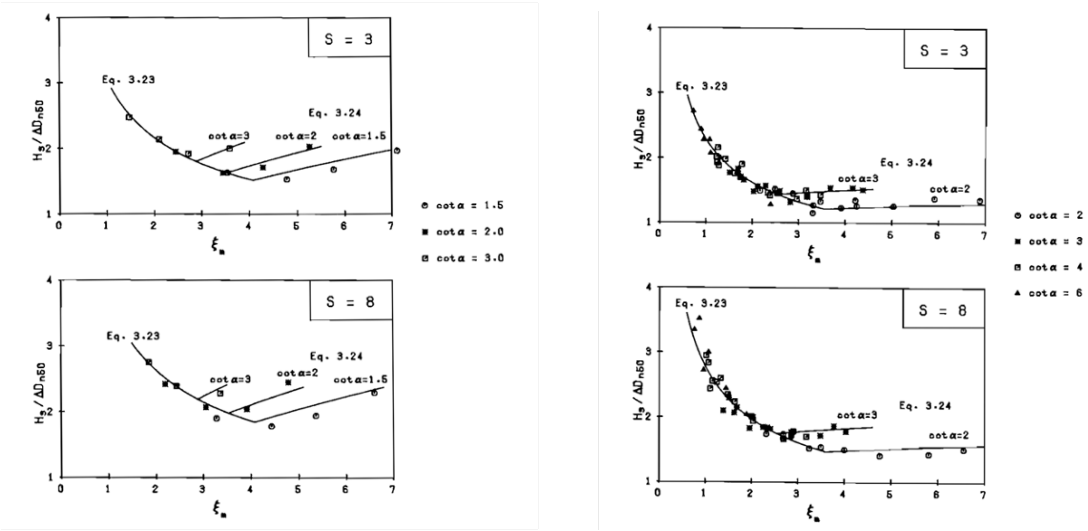

(a) Impermeable layer composition (P = 0.1)

(b) Permeable layer composition (P = 0.5)

Figure 2.3: Stability number with respect to Iribarren number for a) impermeable and b) permeable layer compositions tested for N = 3000 (Van der Meer, 1988).

Two different mechanism influencing stability characterising a permeable and an impermeable core under wave attack are respectively transmission and reflection. Transmission represents the principle of water penetrating to the core of the structure, resulting in a less violent action on the layer composition. In contrast to reflection, where the water flow cannot penetrate to the core, which leads to relatively greater forces in the armour layer during run-down (Jumelet, 2010).

Another effect on stability is observed for the relative higher Iribarren numbers. Due to increasing wave periods with corresponding higher Iribarren numbers, more water can percolate and flow down through the core. This mechanism reduces the forces on the layer composition and stabilizes the slope of the structure (Jumelet, 2010).

- **Slope angle**

  The slope angle ($\cot \alpha$) is strongly related to the stability because of the influence on the Iribarren number (section 2.1.4) and other processes. For example, the change in dominant transportation direction of stones for a varying slope influences the evolution of damage characteristics.

  In this research, steep slopes are defined as in the Rock Manual (CIRIA, 2007) as the range of validated structure slopes in the deep water formulae by Van der Meer(1988)[b]. Consequently, mild slopes are defined as a structure slopes more gentle than 1:6.

- **Stone shape**

  The shape is described by the roundness or angularity of the stone, but also by the surface texture (type of material). This property is not considered as a governing variable on stability in tests of

Van der Meer (1988). However, research of Van Gent et al. (2003) shows that the shape, especially roundness, would have a considerable influence on stability.

2.1.3 Stability number

The stability number is one of the most important variable in a stability formula. Van der Meer (1988) states that the wave height to be used in stability formulae is always the wave height in front of the structure. The stability number varies for different structure slopes. Commonly, more gentle slopes resulting in higher stability values. The stability number N_s is expressed in the Rock Manual (CIRIA, 2007) as depicted in equation 2.18:

$$N_s = \frac{H_s}{\Delta d} \tag{2.18}$$

By use of the formulas 2.13 and 2.14 of section 2.1.2, equation 2.19 is formulated to describe the stability number N_s:

$$N_s = \frac{H_s}{\Delta d_{n50}} \tag{2.19}$$

The basic stability relations are investigated by linking the stability number to the damage parameters (section 2.2.1). For mild slopes the stability is considered higher than for steep slopes. Also different types of coastal protection structures can be compared using the stability number (Van der Meer, 1988).

2.1.4 Iribarren number

The Iribarren number ξ, also known as the surf similarity parameter or breaking parameter, is a dimensionless parameter to model the effects of wave breaking on beaches and coastal structures (Iribarren, 1938). For example, for a shore with a flat beach, the type of breaker can be predicted on the basis of the Iribarren number ξ (Holthuijsen, 2007). The Iribarren number ξ has been defined by later research by Iribarren (1938) as depicted in equation 2.20:

$$\xi = \frac{\tan\alpha}{\sqrt{s_0}} \tag{2.20}$$

where:

$\tan\alpha$ = tangent of structure slope
s_0 = wave steepness for deep water waves (= H/L_0)

The breaker wave types (surging, collapsing, plunging and spilling), shown in figure 2.4, are categorized on the basis of the Iribarren number ξ.

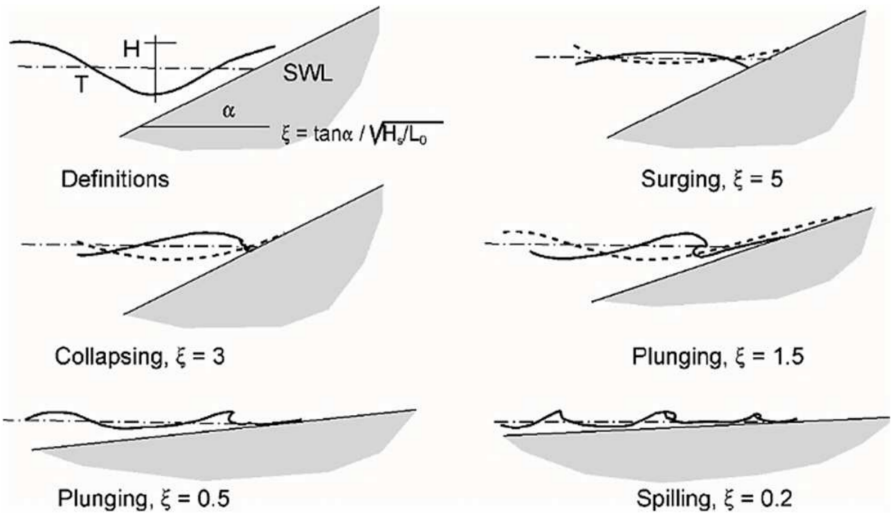

Figure 2.4: Breaker waves type with typical Iribarren number (Schiereck, 2016).

The Iribarren number is interchangeable for a different wave steepness because of the corresponding wave periods. Which means, the wave steepness changes for the use of a peak period T_p (equation 2.21), mean period T_m (equation 2.22) or spectral mean period $T_{m-1,0}$ (equation 2.23):

$$\xi_p = \frac{\tan\alpha}{\sqrt{s_{0,p}}} = \frac{\tan\alpha}{\sqrt{\frac{2\pi H_s}{gT_p^2}}} \quad (2.21) \qquad \xi_m = \frac{\tan\alpha}{\sqrt{\frac{2\pi H_s}{gT_m^2}}} \quad (2.22) \qquad \xi_{m-1,0} = \frac{\tan\alpha}{\sqrt{\frac{2\pi H_s}{gT_{m-1,0}^2}}} \quad (2.23)$$

where:

ξ_p = Iribarren number based in spectral peak period T_p
ξ_m = Iribarren number based in spectral mean period T_m
$\xi_{m-1,0}$ = Iribarren number based in spectral mean period $T_{m-1,0}$

Van der Meer (1988) used ξ_m for his tests and Mossinkoff (2019) and Van Wijland (2020) used ξ_p. The ratio $\frac{\xi_p}{\xi_m}$ is equal to $\frac{T_p}{T_m}$ for the same slope angle α and significant wave height H_s. For example, ξ_p is larger than ξ_m for the same slope angle α and significant wave height H_s. All forms of Iribarren numbers are discussed in this research, because a comparison is made with all of the mentioned literature.

In this research, the focus is on plunging and spilling breaker wave types. For plunging waves, the crest of the wave becomes much steeper than for spilling waves. A plunging waves becomes almost vertical, then curls and falls at the bottom of the wave. Differences in pressure arise here, due to entrained air which cause turbulence (Battjes, 1974). This mechanism is named a plunging jet (figure 2.5), whereby the peak of the energy dissipation is more centered. This is one of the most important aspects why the wave formation of plunging jets has a different effect on the damage on the slope in comparison with spilling waves.

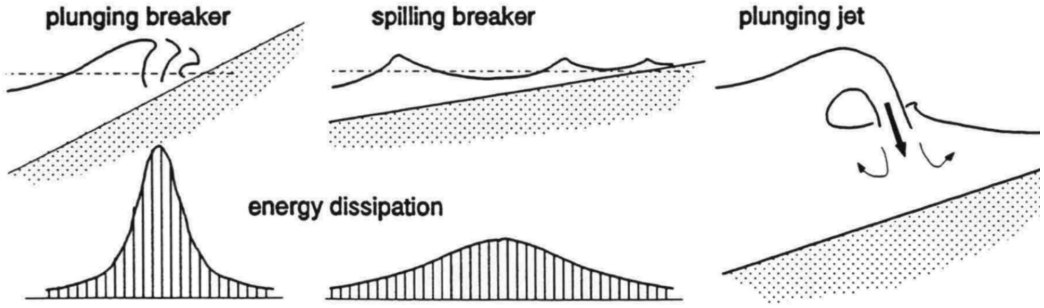

Figure 2.5: Energy dissipation for spilling and plunging breakers with an example of a plunging jet phenomenon (Shiereck et al., 1994)

The distribution between plunging and spilling waves for slopes 1:8 and 1:10 is shown in figure 2.6:

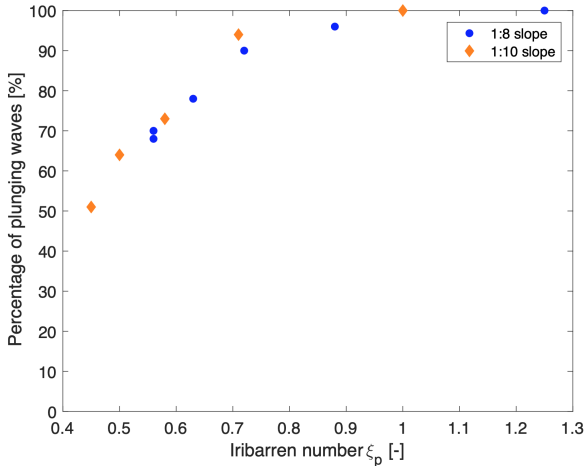

Figure 2.6: Distribution of spilling and plunging breaker waves for slope 1:8 (Van Wijland, 2020) and 1:10 (Mossinkoff, 2019)

Based on figure 2.6, the expected distribution for slope 1:6 is approximately 90 percent and 100 percent plunging waves. Based on wave steepness between $s_p = 0.01$ and $s_p = 0.05$ with corresponding Iribarren numbers, respectively, $\xi_p = 1.8$ and $\xi_p = 0.8$.

2.2 Damage characteristics

Stability of the structure is described by damage. A distinction is made within the damage characteristics between damage parameters in subsection 2.2.1 and damage profiles in 2.2.2. Each damage parameter or profile discussed is based on different principles, for instance erosion area or the number of entrained rocks, that indicates a certain form of damage on a structure. The damage parameters are mainly based on erosion depths and areas relative to the nominal stone. The limits of the damage parameters are generally increasing for more gentle structure slopes. The formation of damage profiles is mainly dependent on the dominant transportation direction, which is especially influenced for varying structure slope, wave steepness and significant wave height.

2.2.1 Damage parameters

The profile based damage parameters described in this section can be distinguished two-dimensional (2D) and three-dimensional (3D) damage parameters, shown in figure 2.7. The physical difference is

that 2D-parameters are based on the damage from a width-averaged profile (figure 2.7 a). The 3D-parameters (figure 2.7 b) could be interpret as a spatial moving average covering the entire slope based. In this section, various damage parameters are introduced:

A clearly defined damage level (Broderick & Ahrens, 1982), S, was introduced by coupling the cross-sectional eroded area A_e with corresponding characterization width w (figure 2.7b) to the square of the nominal diameter of the armour stones, d_{n50A}. This gives the dimensionless parameter damage parameter S as depicted in equation 2.24:

$$S = \frac{A_{(e),w}}{d_{n50A}^2} \tag{2.24}$$

where A_e is the eroded area comparing the initial profile with the profile after wave attack. This profile is width-averaged over the test section w de Almeida et al. (2019).

Van der Meer (1988) discussed two failure criteria: initial damage and failure of structure. Only damage parameter S was used to identify these failure criteria. Depending on the range and datasets (Thompson & Shuttler, 1975) of slopes tested (1: 1.5 - 1: 6), the onset of damage varied between S = 2 and S = 3, respectively. Before the failure of the structure, this was S = 8 and S = 17, respectively. thus, higher damage limits can be expected for gentler slopes. The damage limits for this investigation as well as several are shown in table 2.5.

Damage parameter S only considers the largest erosion area and the damage parameter S_{all} considers all the damage on the slope, as denoted in equation 2.25:

$$S_{all} = \frac{A_{1(e),w} + A_{2(e),w} + ... + A_{n(e),w}}{d_{n50A}^2} \tag{2.25}$$

A possibility within the use of this method for S_{all} is to apply a minimal erosion area $A_{min(e),w}$ which can be used in order to use a threshold to only consider significant erosion areas $A_{(e),w}$.

Wit (2015) presented a method to estimate the start of damage, based on the assumption that the erosion depth d_e is independent of the structure slope and therefore considered constant. This method is expressed in equation 2.26

$$S_{all} = S_{start} * \frac{sin(\alpha_{start})}{sin\alpha} \tag{2.26}$$

An example considering the start of damage for this method for slopes 1:6, 1:8 and 1:10 is given as, respectively, S = 3, S = 4 and S = 5.

The approach of damage in the form of parameter E_{2D} has been considered by Hofland et al. (2011), based on the study by Melby and Kobayashi (1998), as denoted in equation 2.27:

$$E_{2D} = \frac{max[(d_e)_w]}{d_{n50}} \tag{2.27}$$

Where d_e is the maximum depth of erosion perpendicular to the slope in the tests, based on the average profile over the test section (de Almeida et al., 2019).

The damage parameter E_{3D} is based on the same characteristic, maximum erosion depth d_e, as E_{2D}. This approach of damage in the form of parameter E_{3D} has been considered by Hofland et al. (2011), also based on the study by Melby and Kobayashi (1998), as denoted in equation 2.28:

$$E_{3D,m} = \frac{max[(d_e)_{m*d_{n50}}]_w}{d_{n50}} \tag{2.28}$$

Where d_e is the maximum depth of erosion perpendicular to the slope, based on a moving average over a circular area of $m * d_{n50}$ (Hofland et al., 2014) within a given characterization width w. A higher

m-value leads to an increase in the spatially moving circle, which is accompanied by a lower acceptable value for initial damage, intermediate damage and failure of the structure.

The described damage parameters S, S_{all}, E_{2D} and $E_{3D,m}$ are all profile based damage parameters and a visualisation of their defined main characteristics (erosion area A_e, erosion length L_e, maximum erosion depth $max[d_e]$ and characterization width w are given in figure 2.7:

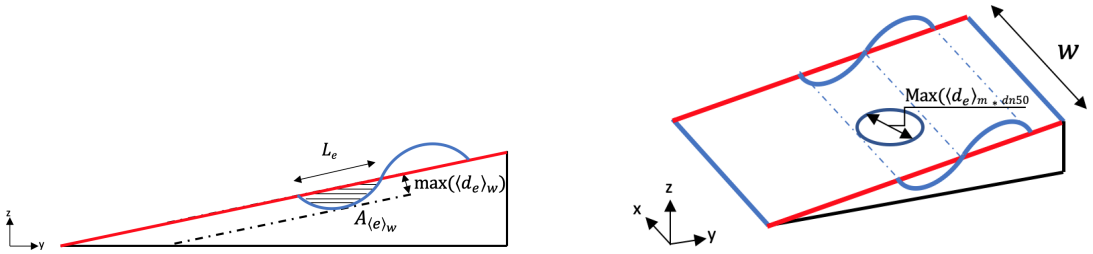

(a) Main characteristics of 2D damage parameter

(b) Main characteristics of 3D damage parameter

Figure 2.7: Defined main characteristics related to a) 2D and b) 3D damage parameters (Van Wijland, 2020).

The Rock Manual (CIRIA, 2007) describes a different interpretation of damage than the profile-based damage parameters, which is based on the number of displaced rock units of the armour layer N_{od} as denoted in equation 2.29:

$$N_{od} = \frac{n_{tot} d_{n50}}{w} \tag{2.29}$$

Where n_{tot} is the number of displaced rock units. This parameter could be used if one want to gain insight into the static stability of a structure, as any loose stone that moves is seen as damage. The damage parameter N_{od} requires that all individual measured rock displacements are taken into account as damage. However, this method is less interesting for an efficient design method, as a moving stone at another location may be of added value in terms of stability of the slope. A difficulty in using this damage parameter is the measurement errors that are almost inevitable because the stones within the same color strip of a test set-up (see: figure 3.2) are not yet clearly distinguishable.

Previous studies in this series, including Mossinkoff (2019) and Van Wijland (2020), have concluded that $E_{3D,3}$ represents the best approximation of local damage and is therefore preferred. In order to also make a comparison with the research of Van der Meer (1988), the focus will initially be on damage parameters S and $E_{3D,3}$. Hofland et al. (2011) suggested that the failure limit of a thicker layer than $2 * dn50A$ could estimated as $E_{3D,3,failure} = ((1.5-1.6)+(T_{>2d_{n50}}-2))$. According to this relation, the failure limit of a layer thickness of $2.5d_{n50}$ would be equal to a value around $E_{3D,3} = 2.0$. For the intermediate damage limit, Hofland et al. (2011) provides an estimate $E_{3D,3,int} = (0.5-0.6) * (T/2)$. For the research of Van Wijland (2020), this gives a quite accurate range of $E_{3D,3,int}$ between 0.625 and 0.75 for the observed intermediate damage value of 0.6.

The damage limits of damage parameters S, E_{2D} and $E_{3D,3}$ of earlier described researches are presented in table 2.5:

Table 2.5: Damage limits for damage parameters S, E_{2D} and $E_{3D,3}$ for various test conditions.

Description	S **(Van der Meer, 1988)**	E_{2D} **(De Almeida et al., 2019)**	$E_{3D,3}$ **(Hofland et al., 2011)**	$E_{3D,3}$ **(Mossinkhoff, 2019)**	$E_{3D,3}$ **(Van Wijland, 2020)**
Layer thickness, t	$2 * d_{n50A}$	$2 * d_{n50A}$	$2 * d_{n50A}$	$2.5 * d_{n50A}$	$2.5 * d_{n50A}$
Slope angle, cot α	1.5 - 6	3	2 - 3	10	8
Initial damage	2 - 3	0.2	0.2 - 0.3	0.5	0.3
Intermediate damage	-	0.5	0.5 - 0.6	1.2	0.6
Failure damage	8 -17	0.9	1.5 - 1.6	2.3	1.5

2.2.2 Damage profiles

Damage profile formation on a structure slope can be categorized as berm and bar profile, as shown in figure 2.8.

(a) Berm profile

(b) Bar profile

Figure 2.8: Damage profiles categorized as a) berm profile and b) bar profile (Van Wijland, 2020).

The damage profile can be schematized by parameters such as angles, heights and length of the formed profile. A berm profile is formed by a net downward transport of rock on the slope, which is accompanied by accretion and erosion on respectively the upside and downside of the slope. And vice versa for a bar profile. The red line in figure 2.8 could be seen as the initial structure profile and the blue line as the formed damage profile after adequate exposure of wave attack. The dominant transportation direction of stones is important for the way in which the damage profile is created. Van der Meer (1988) states that profile development could occur faster than the development of damage, as the resistance to wave action is much smaller for the smaller grains used in dynamically stable structures. One could infer from this that not every form of profile development should be identified as damage, which differs from the statically stable structures.

On the basis of a steeper structure slope, the influence of gravity becomes more decisive, which would mean that stones are more easily transported downwards. The final destination of a stone depends on both the transportation direction and the length. Both characteristics depends on the wave steepness s and significant wave height H_s as shown in figure 2.9:

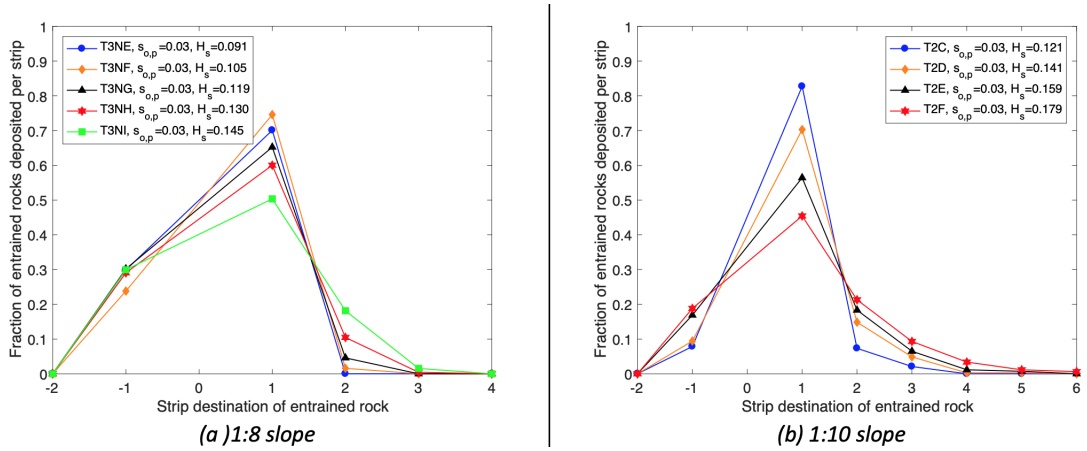

Figure 2.9: Probability graphs of final destination of transported rocks under wave attack for a) slope 1:8 (Mossinkoff, 2019) and b) slope 1:10 (Van Wijland, 2020).

A clear observation by Van Wijland (2020) is that an increasing significant wave height H_s, regardless of the wave steepness s, increases the chance that a single rock will discard one or more strips. Mossinkoff (2019) observed berm profiles for the tests with slope 1:10. Van Wijland (2020) observed a combination bar and berm profiles. By performing physical model tests with a slope 1:6, a combination or mostly bar profiles are expected due to the increased influence of gravity relative to the more gentle slopes.

2.3 Stability of rock under wave attack

Many different studies on the stability of stones on a slope have been carried out. This initial report will only describe substantively at the studies of Van der Meer (1988), Van Gent et al. (2003), Mossinkoff (2019) and Van Wijland (2020) because they are the most important comparison material for the objective of this research.

2.3.1 Research on steep slopes

Van der Meer (1988) made a distinction between surging (equation 2.31) and plunging (equation 2.30) breaker wave type conditions. In addition to the data from his own physical model tests, the formulae of Van der Meer (1988) is also based on additional data from Thompson and Shuttler (1975). The widely used design formulae proposed by Van der Meer (1988) are denoted in equations 2.31 and 2.30:

Plunging waves:

$$\frac{H_s}{\Delta d_{n50}} = 6.2P^{0.18}\left(\frac{S}{\sqrt{N}}\right)^{0.2}\xi_m^{-0.5} \tag{2.30}$$

Surging waves:

$$\frac{H_s}{\Delta d_{n50}} = 1.0P^{-0.13}\left(\frac{S}{\sqrt{N}}\right)^{0.2}\xi_m^{P}\sqrt{\cot\alpha} \tag{2.31}$$

Where $\frac{H_s}{\Delta d_{n50}}$ is equal to the stability number N_s of equation 2.19 in subsection 2.1.3. The transition from plunging waves ($\xi_m < \xi_c$) to surging conditions ($\xi_m \leq \xi_c$) is given by the critical breaker parameter ξ_c:

$$\xi_c = \left[\frac{c_{\text{plunging}}}{c_{\text{surging}}}P^{0.31}\sqrt{tan\alpha}\right]^{\frac{1}{P+0.5}} \tag{2.32}$$

Regardless of the incoming wave conditions and corresponding Iribarren number ξ, Van der Meer (1988) recommended to consider only plunging waves for a structure slopes more gentle than slope 1:4. Van Gent (2004) shows this conservative approach in figure 2.10:

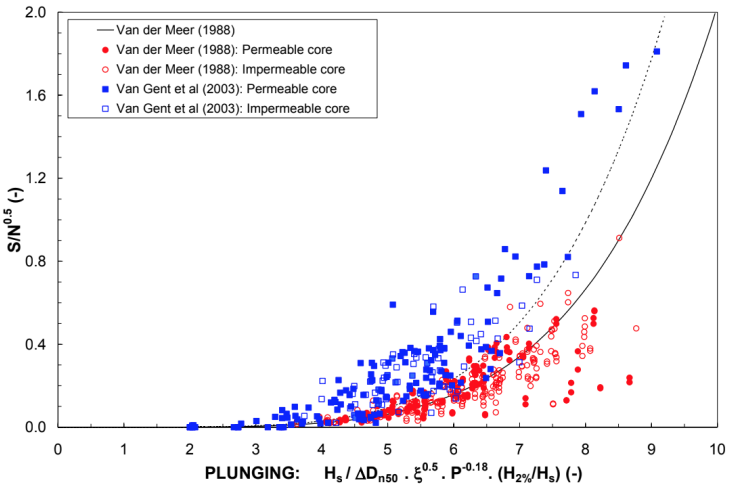

Figure 2.10: Data of Van Gent et al. (2003) compared to formula by Van der Meer (1988) for plunging waves.

The formulae of Van der Meer (1988) is mainly designed on the basis of deep water wave conditions and single-peaked spectra, in contrast to the method of Van Gent et al. (2003). The test data of Van Gent et al. (2003) includes shallow water conditions, which are accompanied by distortions in the spectrum. The difference of the processes that occur in shallow water in comparison with the deep water wave approach of Van der Meer (1988) could lead to a considerable scatter, which results in smaller stone diameter than required (Van Gent, 2014). The tested range from which the stability formulas of Van der Meer (1988) and Van Gent et al. (2003) originated are shown in table 2.6:

Table 2.6: Ranges stability formulae Van der Meer (1988) and Van Gent et al. (2003)

	Stability formulae	
Parameter	**Van der Meer (1988)**	**Van Gent et al. (2003)**
Datasets	**Van der Meer (1988)** **Thompson and Shuttler (1975)**	**Van der Meer (1988)** **Van Gent et al. (2003)**
Slope angle, $\cot\alpha$	1.5 - 6	2 - 4
Relative density, Δ	1.65 - 1.75	0.9 - 2.1
Number of waves, N	162 - 5416	N < 3000
Wave steepness, s_{0m}	0.004 - 0.064	0.004 - 0.063
Breaker parameter, ξ_{0m}	0.7 - 7.6	1 - 5
P	0.10 - 0.60	0.10 - 0.60
$H_{1/3}/\Delta d_{n50}$	0.71 - 4.38	0.63 - 4.38
$H_{1/3}/H_{m0}$	NA	0.68 - 1.01

The formula of Van Gent et al. (2003) is given in equation 2.33:

$$\frac{H_s}{\Delta d_{n50}} = 1.75 \cot\alpha^{0.5}(1 + d_{n50-core}/d_{n50})(\frac{S}{\sqrt{N}})^{1/5} \tag{2.33}$$

Formula 2.33 presents two fundamental differences from the formulae of Van der Meer (1988). First of all, only one formula for plunging and surging waves. Second, the permeability of the structure is

shown as the ratio between nominal rock size of the core $d_{n50-core}$ and armor layer d_{n50}. As a result, for structures with an impermeable core, this method is less accurate in comparison with Van der Meer (1988). An advantage is that for permeable structures the method is more accurate, for both deep water and shallow water conditions (Van Gent, 2014).

2.3.2 Research on mild slopes

Based on the datasets of Mossinkoff (2019) and Van Wijland (2020). The design formula described by Van Wijland (2020) is given in equation 2.34

$$\frac{H_s}{\Delta d_{n50}} = 7.55\ E_{3D,3}^{0.62}\ \xi_p^{-1.10}\ N^{-0.13} \tag{2.34}$$

This formula is verified for data of slopes between 1:8 and 1:10 and for a number of waves N of 15000. The formula is validated for a layer thickness of $2.5 d_{n50}$ on an impermeable core and for Iribarren numbers ξ_p between 0.45 and 1.25, corresponding to plunging and spilling waves. The influence of permeability is not directly incorporated in the formula of Van Wijland (2020).

Equation 2.30 of Van der Meer (1988) for plunging waves is extrapolated for Iribarren numbers ξ_m smaller than 1, as shown in figure 2.11:

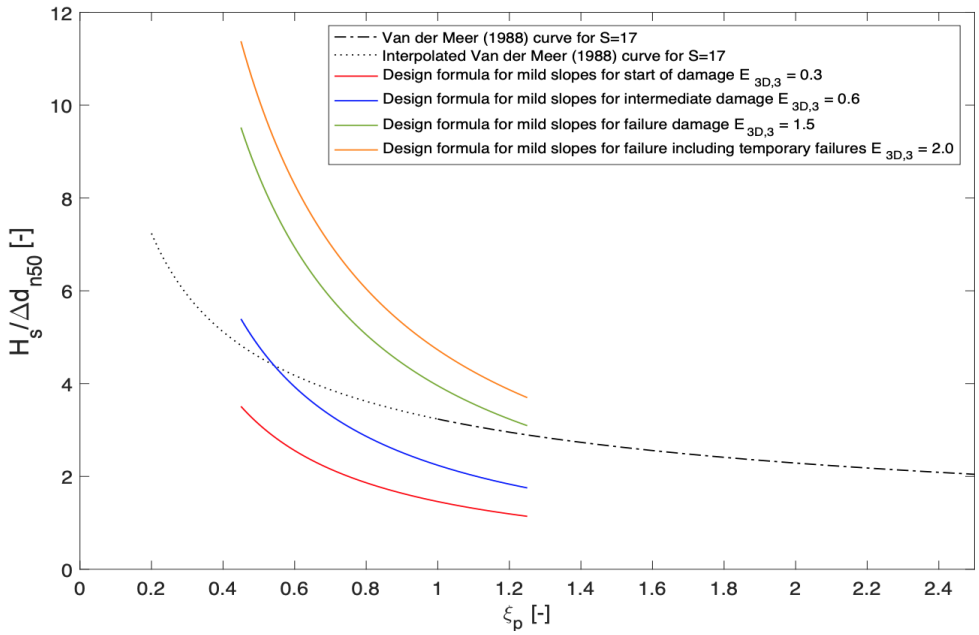

Figure 2.11: Plotted design formula of Van Wijland (2020) and extrapolated Van der Meer (1988) for N = 1000 waves.

From this figure 2.11, Van Wijland (2020) concluded that the design formula presented in this thesis allows higher values of the stability number N_s in comparison with the extrapolation of the method of Van der Meer (1988).

3 Research methodology

To develop an understanding of the ongoing processes regarding stability of mild slopes, the aim of this chapter is to develop an approach to gain real-time insights of the behavior of rocks on mild slopes for a physical model test series. The method for the tests with slopes 1:8 and 1:10 which are described and (re)-performed by Van Wijland (2020) are used as the underlying basic approach. The aim is to be able to answer the research questions (section 1.3) posed by means of this method, with improved processing time with increased accuracy.

3.1 Physical model tests for 1:6 slope

3.1.1 Test set-up

In the Pacific Basin of research institute Deltares, the tests were carried out on a built slope of 6 meters long and 1 meter high, referred to as slope 1:6. The width of the slope is 1 meter and this passage is considered the wave flume. The bottom of the slope in the wave flume consists of wood and the sides of concrete stone. Because the underside is made of wood, it is considered to be completely impermeable. In figure 3.1, the test environment of this slope can be observed along with associated equipment such as wave machines, wave computers, wave gauges and a table to sort the stones by color after each test. The wave machines operate on hydraulics and oil pressure and are able to generate long-crested irregular waves with adjustable characteristics from pre-programmed steering files in the wave computers. The wave paddles are not equipped with automatic compensation for reflection, to take into account the reduction of the reflection, there are wave dampening slopes at the back of the slope structure on the full width of the basin. At the lower part of the built-in slope, two triangular wooden structures have been placed so that the influence of potential formed reflection from the limestone sand structures on the incoming waves is reduced. A top view of this setup is shown in figure 3.2.

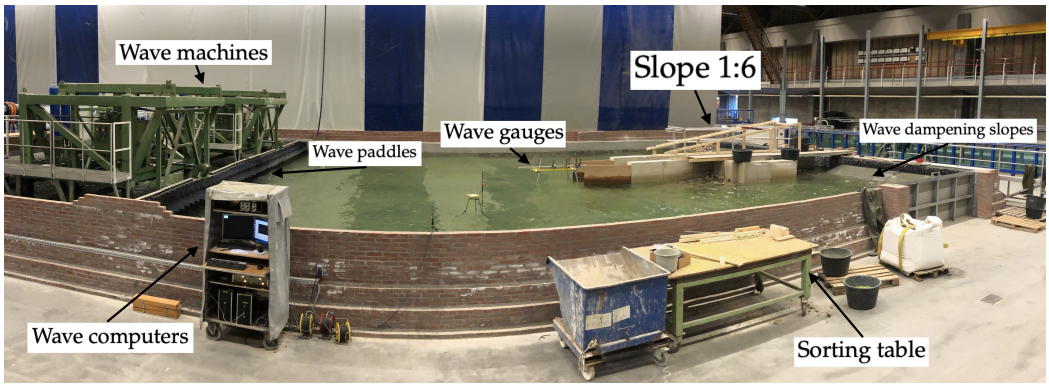

Figure 3.1: Test environment: Pacific Basin of research institute Deltares in Delft, The Netherlands.

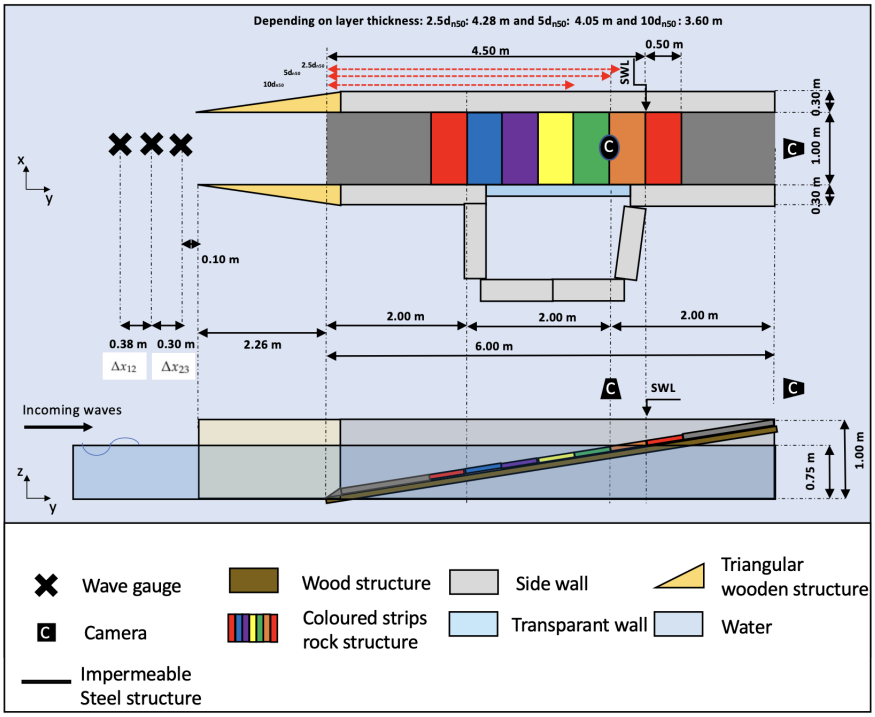

Figure 3.2: Top view test set-up for slope 1:6 based on experiment of Van Wijland (2020) and Mossinkoff (2019).

In figure 3.2, three red dotted arrows are indicated, from the bottom to the top, for a layer thickness of $2.5dn50$, $5dn50$ and $10dn50$. Each arrow represents the distance from the start of the slope to the point where the waterline meets the top of the armour layer in y-direction. SWL is noted as the location where the phreatic surface meets the impermeable layer. A larger layer thickness indicates a greater distance from the initial SWL without the armour layer, indicated by a black arrow. The possible effects of these varying distances will be discussed in subsection 3.2.7 and section 4.7.

The distances between the wave gauges are denoted as Δx_{12} and Δx_{23}. In order to calculate these gauge spacings, the values of each wave condition of the test plan (table 3.3) are calculated with formula 3.1 of Mansard and Funke (1998):

$$D(\Delta x_{12}, \Delta x_{23}, f) = sin^2(k\Delta x_{12}) + sin^2(k\Delta x_{23}) + sin^2(k(\Delta x_{12} + \Delta x_{23})) \tag{3.1}$$

The procedure to obtain the optimal wave gauge spacing according to the method of Mansard and Funke (1998) works as follows:

First, the minimum value D_{min} is calculated over the range of all frequencies ($f_p = 0.37 - 1.71[s^{-1}]$) as $D_{min}(\Delta x_{12}, \Delta x_{23}, f) = min(D(\Delta x_{12}, \Delta x_{23}, f))$. For this range of frequencies multiple values for D_{min} are found. Accounting these values, a local maximum value could be obtained which will provide one specific optimal gauge spacing for this condition. On the basis of the wave conditions (table 3.3), the distance between the wave gauges can be determined as $\Delta x_{12} = 0.38$ m and $\Delta x_{23} = 0.30$ m.

The main characteristics of the physical model tests are shown in table 3.1.

Table 3.1: Main characteristics physical model tests deduced from Van Wijland (2020) and Mossinkoff (2019) in order to compare the results of my test series slope 1:6 with findings of slope 1:8 and 1:10.

Description	Symbol	Value	Unit
Slope angle	$\cot\alpha$	6	-
Wave spectrum	-	JONSWAP	-
Nominal rock diameter	d_{n50}	14.8	mm
Rock grading	d_{85}/d_{15}	1.4	-
Rock density	ρ_s	2944	kg/m^3
Water density	ρ_w	1000	kg/m^3
Relative density	Δ	1.94	-
Water depth	h	0.75	m
Strip width coloured stones	W_{strip}	0.5	m
Dimensions basin (l x b x h)	l, b, h_{basin}	28 x 14 x 1.25	m

- **Slope angle**

  For this series of tests, a slope of 1:6 has been chosen. In order to describe the stability of rocks for this slope angle and to understand the processes on mild slopes, this is essential to conduct. By testing the slope 1:6 in the same test environment as slopes 1:8 and 1:10, a possible comparison can be made with the studies of Van Wijland (2020) and Mossinkoff (2019) on the one hand, and on the other hand, this slope also provides an opportunity for the comparison with tests of Van der Meer (1988). The test with slope 1:6 provides this range of slope stability tests with meaningful information about the transition zone between steep slopes and mild slopes. Based on the distribution of figure 2.6, it is expected that only a small percentage of spilling waves will be present for tests with slope 1:6. With the method of Van der Meer (1988), the presence of spilling waves is not taken into account.

  A certain combination of wave steepness and slope 1:6 can give the same Iribarren number as a slope 1:4 with different wave conditions. For example, it is possible to compare the test results for a slope 1:4 or 1:5 on the basis of corresponding stability and Iribarren numbers.

- **Wave spectrum**

  Since in the design of coastal structures the conditions with steeper waves are decisive, this is the main reason JONSWAP spectrum is considered as the design spectrum and used at the tests of Mossinkoff (2019) and Van Wijland (2020). From the chosen spectrum (frequency domain) and the wave signal (time domain), significant wave heights and wave periods are obtained. The mutual relationships between the various parameters outside both domains are shown in the table 2.3.

  By comparing the PM-spectrum with the JONSWAP spectrum, Van der Meer (1988) obtained results that when the spectral significant wave height and the mean period where almost equal the peak period related to the PM-spectrum was significantly (10% - 15%) smaller. This is because the spectrum evolves towards the lower frequencies. Van der Meer (1988) considered a PM-spectrum to derive his test results, by processing this information into formulas 2.8 and 2.21 a lower peak frequency could lead to higher wave steepness and lower Iribarren number.

- **Rock characteristics**

  The same rock material is used for the 1:6 physical model test as for the comparable 1:8 and 1:10 tests. Before the 1:10 test serie of Mossinkoff (2019), weighing curves from the rock material were collected. It follows that the nominal diameter is 14.8 mm and the grading corresponds to d_{85}/d_{15} = 1.4. This grading is categorized from the EN-13383 as narrow graded gravel (Rock Manual, 2017). By using narrow graded rock material, less spatial variations of damage will occur. Which gives a lower probability of severe local damage due to variations of sizes of individual stones

(CIRIA, 2007). The density of the rocks ρ_s is 2944 kg/m^3, from which the relative density can be calculated as Δ = 1.94 using formula 2.14.

By using the same rock material tests with slope 1:6 as for tests 1:8 and 1:10 there are a number of characteristics to take into account. For milder slopes, the expected amount of spilling breaking waves is higher, which causes less damage for the same wave characteristics. Thus for the same nominal rock diameter (d_{n50}) and same incoming wave characteristics, the stability number (N_s) is expected to increase for decreasing slope. This is mainly due to the increase of the Iribarren number and change of breaker wave type. This reasoning is supported by the design formula of Van Wijland (2020), shown in figure 2.11.

- **Water depth**

  From the perspective of meeting deep water conditions for this study, a water depth is chosen. This is important because Mossinkoff (2019) and Van Wijland (2020) as well as Van der Meer (1988) have used this deep water approach. Mossinkoff (2019) has determined the optimal depth as h = 0.75 m for a slope of 1:10 in the Pacific Basin. This is determined by the minimum depth to simulate deep water conditions and thereby maximize workability by reducing operational filling times of the basin. Based on two criteria about deep water approximation, it was checked whether the approximation is valid for the current test conditions of slope 1:6. Particularly for the larger wave period in the test series, the first criteria of $h/L_0 > 0.5$ (USACE, 2015) is not met. This is based for a range of wave steepnesses (1% - 4%) and significant wave heights (0.02 m - 0.21 m) resulting in h/L_0 = 0.04 - 1.5 by use of formula 2.8. This invokes the criteria of Frostick et al. (2011) which indicates that for a deep water regime, all physical model tests must meet $H_s/h < 0.3$. The highest producible wave height in the Pacific Basin is 0.21 m, which results in H_s/h = 0.28. Therefore the whole range of tests complies with the criteria Frostick et al. (2011). In this test serie with slope 1:6, a water depth of 0.75 m is chosen based on complying of Frostick et al. (2011) criterion as a deep water approach and to compare test results with the tests of Mossinkoff (2019) and Van Wijland (2020).

- **Colour band width**

  The colour band width is referred to as the length of a coloured section of rocks on the slope, as one could observe in figure 3.2. The expected damage domain is important for positioning and determining an useful colour band width. It must be ensured that the moved rocks are situated within the coloured sections after occurrence of the incoming waves. Most erosion and accretion occurs in range $-1.1H_s$ to $+0.6H_s$ for slope 1:8 and $-1.2H_s$ to $+0.4H_s$ for slope 1:10 considering the medians Van Wijland (2020). Since for slope 1:6 with the same colour band width and maximum wave height ($H_s = 0.21m$), a larger vertical range is covered with coloured stones to identify displacements. Therefore, a similar set-up as Van Wijland (2020) is chosen with one strip above SWL and six strips below SWL, each with a width of 0.5 m. It was also decided to perform one test with a strip width of 0.1 m in order to determine the interoperability of the strip width for varying slope angles, because of a possible corresponding changing damage domain.

- **Dimensions basin**

  The total length of the basin is 28 m including the wave generators. The width of the basin is 14 m. The height of the basin inclosure is 1.25 m. The Pacific Basin is shown in figure 3.1. Since the dimensions of the basin are large enough for the waves to disperse, the waves arriving in the wave flume experience minimal impact from processes such as reflection and therefore reduce the occurrence of standing waves. These effects would influence the damage formation of the slope.

3.1.2 Measuring instruments and techniques

The following measuring techniques are used to perform the tests:

1. *Wave gauges to measure incoming wave characteristics*

   As described in subsection 3.1.1 the optimal wave gauge spacing is determined as Δx_{12} = 0.38 m and Δx_{23} = 0.30 m. Before the tests started, calibrations were performed to link the electrical current strength (A) of the wave gauge to a difference in water level (m). By measuring water level in relation to time, insight can be given into wave characteristics such as wave height, wave period and wave steepness of the incoming waves. Figure 3.1 shows where the three wave gauges are positioned in the basin, allowing to distinguish the incident and reflected wave spectra. Figure 3.2 shows the exact distances between the wave gauges and the distances relative to the built-in slope.

2. *Camera to determine the breaking wave type*

   The type of a breaking wave (figure 2.6) can be assessed as spilling or plunging on the basis of Battjes (1974) criteria. A clearly distinguishable difference is the presence of a plunging jet in plunging waves. The distribution between spilling and plunging waves can be determined by analysing the development of each incoming wave in a certain time frame. Figure 3.2 shows the location of the camera at the upper end of the slope pointing towards the incoming breaking waves. The camera is adjusted to visualize the zone of breaking waves, for this a Panasonic HDC-HS200 with a video resolution of 1920 x 1080 pixels is used.

3. *Camera to analyse the normative processes regarding the transportation of rocks*

   To gain a better insight during which phases of an incoming wave the stones are set in motion. Processes such as rocking, entrainment, turbulence and run-down can be properly observed. A camera has been placed one meter above the slope, the position is shown in figure 3.2.

4. *Coloured strips to indicate the entrained and deposited rocks*

   Entrainment and deposition of rocks are measured by counting coloured stones in strips with a certain length. Van Wijland (2020) and Mossinkoff (2019) used a strip width of 0.5 m. To compare with their tests the same strip width is used but also to provide additional information about the impact of the use of varying strip width for a different slope one test serie with a strip width of 0.1 m is performed. This is important because for a different slope angle the height of a slope varies per strip width of 0.5 meters. For example, for a slope of 1:6, a strip width of 0.5 meters requires a height of 0.08 m, compared to a height of 0.06 m for a slope of 1:8. As a result, a single rock has to make a larger vertical displacement to get out of a colour band, therefore more internal transport will occur for slope 1:6.

   By using stereophotogrammetry, a detailed model can be used to count the displaced rocks in 3D. The number of displaced rocks and the transportation length were determined based on this 3D model in Agisoft Metashape. Figure 3.2 shows the position of the coloured strips of 0.5 m on the slope 1:6. In figure 3.12 the test set-up for both used colour band widths can be observed.

5. *Stereophotogrammetry with automatically detectable Ground Control Points (GCPs) to determine damage parameters and damage profiles*

   Stereophotogrammetry involves estimating the 3D coordinates of points on the slope, employing measurements made in multiple photographic images taken from different positions along the

structure. This technique is applicable since the profile can be measured in a relatively simple way, with high accuracy and fine resolution (Hofland et al., 2011). For this test, 63 photos are taken from a wooden frame at a height of 1 meter parallel to the slope. On 21 rows, 3 photos are taken side by side with 0.25 m in between as shown in figure 3.3. Due to the static background, a stereo photo can be simulated for both left and right on the slope, in order to determine the depth of the surface. The 3D model is calculated from a collection of points obtained along an x, y, and z coordinate system. A mesh is applied over the area being compared (indicated by yellow rectangle in figure 3.3), allowing the heights of the damaged profile to be calculated relative to their reference profile. Section 3.2.1 shows how the software processes the input of 63 photos to a model.

In order to be able to calculate the geometric information an image overlap of at least > 30% must be guaranteed across the input dataset of images (Agisoft, 2021). To produce professional quality orthographics, the minimal resolution is 12 Mpx (Agisoft, 2021). For the research a image resolution of 24 Mpx is used. Hofland et al. (2011) stated that a larger amount of data may indicate that the mean profile can be measured with a higher accuracy. Therefore, before processing the xyz-coordinates, masks could be added so that only geometric information is measured for the zone of interest. A mask ensures that the software does not need to include part of the photo in the model calculation and is indicated with red outline and text in figure 3.3. Table 3.6 shows the property differences of two models processed with and without applied masks.

Photos saving in TIFF-files for processing with Agisoft Metashape software. It is recommended using TIFF files due to the fact that less noise (i.e. graininess) appears in TIFF files than in JPEG files (Agisoft, 2021).

Automatically detectable Ground Control Points (GCPs) are used to scale and orient the 3D model. The GCPs have a 12-bit code so that the software assigns a number to each GCP, also referred as target. The xyz-coordinates of the numbered GCPs have been predetermined and can therefore be assigned automatically as a frame of reference in order to align the photos. The reference xyz-coordinates are shown in table 3.2 and are measured with a total station (Leica TCRA1202). The GCPs are positioned to not alter for varying layer thicknesses up to $10d_{n50}$.

The automatically detected Ground Control Points (GCPs) are attached to the sidewalls with a single-turn hinge perpendicular to the side wall, so that the GCPs are locked in x and y direction. The hinges are magnetically attached parallel to the side wall. During the execution phase of the test procedure (subsection 3.1.3), the hinges are closed to reduce any effects of turbulence around the GCPs. So that addition to the already existing effects due to the wall, the presence of the GCPs does not influence the comparability of results from Van Wijland (2020) and Mossinkoff (2019). The margin of error due to the magnetic folding and unfolding of the GCPs is incorporated in the process of the check tests in table I.1.

The GCPs are evenly distributed on the slopes and are not placed exactly at the outer edges of the measurement area. Because the zone with most overlap is in the middle of the measurement area. If GCPs are placed on the outer edges, the overlap is just at the minimum of 2 pictures. For more accurate results, the minimum amount of detected GCPs for each test is increased to 135 projections per 63 photos. Target 1 is projected 6 times, target 12 is projected 9 times and the other numbered GCPs are projected 12 times, as shown in table 3.2

The size of these GCPs depending on the characteristics of the camera used (Canon 750D) and the distance from the camera to the ground. The Ground Sampling Distance (GSD) is depicted as the distance between two consecutive pixel centers measured on the ground. For this setup and camera, the GSD equals 0.029 cm/pixel. The diameter of the middle circle of the GCPs is 14 mm, so that the software is able to very accurately determine the center of the GCP.

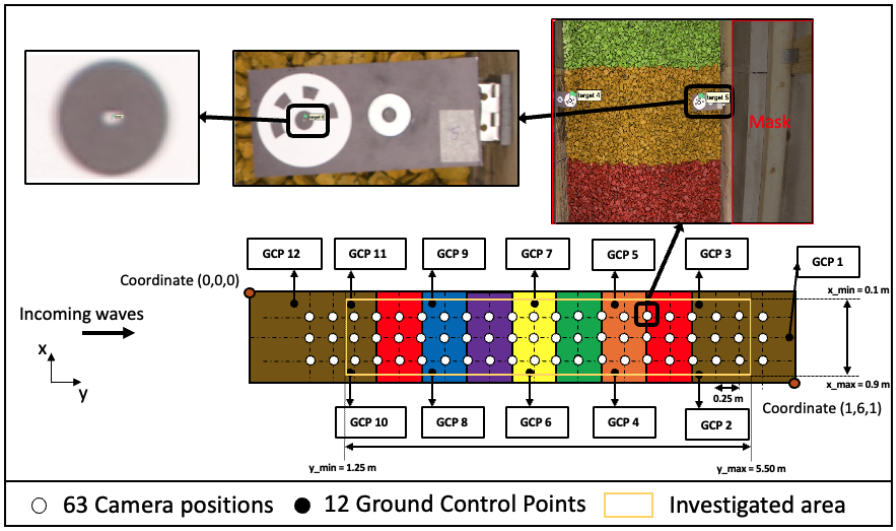

Figure 3.3: Placement Ground Control Points (GCPs).

Table 3.2: Numbered Ground Control Points (GCPs) with reference xyz-coordinates.

	X [m]	Y [m]	Z [m]	Number of projections
GCP 1	0.505	5.738	1.142	6
GCP 2	0.888	5.070	1.060	12
GCP 3	0.129	5.102	1.060	12
GCP 4	0.878	4.121	0.875	12
GCP 5	0.151	4.146	0.875	12
GCP 6	0.867	3.147	0.720	12
GCP 7	0.143	3.166	0.714	12
GCP 8	0.869	2.117	0.553	12
GCP 9	0.146	2.145	0.542	12
GCP 10	0.861	1.195	0.383	12
GCP 11	0.141	1.211	0.389	12
GCP 12	0.136	0.582	0.289	9

3.1.3 Test procedure

This study uses the cumulative method regarding the test procedure. To verify the used method, a single non-cumulative test is performed to compare the damage characteristics. The preference for this method is substantiated by results from studies by de Almeida (2017) and Van Wijland (2020). De Almeida (2017) concludes that cumulative and non-cumulative testing methods presented similar damage results for rock armoured slopes. The tests with slope 1:2 and 1:3 shows small variations (from 0%- 5%) in measured damage according to both S and $E_{3D,5}$ parameters between the two methods. Van Wijland (2020) shows that all associated damage parameters of 5 non-cumulative tests are within a 90 percent confidence interval (90 % CI = $\mu \pm 1.833\ \sigma/\sqrt{10}$) compared to the damage parameters of one cumulative test with the same wave conditions at that particular time in the test series.

An advantage of the cumulative method is that a larger amount of slope data can easily be collected in a relatively shorter time because the slope is not rebuilt within a test serie.

The test procedure of this research consists of three phases: preparation phase, execution phase and completion phase. Each phase is elaborated on the basis of a number of steps to be followed.

- **Preparation phase**
  1. Build up the slope according to the test setup for the specific layer thickness ($2.5d_{n50}/5d_{n50}/10d_{n50}$).
  2. Record the reference profile using 63 photos taken from the frame.
  3. Process the reference profile as a Digital Elevation Model (DEM). An explanation how to process a DEM is shown in appendix G. A DEM is used to check whether the slope is built uniformly. If necessary, adjust local unevenness on the slope and process a new reference profile.
  4. Prepare steering files as input for the wave machines. This is done according to estimations of the start of damage with calculations based on design formulas of Van Wijland (2020) and Van der Meer (1988).
- **Execution phase**
  1. Attach the GCPs to the magnets on the side of the wave flume.
  2. Fill the basin, wait until the water is in a calm state, measure with the water depth with the gauge needle at 0.75 m.
  3. Set the three wave meters to a reference voltage of zero.
  4. Turn on the cameras.
  5. Perform visual inspection of the slope.
  6. Power on the wave machine.
  7. Stop wave machine when duration of the test is reached.
- **Completion phase**
  1. Drain the basin.
  2. Make the GCPs visible again by folding out the hinge.
  3. Record the damaged profile using 63 photos taken from the frame.
  4. Apply the on-site check (Appendix G) to validate the number of 135 GCP projections and to comply with the pixel error limit of 1 pix.
  5. Continue from the beginning of the execution phase until the slope is failed which is indicated by complete removal of the armour layer.

3.1.4 Test plan

The wave steepness (s_{op}) and thus the Iribarren number (ξ_p) are kept around the values indicated in the table for each test series. N = 1000 indicates that for each test iteration the slope is exposed to approximately 1000 waves. As introduced in subsection 2.1.2, the notional permeability could be estimated following the empirical method of Eldrup and Andersen (2019). For the layer thicknesses $2.5d_{n50}$,$5d_{n50}$ and $10d_{n50}$ the estimated values of are, respectively, P = 0.1, P = 0.48 and P = 0.57. These P values are initially used to couple the expected damage limits and the associated significant wave heights per test serie. This relation is based on design formulas (equation 2.30 and 2.34) and damage limits (table 2.5) described by Van der Meer (1988) and Van Wijland (2020). An estimation can be determined for which significant wave height the initial damage would be observed. The chosen value for that specific significant wave height was based on the most conservative expectation between both methods so that tests where initial damage occurs are included in each test serie. The tests continued from the initial test iteration until the slope completely failed based on visual observation.

Tests 1 to 3 examine the effect on damage with increasing significant wave height per test iteration and can be compared on the basis of different wave steepness and Iribarren number per test serie. Test 4 provides information about the relationship with regard to an increasing number of waves. Test 5 is

performed according to the non-cumulative method, which allows comparisons to be made with the cumulative method and more insight into the variability of the damage parameters. Test 6 was performed with a strip width of 0.1 meter which can provide more insight into damage parameters based on the number of entrained and deposited rocks per colour band. Test 7,8,9 are comparable with test 1,2,3 in terms of researched effect, but with a twice as thick armour layer ($5d_{n50}$) to additionally research the effects of a varying armour layer thickness on stability. The slope of test 10 has experienced the same wave characteristics (s_{op}&ξ_p) as tests 3 and 9, but with a layer thickness of $10d_{n50}$.

The executed test plan for slope 1:6 is given in table 3.3.

Table 3.3: Executed test plan slope 1:6.

Test series	$\mathbf{s_{op}}$	$\xi_\mathbf{p}$	$\mathbf{H_s}$	**N**	**P**	$\mathbf{t_A}$ $*d_{n50A}$	**Number of tests**	**Researched effect on damage parameters**
1	0.01	1.67	0.03 - 0.09	1000	0.12	2.5	8	H_s & ξ
2	0.03	0.96	0.02 - 0.15	1000	0.12	2.5	11	H_s & ξ
3	0.04	0.83	0.04 - 0.15	1000	0.12	2.5	8	H_s & ξ
4	0.04	0.83	0.06	250 - 20000	0.12	2.5	8	N
5	0.04	0.83	0.09	1000	0.12	2.5	5	Variability (non-acc)
6	0.04	0.83	0.04 - 0.12	1000	0.12	2.5	7	Colour band (W $\approx$ 0.1m)
7*	0.03	0.96	0.05 - 0.18	1000	0.48	5	10	Layer thickness & P
8	0.01	1.67	0.03 - 0.11	1000	0.48	5	11	Layer thickness &P
9	0.04	0.83	0.05 - 0.21	1000	0.48	5	13	Layer thickness &P
10	0.04	0.83	0.02 - 0.14	1000	0.57	10	14	Filter layer & P
$\sum$							95	

Now that the nominal rock diameter and the test conditions are known we could calculate the expected Reynolds number. The smallest significant wave height H_s of 0.02 m gives Re = 2904 and the largest significant wave height H_s of 0.21 m gives Re = 30489. According to the scaling limits of Van der Meer (1988) described in subsection 2.1.1 the lower limit of the Reynolds number (equation 2.12) is given by $1 * 10^{-4}$. For a nominal rock size of 0.148 m and the assumption $g = 9.81 m/s^2$ and $\nu = 1 * 10^{-6}$ this gives a minimal significant wave height of $H_s = 0.069m$. So there is a chance that for the lowest wave heights tested the stability of the stones is subject to scale effects.

Wave heights smaller than 0.02 m are also often not recommended because the pore pressure and viscous effects in the model are decisive and therefore not representative. When using a filter and core it is important that the proportions are properly scaled or that you match the slope of the target with the prototype. There are therefore different scaling rules, which are outside the scope of this study.

3.2 Processing the stereophotogrammetry and analyzing damage parameters

The implementation of the stereophotogrammetry technique in the Agisoft Metashape is used to reconstruct high quality 3D models from the photos. The 3D models with slope 1:10 Mossinkoff, 2019 and slope 1:8 Van Wijland, 2020 are processed with respectively, 48 photos and 63 photos per test iteration. Appendix D provides a step-by-step plan on how to build a model with Agisoft Metashape. The explanation is based on a processing path with automatically detectable GCPs. The overall process of stereophotogrammetry and analysizing damage parameters is presented in figure 3.4:

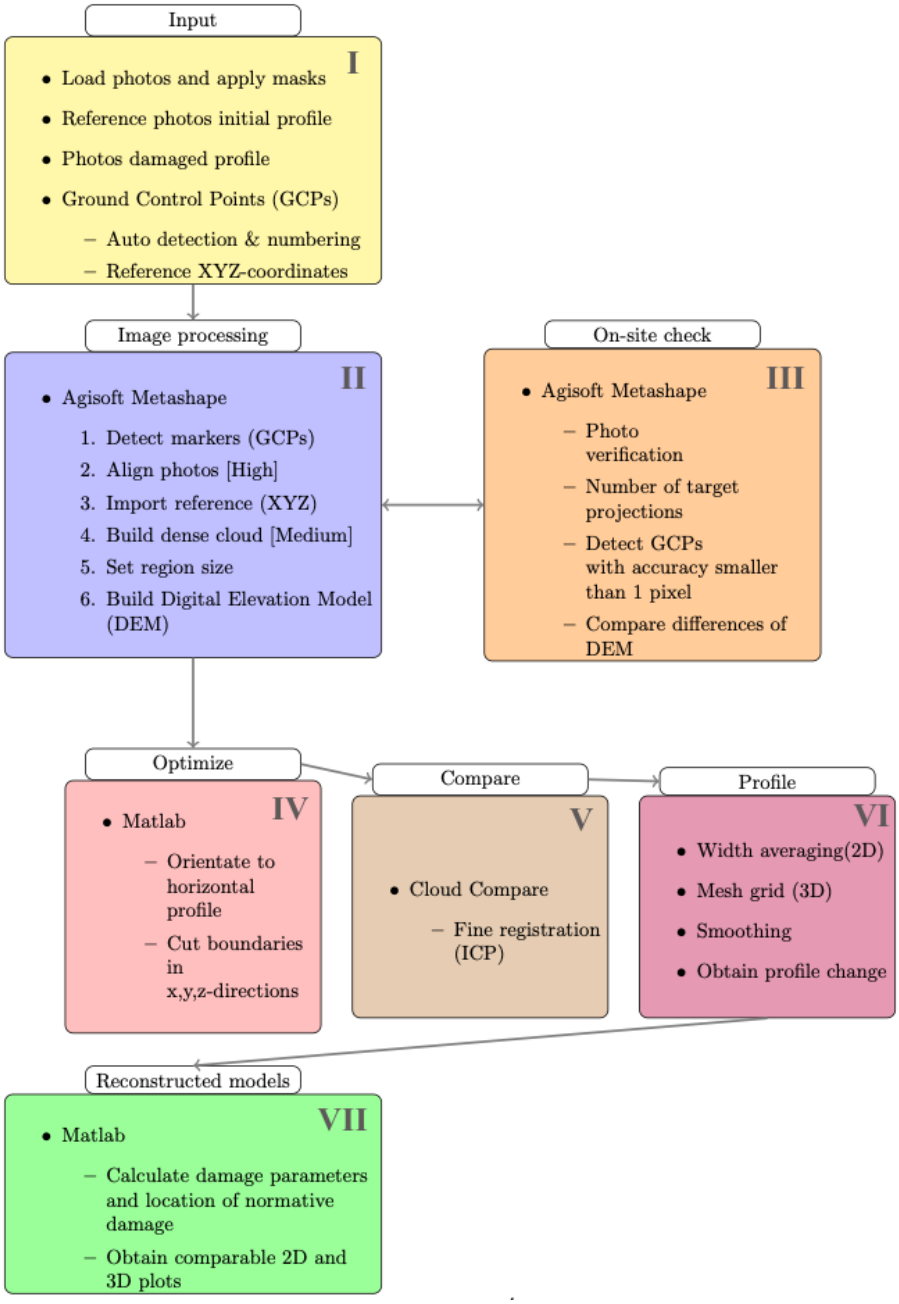

Figure 3.4: Process of stereophotogrammetry in order to reconstruct high quality 2D and 3D models.

3.2.1 Stereophotogrammetry workflow

Figure 3.4 provides an overview of the stereophotogrammetry workflow. On the basis of this figure 3.4, further explanation is given per step:

I **Input**

In order to obtain 3D models from the photos used as input for the stereophotogrammetry method, a number of stages in the process must first be completed. The required input for the method relates to 63 photos of both the initial profile and the damaged profile after each test iteration. The GCPs can be automatically detected and numbered by the software. After the GCPs are fixed at strategic points on the slope, the reference xyz-coordinates are measured.

II **Image processing**

The software Agisoft Metashape is used to process all the input into point clouds, dense clouds and Digital Elevation Models (DEM) during the completion phase of the test procedure (compare section 3.1.3).

III **On-site check**

The software Agisoft Metashape is used to process all the input into point clouds, dense clouds and Digital Elevation Models (DEM) during the completion phase of the test procedure (compare section 3.1.3). In order to continue to the next test iteration with the guarantee that the software is capable of contructing the 3D model in an early stage of the process, an on-site check is developed. During this check, confirmation is given of the number of photos and the total number of projected targets. If the number of photos and the total number of projected targets are in line with the expectations of table 3.2 it implies that all photos were taken sharp. Because the check also shows how often each target has been projected, it also confirms that no duplicate photos were taken. For all GCPs it can be seen what the difference is with the pre-measured reference coordinates. If a single GCP has a deviation greater than 1 pixel, the method will be checked again. It is also possible to compare the DEM of two test iterations. In the regions where no rocks have been moved between 2 tests, the difference in height should be smaller than the accuracy threshold (0.5 mm) following from subsection 3.2.2.

IV **Optimize**

After the on-site check has been successfully performed, within 15 minutes, the next test iteration can be performed. The relatively short processing time of this check is relevant because it can be performed between two tests without causing a delay in the test procedure (section 3.1.3). When all test iterations have been performed, the optimization process in MATLAB starts. Here the profile of the slope is first oriented to a horizontal profile and then the boundaries in xyz-directions are cut. This is essential to enable comparison of the datasets then compare (V) the datasets with Cloud Compare.

V **Compare**

The profiles are aligned even more precisely by means of a Iterative Closest Point (ICP) algorithm of Cloud Compare. ICP is a method which can automatically finely registers two clouds (CloudCompare, 2016). To use this function within Cloud Compare, two conditions must be met. First, both clouds must be already roughly registered and secondly both clouds should represent the same object (CloudCompare, 2016). With the current workflow and this test setup, both requirements for the use of the ICP method are met. The software of Agisoft Metashape already registered the point clouds, which fulfils the first requirement. Per test and test iteration the zone of the slope that still represents the same objects can be different due to wave impact. In particular, the bottom and top have a large undamaged overlapping area. Per test, a theoretical overlap of $\sim 60\%$ is specified in the settings. A large section of the slope is captured by the stereophotogrammetry procedure resulting in overlapping parts on the upper and bottom parts of the slope even when much damage on the slope is present. Van Wijland (2020) used this method to better fit the ends

of the profiles for slope 1:8 and slope 1:10. Since the aim is to develop a method that is comparable to the research of Van Wijland (2020) and Mossinkoff (2019), the ICP method is also used in this research.

VI **Profile**

To obtain the profile change, width averaging and smoothing (figure 3.6) is applied for 2D and a mesh grid is used for 3D.

VII **Reconstructed model**

The method of how the damage parameters are calculated from the models are explained for 2D in subsection 3.2.3 and 3D in subsection 3.2.5. For the determination of the 2D parameter, a threshold is determined to differentiate real damage from measuring errors of the stereophotogrammetry method. This is explained in subsection 3.2.4. This threshold value is also used to quantify the accuracy of the measuring method for the 3D parameters in subsection 3.2.6. The method on how to describe damage domain and location is given in subsection 3.2.7.

3.2.2 Verification of stereophotogrammetry accuracy and effect on damage parameters

If the accuracy of the described method can be verified, then the effects on the damage parameters can be quantified. To quantify the accuracy threshold of this method a check test is performed.

The check test is based on distances between datasets of test iterations. This test consists of 8 iterations with no change in the slope due to wave attack. In between each iteration, the GCPs are folded in and out on the hinge. Before the dense cloud of test iteration is compared with the software Cloud Compare, the ICP tool is first applied to the datasets. As a result, exactly the same stages were completed for both the check tests and the regular tests in order to determine the accuracy and effects on damage numbers. The method accuracy based on check tests is given in table I.1, which shows deviations between different test iterations that are not related to actual slope damage. The mean distance and standard deviation between two dense clouds are estimated with the tool cloud-cloud distances of Cloud Compare. The calculation of distances between two models is performed based on a quadratic function with 6 parameters ($Z = aX^2 + bX + cXY + dY + eY^2 + f$). This selected quadratic model is known for the highest fidelity to the local geometry compared to the other models of this tool. Furthermore, the calculation time of approximately 6 seconds per model comparison. By default, it is recommended by Cloud Compare (2015) to use the quadratic model because it is versatile in the way different shapes are represented.

The accuracy limit is determined on the basis of the 72 check tests results from table I.1 and is shown in figure 3.5:

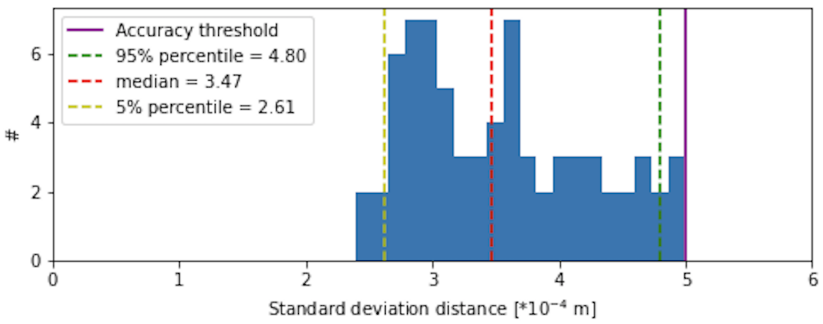

Figure 3.5: Determination of accuracy based on maximum std distance of check tests.

The median, 5% and 95% percentiles are indicated in the histogram. The accuracy threshold for the check test method is determined by selecting a value that is greater than the outliers of the standard deviation distances, which is chosen as $5 * 10^{-4}$ m. This accuracy limit is set as the maximum bias that could occur over a wider area on the slope, for the identical undamaged profiles.

The purpose of using the accuracy limit in the damage assessment is to distinguish between accountable damage and small errors due to measurement inaccuracy. A certain part of the slope has a small difference from the other profile, this is due to the stereophotogrammetry measurement method. A distinction must be made here in order to identify damage caused by a difference in displaced rocks between two profiles.

3.2.3 Determination of 2D parameters

With regard to the overview of the stereophotogrammetry workflow, given in figure 3.4, the last steps from '*V* - compare' to '*VI* - profile' to '*VII* - reconstructed models' are considered in order to eventually determine 2D damage parameters S, S_{all} and E_{2D}, damage locations and plots. From the difference between the initial profile and the wave attack damaged profile it is possible to derive this information, but to do this a number of steps will have to be explained first.

The first step of the '*VI* - profile' stage is to average the profile across the width from the aligned dense clouds. Width averaging is applied per grid size in x-direction. This gives 160 sections of 0.5 cm, one-third of the used nominal rock size ($\frac{1}{3} * d_{n50}$), which contains between 3000-4000 points of the dense cloud.

The second step of the '*VI* - profile' stage is to apply the smoothing principle of Hofland et al. (2011) by use of a $3d_{n50}$ moving average in the direction of the slope. Since the 2D parameters arise from an integral over the length of the profile, its accuracy is expected to be slightly larger than the local damage depth accuracy d_e (Hofland et al., 2011). This is the reason why the smoothing with a moving average is required for this method. By applying the smoothing principle to the profiles, the estimated erosion depth d_e will become less. Hofland et al. (2011) tested the smoothing principle for three different moving average widths: $1d_{n50}, 3d_{n50}$ and $5d_{n50}$. A moving average of $3d_{n50}$ seems sufficient regarding the influence on the estimated damage depth in combination with a small reduction on the calculated damage parameters (Hofland et al., 2011). The effect of the smoothing principle is visualized in figure 3.6:

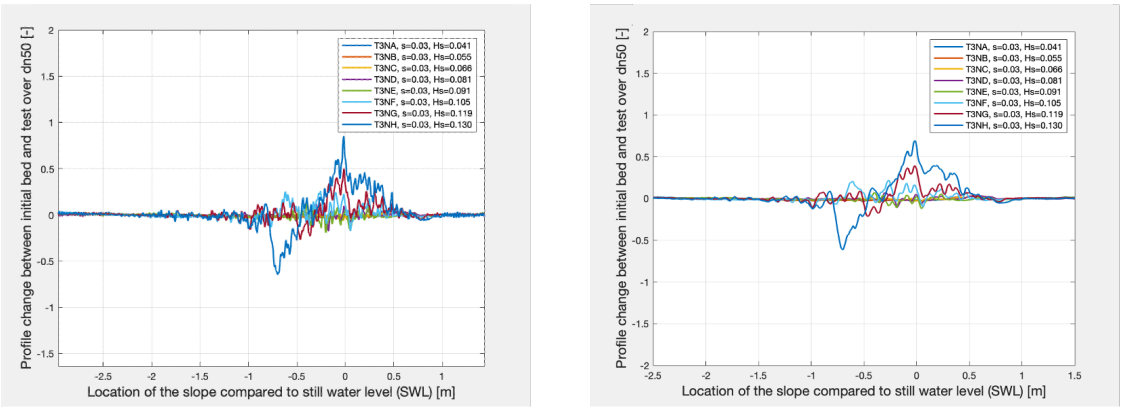

(a) Without applying smoothing principle

(b) With applying smoothing principle by use of 3*d_{n50} moving average

Figure 3.6: Profile changes in y-direction a) without applying smoothing principle and b) with applying smoothing principle by use of $3d_{n50}$ moving average.

When smoothing the results, measurement errors due to the stereophotogrammetry process are aver-

aged out. To show the effect of applying smoothing in more detail, the check tests are compared with and without smoothing in figure I.1. One could observe in this figure I.1, that the smoothing principle ensures that the profile is less sensitive to inaccuracies and profile changes in the order of size of $0.03d_{n50}$, which is around 8 % of the used grid size ($0.5cm$). This reduces the influence of small measurement changes (±8%) with regard to the comparative profiles used for the damage calculations.

The 'reconstructed models' stage is completed by applying the described formulas 2.25, 2.24 & 2.27 of section 2.2.1 to the obtained profile changes. An example on how to determine the damage parameters S, S_{all} and E_{2D} is shown on the basis of figure 3.7:

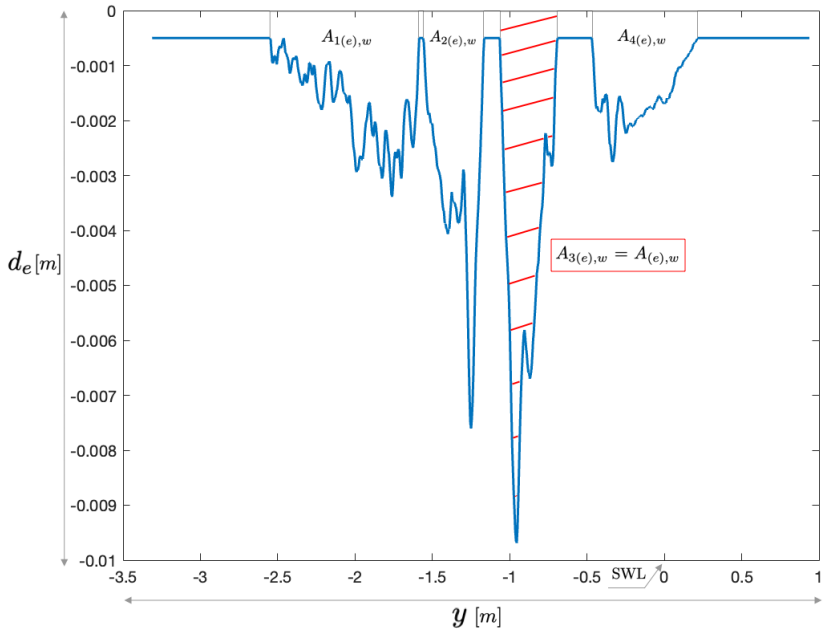

Figure 3.7: Determination of damage parameters S and S_{all} with test 10_8 as example.

Damage parameter S only considers the largest erosion area. For this example S is calculated based on the normative area $A_{3(e),w}$. S_{all} is calculated as $S_{all} = A_{1(e),w} + A_{2(e),w} + A_{3(e),w} + A_{4(e),w}$ which covers all the damage on the slope. The threshold value for d_e is equal to $5 * 10^{-4}$ m based on the largest standard deviations of the check test (figure 3.5). The MATLAB script is able to automatically find the correct intersection points with the threshold value and then calculate the integral of the area indicated with red stripes. This integral corresponds to the largest area $A_{(e),w}$ and thus S can be calculated following equation 2.24. The value of E_{2D} is determined based on the maximum erosion depth ($d_{e,w}$) following formula 2.27.

For the determination of damage parameter S_{all}, the specific range of accumulated damage is determined according to the range in height (z-direction) expressed in the normative (i.e. largest) significant wave height (H_s) per layer thickness. These ranges are given in figure 3.8:

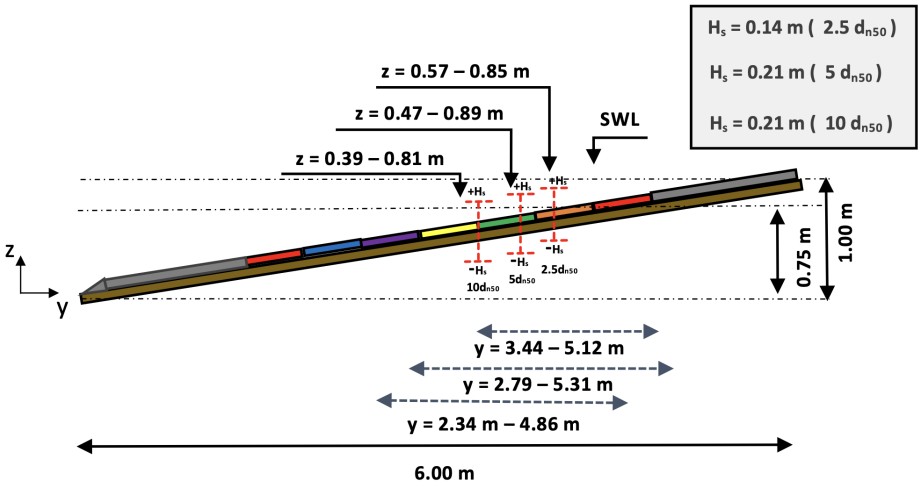

Figure 3.8: The range in z and y direction for the determination of S_{all} for different layer thicknesses.

From the location where the phreatic surface meets the top of the armour layer on, the vertical range of -Hs/+Hs is applied. This location is different for each layer thickness and the corresponding y-coordinates are given in figure 3.2.

3.2.4 Quantification of accuracy threshold on 2D damage parameters

After determining the way in which the 2D damage parameters are used with regard to the measurement method, it is also important that information can be given with a quantified certainty within which confidence interval the relevant damage is located.

This was done on the basis of the previously found (subsection 3.2.2) threshold value of 0.5 mm. This threshold value is both subtracted and added from the initial profile. After that, the usual process is applied for each test iteration. Different damage numbers are obtained for both situations, these differences are regarded as the maximum differences based on deviations in the measurement method. The values of the damage parameters for the two described situations (+/-) are compared with the original damage numbers. These absolute differences are investigated to add values to the confidence intervals of the used damage parameters.

For the investigated tests in 2D, a distinction was made between different layer thicknesses ($2.5d_{n50}$ & $5d_{n50}$ & $10d_{n50}$) and two different ranges in damage S ($S > 2$ & S = 2-17). The characterization width of $54d_{n50}$ is used because the measurement inaccuracy for the entire area is taken into account. Van der Meer (1988) used the indicated range of S = 2-17 for his tests. The reason to investigate this range it because it offers more possibilities for a comparison with the current measurement method and the method of Van der Meer (1988).

A boxplot is used as way of displaying the distribution of the absolute damage differences. Every boxplot highlights the median, 5% percentile and 95% percentile. For damage parameter S, the data is clearly skewed towards the lower differences, as one could observe in figure R.5 of appendix R.1. For damage parameter S_{all}, the data is more centered as shown in figure R.10 of appendix R.2. The absolute difference per layer thickness and damage range are determined and shown in table 3.4:

Table 3.4: Absolute and normalised differences of 2D damage parameters (S & S_{all}) per layer thickness and damage range.

Description		S	S_{norm} **(%)**	S_{all}	$S_{all,norm}$ **(%)**
t = 2.5dn50	95%	±2.05	±60	±3.77	±49
($S > 2$)	median	±0.75	±22	±1.79	±20
t = 5dn50	95%	±3.06	±57	±4.49	±66
($S > 2$)	median	±1.14	±16	±2.78	±17
t = 10dn50	95%	±2.51	±51	±4.82	±38
($S > 2$)	median	±1.10	±21	±1.89	±14
All tests	95%	±2.84	±37	±4.81	±79
($S = 2 - 17$)	median	±0.94	±16	±2.40	±33
All tests	95%	±3.42	±26	±4.80	±69
($S > 2$)	median	±1.34	±11	±2.47	±20

The normalised damage parameters are calculated as the difference divided by the original damage number. For a comparison of 2D test results with the damage parameters S and S_{all} from Van Wijland (2020) and Mossinkoff (2019) it can be used that with 95% certainty it can be said that S = S_{test} ± 3.42 and $S_{all} = S_{all,test}$ ± 4.80. For the comparison with test results of Van der Meer (1988), these ranges are S = S_{test} ± 2.84 and $S_{all} = S_{all,test}$ ± 4.81. What is striking from the data in table 3.4 is that with a larger range of damage number S (S>2) the normalized values are smaller compared to range of S = 2-17. This indicates that for the smaller damage numbers the normalized difference is proportionally larger than for the larger S damage numbers (S > 17).

3.2.5 Determination of 3D parameters

With regard to the overview of the stereophotogrammetry workflow, given in figure 3.4, the last steps from '*V* - compare' to '*VI* - profile' to '*VII* - reconstructed models' is considered in order to eventually determine 3D damage parameters ($E_{3D,1}$, $E_{3D,3}$ and $E_{3D,5}$), damage locations and plots. These steps are visualised in figure K.1 of appendix K.

First, it is described how the workflow evolves from '*V* - compare' to '*VI* - profile'. Mesh grids are now applied to the ICP edited profiles using the software MATLAB. This can be visualized as an idea net that is placed over the profile with square blocks. The size of a square block is called 'grid size' and is taken as 0.5 cm, which for this test series is approximately equal to $\frac{1}{3}d_{n50}$. For the 1:6 slope tests, a grid field is specified from 160 grids in width and 850 grids in length (figure K.1). This corresponds to the area of 0.80 m wide and 4.25 m long across the slope, as shown by the yellow rectangle in figure 3.3. Each grid cell contains between 33 and 36 xyz-coordinates, which is an improvement due to the early appliance of masks in the stereophotogrammetry process. The $E_{3D,m}$ (equation 2.28) is defined as the maximum erosion depth d_e averaged over a moving circle with a diameter of $m * d_{n50}$ within the characterization width w. Each grid cell uses the surrounding grid cells to simulate this spatial moving average containing a circle with a diameter of $m * d_{n50}$. For $E_{3D,1}$, $E_{3D,3}$ and $E_{3D,5}$ the way the spatial moving average is simulated is shown in figure K.1. The approximation of a spatial moving average of E_{3D1} corresponds to 3 grids, which is approximately equal to $1dn50$. Each grid is assigned a height using linear interpolating in MATLAB. By calculating the height per grid using the spatial moving average that corresponds to the damage parameter of interest, the difference of the grid fields of the initial profile and damaged profile can be analyzed.

The '*VII* - reconstructed model' stage of the 3D parameter determination is to apply the described formula 2.28 of section 2.2.1 for m = 1, m = 3 and m = 5 to the obtained profile changes.

The 3D damage parameters are determined for the entire characterization width ($54d_{n50}$) and one section of $27d_{n50}$, as shown in figure 3.9:

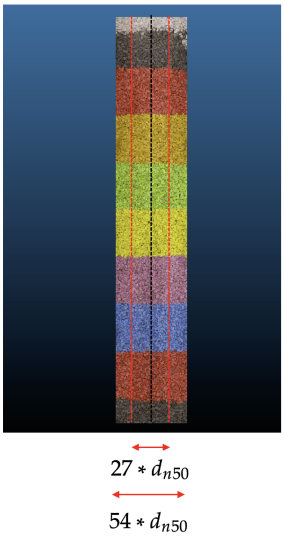

Figure 3.9: Applied characterization width of $27d_{n50}$ and $54d_{n50}$.

Almeida et al. (2019) stated that a characterization width of approximated $25d_{n50}$ is optimal. Van Wijland (2020) splitted the section of $54d_{n50}$ into two different sections of $27d_{n50}$. In this method a centered (black line, figure 3.9), characterization width of $27d_{n50}$ is applied for the comparison of damage parameters with different characterization widths. The preference for a width of $27d_{n50}$ comes from the consideration of using the same absolute characterization width to compare the results with Van Wijland (2020) and Mossinkoff (2019) and still in line with the recommended characterization width of $\approx 25d_{n50}$. The decision for a centered approach was made because the edge effects are reduced as much as possible in the center of the flume.

3.2.6 Quantification of accuracy on 3D parameters

The quantification of the measurement inaccuracies of the method for 3D are determined in the same way as for the 2D parameters, as described in subsection 3.2.4. The principle of subtracting and adding the threshold accuracy from subsection 3.2.2 to the initial profiles in order to subsequently investigate the absolute differences remains the same.

For $E_{3D,1}$, $E_{3D,3}$, $E_{3D,5}$, a confidence interval is derived from the data. This allows a range per 3D damage parameter to be identified in table 3.4:

Table 3.5: Absolute and normalised differences of 3D damage parameters ($E_{3D,1}$, $E_{3D,3}$, $E_{3D,5}$).

Description		$E_{3d,m}$	$E_{3d,m}$ **norm (%)**
m = 1	95%	±0.37	±45
	median	±0.07	±11
m = 3	95%	±0.11	±13
	median	±0.04	±5
m = 5	95%	±0.20	±16
	median	±0.06	±6

Van Wijland (2020) and Mossinkoff (2019) concluded that the $E_{3D,3}$ parameter best represents the damage for mild slopes with regard to the different stages in which the slope changes from undamaged profile to failure criteria. Relative to both the 2D and the other 3D parameters, $E_{3D,3}$ shows the most reliable

interval with deviations from $E_{3D,3} = E_{3D,3,test} \pm 0.11$ and a normalised deviation of 13% for the 95% percentile.

3.2.7 Determination of damage domain and location

The damage domain of a profile can be determined by the location on the slope where a certain form of erosion occurs. In order to be able to investigate at a specific level of detail at which location on the slope erosion occurs, we use a Digital Elevation Model (DEM) of the software Agisoft Metashape. With this it can be clearly determined what the change is between two profiles with regard to the change of a stone. It is also possible to determine the location of erosion within color bands. This helps to assign the damage domains and locations to the damage profile after each test iteration. This classification of five damage locations is based on Van Wijland (2020) and is formulated as follows:

- Low: Referred to as the downslope location where erosion of an individual rock occurs.
- Mid-Low: Referred to as the downslope location where erosion of two rocks in the same width section occurs.
- Low-Area: Referred to as the downslope location where randomness of entrained rocks does not occur anymore.
- Mid-High: Referred to as the upslope location where erosion of two rocks in the same width section occurs.
- High: Referred to as the upslope location where erosion of an individual rock occurs.

An example of the determination of the damage locations is shown in figure 3.10:

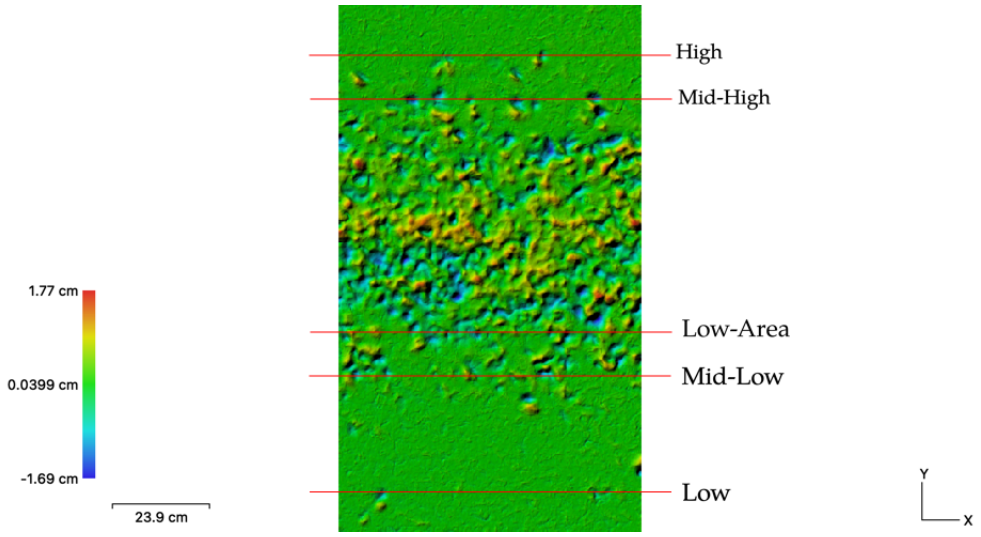

Figure 3.10: Damage domain and location identification by use of Digital Elevation Model (DEM).

The y-coordinate associated with the relevant damage location is used to make the conversion to a damage range in z-direction expressed in normative significant wave height (H_s). Since there is a different normative H_s per layer thickness and also a different location in y-direction where the phreatic surface meets the armour layer, it was decided to include this in the conversion to the vertical range expressed in H_s. This is similar to the determination of S_{all} as shown in figure 3.8.

The additional results that follow provide an improved insight into damage formation and location with respect to different layer thicknesses. To give an example of this, at a slope of 1:6, with a d_{n50}, the

waterline touches the impermeable core at 4.5m, this is referred to as SWL. With a d_{n50} of 0.0148 m and a layer thickness of $2.5d_{n50}$, the phreatic plane touches the armour layer at z = 0.71 m with a normative H_s of 0.14 m. At a layer thickness of $10d_{n50}$ this is equal to z = 0.60 m and H_s = 0.21 m. This analyses is performed for the results of slope 1:6 and are shown in figure 4.15.

For a direct comparison with the slopes of 1:8 and 1:10 it is therefore important that only the same layer thickness is used. The damage locations are expressed in the normative H_s per layer thickness. This comparative results are shown in figure 4.14.

3.2.8 Re-analysis damage parameters Van Wijland

During the process of recalculating the results of Van Wijland (2020) it was found out that the Random Sampling Limit (RSL) of the ICP tool (appendix H) ensured that it was not possible to exactly calculate the same values for the damage parameters again. The difference between two random picked datasets for the tests with the default value of RSL = 50000 and RSL which is larger than the number of coordinates in the dataset are calculated so that this random sampling limit no longer actually affects the final results. The size of a dataset with xyz-coordinates is shown in the table for two examples of slope 1:6 and slope 1:8.

Table 3.6: The number of coordinates of a dataset for two random picked datasets with slope 1:6 and 1:8.

Slope	**Size RAW dataset [$*10^6$]**	**Size CUT dataset [$*10^6$]**	**Masks applied**	**Data for reconstructed model (%)**
1:6	≈ 10	≈ 4	Yes	40
1:8	≈ 50	≈ 2.5	No	5

In the stereophotogrammetry method, often a trade-off has to be made between higher precision coupled with long calculation times or slightly less sophisticated calculations that can be performed faster. From table 3.6 can also be concluded that by applying the masks at an early stage of processing, approximately 8 times more calculated data is used in percentage terms for the reconstructed models. This additional data contributes to the recognition of difference in measurement efficiency associated with this new addition to the process for the stereophotogrammetry measurement method.

3.3 Analysing wave breaking types by observations with video material

This study focuses on obtaining information about damage formation on mild slopes and to do so it is important to distinguish between different formation of breaking waves. The breaker wave types that this research focuses on are primarily spilling and plunging waves. Each type has different properties (2.4) and this can influence damage formation on the slope. An expectation of the breaker wave type can be given by calculating the Iribarren number (equation 2.20) for the investigated slope. Spilling waves are mostly present for $\xi_p < 0.5$. For plunging waves this range is $1.5 < \xi_p < 0.5$. Within these intervals it is likely that the respective forms of wave breaking are most present (Battjes, 1974).

To find out more about the mutual distribution between spilling and plunging waves for different Iribarren numbers, Van Wijland (2020) and Mossinkoff (2019) analyzed this distribution for slopes 1:8, 1:10 (figure 2.6). To be able to add results for slope 1:6, the analysis of camera images was used. The camera is positioned upslope of the slope, with the camera oriented perpendicular to the incoming waves (figure 3.2) to identify the breaker wave type of each wave.

To investigate the distribution of spilling and plunging waves for slope 1:6, the videos from the last test iteration of each test were analyzed. This test iteration was chosen because the different characteristics of

the largest observable waves can best be identified. The distribution was mapped out on the basis of the first fully generated 100 waves. The same method as Van Wijland (2020) and Mossinkoff (2019) is applied.

There are a number of distinguishable aspects on which the plunging and spilling waves can be identified, as presented in figure 3.11:

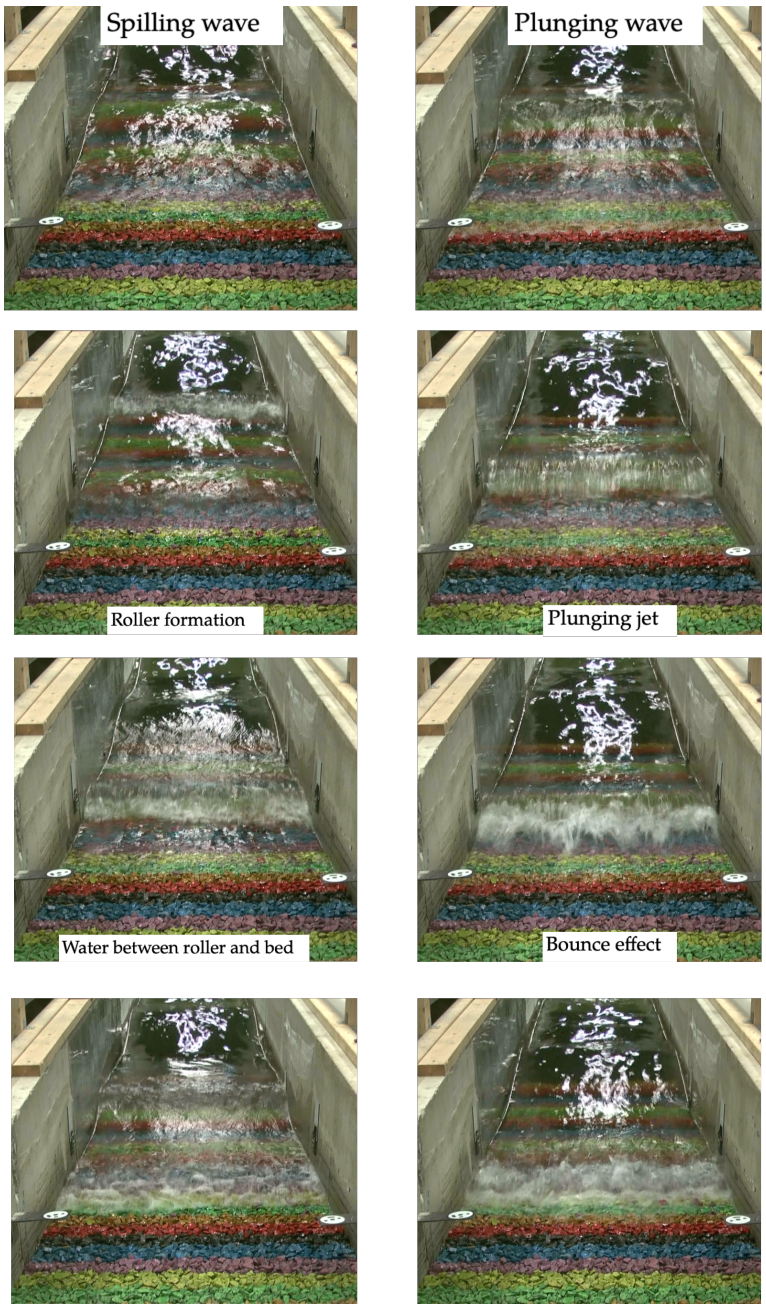

Figure 3.11: Identification of spilling and plunging waves.

A plunging wave is characterized by a steep wave crest, followed by a curling formation that creates a plunging jet that breaks on a relatively short section of the slope, causing a bounce of the water on the bed. A spilling wave is characterized by a milder wave crest, after which a roller formation occurs, as a result of which the wave energy is already spread over a longer range (in y-direction). The results of

this analysis are presented in section 4.4 for slope 1:6 - 1:10.

3.4 Processing the entrained and deposited coloured rocks for different colour band widths

Colour bands are used to identify entrained and deposited rocks, with their corresponding transport lengths. More insight can be developed about, for example, where one rock originated after displacement compared to an overall damage plot of the slope. In combination with the corresponding wave characteristics, the force which is needed to facilitate such a displacement is known. Upward and downward transport can also be easily visualized by identifying a different colour stone in the colour band. Because it is expected that the measurement inaccuracy for the determination of the number of displacements will increase for steeper slopes.

By use of colour bands in combination with stereophotogrammetry, the difference between mobility and erosion is investigated based on the ratio of damage parameters N_{od} (equation 2.29) and S (equation 2.24). To gain more insight into the influence of a varying colour band width on the damage numbers based on the number of displacements, a test was performed with a colour band width of 0.1 m (figure 3.12). The analysis that is performed consists of two parts:

1. Analyse the damage numbers based on the number of displacements (N_{od}, S_{od}, MP) for the colour band width of 0.1 m. Any movement of a stone to a different colour band is taken into account.
2. Analyse the damage numbers based on the number of displacements (N_{od}, S_{od}, MP) for the colour band width of 0.5 m. When counting the displaced rocks, the five different colour bands with w = 0.1 are merged as if it were a single color band of 0.5 m, only the stones that displace from outside the merged band are taken into account.

To identify each rock that has been deposited in a different colour band, information about this displacement is tracked in two ways:

1. Identifying upward/downward transport of the rock.
2. Identify which specific coloured strip the entrained rock deposited.

By using this approach, information can be given about the displacements per colour band. These numbers can be referred to as n_{gross} and n_{net}. Where n_{gross} represents the gross number of rocks, which is the sum of all displaced rocks from their original colour band to another. n_{net} represents the net number of eroded rocks, which is given as the sum of the deposited rocks minus the eroded rocks for all colour bands.

The sum of all net eroded rocks that have been displaced out of every coloured strip. For this method, n_{net} is used to determine the damage parameter N_{od} (equation 2.29). As described in subsection 2.2.1, the damage parameter N_{od} is determined according to all individual measured rock displacements (n_{tot}). But the problem with the use of n_{tot} is that the used method only counts coloured rocks that moved out of their strip, which means that the displacements within a coloured strip are not taken into account. Therefore the net number of eroded stones n_{net} is used to calculate damage parameter N_{od} in this method. These unobserved rock movements within a strip are considered to be a measuring error and give and therefore give an underestimation of the number of displacements. This measuring error is logically smaller for a smaller color band

By taking into account the porosity of the bed layer and assuming that all displaced rocks are removed from the erosion hole, the obtained damage number based on displacements (N_{od}) can be related to damage number based on profile properties (S_{od}). According to the following relation given in equation 3.2 (USACE, 2015) :

$$S_{od} = \frac{N_{od}}{1 - porosity} \tag{3.2}$$

This makes sense as S_{od} can be compared to other profile based 2D damage parameters as S and S_{all}. The same porosity value of 0.4 for the bed layer composition of 0.4 is used based on the assumption of Mossinkoff (2019) and Van Wijland (2020).

From test 6 ($s_{op} \approx 0.04$), with a respective colour band width of 0.1 m (lower figure 3.12) and merged 0.5 m (upper figure 3.12), the comparison of damage numbers (N_{od} and S_{od}) could give insight into the applicability of different colour band widths. For example to specify the effects following from varying number of observed rocks between colour bands. The two used approached are visualised in figure 3.12:

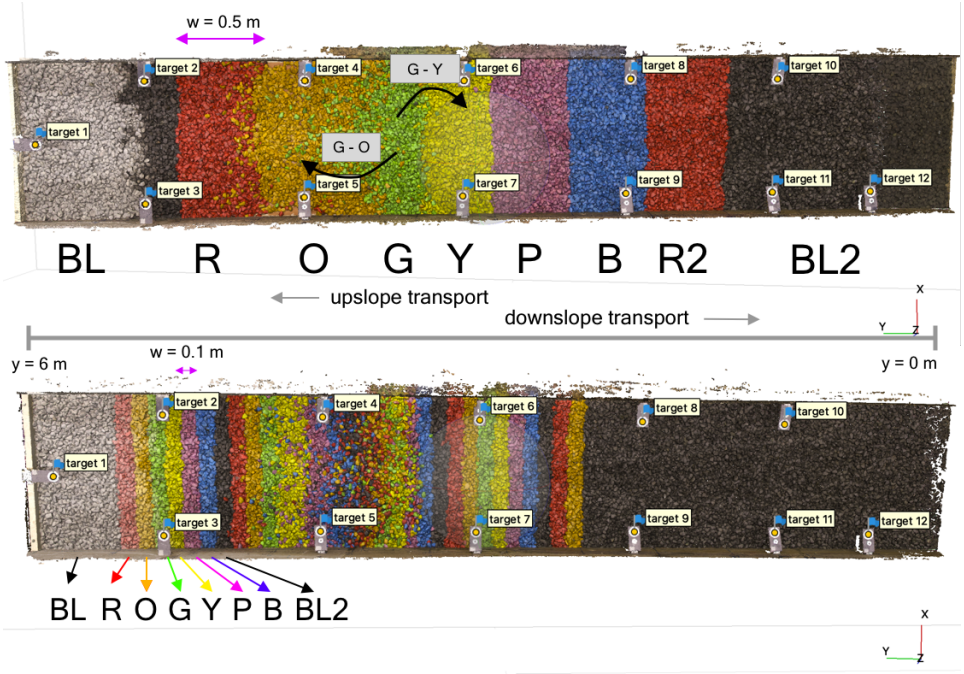

Figure 3.12: Determination of displacements with different colour band width

The added value of performing the test based on the two approaches considering a different colour band width is, firstly, that it possibly could give more insight into the measurement inaccuracy that has been incorporated in previously performed tests with a colour band of 0.5 m for slope 1:6 - 1:10. The second, the damage parameters N_{od}, S_{od} and S_{all} can provide insight into the processes of mobility and erosion with respect to differences between mild and steep slopes. At last, insight can be gained from this method that can be used to make a recommendation about scaling colour band width in combination with testing for different slope angles because of the effects of using too large colour bands can produce misleading results.

Section 4.5 describes the results of this method. Figure 4.17 shows sensitivity to misleading interpretations based on displacements, areas of erosion and colour bands where maximum erosion or accretion occurs. A comparison is provided to observe differences with use of small colour bands (w=0.1 m) and merged colour bands (w=0.5m). Figure 4.18 shows S_{od}/S_{all} to compare mobility and erosion. Figure 4.19 shows the measurement error between damage parameter N_{od} based on displacements n_{net} and the width averaged erosion parameter S_{all}.

4 Results

Chapter 4 presents and discusses the results of the performed test series of physical model tests at Deltares for slope 1:6, 1:8 and 1:10. The analysis consists of visual observations during the execution phase of the testing. In addition, the influences of the governing parameters are explained on the basis of results of the calculations of the profile-based damage parameters (S, S_{all}, E_{2D}, $E_{3D,1}$, $E_{3D,3}$ and $E_{3D,5}$). Furthermore, the results of the test serie are used to gain insight into the use of damage domains and colour bands. An estimation for the distribution of plunging waves is presented based on the test data. Additionally, the design formula is given that represents the test series for mild slopes with associated damage limits. Thereafter, the results of the analysis are discussed.

4.1 Visual observations

While performing the tests, a visual inspection was performed after each test iteration. Notable displacements or damage are listed in order to substantiate results using visual observations during the execution phase of the test procedure (3.1.3). The two main visual observations are divided into two different categories: different types of damage formation with dominant transport direction (4.1.1) and boundary effects due to side walls (subsection 4.1.2). For both observations, the visual features will be described and a possible cause will be explained.

4.1.1 Damage formation and dominant transport direction

A striking observation from the visual inspections was that tests with the same incoming wave characteristics, but with varying layer thicknesses, produced different types of damage profiles (figure 2.8). This could be observed by determining where on the slope the rocks are placed after test iterations with the larger wave load. The dominant transportation direction could be determined from these observations and the outcomes are shown in figure 4.1 for all tests for which different layer thicknesses have been tested in the range 1:6 - 1:10.

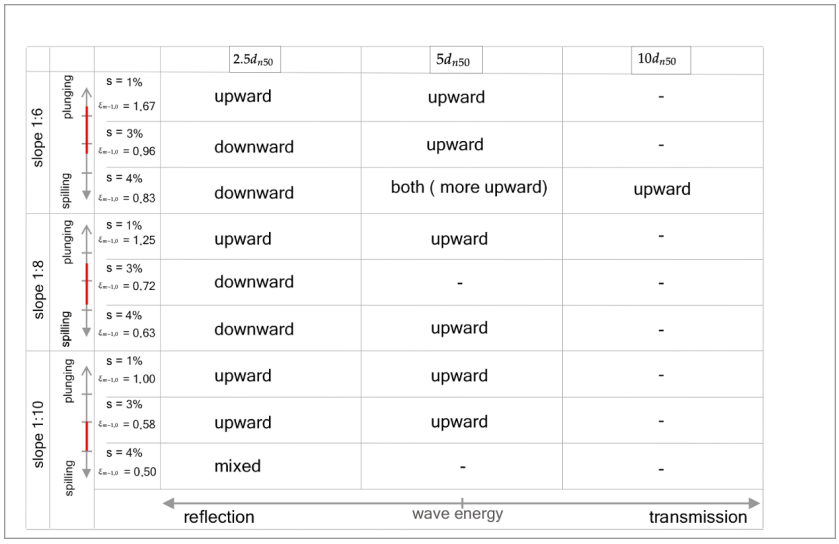

Figure 4.1: Dominant transport direction for various layer thickness, slope angles and wave steepness ('-' means not tested yet).

Especially the results with wave steepness 4% for slope 1:6 shows the varying damage formations for similar incoming wave characteristics. This process could be observed according to 2D results for tests with layer thicknesses 2.5d_{n50}, 5d_{n50} and 10d_{n50} in figure 4.2:

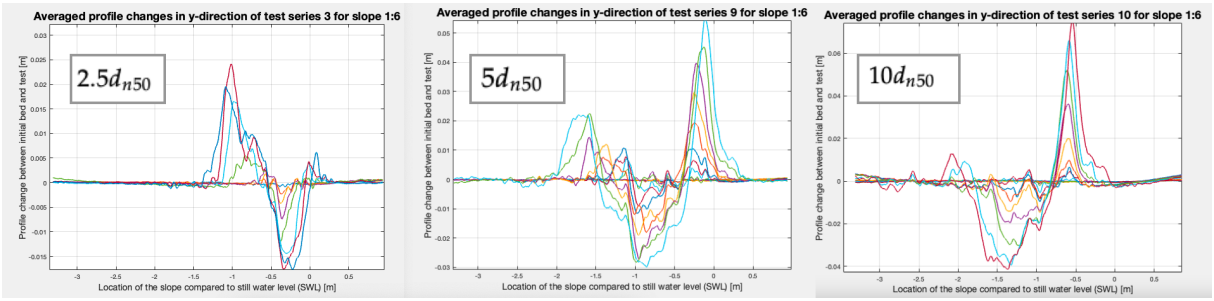

Figure 4.2: 2D damage profile for layer thickness 2.5d_{n50}, 5d_{n50} and 10d_{n50} with wave steepness 4%.

For the test with a layer thickness of 2.5d_{n50}, a clear bar profile is formed by dominant transport downwards. For a layer thickness of 5d_{n50}, an accumulation is visible downwards of the slope, which appears equal in size as the upslope accumulation (see: figure 4.3). This is a clear combination of a bar and a berm profile. Only for a slope angle of 1:6 a layer thickness of 10d_{n50} has been tested, it is interesting to see that a dominant transport direction upslope is observed which corresponds with a berm profile. To substantiate these visual observations, the 2D averaged profile results for the test iterations 3_7, 9_7 and 10_8 can be observed in figure 4.3:

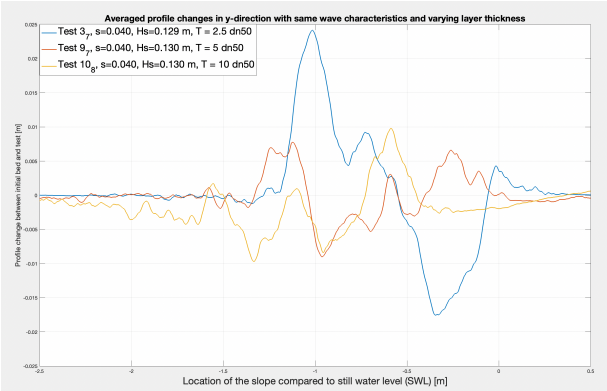

Figure 4.3: 2D profile of tests with same incoming wave characteristics ($H_s = 0.13m, s = 0.04$) and layer thicknesses $2.5d_{n50}$, $5d_{n50}$ and $10d_{n50}$.

From figure 4.3 it can be seen that $T = 2.5d_{n50}$ gives a bar profile. $T = 5d_{n50}$ gives a combination of equal volume rock accumulation downslope and upslope. $T = 10d_{n50}$ gives a berm profile accompanied by dominant upward transport.

Different types of layer compositions may involve different hydraulic and structural processes. For tests with layer thickness $2.5d_{n50}$, most of the rocks are pulled downwards after wave attack. A feasible explanation for this would be that turbulent forces and wave energy act through this entire armour layer up to the impermeable core. The water flow can not penetrate to the core, which leads to relatively greater forces in the armour layer during run down (Jumelet, 2010). This process is referred to as reflection, which is a run-down normative process which relates to a downward transportation direction and a bar profile. For tests with layer thickness $5d_{n50}$, less stones are pulled downwards compared to $10d_{n50}$. Also upward transport is observed. The present downward transport shows that there is still exposure to the run-down mechanism. For tests with layer thickness $10d_{n50}$, most rocks are pushed upwards. Due to the increased layer thickness and volume of voids between the top of the armour layer and the impermeable core, the water flow can dissipate more easily into the thicker layer. Therefore, the outer rocks of the armour layer are barely exposed to the strong wave run-down. The run-down mechanism is less significant because of increased permeability of the bed, which corresponds with the process of transmission (Jumelet, 2010).

4.1.2 Boundary effect

Boundary effects were also observed during previous studies by Van Wijland (2020) and Mossinkoff (2019). These boundary effects are identified within 10 cm of the side wall accompanied by heavy erosion, especially while this is not yet the case in the rest of the armour layer. It is important that during the stereophotogrammetry workflow (subsection 3.2.1) the profile is cutted to minimize the effects that the boundary effects could have on the damage numbers. An example of a cutted profile with characterization width of $54d_{n50}$ is shown in figure 4.4:

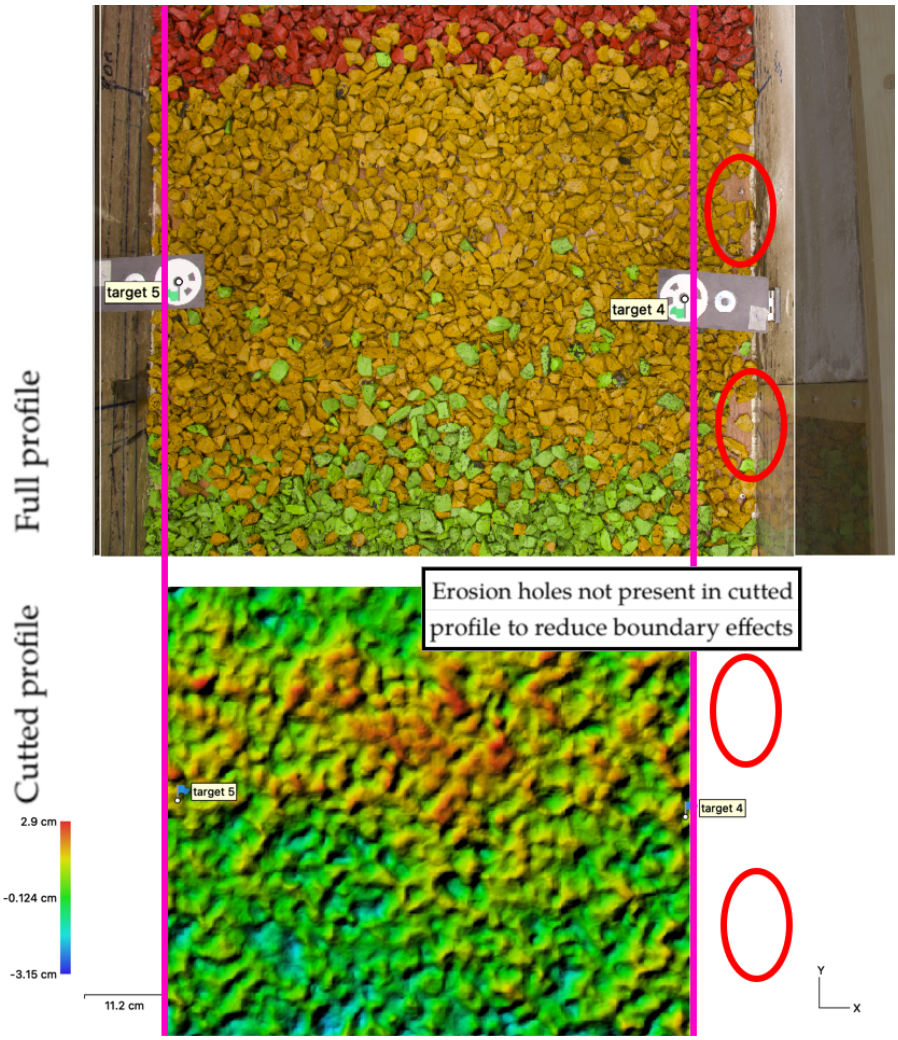

Figure 4.4: Full profile with identified boundary effects compared with cutted profile ($54d_{n50}$) to reduce boundary effects.

An obvious cause for the occurrence of the boundary effects could be that the water forces of a breaking wave (particularly the plunging jet) dissipate less easily at the sides. The energy of perpendicular hydro forces (x-direction) on the slope are mostly deflected downslope (y-direction). This could strengthen the run-down mechanism in those places. If you compare this to the middle of the slope with regard to the width, the water can move in multiple directions so that the effect of reflective forces is more present on the sides of the wave flume.

4.2 Damage parameters

This section presents the results regarding the 2D and 3D damage numbers. The determination of these damage numbers ($S, S_{all}, E_{2D}, E_{3D,1}, E_{3D,3}, E_{3D,5}$) from the models obtained from the stereophotogrammetry method are explained in subsections 3.2.3 and 3.2.5. In total 95 tests were performed for slope 1:6. The 84 tests performed by Van Wijland (2020) for 1:8 and the 47 tests performed by Mossinkoff (2019) for slope 1:10 are also included in the results in order to gain insight of the hydraulic and structural influences related to the damage numbers in the range 1:6 - 1:10. In order to determine general trends to determine the influences on stability, all obtained damage numbers are looked at. To perform a

more specific analyses, a single test could be investigated per damage parameter, with particular focus on damage number $E_{3D,3}$. This damage number is often used for the in-depth analysis because it is described by Van Wijland (2020) and Mossinkoff (2019) as the most useful damage figure for mild slopes and also gives the most reliable parameter from the analysis for stereophotogrammetry accuracy (table 3.5).

4.2.1 Variability and accuracy

Test 5 of the executed test series for slope 1:6 (table 3.3) contains five test iterations with same wave characteristics of $s_{op} \approx 0.04$ and $H_s \approx 0.085m$. After each test iterations, the slope is rebuilt and a new reference is processed. This is according to the non-cumulative test method, which was also used in the research of Van der Meer (1988). The purpose of this subsection is to provide insight into the reliability of comparing damage numbers results of non-cumulative tests and cumulative tests. To be able to validate these results, a comparison was made with test iteration 6_{05} because after this iteration the slope has processed the same incoming wave characteristics from a cumulative method as for all iterations of non-cumulative test 5. A t-distribution is used to determine the 90 percent confidence intervals which are presented in table 4.1:

Table 4.1: Damage results of test series 5 (non-cumulative) with a 90% confidence interval for $w = 54d_{n50}$. Results of test 6_{05} (cumulative) are presented to compare cumulative and non-cumulative damage results.

Damage parameter	**Mean (μ)**	**Std (σ)**	**Variation ($\frac{\sigma}{\mu}$)**	**Lower boundary 90% percentile**	**Upper boundary 90%** percentile	Test 6_{05}
S	2.63	0.77	0.29	1.74	3.48	3.07
S_{all}	3.21	0.86	0.27	2.15	4.02	3.10
E_{2D}	0.24	0.04	0.15	0.20	0.28	0.27
$E_{3D,1}$	1.53	0.14	0.09	1.38	1.68	1.18
$E_{3D,3}$	0.79	0.09	0.11	0.71	0.90	0.76
$E_{3D,5}$	0.53	0.08	0.14	0.44	0.62	0.57

The damage parameters of test 6_{05} which are within the lower and upper 90% confidence interval are validated. This representation indicates that the comparison of the cumulative method and the non-cumulative method is valid. All the tested values are within the range, except for the damage parameter $E_{3D,1}$. This indicates that for damage number $E_{3D,1}$, further research is needed to establish a direct link between results from non-cumulative and cumulative methods. A possible cause for the deviation from the confidence range is that $E_{3D,1}$ uses the smallest moving average of the 3D parameters and this can ensure that a small deviation of a number of stones can cause a relatively large difference in $E_{3D,1}$. Van Wijland (2020) stated: 'the smaller the circle of the spatial moving average is within the damage parameter E3D,m, the higher is the offset', which substantiate this result.

The damage parameters are determined by use of a characterization width of $54d_{n50}$. For the other damage parameters that are within the 90% confidence interval the assumption is made that the damage parameters for $w = 27d_{n50}$ will also hold. This assumption is based on research by (de Almeida, 2017), which shows that for the 2D parameters the damage becomes increasingly stable with a characterization width larger than $25d_{n50}$. For 3D parameters the probability of observing a larger damage value will increase for a larger characterization width, so the variability in table 4.1 is actually larger than for $27d_{n50}$. The characterization width of $27d_{n50}$ is used for the result section.

4.2.2 Influence of wave height, wave steepness and slope angle

- **Influence of significant wave height H_s**

  In general, a positive correlation can be observed between the significant wave height and all determined damage numbers. This means that a higher significant wave height, whose waves contain more energy, have a greater force impact on the slope. This results in higher damage parameters, as presented in figure 4.6.

  When looking at the mutual relationships between each test iteration, a number of deviations from this general statement can be observed. This is expressed in a deviation of the general trend which occurs within a test between two successive test iterations. To give an example for slope 1:6 for damage number $E_{3D,3}$, where in various tests it happens that for a test iteration with a higher significant wave height H_s a lower damage number is obtained. However, this deviation is only lasting for a single iteration. Which means that the damage parameter ($E_{3D,3}$) of the test iteration that follows is larger than those values of the two test iterations before. The most feasible causes for these deviations are due to measuring inaccuracy following from the stereophotogrammetry method. Table 3.5 shows that when investigating damage parameter $E_{3D,3}$ a deviation of ±0.11 is considerable for this measuring method. Also the variability of the damage parameters could be taken into account, which for this specific example the variation ($\frac{\sigma}{\mu}$) of $E_{3D,3}$ following from the variability tests (table 4.1) is depicted as 0.11.

- **Influence of wave steepness $s_{o,p}$**

  A general trend in wave steepness $s_{o,p}$ that can be inferred from the damage plots in figure 4.6 is for a larger wave steepness, lower values of damage parameters are obtained for a comparable significant wave height.

  The impact on the distribution between spilling and plunging waves due to changes in wave steepness is less sensitive to slope 1:6 compared to slope 1:8 and 1:10. For slope 1:6, the lowest obtained Iribarren number is 0.8. For an Iribarren number of 0.8 for slope 1:8 the percentage of spilling waves is expected less than 10%, based on figure 2.6. Because for slope 1:8 and 1:10 the total range of wave steepness ($s_{o,p} = 0.1 - 0.5$), inherent to a certain range of Iribarren numbers, realises a significant increase of the percentage of spilling waves. For slope 1:8, the lowest Iribarren numbers give approximately 30% spilling waves and for 1:10 this ratio is around 50% (figure 2.6).

  So for slope 1:8 and 1:10, a larger wave steepness $s_{o,p}$ shows lower damage parameters, which is associated with a higher percentage of spilling waves. Spilling waves dissipate energy in a longer distance (y-direction) compared to plunging waves (see figure 2.5) and therefore results in lower wave impact on the slope which expects to lead to lower damage parameters. This expectation is supported by the results, presented in 4.5:

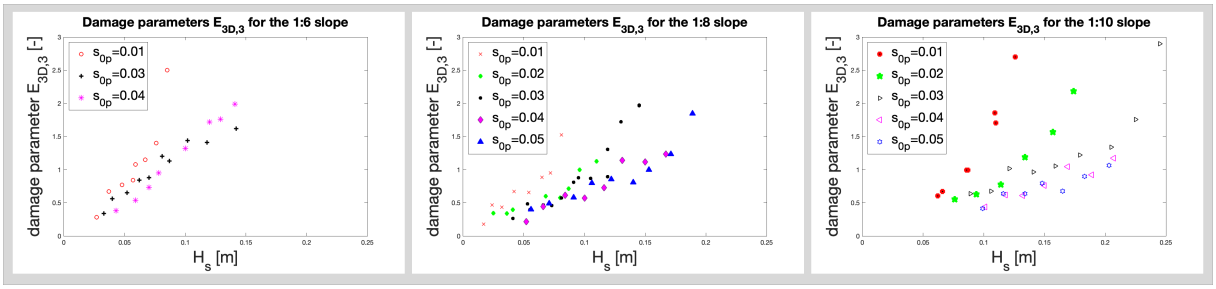

Figure 4.5: Damage parameter $E_{3D,3}$ compared to significant wave height H_s for varying wave steepness and slopes 1:6, 1:8 and 1:10.

The effect of an increasing number of spilling waves on damage can be clearly observed in figure 4.5. For slope 1:6 the ratios between the extreme tested wave steepnesses are smaller than for

slope 1:8, which in turn is smaller compared to slope 1:10. For example, by drawing an imaginary straight line through the data points of $E_{3D,3}$ in figure 4.5, this gives the insight that for slope 1:6 the slope coefficients of these lines are close to parallel. Compared to diverging lines for slope 1:10, this corresponds to the enhanced effect of less damage due to the influence of an increased percent of spilling waves.

- **Influence of slope angle** α

  For a steeper slope angle (in range 1:6 - 1:10), the damage parameters are increasing for a comparable significant wave height H_s. The same explanation as for the influence of wave steepness regarding the change of the Iribarren number also applies here. A steeper slope, inherent to an increasing Iribarren number, leads to a lower percentage of spilling waves.

  Another considerable effect for steeper slopes is the impact of gravity on transporting rocks. Although, for slope 1:6 the dominant transportation direction is not necessarily downslope for all wave characteristics. But especially for the steeper waves on a 1:6 slope, where more downward transportation is observed (figure 4.1) than for low wave steepness. It is obvious that gravity contributes more to downward displacements than in the case of slope 1:10, where the dominant direction of transport appears to be upward (Mossinkoff, 2019).

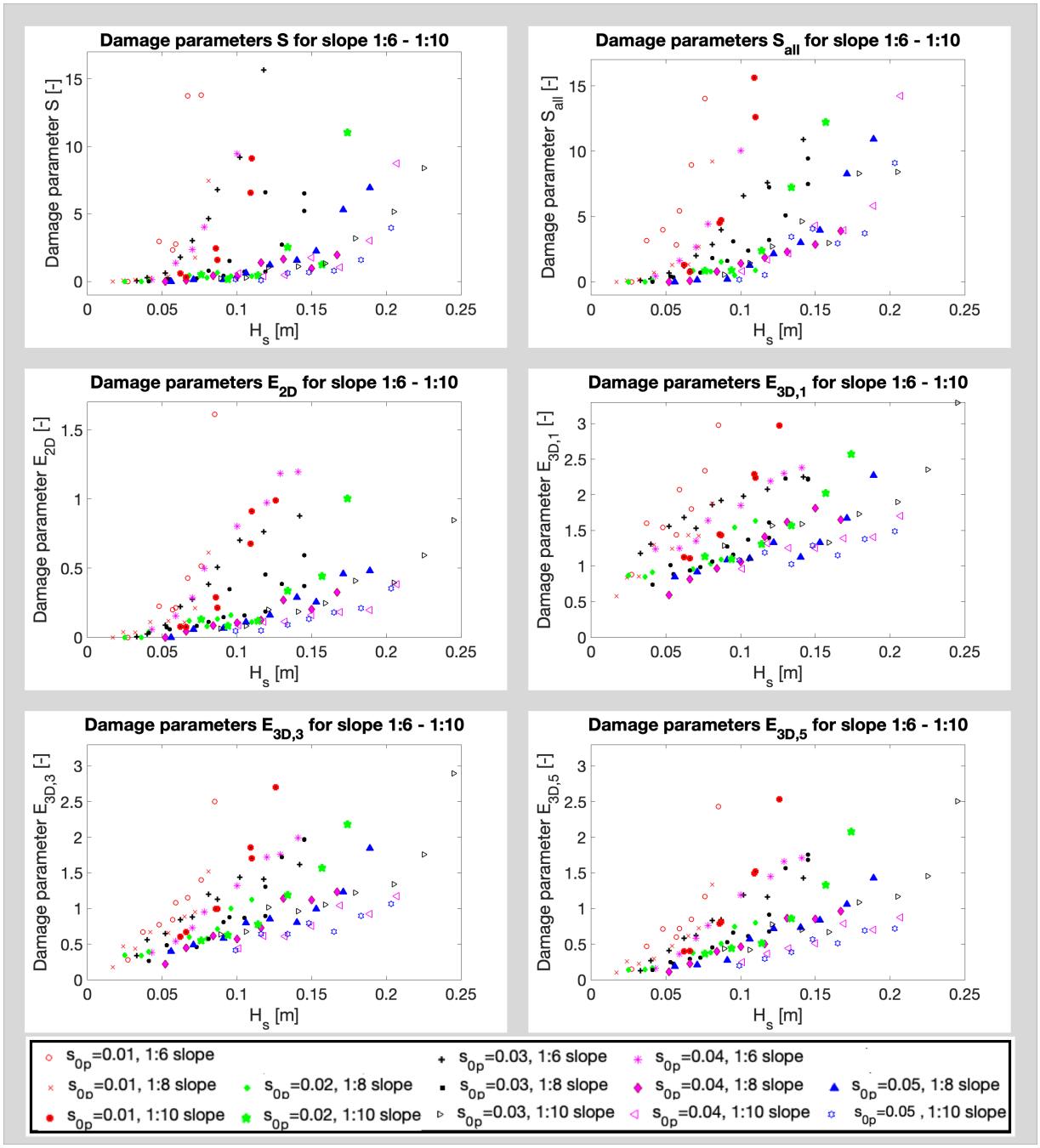

Figure 4.6: Profile based damage parameters related to significant wave height Hs distinguishing between different wave steepnesses s_{op} and slope angles α after 1000 incoming waves.

4.2.3 Influence of layer thickness

For the slope range 1:6 - 1:10, the physical model tests were performed for wave steepness $s_{op} = 0.01$ and $s_{op} = 0.03$ for layer thicknesses $T = 2.5d_{n50}$ and $T = 5d_{n50}$ to make this series complete. Additional tests for slope 1:6 for wave steepness $s_{op} = 0.04$ are performed for three different layer thicknesses ($T = 2.5d_{n50}$, $T = 5d_{n50}$ and $T = 10d_{n50}$) to gain insight into the influence of layer thickness in relation to the stability of rocks. All tests were performed with an impermeable core, without a filter layer and a nominal rock diameter d_{n50} of the armour layer of 0.0148 m.

Van Wijland (2020) stated in his report that the layer thickness has no influence on the stability for slopes 1:8 and 1:10. It is more complicated to observe a general trend compared to the previous discussed influences on stability described in subsection 4.2.5. Therefore, the investigation of the influence of layer thickness needs a more in-depth analysis by showing the damage limits of $E_{3D,3}$ (0.3, 0.6 and 1.5) based on the indicated failure limits presented by Van Wijland (2020) for a layer thickness of T = $2.5d_{n50}$ (see table 2.5). The results of $E_{3D,3}$ per slope and wave steepness are shown in figure 4.7:

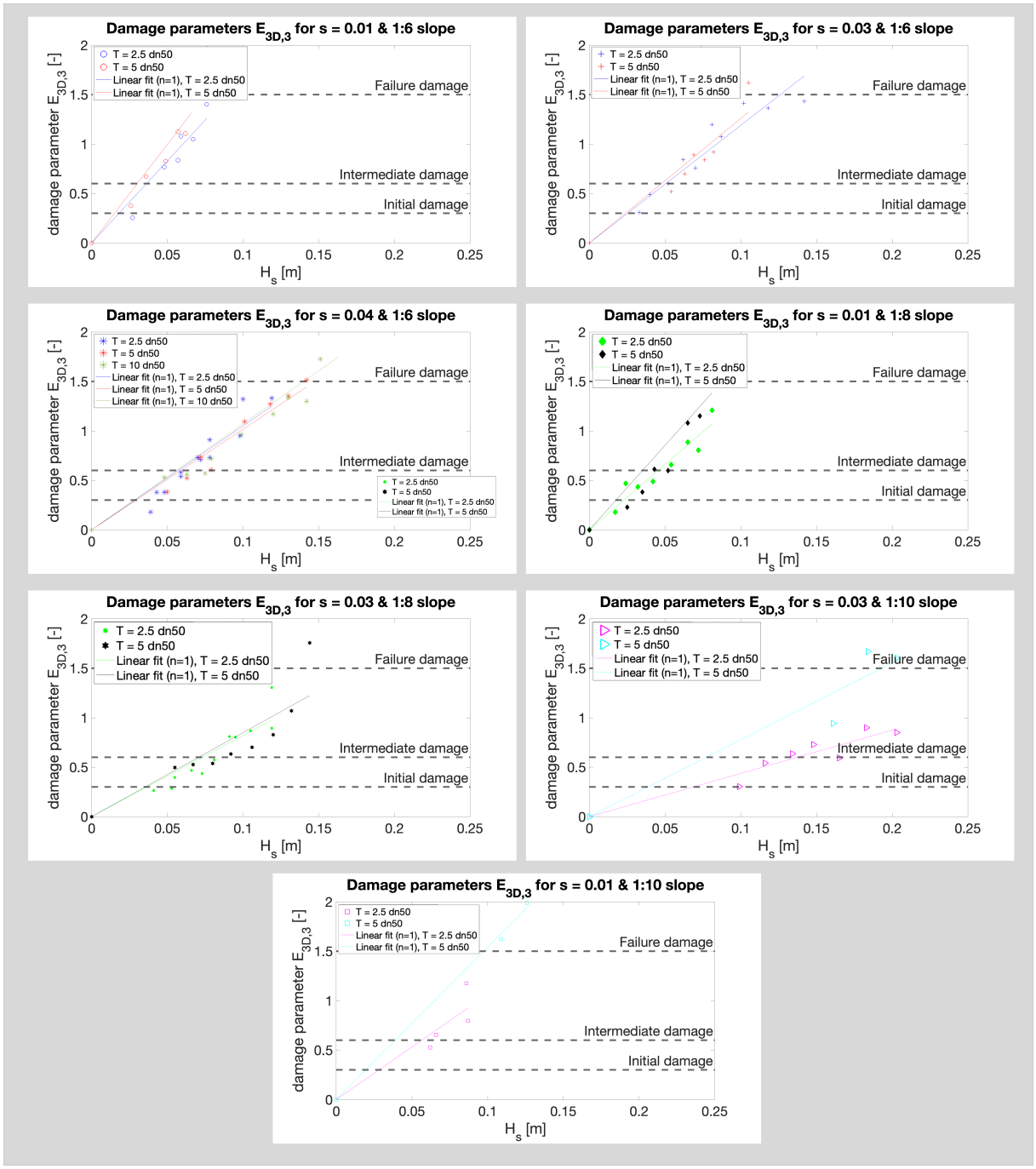

Figure 4.7: Damage parameter $E_{3D,3}$ compared to significant wave height H_s for varying layer thicknesses and slopes with presented damage limits corresponding with T = $2.5d_{n50}$ and optimal linear fitted lines.

Figure 4.7, takes into account the fact that when the slope fails, the impermeable core is partially exposed. The event of which the impermeable core becomes visible for varies per layer thickness and occurs at lower $E_{3D,3}$ damage numbers than for $2.5d_{n50}$ compared to the tests with layer thickness $5.0d_{n50}$ and $10d_{n50}$. After exposure of the impermeable layer, the parameter d_e on which $E_{3D,3}$ is partly based (formula 2.28), can grow less in the case of a layer thickness $2.5d_{n50}$ compared to a similar damage number achieved for a test with a thicker layer from which the impermeable layer has not yet been exposed. This has been included in the analysis of figure 4.7 by not including tests for which the slope has already failed.
Analyzing the plots from figure 4.7 leads almost equal damage trends between performed tests with the same incoming wave characteristics but only with a different layer thickness. No significant difference can be derived for the tests with slope 1:6 and 1:8. For the slope 1:10, the thicker layer seems to cause less damage for a similar wave attack, but this is based on a relative low total of five tests for a layer thickness of $5d_{n50}$. Therefore, the conclusion of Van Wijland (2020) is maintained that no significant difference in damage can be observed from the tests.

For a second analysis for the influence of permeability, the tests are divided into four $E_{3D,3}$ damage zones:

- Zone 1: $0.4 < E_{3D,3} < 0.7$
- Zone 2: $0.7 < E_{3D,3} < 1.0$
- Zone 3: $1.0 < E_{3D,3} < 1.3$
- Zone 4: $1.3 < E_{3D,3} < 1.5$

The stability with corresponding Iribarren numbers $\xi_{m-1,0}$ is presented per indicated damage zone per layer thickness in figure 4.8:

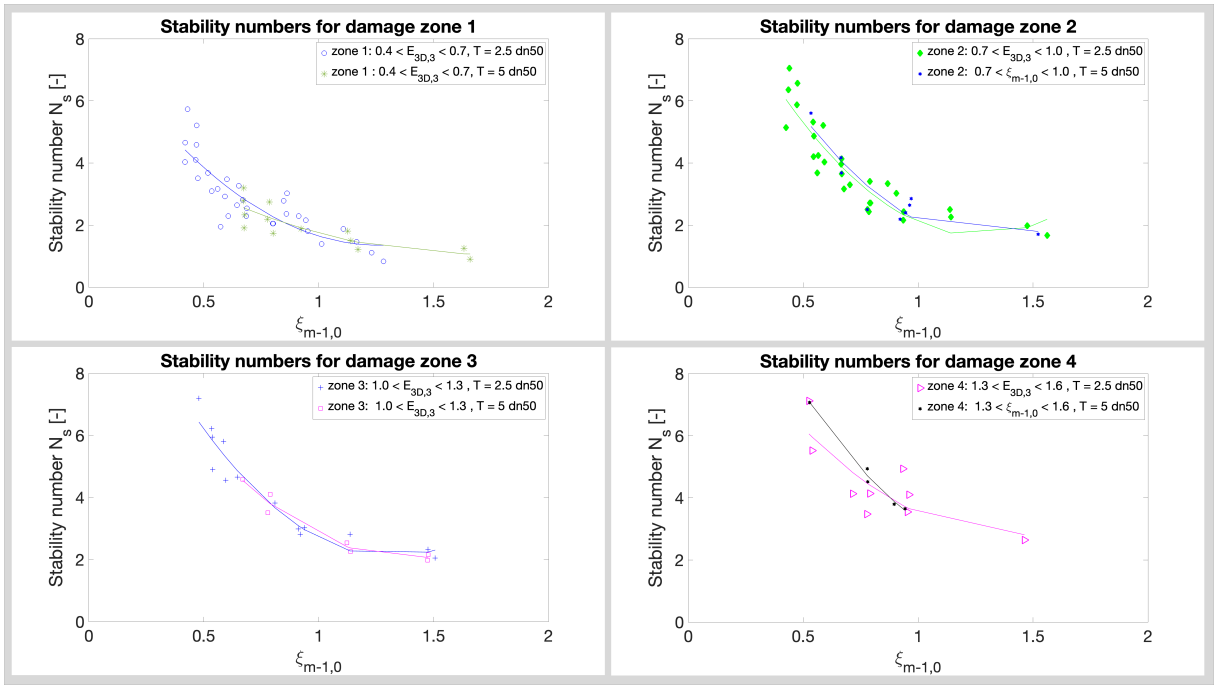

Figure 4.8: Trends of stability number N_s and Iribarren $\xi_{m-1,0}$ divided in damage zones.

In figure 4.8 again no significant difference in stability can be observed with regard to different layer thicknesses ($2.5d_{n50}$ and $5d_{n50}$).

Since per slope angle and per wave steepness, which are combined in the Iribarren number, the damage formations are varying with respect to layer thickness (see figure 4.1), a double variability for layer thickness T, Iribarren $\xi_{m-1,0}$ occurs. A reason could be the impact of permeability P due to reflective and transmissive processes which are also interacting with layer thickness T and Irribarren $\xi_{m-1,0}$. Despite the different damage formations (bar/berm profile) and dominant transport direction, no significant difference in damage parameter $E_{3D,3}$ and stability (N_s) was observed.

For slope 1:10 and layer thickness $5d_{n50}$ only five tested are performed. From these tests only one value of the $E_{3D,3}$ damage parameter is below the indicated failure criterion of 1.5 Van Wijland (2020). Therefore, this test can hardly be compared to the tests with layer thickness $2.5d_{n50}$ for the same method. All the tests for the different used damage parameters are presented in figure 4.9:

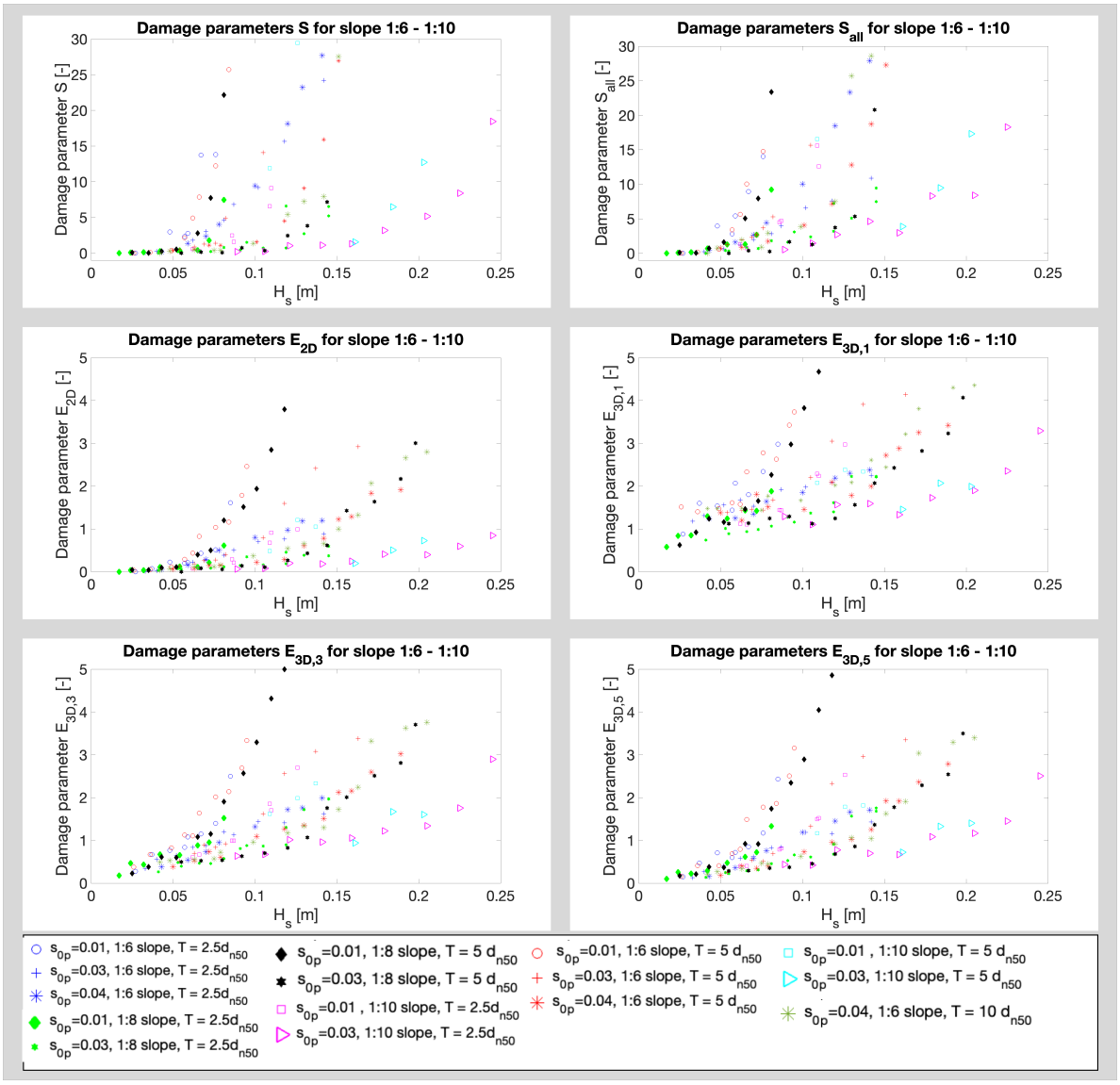

Figure 4.9: Profile based damage parameters related to significant wave height Hs distinguishing between different layer thicknesses T and slope angles α after 1000 incoming waves.

4.2.4 Influence of (notional) permeability

This analysis focuses whether it is useful to assign a constant notional permeability value to a certain layer composition for a mild slope design method. And if not, to gain knowledge how permeability could be still taken into account for the design. To obtain the starting value of notional permeability for this analysis, the assumption is made that the method of Eldrup and Andersen (2019) is valid outside the applicability range of 1:1.5 - 1:6.

Regarding slope 1:6, the research of Van der Meer (1988) only showed results for slope 1:6 with an impermeable core with a notional permeability of P = 0.1 (figure 2.3). With the structural parameters of slopes 1:6, 1:8 and 1:10, an estimation of the notional permeability is made based on the method of Eldrup and Andersen (2019). Table 4.2 provides the expected values for the notional permeability of the mild slope test series:

Table 4.2: The notional permeability for layer compositions without filter layer calculated with the method of Eldrup & Andersen (2019).

Layer composition			**Notional permeability**
Description	**Armour**	**Core**	**based on method of Eldrup & Andersen (2019)**
Impermeable			0.1
$2.5 * d_{n50}$	$2.5d_{n50}$	Impermeable	0.12
$5 * d_{n50}$	$5d_{n50}$	Impermeable	0.48
$10 * d_{n50}$	$10d_{n50}$	Impermeable	0.57
Permeable			0.6

Van Wijland (2020) and Mossinkoff (2019) used the method of Eldrup and Andersen (2019) to quantify the layer compositions with respect to the notional permeability factor P. Van der Meer (1988) used extreme values for an impermeable core (P = 0.1) or a permeable core (P=0.6). Notional permeability P values for other layer compositions are considered to be between these two extremes. As described in subsection 2.1.1, Eldrup and Andersen (2019) developed this empirical method based on studies with several layer compositions (appendix B) for a damage range of $S = 2 - 17$ and slope angles between 1:1.5 - 1:6.

The test results give the required wave height (H_s), 2D damage (S), number of waves (N) and the Irribarren number (ξ_m) which are necessary for the use of equation 2.30. By combining the concepts of notional permeability of Eldrup and Andersen (2019) and plunging wave damage (equation 2.30), it is possible to gain insight into the relation of notional permeability P and layer thickness compositions with an impermeable core in slope range 1:6 - 1:10. Only tests iterations in damage range S = 2 - 17 are used and a conversion method of accumulated damage tests is applied (subsection 2.1.2) which results in a higher number of waves N than initially was taken into account. Based on the conversed number of waves for the specific tests within the damage range, the notional permeability value can be compared. The implementation of the test results for slope 1:6, 1:8 and 1:10 combined with the method of Eldrup and Andersen (2019), including taking into account accumulated tests are shown in figure 4.2.4:

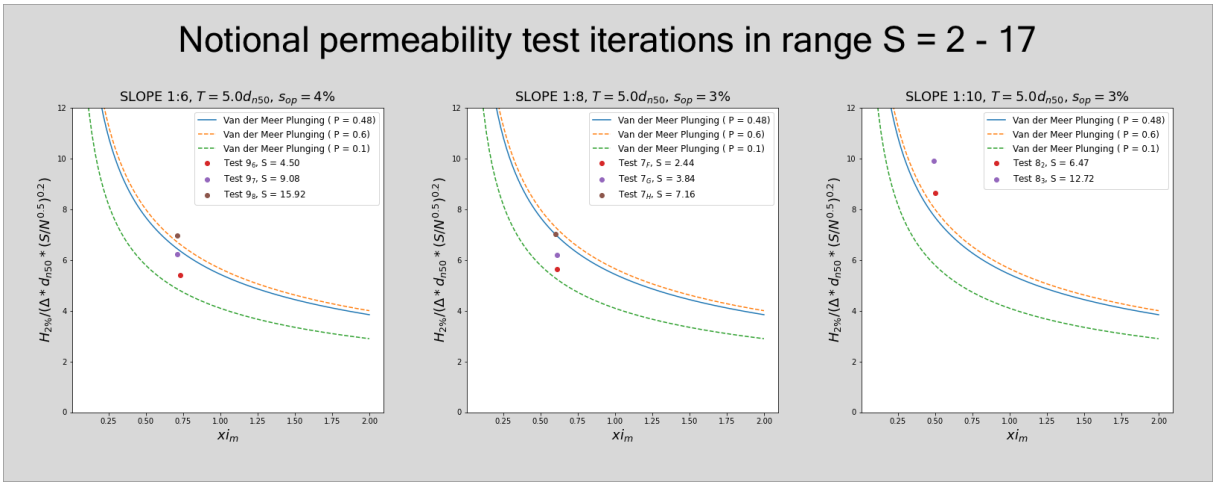

Figure 4.10: Implementation of test results processed by method of Eldrup and Andersen (2019) for slope 1:6, 1:8 and 1:10.

Figure 4.2.4 shows that varying values of notional permeability P are found based on the test results processed according to the method of Eldrup and Andersen (2019). As a result, it does not initially seem obvious to use a fixed value for the notional permeability P per layer composition for the use of the design formula based in the results of slope 1:6, slope 1:8 and slope 1:10. Underlying is also the fact that no method is yet available to analyze this for mild slopes. After all, the Eldrup and Andersen (2019) method is not based on test results with a more gentle slope than 1:6. It was therefore expected that the tests should be more accurate for a 1:6 slope than for slope 1:8 and 1:10. The difference in expected values (dashed lines) and calculated point values increases as the slope decreases. Further visualization on the analysis is presented in figure T.1 of appendix T.

The outcomes of notional permeability numbers obtained with test results and the formula of plunging waves by Van der Meer (1988) differs from the estimated notional permeability of Eldrup and Andersen (2019) obtained by structural parameters of the slope. Therefore, the method of Eldrup and Andersen (2019) could not have been validated yet as application for mild slopes design. An possible outcome could lie in including the layer thickness in the design formula in order to take into account different layer compositions.

4.2.5 Influence of number of waves

For slopes 1:6, 1:8 and 1:10, tests were performed in which the number of waves was steadily increased and the other wave characteristics were kept constant. The maximum number of waves N tested for these slopes are, respectively, 20000, 15000 and 11000. The wave heights used for the tests with slope 1:6 are about two times smaller than with slope 1:8 and 1:10. Therefore, an accumulated number of 20000 waves was tested for slope. This was executed without achieving failure of the slope by exposure the impermeable layer of the slope.

A re-analysis of Van der Meer (1988) on the physical model tests of Thompson and Shuttler (1975) provides a relation where the damage parameter S is positively correlated to the square root of the number of waves N ($S \sim \sqrt{N}$) for a maximum tested number of waves of 15000. Van der Meer (1988) established a number of theoretical requirements to describe the influence of number of waves on stability. Since the test results of slope 1:6 are in the valid slope range, an experiment was performed to check the comparability of these results. The number of waves N is shown in comparison to damage parameter S in figure 4.11:

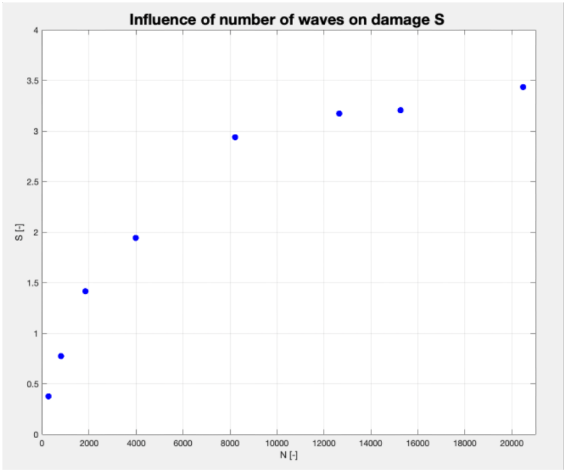

Figure 4.11: Influence number of waves on damage parameter S for slope 1:6.

From N = 0 - 1000 the function should be almost linear as only high wave groups will cause the first damage (Van der Meer, 1988). Figure 4.11 shows that the damage for the first 1000 waves is expanding with the largest ratio. It is expected that for large N numbers a limit to the damage is reached which relates to an equilibrium. Van der Meer (1988) describes this with equation 2.11. The curve fitting coefficient of Van der Meer (1988) are a = 1.3 and b = $3 * 10^{-4}$ and are used to make a comparison with the results. a = 1.3 insinuates that the damage is limited to 1.3 times the damage found after N = 5000. For $N > 8500$ the maximum damage can be set at $S = 1.3 * (S(5000)$. For this test that would be $S_{max} = 3.25$, with $S(5000) = 2.5$. The test also complies with the criteria that after 5000 waves the damage is at least equal to S = 2. The damage at the maximum number of waves (N = 20000) divided by the damage at N = 5000 is equal to $S(20000)/S(5000) = 3.43/2.5 = 1.37$. This result is comparable to the value of 1.3 of Van der Meer (1988). This indicates that the test performed with slope 1:6 corresponds to the expectations of constant damage progression when testing the influence of stability in relation to the number of waves. The damage formation was observed to stabilize for an increasing number of waves for slope 1:6, also following the same interpretation as Van der Meer (1988).

The general trends for slope 1:8 and 1:10 visible from the plots for all obtained damage numbers (figure 4.12) have not yet reached equilibrium. For the 2D parameters, a linear upward trend is observed. The results in 3D also shows a linear upward trend. This is different from the trend of slope 1:6, which seems to reach an equilibrium in 3D. Therefore, as Van Wijland (2020) already stated, the correlation between the number of waves N and damage might be different for mild slopes compared to steeper slopes. When considering the influence of the number of waves N, the expectations for steep slopes of Van der Meer (1988) still correspond to the results from the physical model tests of slope 1:6.

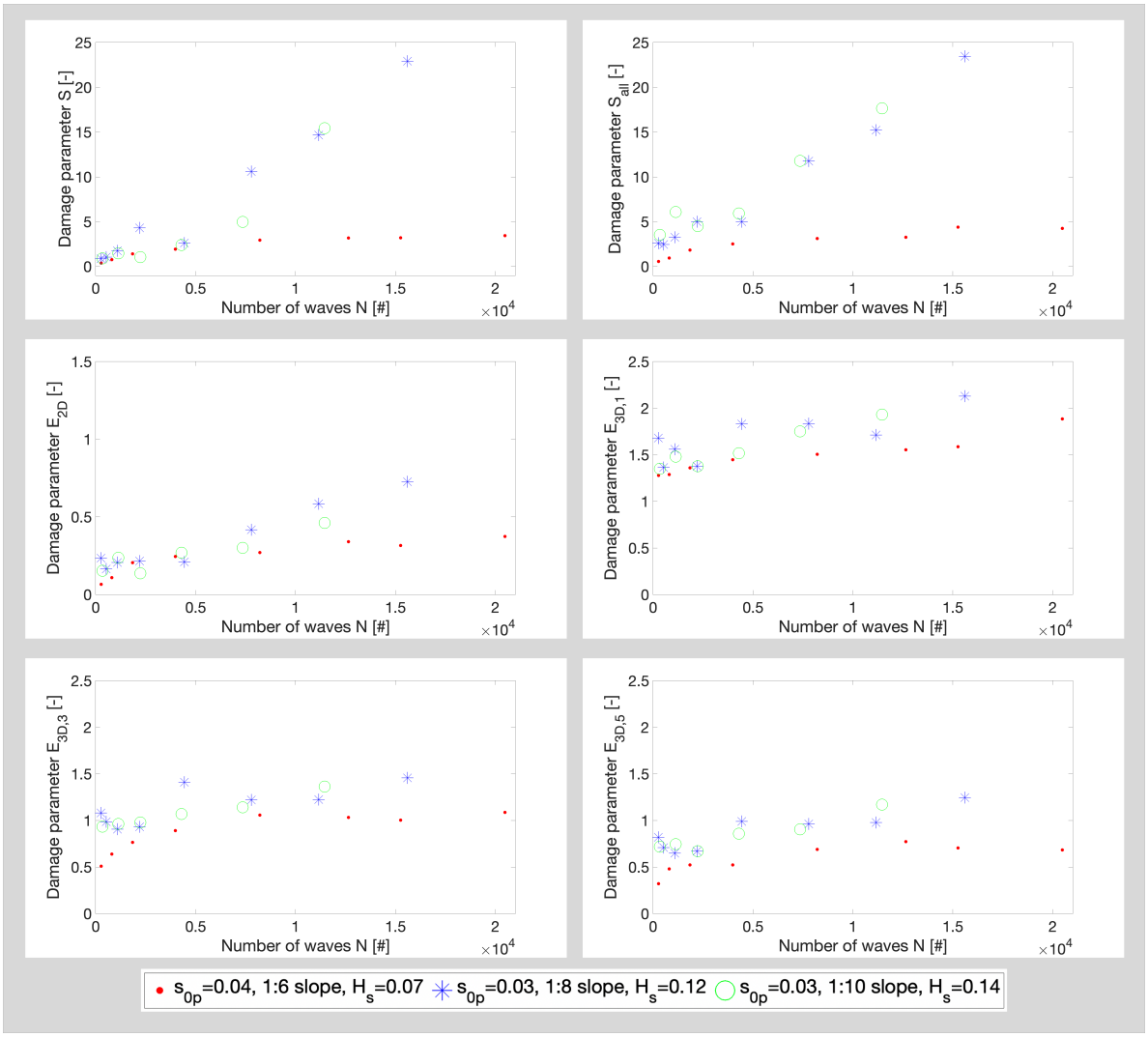

Figure 4.12: Profile based damage parameters related to number of waves N for slopes 1:6, 1:8 and 1:10.

4.3 Damage domain and location

In this section a distinction is made between:

1. Damage domain according to the classification of five damage locations as described in section 3.2.7
2. Maximum damage location per damage parameter

The damage domains are presented in the left part of figure 4.13. At the right part, the median values expressed in the maximum significant wave height H_s for each damage zone are displayed.

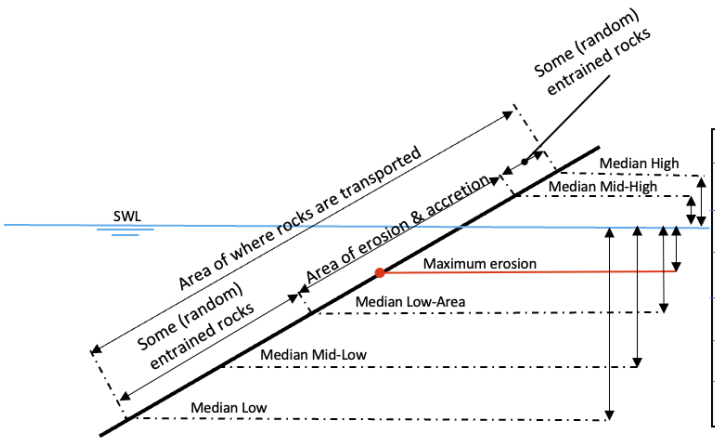

	1:6 slope	1:8 slope	1:10 slope
Med H	0.39	0.70	0.46
Med MH	0.34	0.59	0.39
Max E_{3D,3}	- 0.25	- 0.41	- 0.76
Med LA	- 0.46	- 1.11	- 1.24
Med ML	- 1.02	- 1.58	- 1.81
Med L	-1.66	- 2.27	- 2.27

Figure 4.13: Damage domains expressed in H_s

The added test series provide insight into the damage domains and maximum damage limits from range 1:6 - 1:10. The results of this are based on the tests with a layer thickness of $2.5d_{n50}$. Variability and number of wave tests are not included as only tests with varying wave height are used. The results are presented in figure 4.14.

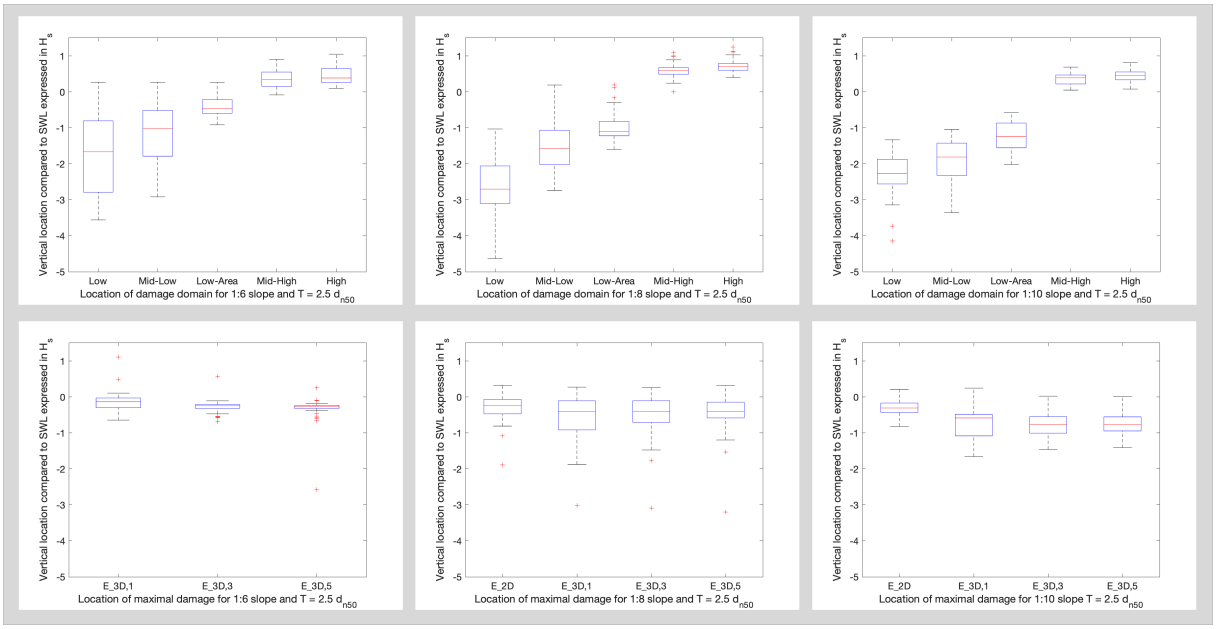

Figure 4.14: Upper: boxplot of damage domains according to five locations for slope 1:6, 1:8 and 1:10. Lower: boxplot of maximal damage location of damage parameters for slope 1:6,1:8 and 1:10.

What is striking about the results in figure 4.14 is that the upper and lower boxplot limits (25th & 75th percentiles) vary in distance, but when looking at the median values of the comparable damage domains for different slope angles (figure 4.14), they are no further than $1 * H_s$ apart. The maximum damage for slope 1:6 is more centered compared to slope 1:8 and 1:10. The medians of maximum damage for $E_{3D,3}$ for slope 1:6 and 1:10 differ $0.5 * H_s$. Where the maximum value of $E_{3D,3}$ is closer to SWL as the slope angle becomes steeper.

Also, the results of slope 1:6 for tests with different layer thicknesses ($T = 2.5d_{n50}$,$T = 5d_{n50}$ and $T = 10d_{n50}$) were analyzed to gain more insight into the effect of varying layer thicknesses on the damage domain and the location of maximal damage. The results are presented in figure 4.15:

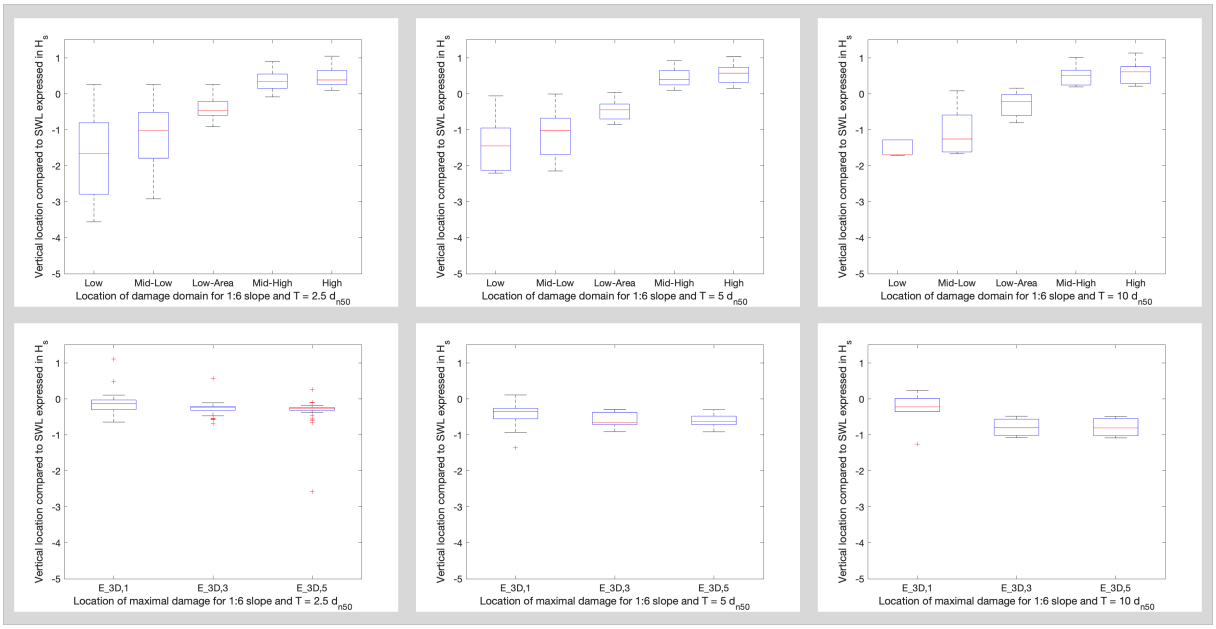

Figure 4.15: Upper: boxplot of damage domains according to five locations for slope 1:6 and varying layer thickness. Lower: boxplot of maximal damage location of damage parameters for slope 1:6 and varying layer thickness.

In particular, the 'Low' damage zone with layer thickness $2.5E_{3D,3}$ shows a large spread compared to the other layer thicknesses. In contrast, the maximum damage shows a more centered ratio. The median of the $E_{3D,3}$ maximum damage location is closer towards SWL for smaller layer thickness.

4.4 Breaker wave types

The test iteration with the highest significant wave H_s of each test is used for the determination of the distribution of plunging and spilling waves. This analysis, as described in section 3.3, was performed for all tests with slope angle 1:6. No other influences on the investigated distribution were found, such as the influence of layer thickness.

From the data of Van Wijland (2020) and Mossinkoff (2019) a relation between the distribution of spilling and plunging waves and the Iribarren number was already observed. As described in subsection 2.1.4, the expected distribution for slope 1:6 would vary between 90% and 100% plunging waves. This is in line with the obtained results, which are shown in figure 4.16:

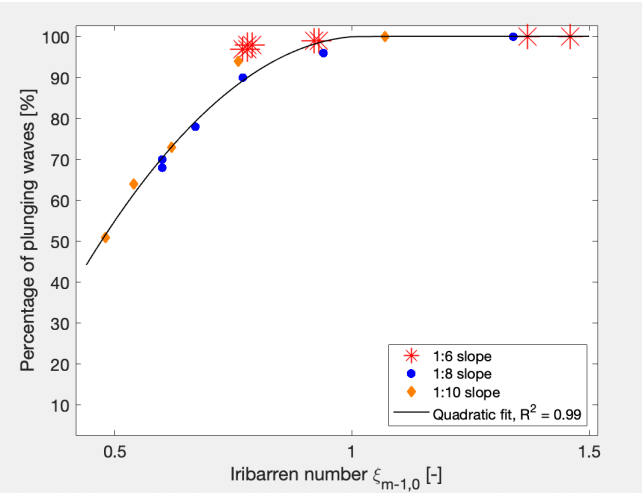

Figure 4.16: Distribution of spilling and plunging waves for slopes 1:6, 1:8 and 1:10.

From figure 4.16 it can be concluded that a different slope angle, but an equal Iribarren number, gives almost the same distribution between plunging and spilling waves. This supports the hypothesis that the distribution of the breaker wave type is dependent on the Iribarren number. A quadratic fit ($R^2 = 0.99$) is applied to the data, which results in equation 2 to estimate the fraction plunging or spilling waves:

$$\begin{cases} 0.4 \leq \xi_{m-1,0} < 1; & F_p = \frac{N_{plunging}}{N_{total}} & = & -1.6\xi_{m-1,0}^2 + 3.3\xi_{m-1,0} - 0.7 \\ 1 \leq \xi_{m-1,0} \leq 1.7; & F_p = \frac{N_{plunging}}{N_{total}} & = & 1 \end{cases} \tag{4.1}$$

After the distribution reaches 100% plunging waves at approximately $\xi_{m-1,0} = 1$, the distribution is considered to be fully plunging and therefore this value is fixed at $F_p = 1$, up to the largest tested value of $\xi_{m-1,0} = 1.7$. For higher numbers of Iribarren outside the tested range, there is a chance of the presence of surging waves.

4.5 Colour bands

For the current research series, the same characterization width w is used for the range slope 1:6 - 1:10. As the slope becomes steeper, the measurement inaccuracy on N_{od} is expected to increase for the mild slope range due to the effect of a higher ratio of the total displacements that occurs within the same colour band, also called internal displacements. This is substantiated by the maximum damage graphs from figure 4.14. The location of maximal damage for slope 1:6 is more concentrated compared to slope 1:8 and 1:10, so most damage is expected to be within a smaller number of colour bands. One can also take into account the area where rocks are transported, which ranges from 'Median Low' to 'Median High' as presented in figure 4.11. When taking the values of these ranges into account, slope 1:6 gives a tighter range over which rocks move compared to slope 1:8 and 1:10.

To gain more insight into the influence of the colour band width on displacement trends and damage numbers based on the number of displacements, a test 6 for slope 1:6 was performed with a characterization width of 0.1 m (figure 3.12). The analysis that is performed consists of two approaches described in section 3.4, consisting of a characterization width of 0.1 m and a considered merged characterization width of 0.5 m.

Test iteration 6_{07} was chosen to analyse because this iteration is associated with the highest significant wave height and the largest number of displaced stones of this test serie. The results for strip widths of w = 0.1 m and merged w = 0.5 m are given in figure 4.17:

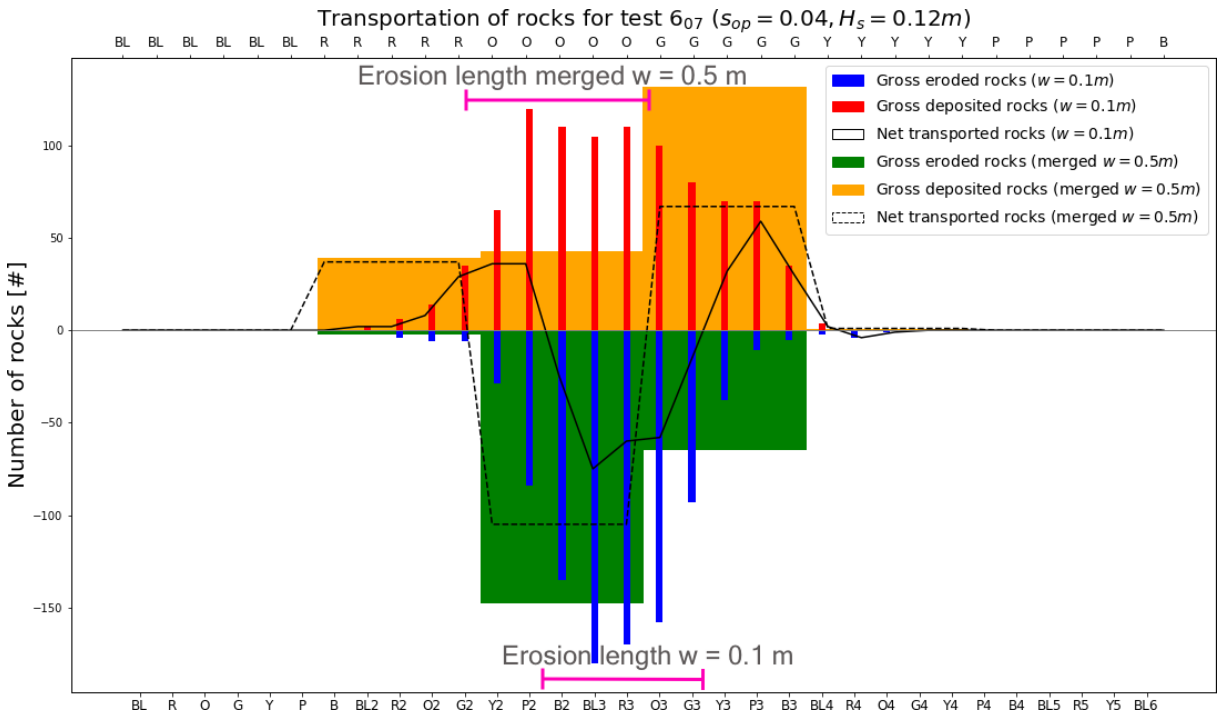

Figure 4.17: Transportation of rocks for test 6_{07}, analysed with merged approach of $w = 0.5m$ (upper x-axis) and $w = 0.1m$ (lower x-axis).

Figure 4.17 shows that a number of misconceptions can arise from analyzing a low-resolution colour band graph with a relatively large strip width. For the test with merged $w = 0.5m$, it can be observed that the maximum erosion takes place in the orange colour band (see: upper O strip), in the range within in that strip ($w = 0.1m$) both the maximum erosion (see: lower BL3 strip) and the lower peak of accretion (see: lower Y2 strip) occurs. This means that the erosion characteristics of slope differs in erosion length (y-direction) and location of maximum erosion (and accretion). For this test iteration it shows that at the location where the largest erosion is expected for $w = 0.5m$ there is actually an accumulation of rocks upwards. The erosion length for a smaller colour band width is smaller. One can observe that there are regions with a relative high number of displacement, but with net accretion. Based on the above findings from figure 4.17, it can be stated that a colour band of $w = 0.1m$ is better for the determination of N_{od} and S_{od}. The test with color band width of 0.1 m is used to gain insight into the process of mobility and erosion. The use of the damage number N_{od} with a smaller colour band gives more insight into the obtained measurement inaccuracy as a result of the internal displacements. In addition, the application of this insight shows a stronger relation to the original definition of N_{od} of USACE (2015).

The counted displacements can be expressed in damage numbers N_{od}. By use of equation 3.2 the conversion is made to S_{od} by taking porosity of the armour layer into account. A steep slope is characterized by the fact that all displacements instantly contribute to erosion, which can be indicated as $S_{od} = S_{all}$. By analyzing the relationship between S_{od} and S_{all}, mobility and erosion processes on mild slopes can be considered. This ratio S_{od}/S_{all} compared to wave height H_s is presented in figure 4.18:

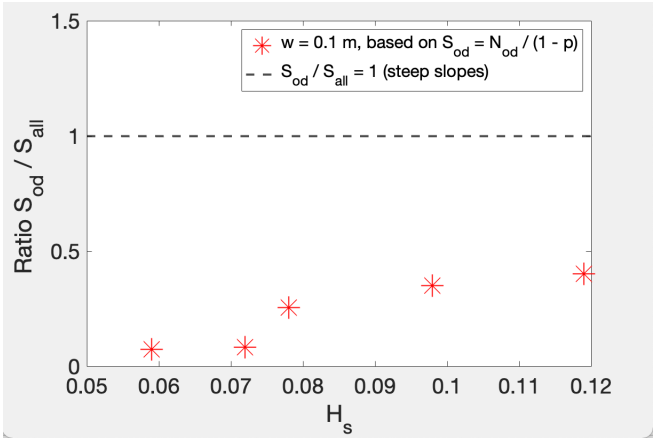

Figure 4.18: Ratio of mobility and erosion compared for mild slope values and steep slope interpretation

Figure 4.18 provides insight into the physical process with regard to erosion and mobility. The erosion is represented by S_{all} and the displacements by S_{od}. As a result, the ratio S_{od}/S_{all} is smaller than 1 for mild slopes. This value indicates that the mobility in relation to the erosion is larger than for a steep slope. For a steep slope this ratio is around 1 (USACE, 2015), which means that every displacement is counted as erosion.

The ratio S_{od}/S_{all} gives lower values for a smaller significant wave height H_s. This can be explained by the fact that while damage is already observed by the calculation of S_{all}, the moving rocks are not taken into account because they displace with a smaller length than one colour band. This is in line with the findings of Van Wijland (2020) for tests with a colour band of 0.5 m and slope angle 1:8 and 1:10. The ratio S_{od}/S_{all} gives higher values for a larger significant wave height H_s, explained by the fact that for larger waves the rocks displace outside their original colour band. At this stage, a clear trend in the erosion profile is formed. This allows a clearer distinction to be made between erosion and accretion areas on the slope.

For mild slopes, situations can arise in which there are more displacements than actual erosion on the slope, because rocks move back and forth without causing erosion. For example, if a stone is counted as displacement but remains in the same erosion area ($A_{(e),w}$) for the determination of S_{all} (see figure 3.7). Displaced rocks on steep slopes often fall directly to the toe. For the design of steep slopes, each displacement is therefore linked to erosion, making the ratio S_{od}/S almost equal to 1. This ratio is equal to 1 for steep slopes and decreases sharply with mild slopes, so that the values of mobility (S_{od}) and erosion (S) diverge strongly. The described mechanism explains why the ratio S_{od}/S_{all} will deviate for mild slopes in comparison with steep slopes.

Measurement errors are also included in this analysis. These can be analyzed by comparing damage parameter N_{od} calculated in two different ways. The first way is to calculate N_{od} based on counted displacements n_{net} according to equation 2.29. This is compared by the conversion of 3.2 based on the width-averaged erosion parameter S_{all}. Both values of N_{od} are presented in figure 4.19:

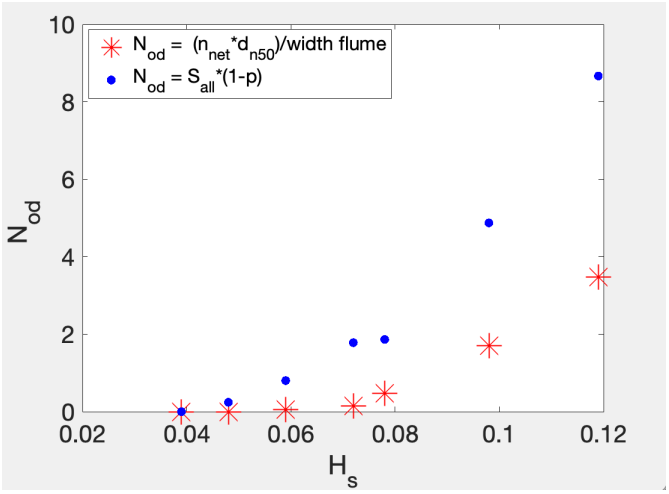

Figure 4.19: Difference in N_{od} based on displacements (n_{net}) and width-averaged erosion of the slope (S_{all}).

It is expected that the values of N_{od} based on n_{net} should be close to N_{od} based on S_{all}. For the largest wave height measured (Test 6_{07}), N_{od} based on S_{all} is 2.5 times larger than N_{od} based on n_{net}. These differences can be explained by a number of measurement inaccuracies. For the calculation of S_{all}, the sides of the flume (two times $\approx 10cm$) are not counted because of edge effects. Also, S_{all} is not determined over the total slope area, but an approximation is used based on the maximum significant wave height, as shown in figure 3.8. The entire flume width and slope area is taken into account to determine the number of displacements n_{net}. The used colour band of 0.1 m is roughly equal to $7d_{n50}$ for this test. Therefore, still the number of counted displacements is underestimated as it is common that all rocks that move with a larger distance than $1dn50$ are counted.

4.6 Design formula mild slopes

This section presents a design formula based on physical properties of the test characteristics for slopes 1:6 - 1:10. By means of the correlations arising from the results, the relationships between the variables and the fitting parameters can be determined.

4.6.1 Evaluation of damage limits

For the evaluation of damage limits for the design formula for mild slopes, the damage profiles of the tests are analysed according to the definitions for initial, intermediate and failure damage. To provide more insight into this, matching damage profiles have been found per slope for each described definition of a damage limit. The definitions that are used to describe the damage limits are as follows:

- *Initial damage*: when the first rocks start to move randomly on the slope.
- *Intermediate damage*: random displacements of individual rocks changes to groups of rocks that are transported to and from the same position.
- *Failure damage*: impermeable core (or filter layer) starts to become visible.

The stereophotogrammetry models are used for the analysis to link a test profile to a certain damage limit. The eligible tests per slope angle and damage limit are presented in appendix V. The S and $E_{3D,3}$ damage parameters of the chosen tests are statistically analysed to give the 5% and 95% percentiles and

the corresponding mean values. Based on the quality and numbers of the matched profiles choice is made per slope angle and damage limit. In total 45 profiles are matched to a certain damage limit for the range of slopes 1:6-1:10. The values according to the damage limits per slope, layer thickness and damage parameter (S and $E_{3D,3}$) are presented in table 4.3:

Table 4.3: Evaluation of matching profiles based on defined damage limits for damage parameters S and $E_{3D,3}$ for slopes 1:6 - 1:10 (* means could not be determined based on executed tests).

		T = $2.5d_{n50}$		**T =** $5d_{n50}$	
Slope	**Damage limit**	**S**	$E_{3D,3}$	**S**	$E_{3D,3}$
1:6	start	0.2	0.3	0.2	0.3
	intermediate	2	0.6	2	0.6
	failure	18	1.5	*	*
1:8	start	1	0.3	1	0.3
	intermediate	3	0.6	3	0.6
	failure	20	1.5	*	*
1:10	start	3	0.3	3	0.3
	intermediate	4	0.6	4	0.6
	failure	22	1.5	*	*

The first finding after analyzing the matched profiles was that the start of damage is not influenced by the varying use of layer thicknesses ($2.5d_{n50}$ and $5d_{n50}$) for slopes 1:6 - 1:10. This finding is in line with the statement of Hofland et al. (2011), that initial damage is only an indication of the start of damage and therefore the definition stays the same regardless of layer thickness.

The used definition for intermediate damage for this test serie is based on the first removal of rocks in groups. It can be added to this that the observed displacements are no longer random but show more structured displacements, for example the first indication of a bar or berm profile. One could observe from figure 4.8, that the stability remains practically unchanged at different layer thicknesses for slope ranges 1:6 - 1:10. Based on these results, in combination with the matching profiles, an equal intermediate damage for different layer thicknesses was found. For example, if the proposed equation of Hofland et al. (2011) for intermediate damage would be used for a layer thickness of $5d_{n50}$, this gives an estimated intermediate damage limit between $E_{3D,3} = 1.3 - 1.5$. A matching profile according to this limit is for example profile 9_{09} of test serie slope 1:6, which significantly exceeds the level of profile development described by the definition of intermediate damage. The damage limits for S and $E_{3D,3}$ for start of damage and intermediate damage remain the same for varying layer thickness between $2.5d_{n50}$ and $5.0d_{n50}$, based on the supposed definitions of damage. The definitions of initial and intermediate damage describe the transport of rocks and groups of rocks. This relates to movements and mobility. This is different from the definition of failure damage, which is based on the properties of the armour layer of the construction.

So the slope fails if the impermeable layer or filter layer becomes visible. When this event occurs, the damage parameters are affected because the underlying layer influences the process of damage development. In the case of the mild slope test series, a wooden plank is used as an impermeable layer, so the depth can no longer increase with regard to the damage calculation. The failure limit is defined based on the visualization of the impermeable layer of the construction. Therefore a higher value of $E_{3D,3}$ damage is accepted after visual inspections of the damage profiles for thicker layers. This is in line with the stated expectation of Hofland et al. (2011) that the requirements of a structure could depend on the depth of the local damage depth. In this test series, this expectation could be confirmed by analyzing the profiles associated with the stated definition of failure. Although this study showed that the damage limit is higher due to the use of a thicker layer ($5d_{n50}$). The results indicate an equal stability number N_s for comparable wave attack. A higher stability number N_s for failure is accepted for a thicker layer ($5d_{n50}$), because the impermeable will become visible after higher wave attack. These higher values of stability N_s and damage result in an increase of the bed mobility, so a larger number of rocks are being

transported on the slope.

The damage limits for damage parameter $E_{3D,3}$ are found constant for different slope angles (1:6 - 1:10). Where the damage parameter S shows higher allowed numbers for a decreasing slope compared to constant $E_{3D,3}$ values. This is comparable to previous results Van der Meer (1988) for steep slopes. There the damage limits also vary by slope for the S parameter for a layer thickness of $2d_{n50}$, as shown in table 2.5. For example, the filter layer for slope 1:2 becomes visible at S = 8 and for slope 1:5 this occurs for S = 17. This is explained by the fact that for milder slopes there are more rocks around the still water level (SWL) that have to be displaced before the filter layer becomes visible.

The damage limit for failure is found to increase for increasing layer thickness. The maximum tested damage number for layer thickness $5d_{n50}$ is $E_{3D,3}$ = 2.5. For these values, the impermeable layer is not yet visible and therefore the damage limit of failure could not be determined yet. For layer thickness $2.5d_{n50}$ the slope fails at a damage level of $E_{3D,3}$ = 1.5. In general, the failure damage limit of S increases for decreasing slope angle, but also for a thicker layer.

This analysis supports the use of $E_{3D,3}$ in the design formula as the representation of the most applicable profile based damage parameter of mild slopes. Since the damage limits of the S parameter vary per slope angle (α) and also Iribarren number ($\xi_{m-1,0}$), this will give different results in terms of stability which differences are not present in the use-case of damage $E_{3D,3}$.

4.6.2 Design formula and applicability range

Based on the relationships obtained in the results of the test series for mild slopes in range 1:6 - 1:10 for layer thicknesses in range $2.5d_{n50} \leq T \leq 5d_{n50}$, the data from the physical model tests is compared with the design formula. The empirical design formula, valid for the application range of table 4.4 and based on figure 4.21, is given as equation 4.2:

$$\frac{H_s}{\Delta d_{n50}} = \frac{6.3 * E_{3D,3}^{0.84}}{\xi_{m-1,0} * N_{plunging}^{0.11}} \tag{4.2}$$

where:

initial damage limit	$E_{3D,3}$	= 0.3
intermediate damage limit	$E_{3D,3}$	= 0.6
min. failure damage limit	$E_{3D,3}$	= 1.5
max. $E_{3D,3}$ (T)		$= \frac{2}{5} * T + 0.5$
$N_{plunging}$		$= N_{total} * F_p$
F_p	$(0.4 \leq \xi_{m-1,0} < 1)$	$= -1.6\xi_{m-1,0}^2 + 3.3\xi_{m-1,0} - 0.7$
F_p	$(1 \leq \xi_{m-1,0} < 1.7)$	= 1

The applicability range of associated hydraulic and structural parameters of the performed tests for slope 1:6 - 1:10 are given in table 4.2:

Table 4.4: Applicability range of design formula 4.2.

Variable	Expression	Range
Stability parameter	$N_s = \frac{H_s}{\Delta d_{n50}}$	0.9 - 7.2
Slope angle	$\cot \alpha$	6 - 10
Iribarren based on $T_{m-1,0}$	$\xi_{m-1,0}$	0.4 - 1.7
3D damage	$E_{3D,3}$	$\leq \frac{2}{5} * T + 0.5$
2D damage	S	depends on slope angle (see table 4.3)
Wave steepness	s_{op}	0.01 - 0.05
Number of waves	N_{total}	250 - 20000
Layer thickness	T	2.5 - 5 d_{n50}
Fraction plunging waves	F_p	0.5 - 1.0

The acquired data is based on JONSWAP wave spectrum and the assumption of deep water wave conditions. The used characterization width w from which the calculated damage parameter $E_{3D,3}$ is determined is equal to $27 d_{n50}$. Only profiles that have not yet failed are included in the applicability range for the design formula. Therefore, the maximum damage $E_{3D,3}$ depends on the layer thickness T according to: $E_{3D,3} \leq \frac{2}{5} * T + 0.5$. Tests below $H_s < 0.02$ m are not taken into account, because these conditions are relatively sensitive to scale effects due to low Reynolds numbers.

4.6.3 Statistical measures

The design formula from equation 4.2 has been established by comparing statistical error properties. In case of a possible fit, a coefficient is assigned per variable. The optimal coefficient matching the best statistical measures can be calculated based on the relationship between the variable and the data from the physical model tests. The optimal fitting coefficients of the design formula are calculated with MATLAB programming by use of the 'lsqnonlin'-function in combination with the 'trust-region-reflective' algorithm. The 'lsqnonlin'-function solves nonlinear least-squares curve fitting problems. Randomly generated starting points within the specified lower and upper limits of the coefficients are executed for 100 iterations to find the values for the coefficients that are providing the best fit following the statistical measures ($RMSE$ and R^2). The initial start values are taken in a larger range for the first series of iterations. After completing the first series of iterations, the starting values can be fine-tuned based on the results of the coefficients. When the statistical measures are hardly improving anymore, the series of iterations is completed.

The statistical measures of the model are described as following:

1. The coefficient of determination (R^2): The R^2-value indicates how much variation of a dependent variable is explained by the independent variables in a regression model. So, if the value of R^2 provided by the MATLAB calculations is 0.50, then approximately half of the observed variation can be explained by measured data input of the model. If the value of R^2, the fitted line exactly matches the data points of the physical model tests. The traditional computation of R^2 is used by comparing the variability of the estimation errors with the variability of the original values

$$R^2 = [\frac{(n \sum xy - (\sum x)(\sum y))}{\sqrt{n \sum x^2 - (\sum x)^2} * (\sqrt{n \sum y^2 - (\sum y)^2})}]^2 \tag{4.3}$$

where:

n = number of physical model test results
x = estimated $E_{3D,3}$ following design formula
y = measured $E_{3D,3}$

2. Root Mean Squared Error (RMSE): Squared root of the quadratic mean of the differences between the predicted values of the model and the measured data. The RMSE gives insights into the performance of the regression machine learning model in MATLAB.

$$RMSE = \sqrt{\frac{1}{n}\sum_{i=1}^{n}(x-y)^2} \tag{4.4}$$

where:

n = number of physical model test results
x = estimated $E_{3D,3}$ following design formula
y = measured $E_{3D,3}$

The design formula with corresponding coefficients, statistical measures ($RMSE\&R^2$), regression line and 95% prediction interval is given in figure 4.21:

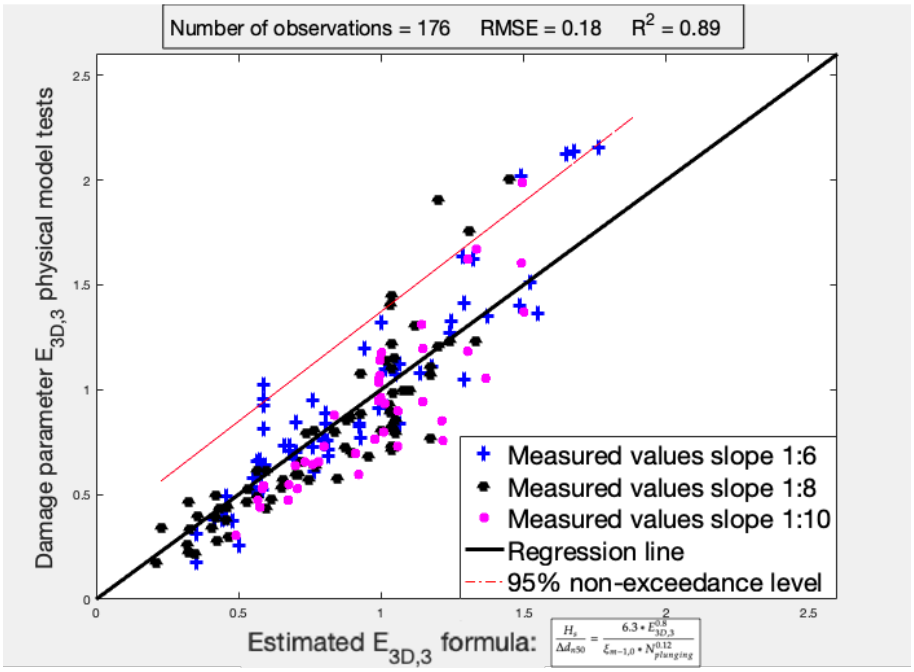

Figure 4.20: Observed damage values of physical model tests compared with predicted damage of design formula 4.2.2 for slope range 1:6 - 1:10.

Most of the observed outliers with a larger measured damage of physical model tests than predicted by use of the design formula are within range $1.5 \leq E_{3D,3} \leq 2.5$. This can be explained by the fact that only a relatively small part ($\approx$ 7%) of the tests are performed within that particular damage range. When looking for a range $E_{3D,3}$ smaller than 1.5, the outliers are tests with larger number of waves than 15000 and the test with steepest waves for slope 1:6, which gives relative higher damage compared with the other wave steepnesses of all the other performed tests.

The standard deviation σ is given as 0.27. μ as the best fit value of equation 4.2, which equals 6.3. The 95% non-exceedance value is determined by '$\mu + 1.64 * \sigma$', which gives 5.9.

To validate the reliability of the MATLAB model, the measurement results of Van Wijland (2020) and Mossinkoff (2019) were used as input for the model. The model provides the optimal coefficients

which are almost equal to the presented equation design formula of Van Wijland (2020) (equation 2.34) with a slightly smaller value RMSE. This indicates that the model works correctly and can be used for optimization purposes and also processing possible extensions of the design formula.

4.6.4 Stability of design formulas for mild slopes and Van der Meer plunging waves

As explained in the problem analysis 1.2, the reason for starting this research series for mild slopes was that the extrapolated Van der Meer (1988) plunging wave method (equation 2.30) probably reflects too conservative rock sizes due to variable influences on mild slopes. For example, the impact on the slope from spilling breaking waves. However, the plunging wave equation 2.30 is still advised in The Netherlands to be used for the design of mild slopes while this is only empirically derived for $0.75 \leq \xi_{m-1,0} \leq 7.5$. To make a comparison between the design formula for mild slopes (equation 4.2) and the plunging wave equation 2.30 of Van der Meer (1988), both graphs are displayed in figure 4.21 for Iribarren ($\xi_{m-1,0}$) with corresponding stability number (N_s):

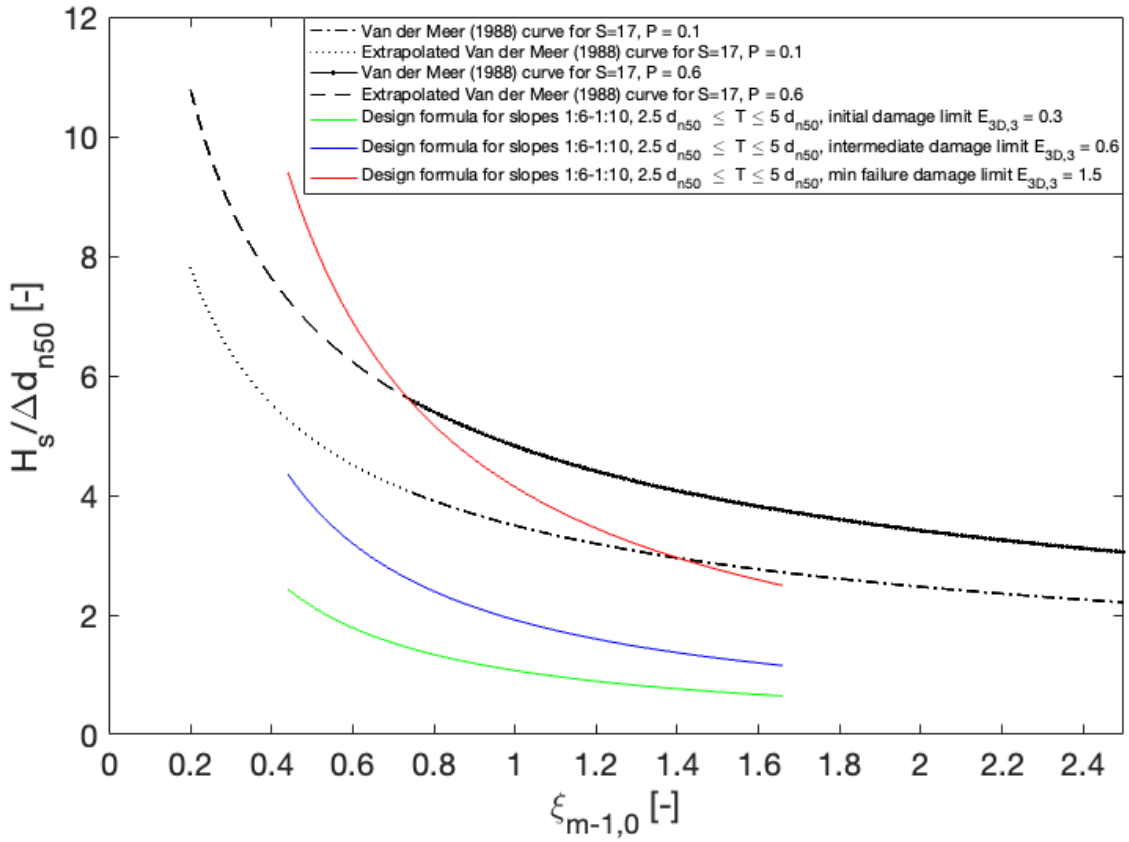

Figure 4.21: Stability (N_s) and Iribarren ($\xi_{m-1,0}$) based on design formula (equation 4.2) and Van der Meer plunging waves (equation 2.30).

Van der Meer (1988) has used the mean wave period T_m with a P-M spectrum (equation 2.5). In the Netherlands, the $T_{m-1,0}$ is used because it is seen as the period that represents wave run-up, overtopping and stability. So in practice, where a standard spectrum shape does not exist, the spectral mean energy period $T_{m-1.0}$ gives a realistic representation which can be used for the slope design (Van Gent et al., 2003). The used peak period T_p of the design formula of Van Wijland (2020) is not suitable for Dutch sea states, because the corresponding spectra can take on an odd shape in shallow water. The expected spectrum in practice is much more peaked in comparison with the used P-M spectrum of Van der Meer

(1988) and therefore the ratio T_p/T_m also varies because the spectra vary in shape. The ratio will vary if wave breaking occurs before the wave reaches the construction, then the wave periods will diverge. Since the tests were performed for deep water conditions, the conversion from T_m to $T_{m-1,0}$ may be done using a factor depending on the spectrum shape. Van der Meer (1988) has a ratio around 1.1 for T_p/T_m. It has been assumed that the ratio of the conversion for deep water in the JONSWAP spectrum is $T_{m-1,0}/T_m = 1.07$.

So the comparison shows that structures allow larger stability numbers N_s before failure occurs. A significant contributing factor is the increase of, less damaging, spilling waves for smaller Iribarren numbers $\xi_{m-1,0}$. The impact of this can be quantified by means of an example where the Dutch sea state is depicted with a certain wave steepness of 4%. For the design of a 1:6 slope, a corresponding Iribarren number of $\xi_{m-1,0} = 0.75$ can then still be used within the applicability range of Van der Meer (1988). If the stability of the design formula for mild slopes (red line) is compared with the plunging wave equation (black 'point-dot' line) for failure damage with a layer thickness of $2.5d_{n50}$ and impermeable core this results in a stability ratio of $N_{s,mildslopes} = 1.37 * N_{s,VDM}$. A higher allowable stability (N_s) results in a proportional smaller nominal rock size (d_{n50}) for the slope design. For the lowest point of the mild slope applicability range ($\xi_{m-1,0} = 0.44$), a similar comparison gives the stability ratio as $N_{s,mildslopes} = 1.78 * N_{s,VDM}$.

The line for the formula of mild slopes is close to the plunging wave equation for higher Iribarren values towards steep slopes. For failure damage and $\xi_{m-1,0} > 1.4$ the mild slopes formula gives more conservative values in comparison with the plunging wave equation 2.30. This is a small difference (< 10%) and may be due to a relatively small number of tests in that range of Irribarren (slope 1:6, low wave steepness) compared to the amount of tests available in that range for Van der Meer (1988).

4.7 Discussion of results

First, a discussion based on how the results were obtained and the possible effects that could influence the results.

- **Deep water wave conditions**

  Ratio of $T_p/T_{m-1,0}$ should be expected to be constant around 1.07 for a deep water approach. This is why it is possible to use this as a conversion factor. For the performed tests at Deltares, a minimum depth of 0.75 m is chosen to simulate deep water conditions. The first deep water criteria of $h/L_0 > 0.5$ (USACE, 2015) is not met for the longer waves. The longest waves of the test give a ratio $h/L0$ below 0.2. For these tests, the ratio $T_p/T_{m-1,0}$ varies between 1.08 - 1.14. Thus, for tests whose fulfillment of the deep water criterion can be questioned, the ratio $T_p/T_{m-1.0}$ changes. So the peak period and the energy period are further apart, which means that the spectrum is less peaked for these tests. To reduce possible effects due to differences in wave spectra maybe a larger water depth in the basin could be used.

- **Placement of rocks on slope for specific layer thickness**

  The way the slope is built requires precision. The armour layer is built up with different colours of rocks that must be able to be considered separately but also equal in layer thickness. Over the entire length of the slope, it is important that the slope is built up with this pre-specified layer thickness. In this test series, the layer thickness varied between $2.5d_{n50}$ and $10d_{n50}$, which is respectively, $\sim 0.04m$ and $\sim 0.15m$ for the used nominal rock size. These are reasonably small distances in which small differences of a number of stones can have a relatively large impact when the impermeable layer becomes visible for a certain wave attack.

- **Colour band width per slope angle**

  The reason why a test was performed with a different color band width, was because of the fact that this structural parameter influenced the equation for damage parameters based on displacements for different slope angles. As a result, an individual rock must be transported with a greater vertical distance for a steeper slope than a shallower slope to be counted as a displacement.

  When using smaller colour bands and the same amount of colour variation, it is possible that after identifying a different colour rock in a particular colour band, doubt may arise whether this is due to upward or downward transport. The DEM map, as shown in figure 3.10, can help to provide accurate insight into places where erosion occurs and therefore provides additional knowledge of the overall stereophotogrammetry method in combination with the use of colour bands.

- **Automatic detectable GCPs on hinges**

  GCPs are essentially fixed coordinates which are used to acquire the real distance in the images (section 3.1.2). By placing the GCPs on a hinge with one freedom of movement, it is managed to simulate a fixed coordinate. However, there will be a small variability in the stereophotogrammetry process. If the GCPs were fixed to the inside of the wave flume but had to be clearly visible for the pictures taken from above, the GCPs would interfere with the incoming waves. This is expected to have greater effects on the observed mechanisms and calculated damage parameters.

  In the previous studies for mild slopes, manual determination of GCPs was used, which meant that for each photo it had to be determined manually what the location of a GCP was and which number belonged to it. Recalculating the models for slope 1:8 and slope 1:10 is therefore labour-intensive. Conservatively, this method saves 20 minutes per test iteration, assuming it takes 20 seconds per photo to accurately number and identify all displayed GCPs. This equates to approximately 32 hours of work for 95 tests assuming that each manual entry of GCPs was directly completed within the stated margin of error of 1 pixel relative to the reference coordinates.

- **Scaling limits smallest waves**

  If the scale limits for physical model tests of Van der Meer (1988) are adhered to, the tests with a significant wave height H_s smaller than 0.069 m could be influenced by scale effects. The principle of cumulative testing assumes that the previous test iteration does not affect the next test. Based on this assumption, the scaling effects for small wave heights will be less pervasive in the results of tests with larger waves.

- **Use of ICP method**

  Using ICP with an initial profile as a reference profile in combination with a damaged slope can cause both profiles to be placed closer together, resulting in less damage than without using ICP. To take into account this effect, the threshold accuracy resulting from the check test method is used to both subtract and add this value ($5 * 10^{-4}$) from the profile. So that the largest possible error is calculated. Independent if there would be less or more damage following from the use of the ICP method.

- **Measurement accuracy of physical model tests**

  The measurement accuracy of the physical model tests for mild slopes is characterized by the check test accuracy, the stereophotogrammetry accuracy, the variability and the sampling error.

  The check test method is used to measure the maximum difference between identical undamaged profiles. Based on 56 comparable inputs (table I.1), the largest observable measurement error from the check tests is given as $5 * 10^{-4}$. This value could be taken smaller using a 90% or 95% percentile value. This could affect the determination of damage parameter S, in which this threshold value is used to find the area for the maximum erosion area greater than that threshold. Of course, if another surface is seen as the normative erosion area $A_{(e),w}$, then the damage parameter S can also be influenced. This check test accuracy is used to determine the accuracy of the stereophotogrammetry method.

The maximum deviation of an undamaged profile is added and subtracted from the reference profile of each test. From this approach, the measurement error can be expressed per damage parameter, as shown in tables 3.4 (2D) and 3.5 (3D).

The variability of the damage parameters can be considered from the results in table 4.1. The variability indicates the differences that can occur if the same steering files are used in the wave machine and the slope is rebuilt in between. For the variability, only 1 test was performed per slope in range 1:6-1:10, so that the number of damage parameters to be compared results from 16 test iterations. To give a more reliable representation of the variability, several tests per damage level should be performed.

The uncertainty for performing completely new tests is described by the sampling error. If the tests had been performed with a slope twice as wide, this would also have influenced the outcome of the damage parameters. For the sampling error, the longitudinal slope can be divided into 5 strips in order to gain more insight into the sampling error and possibly the first quantified insight into longitudinal transport. This has not yet been done and therefore it is difficult to conclude what the measurement accuracy is of the entire physical model test method.

For the comparison of the measurement accuracy between the slopes 1:6,1:8 and 1:10, it is likely that the quality of the camera provides a more accurate representation of the 3D model. The input for the stereophotogrammetry method for slope 1:6 differs from the use of an improved camera due to the use of masks, so that the number of points included for the point cloud contained up to 8 times more data compared to the point clouds of slope 1:8 and 1:10, as shown in table 3.6.

An opportunity would have been to directly compare the data points for slope 1:6 with the similar data points used by Van der Meer (1988) for this slope. These measurement deviates far from the current stereophotogrammetry method, it was considered not to perform this comparison in this way. The measurement method of Van der Meer (1988) used box counting to map the 2D erosion area. This is difficult to compare with the advanced technique with 3D models by use stereophotogrammetry. The plunging wave equation is compared with regard to stability, but no comparisons are made for individual data points.

Discussion from the presented results:

- **Damage parameters**

  For the results various profile based damage parameters have been calculated to investigate relationships between the governing hydraulic and structural parameters. Each damage parameter focuses on specific properties and is based on other fundamentals, which can be discussed for the aim of designing mild slopes.

  S and S_{all} are 2D parameters based on the size of the erosion area ($A_{(e),w}$). These damage parameters do not depend on the depth of the erosion (d_e), while the failure of the slope is defined by exposing the impermeable layer or filter layer. Figure 4.13 shows that the damage domains of slope 1:6 is more concentrated in comparison with slope 1:8 and 1:10. This indicates that for milder slopes the erosion length increases, so it is expected that with milder slopes a higher allowable S value can actually be determined without the impermeable layer already having to be visible. This could also be the other way around if there is a large damage impact on a relatively small area, this phenomenon is considered hidden erosion by de Almeida et al. (2019). This expectation was established by looking for matching profiles in the definitions of the damage limits (table 4.3), in which the maximum permissible S increases for a milder slope. This makes for a difficult representation with regard to the stability graph (figure 4.21). The fact that $S_{failure}$ varies per slope and thus per Iribarren number substantiates that a 3D damage parameter is more suitable regarding the characteristics of mild slopes. E_{2D} does not depend on the erosion area ($A_{(e),w}$) but only on the depth d_e. In theory, this could be used to identify slope failure. If a proper damage limit could be assigned with a maximum allowable damage depth d_e.

  The used 3D parameter ($E_{3D,m}$) are based on a spatial moving average of m = 1, 3 or 5 d_{n50}. A displacement of a single rock, which has a relative low impact to the stability of mild slopes,

can have a large impact on the damage parameter $E_{3D,1}$ because of the used moving average of $1d_{n50}$. Table 4.1 shows that further research is needed to establish a direct link between results from non-cumulative and cumulative methods. $E_{3D,1}$ is considered as sensitive and therefore the measurement accuracy could not have been validated yet. The design formula of mild slopes is based on $E_{3D,3}$, because this parameter gives the most reliable results regarding the stereophotogrammetry (table 3.5) and variability (table 4.1) compared to $E_{3D,5}$. This ensures confidence in the measured damage and the predicted damage. An advantage of using $E_{3D,3}$ is that the value defined as slope failure remains equal for a varying slope (1:6 - 1:10). This makes it possible to make an efficient design for mild slopes independent of the slope angle and identify the different stages of damage development on the slope according to one set of established damage limits of $E_{3D,3}$ (table 4.3). A disadvantage is that the use of damage parameter $E_{3D,m}$ is still very limited in contrast to more widely used damage parameter S.

- **Acceptable damage limits for a design**

  Initial and intermediate damage are described using a definition based on the movement of rocks and groups of rocks. This indicates a process based on displaced rocks and thus mobility. Another approach is used for the failure damage limit definition. This limit is reached when the impermeable layer becomes visible. To define this more specifically, use is made of the property that the 'visibility' of the impermeable layer is indicated by an erosion hole with a diameter of $1d_{n50}$. In theory, failure should then equals $E_{3D,1} = 2.5$ for a layer thickness of $2.5d_{n50}$. From a design point of view, it can be stated that if a layer thickness of at least $1d_{n50}$ is maintained over the entire slope area, this could be an acceptable damage limit for a construction. An acceptable damage limit corresponds to a depth of $1.5d_{n50}$ detected by a moving average of $1d_{n50}$. Therefore, an acceptable damage limit for the design could be assigned as $E_{3D,1} = 1.5$. These two situations can be visualized using figure 4.22:

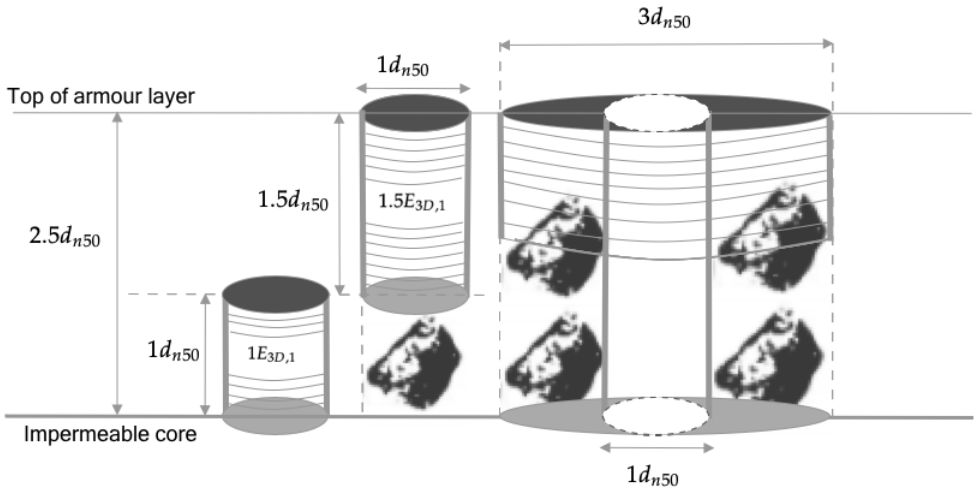

Figure 4.22: Visualization of remaining layer thickness identification for $E_{3D,1}$ and $E_{3D,3}$.

Figure 4.22 illustrates that a moving average of $1 * d_{n50}$ can be used to determine the value for the failure limit. This theoretical value of $E_{3D,1}$ for an acceptable design is compared with the normative damage parameter for mild slopes $E_{3D,3}$ according to the test results.

Since it has been found that stability and hence mobility increases for higher damage levels. A thicker armor layer has no significant influence on this. Therefore, for the layer thickness of $5d_{n50}$,

it is not recommended to use the same approach for a remaining layer of $1d_{n50}$. With increasing load and accepting higher damage levels, the mobility of rocks significantly increases. A more conservative approach to a design value for $T = 5d_{n50}$ is used so that at least half of the remaining layer thickness on the slope is stable. This is equivalent to $E_{3D,3}$ of 1.5. The acceptable damage limits for a mild slope design are presented in table 4.5:

Table 4.5: Acceptable design limits of $E_{3D,3}$ for $T = 2.5d_{n50}$ and $T = 5d_{n50}$.

Initial layer thickness	**Remaining armour layer**	**max(E_{3D1})**	**max(E_{3D3})**
2.5 d_{n50}	1 d_{n50}	1.5	0.9
5 d_{n50}	2.5 d_{n50}	2.5	1.5

An acceptable damage limit for a design of the construction with $T = 2.5d_{n50}$ lies between $E_{3D,3} = 0.6$ (intermediate) and $E_{3D,3} = 1.5$ (failure). It is recommended to remain at least $1d_{n50}$ layer thickness. This corresponds to an $E_{3D,3}$ of 0.9 according to a number of 28 tests. This acceptable damage limit is considered based on the constructional properties of the slope with respect to the remaining layer thickness. Especially for the thicker layer this means that it is possible for a volume of rocks to become mobile. This could have effects on stability, which should be taken into account.

For a construction with $T = 5d_{n50}$, it is recommended to remain half of the armour layer ($2.5d_{n50}$). The acceptable damage limit is indicated as $E_{3D,3} = 1.5$ based on a number of 7 tests and the failure damage limit of $T = 2.5d_{n50}$.

- **Characterization width and length effect**

  The determination of the variability is based on a characterization width of $54d_{n50}$ for the parameters used. The design formula (equation 4.2) and damage limits (table 4.3) are based on a characterization width of $27d_{n50}$. When using a characterization width larger than the optimal $25d_{n50}$ (de Almeida, 2017), the length effect is taken into account. The length effect should be considered regarding the expected maximum damage that can be observed in a structure wider than the one tested in the physical model tests. Research by de Almeida et al. (2019) has shown that there are fundamental differences between 2D and 3D parameters with regard to characterization width and the length effect. This is reflected in the fact that S and E_{2D} become increasingly stable for a characterization width larger than $25d_{n50}$. 3D damage parameters $E_{3D,m}$ will increase with increasing characterization widths. So for the design of mild slopes based on $E_{3D,3}$, the length effect should be taken into account. This also ties in with the fact that longitudinal transport will also play a role for wider characterization widths. This has not yet been taken into account in the results in this test series for mild slopes.

- **Notional permeability**

  The method of Eldrup and Andersen (2019) is investigated to gain insight into the use of the notional permeability factor for mild slopes. The possibility was considered to include this factor P, according to method of Eldrup and Andersen (2019), in the design formula. If you were to assign a constant P-value to the layer composition and make calculations based on that for expected damage, as for example with the formula of plunging waves Van der Meer (1988), you run the risk that other boundary conditions in this fitted parameters get clogged. It is observed that the expected notional permeability P become more inaccurate for slope 1:8 and 1:10 (table 4.10). The notional permeability P is a empirical coefficient which has not been designed for slopes 1:8 and 1:10. In order to use it as intended by Eldrup and Andersen (2019), it is recommended to extend this method based on test data for mild slopes.

- **Stability of bed for mild slopes**

  The stability of the bed is described on the basis of the gained knowledge that the tested range of mild slopes behaved somewhere between statically stable and dynamically stable structures.

Through this test series, damage parameter $E_{3D,3}$, associated damage limits and ratio S_{od}/S are examined as suitable to give an indication of the stability.

Steep slopes are often designed as statically stable structures. This design assumes that any rock that displaces can no longer fulfill a function in terms of stability, so any movement is considered erosion ($S_{od} = S$). Dynamic stability is based on achieving deformation towards equilibrium through a combination of upward and downward transport. A difference in normative transport direction has even been observed for similar wave characteristics with a different layer thickness. In this study it was investigated for which damage numbers of $E_{3D,3}$ the impermeable layer became visible for a layer thickness of 2.5 and 5.0 d_{n50}, which is defined as failure of the bed. If it can be assumed that designing for bed failure based on the tests is possible, then the ratio S_{od}/S should also be critically examined. With the ratio S_{od}/S a measure can be given about how many movements are allowed with regard to erosion. If one assumes that longitudinal transport is also present, it could be that a realistic situation is sketched by the fact that more displacement contributes to erosion, ratio S_{od}/S decreases, than would be the case in the test situation.

5
Conclusion & Recommendations

Chapter 5 provides conclusions and recommendations regarding the research series development in order to contribute to the understanding of stability on mild slopes.

5.1 Conclusion

Section 5.1 concludes the acquired knowledge for an accurate design of mild slope structures, by following the formulated research objective from section 1.3:

'Describe the stability of rock slopes under wave attack in the transition zone of breaking waves between mild and steep slopes to provide insights into governing processes and quantified damage characteristics in order to contribute to an efficient design method.'

In order to meet this objective, 5 research questions have been defined:

1. **How do the governing hydraulic and structural parameters influence the damage on mild slopes?**

   The normative parameters are plotted against the damage in order to observe correlations. The significant wave height has a positive correlation to damage (figure 4.6). This is due to the fact that a higher significant wave height is associated with a larger wave energy. So more energy will be deflected on the bed which gives a larger impact on the damage. Per slope angle, the tests with a higher wave steepness result in lower damage which gives a negative correlation.

   A clearly observable relationship is that for an increasing slope angle, the difference in damage between wave steepnesses is larger. So the slope angle has impact on the strength of the negative correlation between wave steepness and damage (figure 4.5). This knowledge is extended by the observation that for increasing slope angle, the Iribarren number increases and the percentage of plunging waves increases (figure 4.16). Plunging waves have more impact on the slope and cause more damage, so for mild slopes a positive correlation between slope angle and damage is observed. The effects of Iribarren and the distribution of spilling and plunging waves is further described at question 2 and 5.

   The number of waves for slope 1:6 shows a positive quadratic relationship to damage (figure 4.12) and satisfies the stated theoretical requirement of Van der Meer (1988) for this gradient in comparison with damage parameter S (figures 4.11). For slopes 1:8 and 1:10 the damage is linear increasing, tested respectively until 15000 and 10000 waves.

   A varying layer thickness of 2.5, 5 and 10 d_{n50} showed no structural and discernible differences regarding damage parameters based on a comparison with the significant wave height (figure 4.7). Simultaneously, the damage profiles and location of erosion are changing, which is described at question 3. To delve deeper into this analysis regarding quantified damage, four $E_{3D,3}$ damage zones were defined from which the tests could be compared in terms of stability and Iribarren (figure 4.8). These results clearly indicate that the layer thicknesses of 2.5 and 5 d_{n50} have no

influence on the stability. For a layer thickness of $10d_{n50}$ only one test is performed, which offers too little information to draw a conclusion.

Damage based on displacements (N_{od} and S_{od}) are affected by the colour band width. The use of a smaller colour band, $w = 0.1m$ instead of $w = 0.5m$, has the consequence that more displacements are taken into account to calculate damage (figure 4.17). This results in more representative numbers of N_{od} and S_{od}, which could be used to differentiate between mild and steep slope characteristics.

The determination of whether a displaced stone directly contributes to erosion is determined on the basis of the ratio between mobility (N_{od} and S_{od}) and erosion of the entire slope area (S_{all}). As a result, the ratio S_{od}/S_{all} is smaller than 1 for mild slopes (figure 4.19). This value indicates that the mobility in relation to the erosion is larger than for a steep slope. It can be concluded that mild slopes experience more displacements than actual erosion on the slope, because rocks move back and forth without causing erosion. For steep slopes all displacements are considered as erosion, making the ratio S_{od}/S. Therefore, the mobility-erosion ratio is equal to 1 for steep slopes and decreases sharply with mild slopes, so that the values of mobility (S_{od}) and erosion (S) diverge strongly.

2. **How do the influences of the changing distribution of plunging and spilling waves on mild slopes evolve based on the Iribarren number?**

   The influences of the distribution of plunging and spilling waves (figure 4.16) on mild slopes aligns with the positive correlation between Iribarren and damage described at question 1.

   A first observation shows that the general stability of mild slopes increases as the distribution contains a higher percentage of spilling waves. This is due to the characteristic less damaging energy distribution of a spilling wave (figure 2.5). A second observation is that as the percentage of spilling waves shifts to just plunging waves, the influence on stability decreases (4.5). When observing the stability graph of figure 4.21, this effect is visible as a more constant tangent ($\frac{\Delta N_s}{\Delta \xi_{m-1,0}}$) for a shift in the distribution towards plunging waves.

   The fraction of plunging waves for a certain Iribarren number ($0.4 \leq \xi_{m-1,0} \leq 1.7$) can be determined based on a quadratic fit on the distribution of plunging and spilling waves:

$$\begin{cases} 0.4 \leq \xi_{m-1,0} < 1; & F_p = \frac{N_{plunging}}{N_{total}} = -1.6\xi_{m-1,0}^2 + 3.3\xi_{m-1,0} - 0.7 \\ 1 \leq \xi_{m-1,0} \leq 1.7; & F_p = \frac{N_{plunging}}{N_{total}} = 1 \end{cases}$$

   After the distribution reaches 100% plunging waves at approximately $\xi_{m-1,0} = 1$, the distribution is considered to be fully plunging. Since the former used design formula for mild slopes (equation 2.30 of Van der Meer (1988)) is based on only plunging waves, it can be examined how this relates to highest segment of Iribarren numbers for the mild slope test series. This is discussed further in question 5.

3. **How are the damage characteristics on mild slopes quantified and on the basis of which processes and mechanisms does this occur ?**

   3D damage shows a lower bias error compared to width-averaged profiles for mild slopes. This means that local damage based on depth in combination with a spatial moving average ensures that the normative erosion is identified. Based on the highest stereophotogrammetry accuracy and the lowest variability for comparable wave characteristics, $E_{3D,3}$ is considered the normative damage indicator for mild slopes.

   Based on the described definitions of damage limits (start, intermediate and failure) matching profiles have been selected per slope angle that correspond to a certain limit. The values of the damage limits remain constant per slope and layer thickness for start of damage at $E_{3D,3} = 0.3$

and intermediate damage at $E_{3D,3} = 0.6$. Since it has been observed that a doubled layer thickness ($5d_{n50}$ instead $2.5d_{n50}$) does not show significant effect on the stability numbers, but it does affects damage profile development and the location of maximum erosion. The damage limit for failure is found to increase for increasing layer thickness. The maximum tested damage number for layer thickness $5d_{n50}$ is $E_{3D,3} = 2.5$. For these values, the impermeable layer is not yet visible and therefore the damage limit of failure could not be determined yet. For layer thickness $2.5d_{n50}$ the slope fails at a damage level of $E_{3D,3} = 1.5$.

It has been observed that for the same wave characteristics and a varying layer thickness there can be a difference between normative transportation direction 4.1. Figure 4.2 shows in 2D that varying layer thicknesses are subject to different processes that correspond with a specific type of damage development (bar/berm profile). An explanation has been given based on the processes of reflection and transmission in combination with the run-down mechanism. A smaller layer thickness relates with normative downward transport and a bar profile. This is due a higher exposure to the run-down and reflection of the impermeable layer. For tests with an increased layer thickness accompanied by an increased volume of voids, the water flow can dissipate more easily into the thicker layer. This results that for all tests with an increased layer thickness most rocks are pushed upwards, creating berm damage profiles. Therefore, the outer rocks of the armour layer are barely exposed to the strong wave run-down. The run-down mechanism is less significant because of increased permeability of the bed, which corresponds with the process of transmission.

4. **What is an efficient design method for stability of rocks on mild slopes?**

The design method is based on data obtained from stereophotogrammetry and damage calculations of non-failed slope profiles. This data is considered the input for the model to develop a design formula for mild slopes. An improved way of measuring physical model testing through the use of automatically detectable GCPs and the use of masks provides accurate input. An advantage of this is that the results are reproducible and that the automated scripts (appendix F) can be used to process more test results in a shorter time. The input data of the design method can also be visibly checked on the basis of detailed 3D models. By using $E_{3D,3}$ as the normative damage parameter for mild slopes, the input for the model is more reliable. The spectral mean energy period $T_{m-1,0}$ is in general the normative period measure for design with regard to wave run-up, overtopping and stability. The use of correct parameters for mild slope properties contributes the design method presented as:

$$N_s = \frac{H_s}{\Delta d_{n50}} = \frac{c_{pl} * E_{3D,3}^{0.84}}{\xi_{m-1,0} * N^{0.12}}$$

where:

initial damage limit $E_{3D,3}$	$= 0.3$
intermediate damage limit $E_{3D,3}$	$= 0.6$
min. failure damage limit $E_{3D,3}$	$= 1.5$
max. $E_{3D,3}$ (T)	$= \frac{2}{5} * T + 0.5$
$N_{plunging}$	$= N_{total} * F_p$
$F_p \quad (0.4 \leq \xi_{m-1,0} < 1)$	$= -1.6\xi_{m-1,0}^2 + 3.3\xi_{m-1,0} - 0.7$
$F_p \quad (1 \leq \xi_{m-1,0} < 1.7)$	$= 1$

Depending on the design phase, the coefficient c_{pl} can be used as a best fit or 95% non-exceedance value. These corresponding numbers are displayed in table 5.1:

Table 5.1: Coefficients for best fit (μ) and 95% non-exceedance limit for mild slope design method.

Coefficient	**Average value (μ)**	**Standard deviation, σ of the coefficient**	**95% non-exceedance ($\mu - 1.64 * \sigma$)**
c_{pl}	6.3	0.3	5.9

An algorithm was used as a fitting tool to determine the coefficients with the corresponding acceptable statistical measures ($RMSE\&R^2$). In order to agree with safety norms in practice, only the construction with a larger nominal rock diameter would previously be the solution for mild slope design. With this method also a different approach is presented by increasing layer thickness, due to the found constant stability for a varying layer thickness ($2.5 \leq T \leq 5d_{n50}$).

For $T = 2.5d_{n50}$, an acceptable damage limit is $E_{3D,3} = 0.9$, which corresponds to a remaining armour layer of $1d_{n50}$. For $T = 5d_{n50}$, an acceptable damage limit is $E_{3D,3} = 1.5$, which corresponds to a remaining armour layer of $2.5d_{n50}$. A higher wave load results in a higher damage level, higher stability number and more rock displacements. For $T = 5d_{n50}$, a more conservative approach for the remaining layer is important due to the significant increase of bed mobility. Based on the findings, a higher damage limit can be set for a thicker layer thickness, which contributes to an efficient construction method of mild slopes.

The stability graph shown for the acceptable damage design values in figure 5.1:

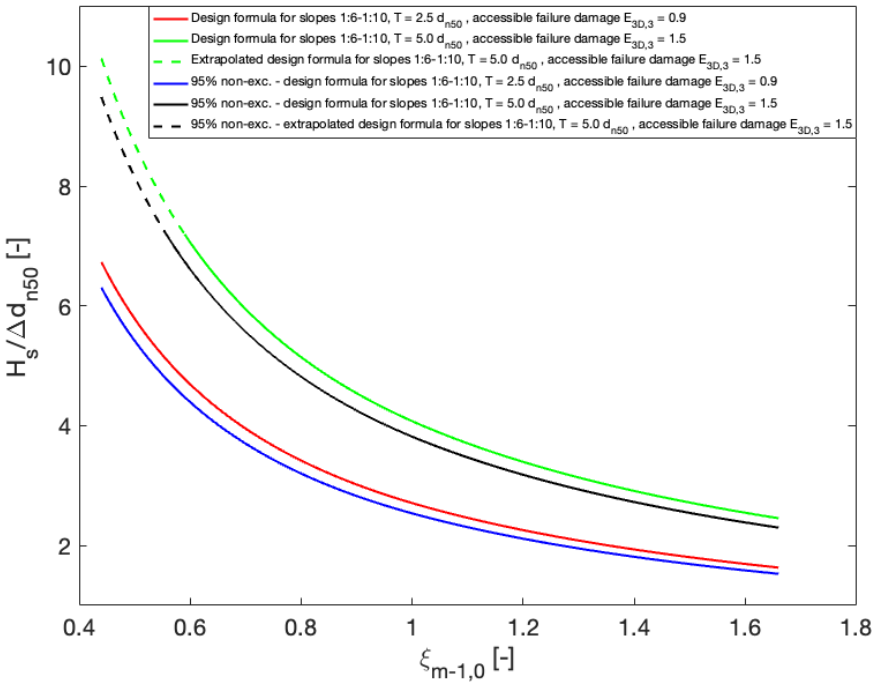

Figure 5.1: Design formula with acceptable damage limits

The green and red lines represent the best fit ($c_{pl} = 6.3$) of the design formula. The 95% non-exceedance value ($c_{pl} = 5.9$) is represented by the blue and black lines. The design formula is valid until $N_s = 7.2$ and can be used up to value for mild slope design. When designing for for higher stability numbers, an extrapolation is indicated by the dotted line, which is not validated.

5. **How is the design method for mild slopes related to the steep slopes test series of Van der Meer (1988)** ?

   The higher segment of tested Iribarren numbers for the mild slopes design method corresponds to the lower segment of Iribarren numbers for the test series of Van der Meer (1988). The region of overlap is indicated as $0.75 \leq \xi_{m-1,0} \leq 1.66$. The tests performed with slope 1:6 are within this overlap region and showed for $\xi_{m-1,0} > 1$ almost only plunging waves (figure 4.16), which in theory fits well with the fundamental determination of the Van der Meer (1988) method for plunging waves.

   To determine how the two methods relate to each other in terms of stability, the wave spectra used must be taken into account. Both methods are based on a deep water wave assumption, with a PM-spectrum used for Van der Meer (1988) and a JONSWAP spectrum for mild slopes design. As a result, a factor of $\xi_{m-1,0} = 1.07 * \xi_m$ was used to make the conversion between both methods regarding stability.

   The ratio between both tests series compared for failure damage for an impermeable core with a layer thickness of $2.5d_{n50}$ is described for four values of Iribarren:

   - Lowest point of mild slopes series: $\xi_{m-1,0} = 0.44$, gives $N_{s,mildslopes} = 1.78 * N_{s,VDM}$. So design formula 4.2 gives a higher stability compared to the extrapolated method of Van der Meer (1988).
   - Lowest point of steep slopes series: $\xi_{m-1,0} = 0.75$, gives $N_{s,mildslopes} = 1.36 * N_{s,VDM}$. So design formula 4.2 gives a higher stability compared to method of Van der Meer (1988).
   - $\xi_{m-1,0} = 1.40$, gives equal stability for both methods.
   - Highest point of mild slopes series: $\xi_{m-1,0} = 1.66$, gives $N_{s,mildslopes} = 0.92 * N_{s,VDM}$. So design formula 4.2 gives slightly less stability compared to method of Van der Meer (1988).

   It can be concluded that for $\xi_{m-1,0} < 1.4$ up to a 78% smaller nominal rock size can be used for the design compared to the previously used (extrapolated) Van der Meer (1988) method.

5.2 Recommendations

In this research series for mild slopes, slope angles 1:6, 1:8 and 1:10 were tested at Deltares by means of physical model tests. Based on this whole series, recommendations are made that can contribute to this research and future analyses. These are described as follows:

- Based on the stereophotogrammetry method, a new measure can be developed with which the layer thickness can be verified in advance when building up the slope as the correct layer thickness within a certain range of deviation. This range of deviation could, for example, be given by a maximum deviation of $\pm 15\% d_{n50}$. This could be achieved by comparing an impermeable layer with an initial profile and only agreeing for the test series if the deviation is within the stated requirement.
- Since the damage profiles of tests with the same wave characteristics but a varying layer thickness differ in bar and berm profile and normative transportation direction, it could be meaningful to analyze at which location the wave breaks on the slope. This can be done by means of the camera images filming the slope from above.
- Using too large colour bands can result in fewer displacements being observed than actually taking place. Creating small colour bands in physical model tests takes much time to construct. An analysis could be performed to scale the colour band width for various slopes and normative wave heights for future physical models tests. Based on this analysis, it might also be possible to create a conversion method to compare damage parameters based on displacements.
- Since designs are made based on damage limits, it is recommended for the execution of future physical model tests to observe the transition between the different damage described damage limit definitions based on the results. An improvement regarding acceptable damage limits for thicker layer can be made based on an integrated design approach regarding mobility, erosion and layer thickness.
- In steep slopes the ratio S_{od}/S is almost 1 because every displacement is linked to erosion. Based on the increase of the S_{od}/S ratio for mild slopes, the possible influence of longshore transport becomes important. It is perhaps too opportunistic to assume that if a displacement does not directly contribute to erosion, then the displaced rock contributes to stability. To gain more knowledge about the contribution to stability of displaced rocks, further research could be carried out with wider slopes and oblique incoming waves. This provides insight into the length effect, longshore transport and possible influence of oblique incoming waves.
- Explore possible extensions to the use of notional permeability regarding the empirical method of Eldrup based on results of the mild slope test serie.
- To give a more reliable representation of the variability, several tests per damage level should be performed. For the sampling error, the longitudinal slope can be divided into 5 strips in order to gain more insight into the quantification of the sampling error.
- It is recommended to perform additional tests for some tests for which less data is available. For slope 1:10, very limited data is available with a layer thickness of $5d_{n50}$. The completion with a $10d_{n50}$ layer thickness for slopes 1:6 - 1:10 for varying wave steepness would provide a more complete conclusion for the influence of layer thickness on stability.
- Sample all fitting coefficients of the design formula of mild slopes using a bootstrap method. As a result, the confidence interval can be determined separately for each coefficient. This insight is useful for probabilistic design of hydraulic structures.

Bibliography

Agisoft. (2021). Agisoft metashape user manual: Professional edition, version 1.7.

Battjes, J. (1974). Computation of set-up, longshore currents, run-up and overtopping due to wind-generated waves.

Broderick, L., & Ahrens, L. (1982). Riprap stability scale effects.

Buckley, W., Pierce, R., Peters, J., & Davis, M. (1984). Use of the half-cycle analysis method to compare measured wave height and simulated gaussian data having the same variance spectrum. *Ocean Engineering*, *11*(4), 423–445. https://doi.org/doi:10.1016/0029-8018(84)90014-3

CIRIA. (2007). The rock manual, the use of rock in hydraulic engineering.

CloudCompare. (2016). Cloudcompare: 3d point cloud and mesh processing software open source project.

de Almeida, E. S. (2017). Damage assessment of coastal structures in climate change adaptation [Erasmus Mundus Master in Coastal and Marine Engineering and Management (CoMEM)].

de Almeida, S., E., Van Gent, M. R. A., & Hofland, B. (2019). Statistical analysis of the stability of rock slopes. *Marine Science and Engineering*, *60*(7). https://doi.org/10.3390/jmse/7030060

DELOS. (2000). Environmental design of low crested coastal defence structures.

Eldrup, M., & Andersen, T. (2019). Stability of rubble mound breakwater - a study of the notional permeability, based on physical model tests. *Water*, *11*(934), 20. https://doi.org/doi:10.3390/w11050934

Frostick, E., L., McLelland, S., & Mercer, G., T. (2011). Users guide to physical modelling and experimentation: Experience of the hydralab network.

Goda, Y. (1986). Effect of wave tilting on zero-crossing wave heights and periods. *Coastal Engineering in Japan*, *29*(1), https://doi.org/10.1080/05785634.1986.11924429, 79–90. https://doi.org/10.1080/05785634.1986.11924429

Hasselmann, K., Barnett, T., Bouws, E., Carlson, H., Cartwright, D., & Enke, K. (1973). Measurements of wind-wave growth and swell decay during the joint north sea wave project (jonswap).

Hofland, B., Disco, M., & Van Gent, M. (2014). Damage characterization of rubble mound roundheads [Coastlab].

Hofland, B., Van Gent, M., Raaijmakers, T., & Liefhebber, F. (2011). Damage evolution using the damage depth [DOI: 10.1142/9789814412216$_0$070].

Holthuijsen, L. H. (2007). *Waves in oceanic and coastal waters* (3rd). New York, Cambridge University Press.

Hudson, R. (1953). Wave forces on breakwaters.

Iribarren, R. (1938). A formula for the calculation of rock-fill dikes.

Jensen, J., O., & Klinting, P. (1983). Evaluation of scale effects in hydraulic models by analysis of laminar and turbulent flows.

Jumelet, D. (2010). *The influence of core permeability on armour layer stability* (Master's thesis). Delft University of Technology.

Kik, R., Van den Bos, J., Maertens, J., Verhagen, H., & Van der Meer, J. (2012). Introduction to bed, bank and shore protection.

Kramer, R. (2016). *Stability of rock on mild slopes under wave attack* (Master's thesis). Delft University of Technology.

Mansard, E., & Funke, E. (1998). The measurement of incident and reflected spectra using a least-square method.

Melby, J., & Kobayashi, N. (1998). Progression and variability of damage on rubble mound breakwaters [124, 286–294].

Mossinkoff, L. (2019). *Stability of stones on mild slopes under wave attack* (Master's thesis). Delft University of Technology.

Ocean Conference, . (2017). Ocean fact sheet.

Pierson, J., W., & Moskowitz, A., L. (1964). Proposed spectral form for fully developed wind seas based on the similarity theory of s. a. kitaigorodskii.

Postma, M. (2016). *Xbeach-g as a design tool for rock on mild slopes under wave loading* (Master's thesis). Delft University of Technology.

Reijmerink, S., Jong, M., & Hout, A. (2020). North sea conditions on 1 and 2 january 2019.

Schiereck, G. (2016). *Introduction to bed, bank and shore protection* (2nd) [updated by H.J. Verhagen]. Leeghwaterstraat 42, NL2628CA Delft, The Netherlands, Delft Academic Press / VSSD.

Shiereck, J., G., Henri, L., Fontijn, W., & Sistermans, J. (1994). Riprap design for wind-wave attack, a laboratory study in random waves.

Thompson, D., & Shuttler, M. (1975). Riprap design for wind-wave attack, a laboratory study in random waves.

USACE. (2015). Coastal engineering manual (cem) 1110-2-1100.

Van der Meer, J. W. (1988). *Rock slopes and gravel beaches under wave attack* (Doctoral thesis). Delft University of Technology.

Van Gent, M. (2004). On the stability of rock slopes [Symposium in Varna].

Van Gent, M. (2014). Oblique wave attack on rubble mound breakwaters. [DOI: 10.1016/j.coastaleng.2014.02.002].

Van Gent, M., Smale, A., & Kuiper, C. (2003). Stability of rock slopes with shallow foreshores.

Van Wijland, J. (2020). *Stability of rock on mild slopes* (Master's thesis). Delft University of Technology.

Wendt, E. (2017). *Stability of stones on mild slopes* (Master's thesis). Delft University of Technology.

Wit, E. (2015). *Stability of gravel on mild slopes in breaking waves* (Master's thesis). Delft University of Technology.

List of figures

List of tables

A Flowchart parameters

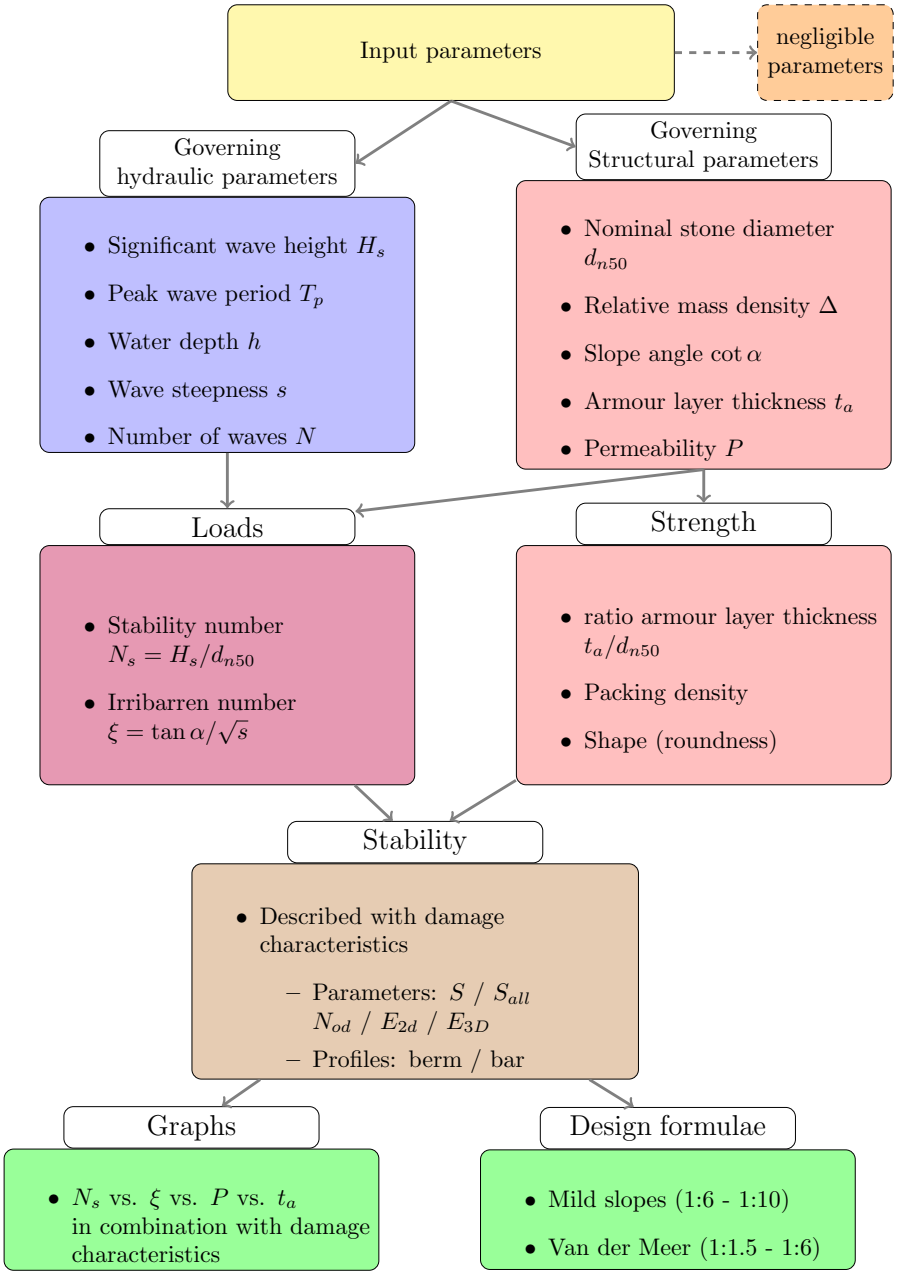

Figure A.1: Flowchart of input parameters to graphs and design formulae

B
Notional permeability

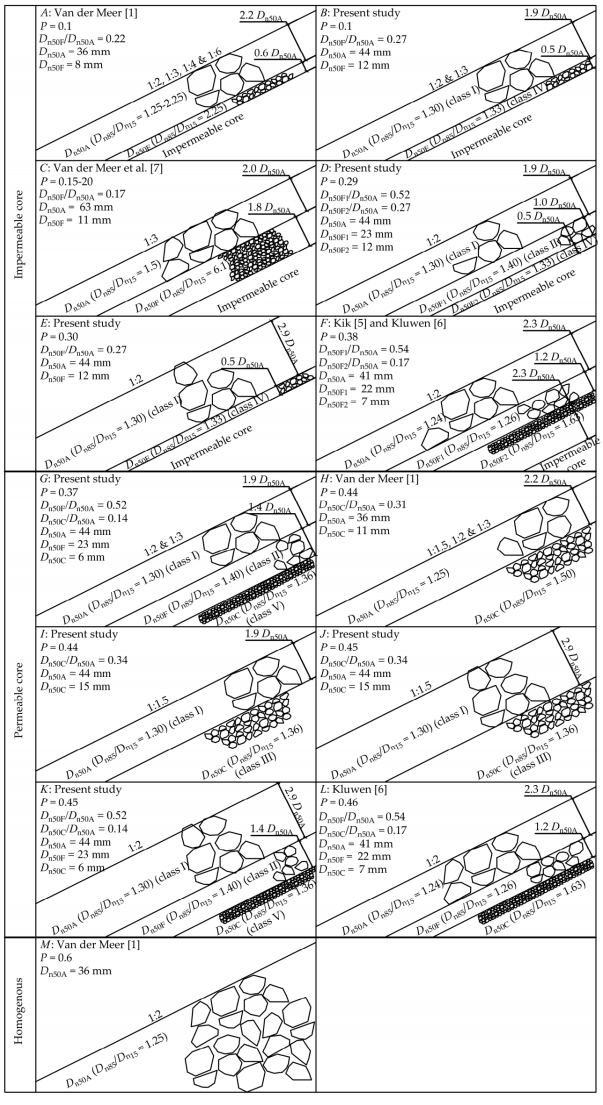

Figure B.1: Fitted notional permeability factor of different layer compositions

A, H and M: Van der Meer ; B, D, E, G, I, J and K: Eldrup et al. 2019 ; F: Kik and Kluwen ; L: Kluwen ; C: Van der Meer et al.

Table B.1: Estimation of notional permeability factor for test conditions slope 1:6 and slope 1:8 (Van Wijland (2020)) and following the method Eldrup and Andersen (2019).

			Impermeable core								
			One rock layer armour ($2.5D_{n50}$)			One rock layer armour ($5D_{n50}$)			One rock layer armour ($10D_{n50}$)		
Description	**Symbol**	**Unity**	**Armour**	**Filter**	**Core**	**Armour**	**Filter**	**Core**	**Armour**	**Filter**	**Core**
Density of the stone	ρ_s	$[kg/m^3]$	2944	-	-	2944	-	-	2944	-	-
Nominal rock size	d_{n50}	[m]	0.0148	-	-	0.0148	-	-	0.0148	-	-
Layer thickness	t_a	[m]	0.037	-	-	0.074			0.148		
Relative layer depth	z_1^*	-	0	2.5	2.5	0	5	5	0	10	10
	z_2^*	-	2.5	2.5	13	5	5	13	10	5 10	13
Integration function	k	-	0.99	0	0	1.20			1.25		
Notional permeability	P	-	0.12			0.48			0.57		

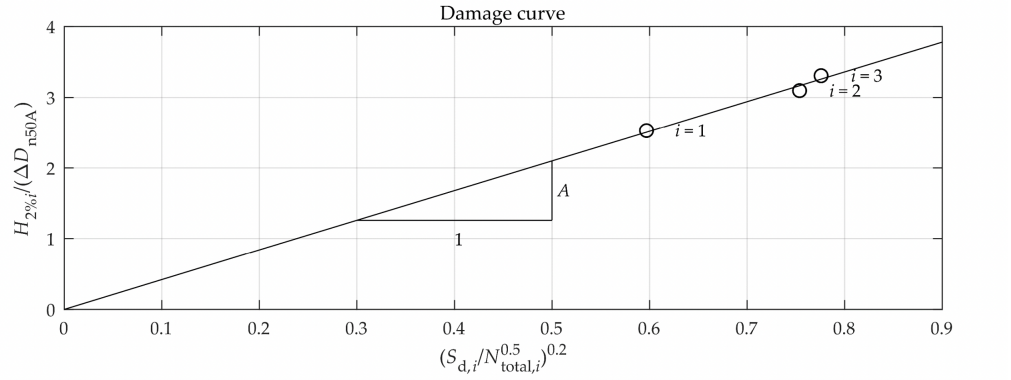

Figure B.2: Damage curve for accumulated tests. The tests are shown with markers and the test iteration number in the wave series is given by i. A and $N_{total,i}$ are found by iterating Equation 2.17 until convergence of A is obtained (Eldrup & Andersen, 2019)

.

- For the accumulated test series (i>1) an extra number of waves is a function of $N_{extra,i}$ were added to the number of waves N_i used in the test. Since the extra number of waves is a function of A, an iterative procedure was applied to equation 2.17 until convergence of A was found.'
- When testing a permeable core, the possible occurrence of scale effects must be taken into account. Relative large pressures from inside the core of the structure could occur, which results in less permeability then estimated initially (Kik et al., 2012).

C
Work scheme Deltares

Phase	Description	Duration in working days	Duration in workweeks
Preparation	Construction of the slope Install automatically detected GCPs Familiarize with equipment Testing photogrammetry including processing Perform 2 check tests	20	4
Testing phase 1	Test series 2 Rebuild slope Test series 3 Rebuild slope Test series 1 Rebuild slope and increase layer thickness Test series 7	3 1 2 1 2 1 2	2.4
Decision	Decision 8a & 8b or 8c & 8d to order stones	1	0.2
Testing phase 2	Rebuild slope Test series 4 Rebuild slope Test series 5 Rebuild slope Test series 6 Rebuild slope	1 2 1 2 1 2 1	2
in-depth tests #1 a & b	When 8ab) Grade stones filter layer Rebuild slope with filter layer	2 1	0.6
in-depth tests #2 c & d	When 8cd) Grade stones core Remove former slope structure Rebuild slope with permeable core	2 0.5 1	0.7
Delay	5 %	2.5	0.5
Duration option #1		48.5	9.7 weeks
Duration option #2		49	9.8 weeks

D
Using Agisoft Metashape

Building a model:

1. Use 'MetashapePro'. The used version is 1.6.5 (64 bit).
2. Load photos: 'Workflow' → 'Load Folder' → 'Single camera'
3. Apply masks with Python API: 'Tools' → 'Run script' → run "masks.py"
4. Detect markers automatically: 'Tools' → 'Markers' → 'Detect markers'
5. Import x,y,z-coordinates of markers: 'Import reference' → open .csv-file with marker coordinates and accuracy
6. Build Point Cloud: 'Workflow' → 'Align photos'
7. Dense Point Cloud: 'Workflow' → 'Build Dense Point Cloud'
8. Export Model" 'File' → 'Export Model'

Detect markers automatically

- Black circle max 30 pix. Black circle GCPs of Deltares are 14 mm so GSD should be smaller than 0.046
- Check camera specifications, Ground Sampling Distance (GSD) and marker size.
- Parameters
  - Marker type: Circular 8 bit
  - Tolerance: 20

Load photos

- Camera output in RAW-files
- Convert to TIFF-files with 16 bts/channel without compression of the files.
- Camera calibration

On-site check

1. Load photos
2. Detect markers automatically with Python API "markerdetection" (Appendix F)
3. Check if the expected number of 135 markers complies with output of the script ('Workspace' → 'Console')
4. Error pixel check must be lower than 1 pix ('Reference' → 'Total error')

E

Camera specifications and settings

Camera specifications

- Camera type: Canon EOS 750D
- Lens type: Tamron 62 mm
- Image width: 6000 pixels
- Image height: 4000 pixels
- Focal length: 18 mm
- Sensor width: 22.3 mm
- Distance (d): 1.4 m
- Ground Sampling Distance (GSD): 0.029 cm/pixel
- Width single image footprint on the ground, D_w: 1.734 m
- Height single image footprint on the ground, D_h: 1.156 m

Before taking first picture of the serie use Automatic Focus (AF) function and then switch to Manual Focus (MF).

Camera settings

Consistency between photos is the most important aspect of camera specifications. The focal-length, focus, ISO, and aperture should remain consistent for best results. To attain consistency, zoom in to the desired setting, focus the camera by depressing the shutter button half-way, and then switch the cameras focus setting from "A" (automatic) to "M" (manual). You should also shoot in "Aperture priority mode," which you can switch to by twisting the dial located on the top-left of the camera to the "A" setting. Once set to aperture priority mode, you can twist the dial located on the upper-back of the camera to alter the aperture. The lowest aperture setting you should use is f/5.6 If possible, shoot at a higher aperture, but keep in mind that the higher the aperture, the slower the shutter speed. If the shutter speed becomes to slow, we recommend setting the camera on a tripod. (UNC,2020)

Summary taking photos:

1. 'Aperture priority' mode ('Av' on Canon dial)
2. High aperture setting (f/ 5.6 minimum)
3. Fixed focal length (i.e. zoom)
4. Fixed focus ('Manual focus')
5. No flash
6. Use a stationary frame

The camera focus should not be changed after the initial photo and the ISO setting should be as low as possible to reduce graininess.

- Manual or Aperture priority (AV)
- Diaphragm F6.3
- Shutter speed: 1″
- ISO: 100 (Low as possible to reduce graininess/noise)
- Output: RAW-file
- One shot
- White balance: 4000k (White TL-light inside)
- Self timer: 2 sec
- Picture style: standard

F
Metashape Python API

```python
#Count the total number of markers detected in a chunk

# IMPORT
import Metashape as mt

# VARIABLES

chunk = mt.app.document.chunk #define the active chunk
cameras = chunk.cameras #define a list of the cameras inside the chunk
n_cameras = len(chunk.cameras) #number of cameras

# EXECUTION

chunk.remove(chunk.markers) #remove previous markers

for camera in cameras:
    chunk.detectMarkers(cameras=camera)
total_markers = len(chunk.markers)
chunk.remove(chunk.markers)
chunk.detectMarkers()

if total_markers >= 135:
    print("The number of expected GCPs has been detected. Continue with the next test in this serie.")
else:
    print("NOTE: The number of GCPs detected is different from 135. Please check for errors.")
```

Figure F.1: On-site number of total markers detection check

```python
#Apply masks to a specific range of images

# IMPORT
import Metashape as mt
import os

# VARIABLES
chunk = mt.app.document.chunk #define the current working chunk
cameras = chunk.cameras #define the cameras in the chunk

img_path = mt.app.getExistingDirectory() # ask the folder path of the masks
tol = mt.app.getInt("Choose tolerance value for masking") #ask for the masking tolerance value
     #change directory to that path

# EXECUTION
chunk.importMasks(path=os.path.join(img_path,'Links_Initial.jpg'),
source=Metashape.MaskSource.MaskSourceFile,operation=Metashape.MaskOperation.MaskOperationReplacement,
tolerance=tol,cameras=cameras[0])
chunk.importMasks(path=os.path.join(img_path,'Links_Regular.jpg'),
source=Metashape.MaskSource.MaskSourceFile,operation=Metashape.MaskOperation.MaskOperationReplacement,
tolerance=tol,cameras=cameras[1:21])
chunk.importMasks(path=os.path.join(img_path,'Midden_Initial.jpg'),
source=Metashape.MaskSource.MaskSourceFile,operation=Metashape.MaskOperation.MaskOperationReplacement,
tolerance=tol,cameras=cameras[21])
chunk.importMasks(path=os.path.join(img_path,'Midden_Regular.jpg'),
source=Metashape.MaskSource.MaskSourceFile,operation=Metashape.MaskOperation.MaskOperationReplacement,
tolerance=tol,cameras=cameras[22:42])
chunk.importMasks(path=os.path.join(img_path,'Rechts_Initial.jpg'),
source=Metashape.MaskSource.MaskSourceFile,operation=Metashape.MaskOperation.MaskOperationReplacement,
tolerance=tol,cameras=cameras[42])
chunk.importMasks(path=os.path.join(img_path,'Rechts_Regular.jpg'),
source=Metashape.MaskSource.MaskSourceFile,operation=Metashape.MaskOperation.MaskOperationReplacement,
tolerance=tol,cameras=cameras[43:64])
```

Figure F.2: Apply masks to specific range of photos in the test serie

G
Workflow methodology of stereophotogrammetry technique

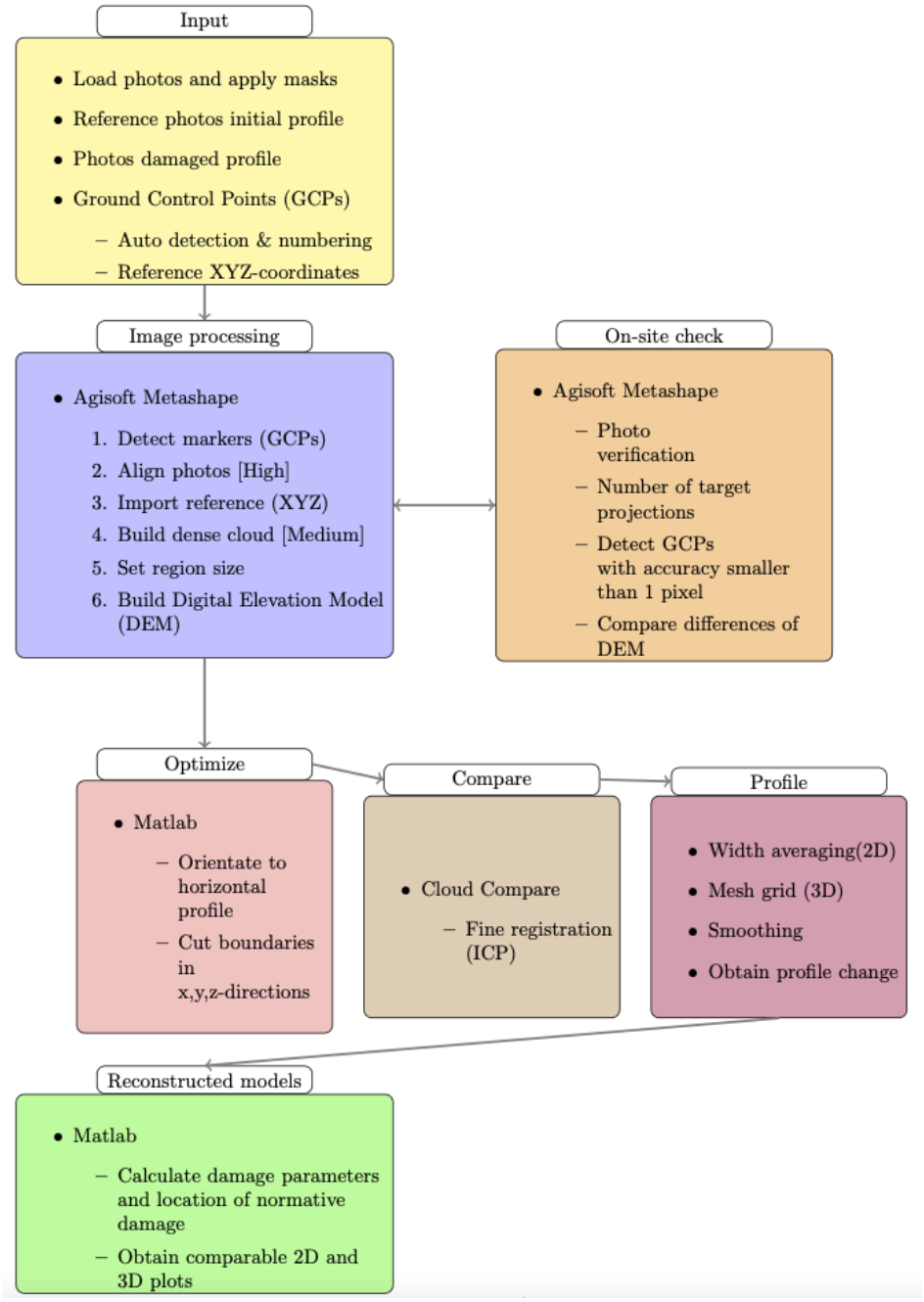

Figure G.1: Workflow methodology image processing

H

Settings and use of ICP tool

H.1 Settings ICP in Cloud Compare

- Theoritical overlap = 60 %

H.2 Exercise possible effects of ICP tool

In this exercise the aim is to investigate the possible effects of using the ICP tool on the collected results. This research stems from the suspicion that the use of the ICP during the check tests (two undamaged profiles) has a different influence on damage numbers than the use of ICP with a damaged and an undamaged profile. This is because when using the ICP tool, overlap between the two point clouds is searched for and they are fitted on top of each other more appropriately. To determine an order of magnitude of the influence, a comparative study is performed for test 1 with and without ICP applied.

To give an indication on the order of magnitude of the possible effects, the profile with and without ICP was compared for each test iteration in figure H.1:

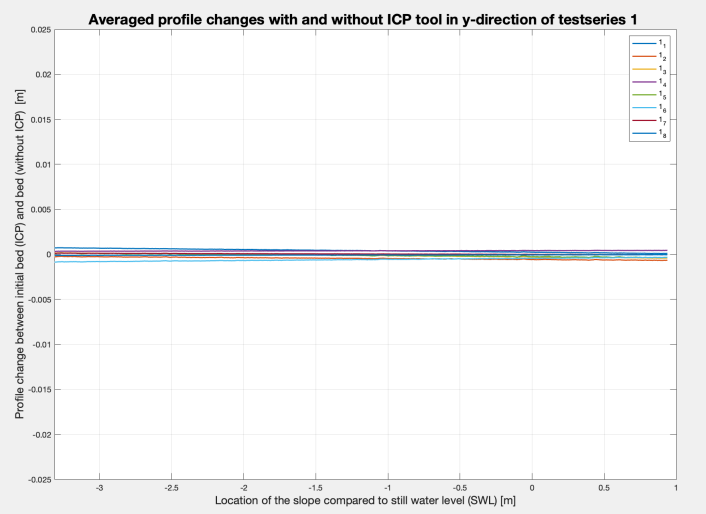

Figure H.1: Influence of ICP tool within accuracy limit regarding the difference of Test 1 with and without ICP tool applied

The figure shows that the differences of each particular test were smaller than the used threshold value of 0.5 mm. There is no clear trend in positive versus negative values in the profiles for increasing damage.

Check tests

Table I.1: Matrix from check test with 8 iterations providing distances with mean (=m) and standard deviation (=std) values compared to reference profile (=ref).

Check tests	distance $*[10^{-4}m]$		distance $*[10^{-4}m]$		distance $*[10^{-4}m]$		distance $*[10^{-4}m]$		distance $*[10^{-4}m]$		distance $*[10^{-4}m]$		distance $*[10^{-4}m]$		distance $*[10^{-4}m]$		distance $*[10^{-4}m]$	
	m	std	m	std	m	std	m	std	m	std	m	std	m	std	m	std	m	std
0_0	ref	ref	2.31	3.19	2.53	2.52	2.83	3.58	2.87	3.05	3.61	3.45	3.12	4.42	3.65	3.74	3.25	4.76
0_1	2.33	2.73	ref	ref	2.20	2.39	2.32	2.88	2.36	3.26	3.35	3.87	2.68	3.19	3.39	3.61	2.87	3.29
0_2	2.50	2.80	2.15	3.16	ref	ref	2.42	3.48	1.72	2.53	3.44	3.92	2.60	4.30	3.47	3.64	4.76	4.58
0_3	2.93	3.38	2.41	2.93	2.56	3.01	ref	ref	3.01	2.76	2.92	3.33	2.58	2.73	3.07	3.04	2.86	2.91
0_4	2.97	3.16	2.45	3.59	2.55	3.00	1.72	2.77	ref	ref	2.90	2.69	2.62	3.99	3.06	3.01	2.92	4.39
0_5	3.80	3.65	3.52	4.02	3.64	3.51	3.03	3.33	3.01	2.76	ref	ref	3.58	4.25	2.57	2.86	3.78	4.65
0_6	3.13	4.16	2.67	3.54	2.63	3.96	2.49	4.78	2.52	4.54	3.41	4.99	ref	ref	3.08	2.81	2.28	2.46
0_7	3.81	4.63	3.54	4.56	3.66	4.47	3.16	4.86	3.14	4.83	2.54	4.93	3.24	4.15	ref	ref	3.21	4.42
0_8	3.29	4.32	2.89	3.71	2.87	4.12	2.82	4.61	2.86	4.69	3.08	2.81	2.32	2.48	2.95	2.94	ref	ref

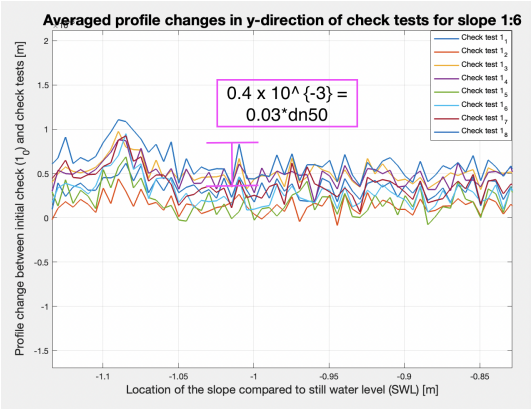

(a) Without applying smoothing principle

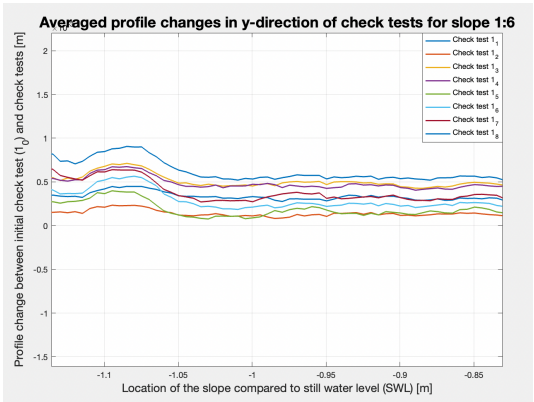

(b) With applying smoothing principle by use of 3*d_{n50} moving average

Figure I.1: Profile changes in y-direction of check tests a) without applying smoothing principle and b) with applying smoothing principle by use of 3*d_{n50} moving average

J Damage determination 2D

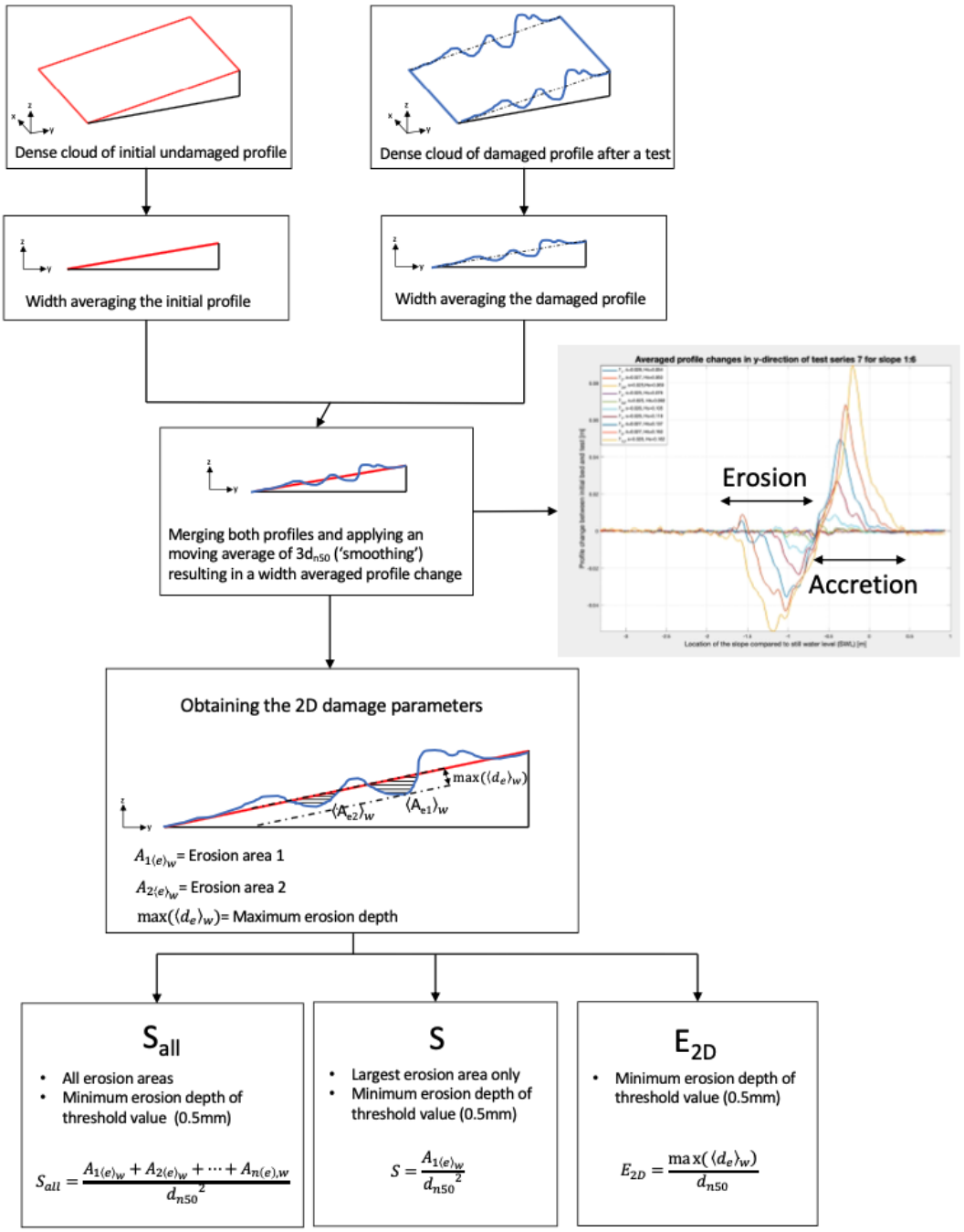

Figure J.1: Determination 2D damage parameter based on work of Van Wijland (2020)

K
Damage determination 3D

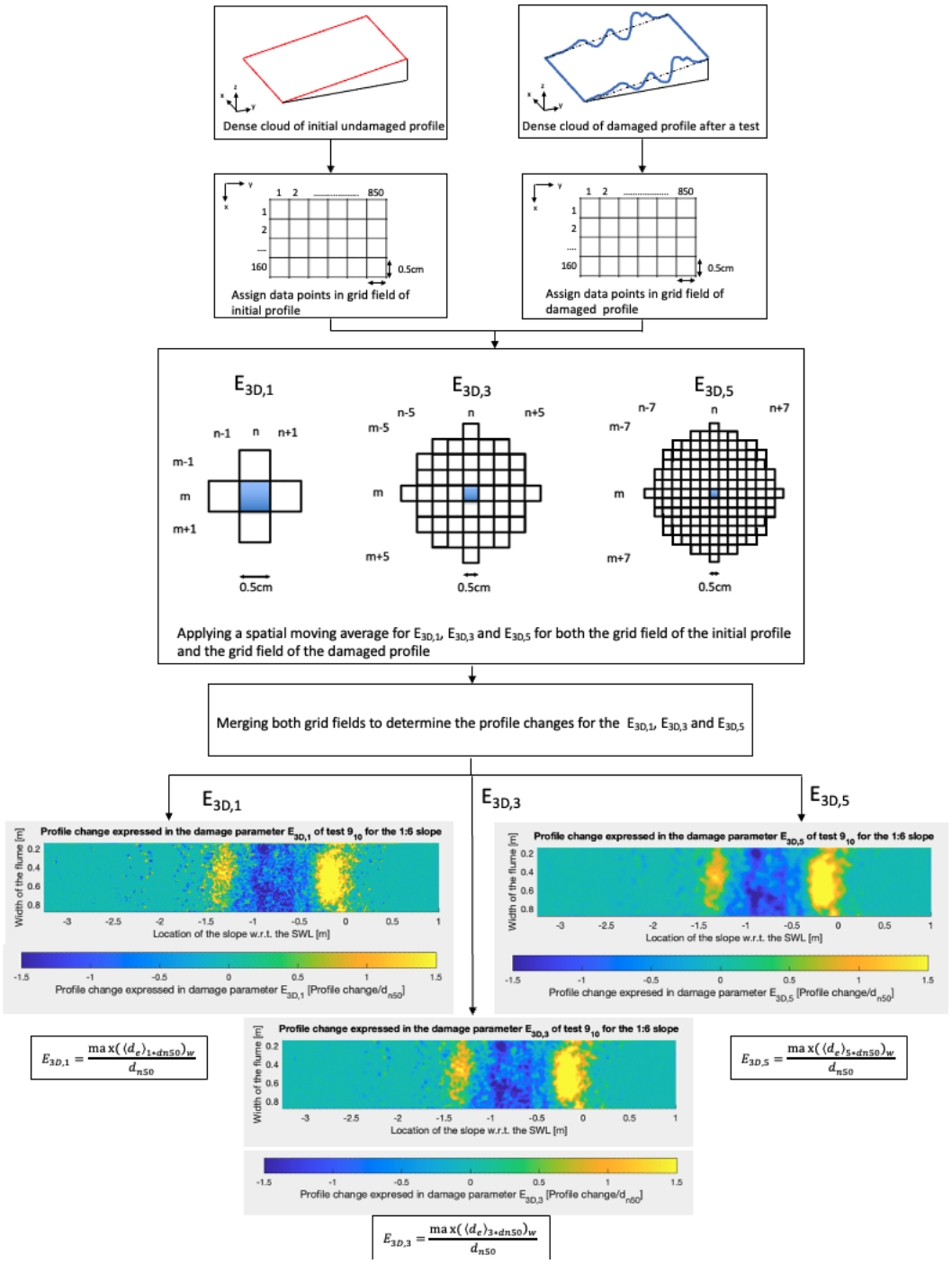

Figure K.1: Determination 3D damage parameter based on work of Van Wijland (2020)

L Results 2D profiles

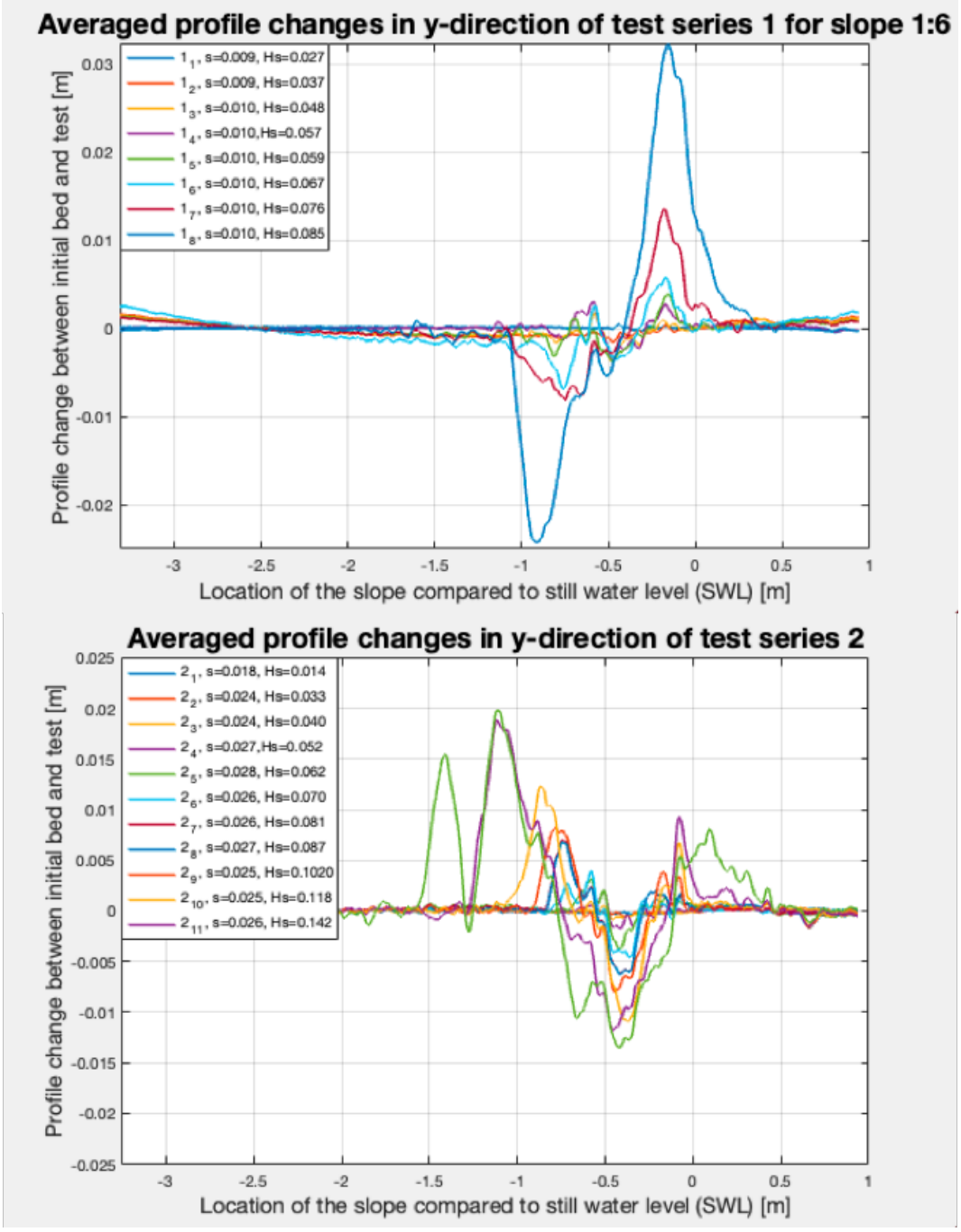

Figure L.1: Results 2D profiles for test 1 and 2

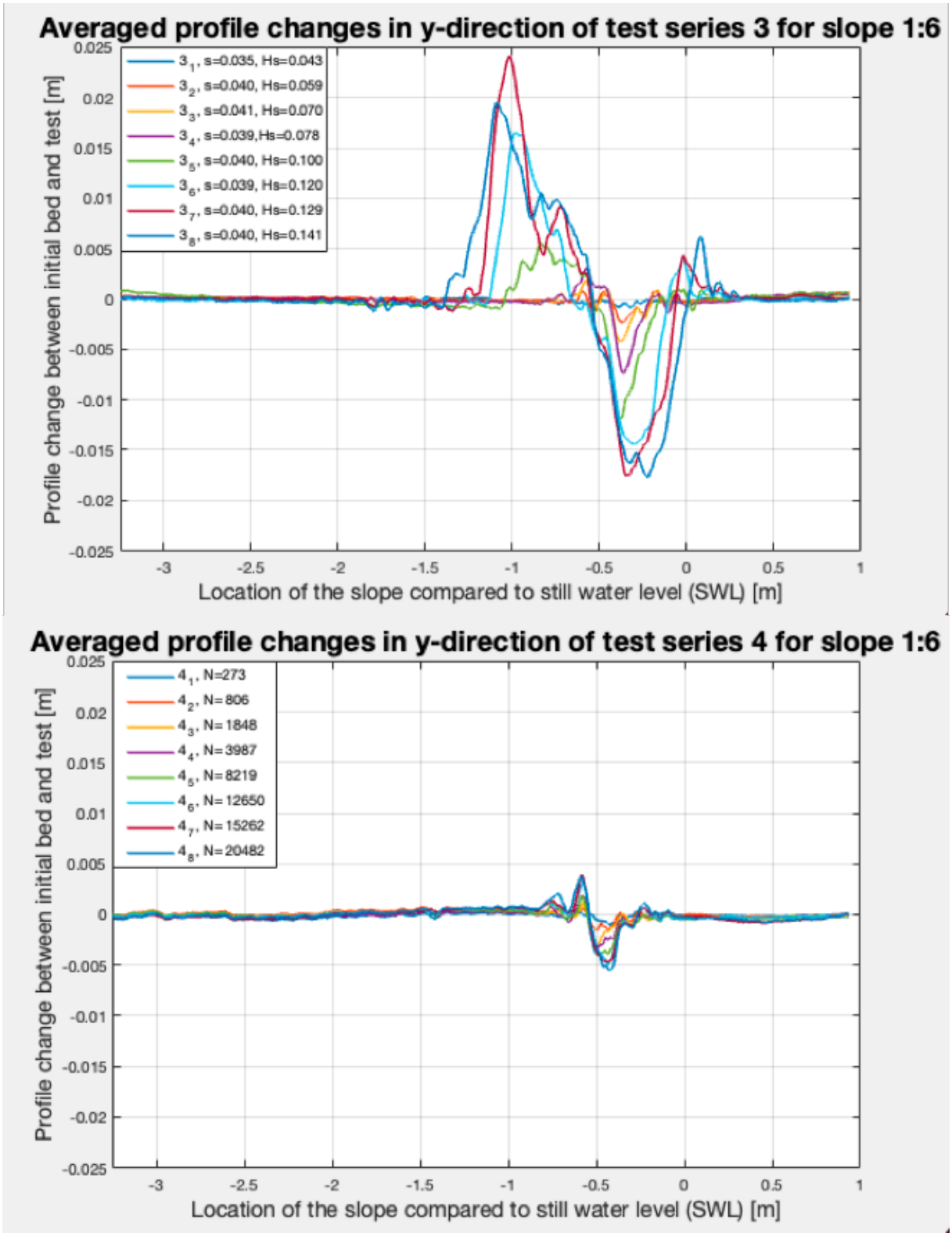

Figure L.2: Results 2D profiles for test 3 and 4

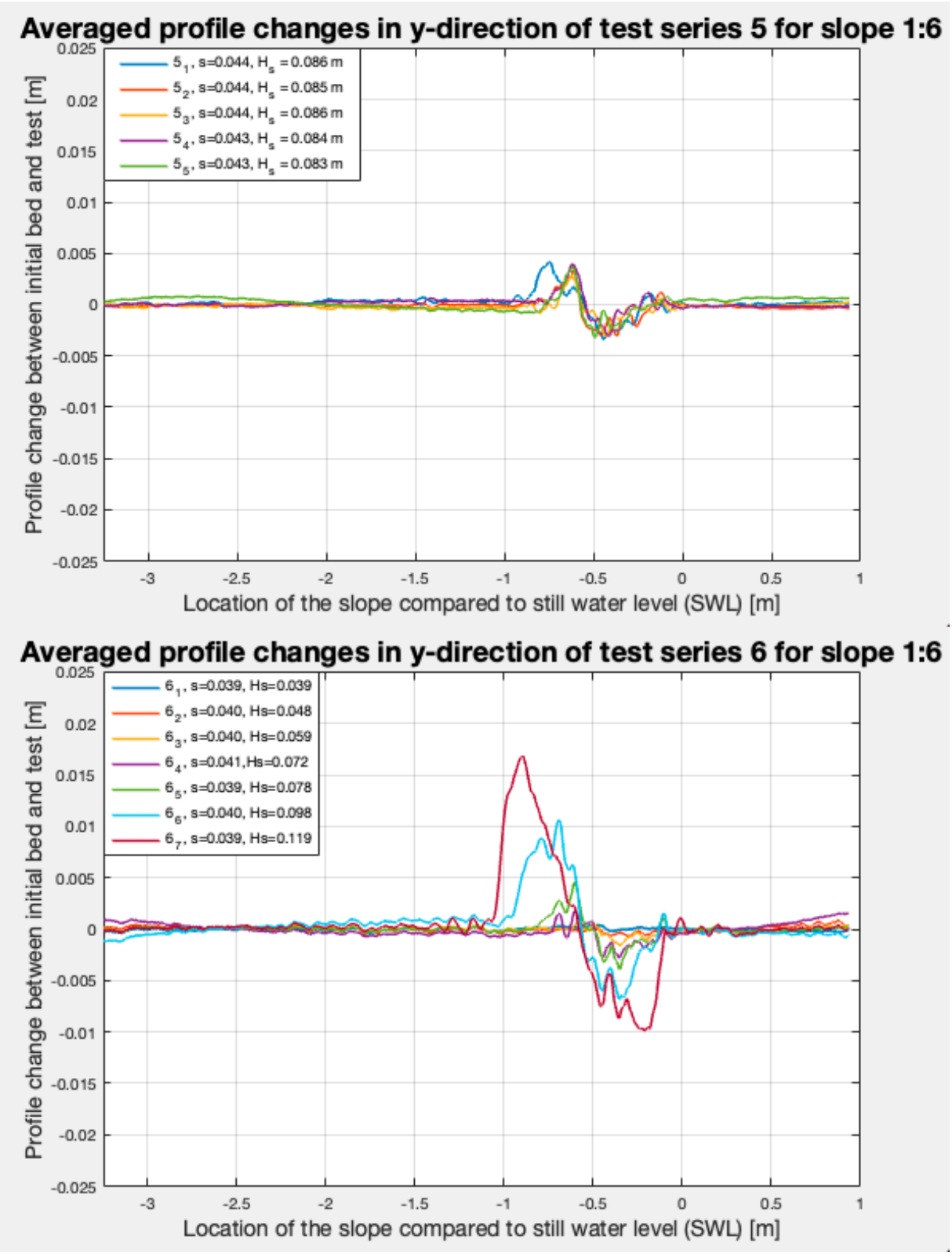

Figure L.3: Results 2D profiles for test 5 and 6

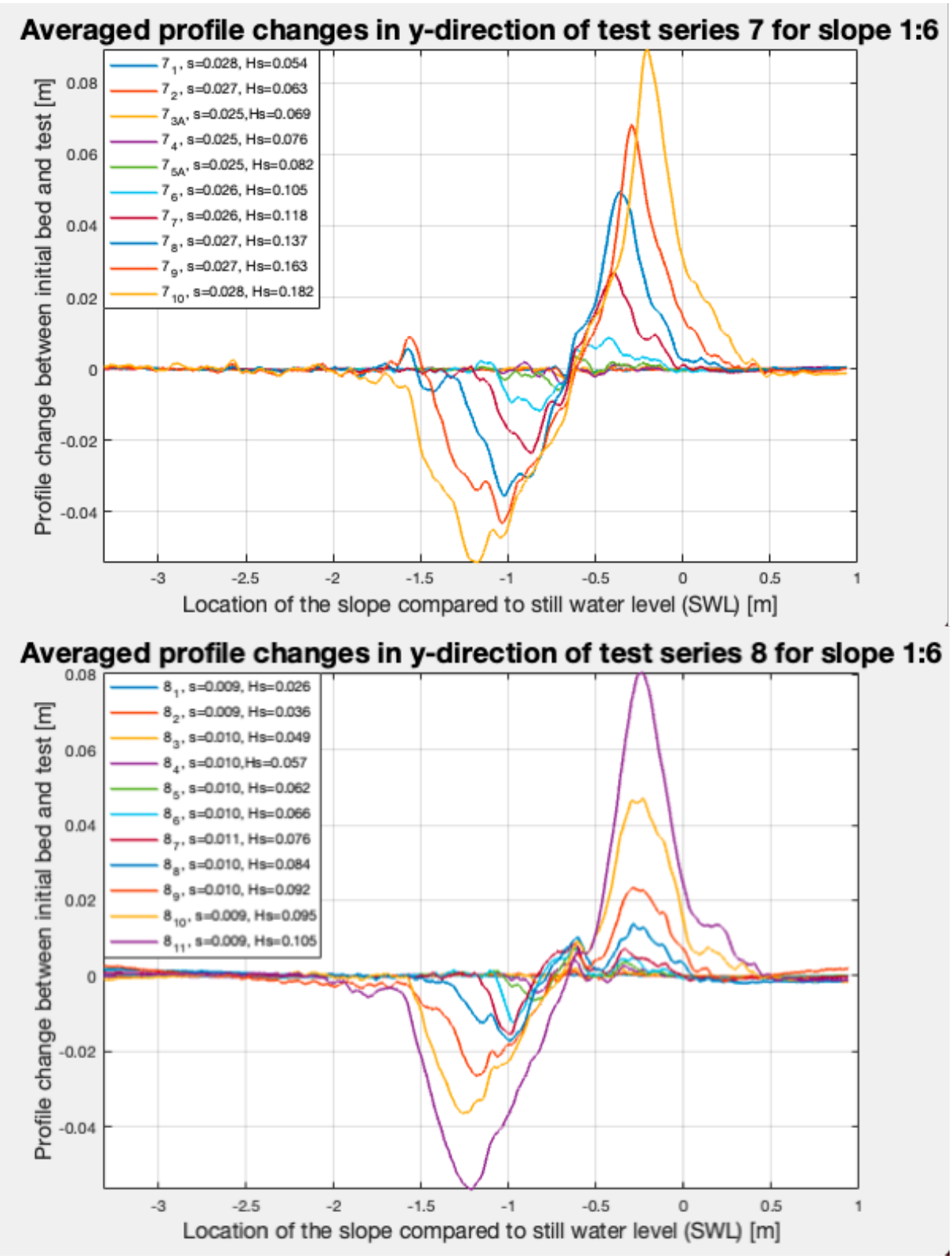

Figure L.4: Results 2D profiles for test 7 and 8

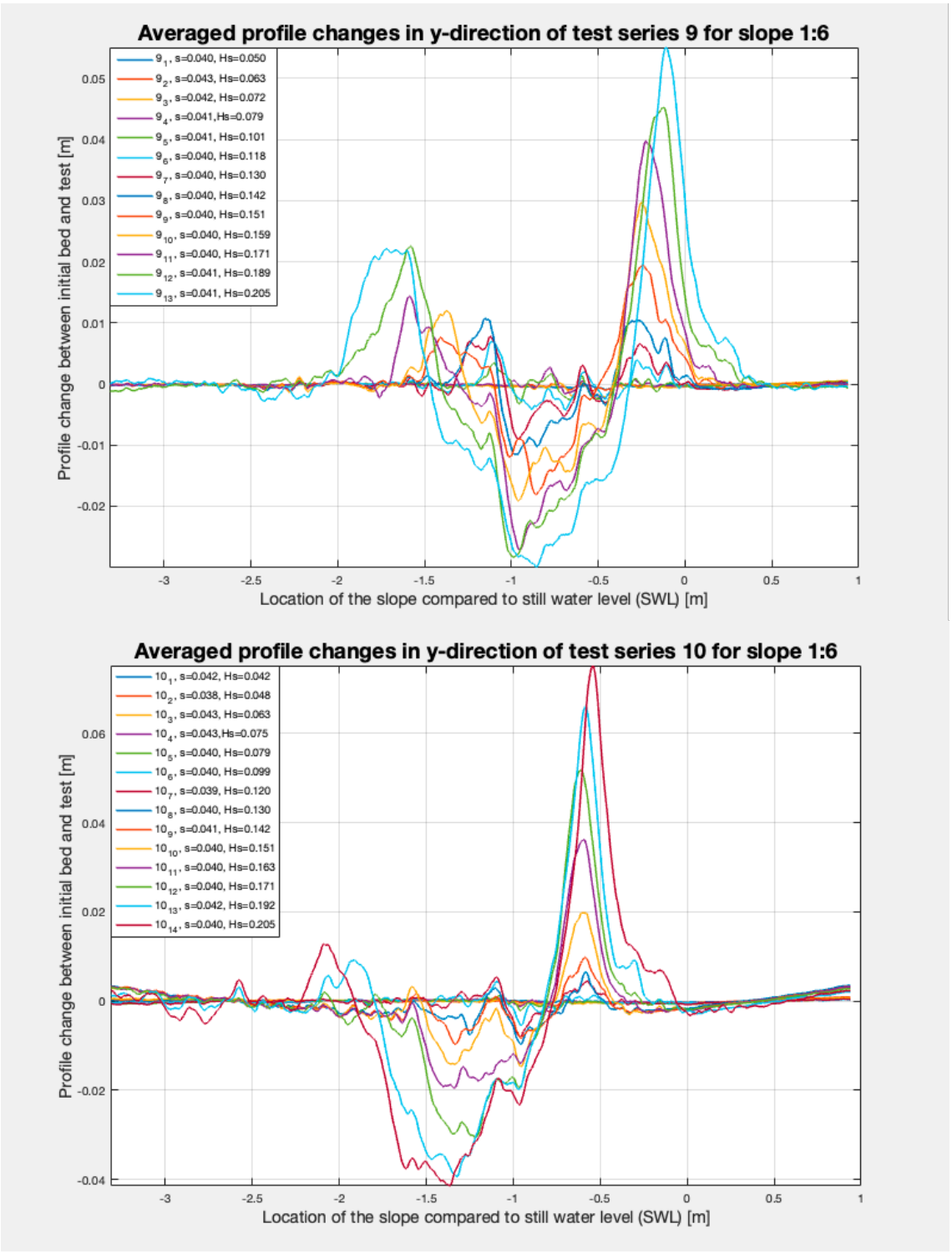

Figure L.5: Results 2D profiles for test 9 and 10

M
Results 3D profiles

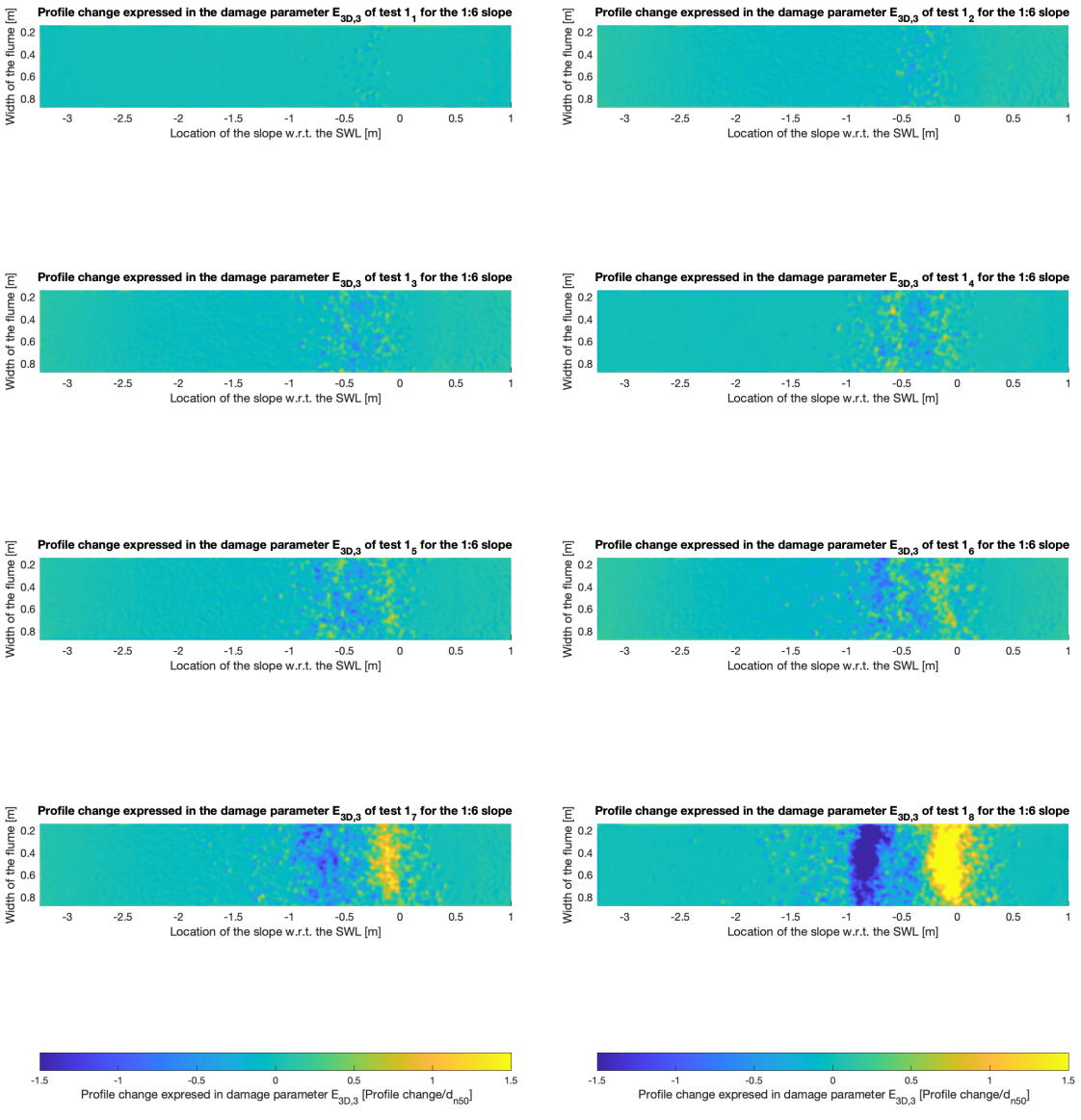

Figure M.1: Results 3D profiles for test 1

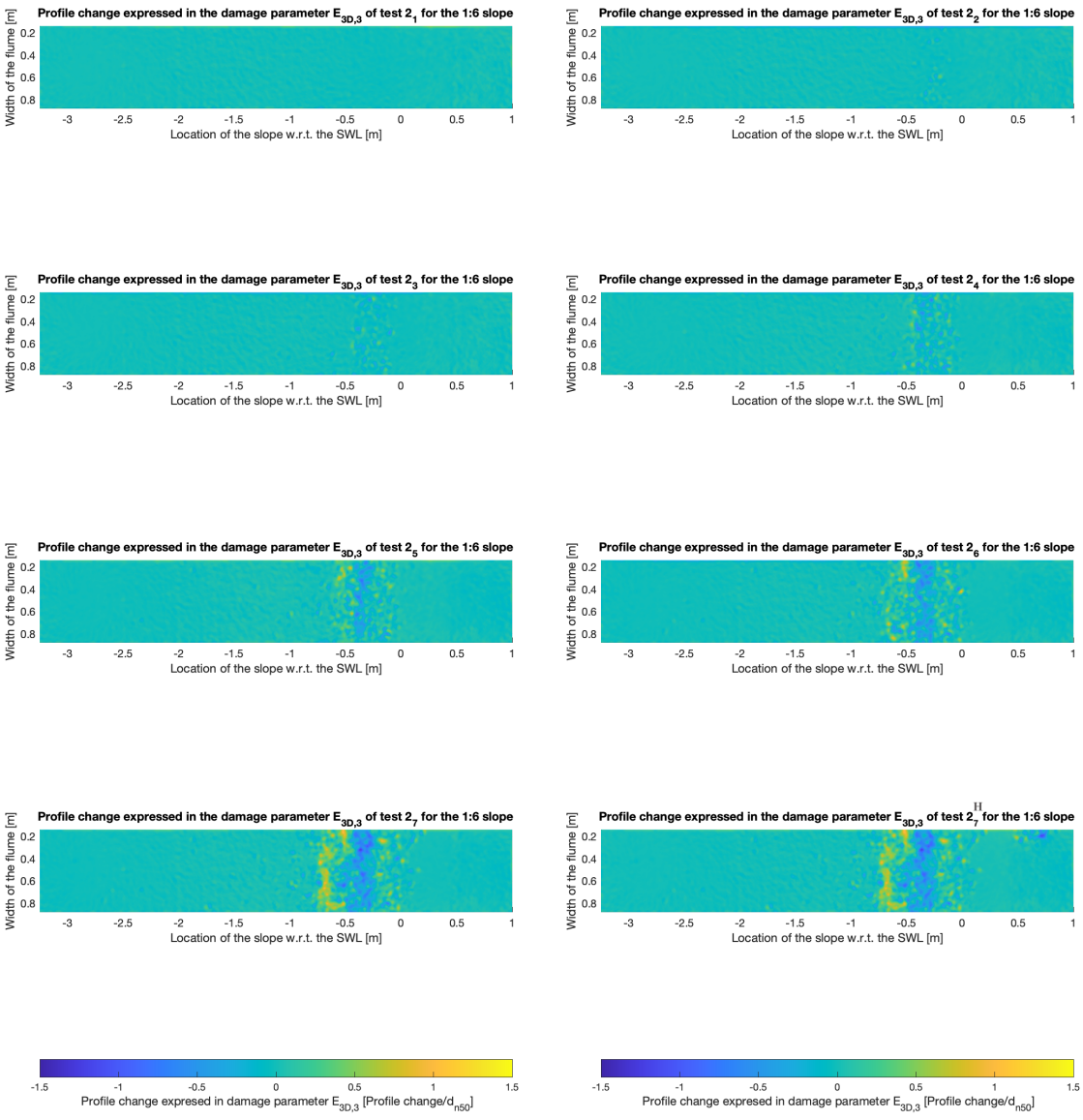

Figure M.2: Results 3D profiles for test 2 (part 1)

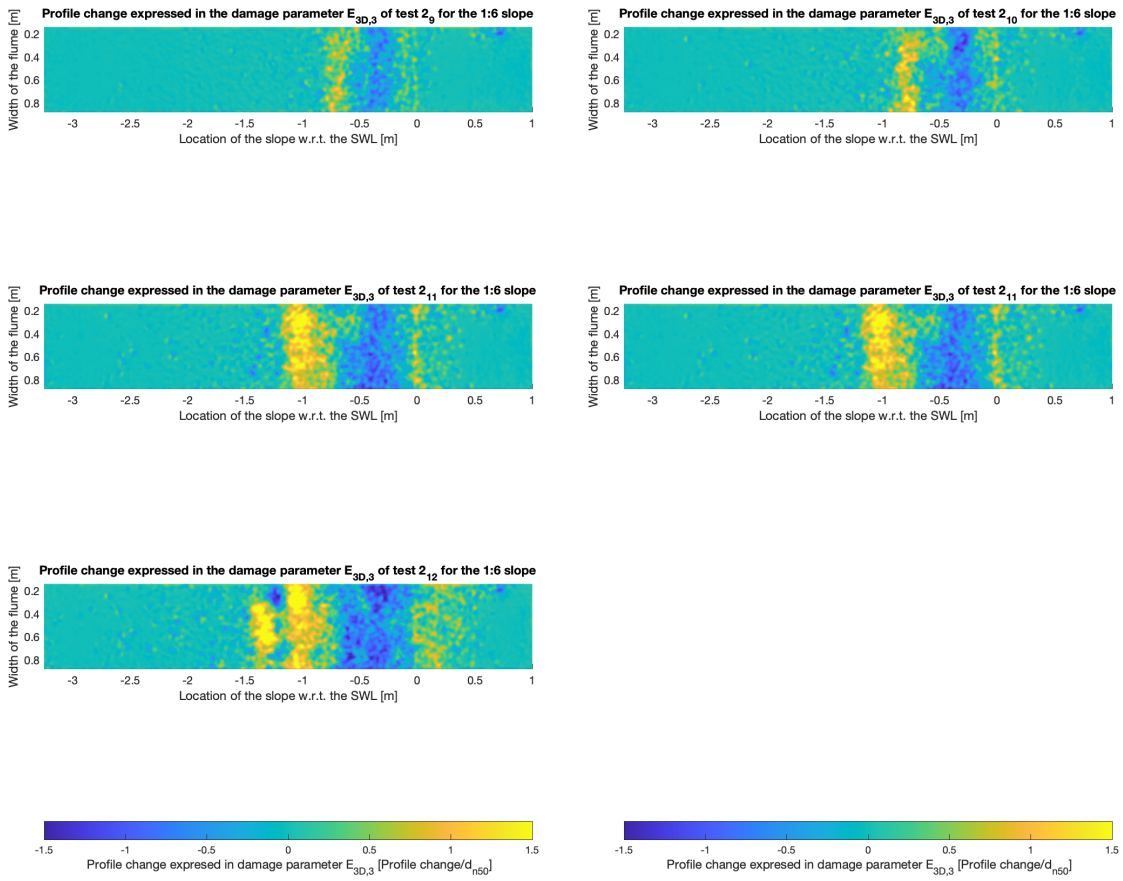

Figure M.3: Results 3D profiles for test 2 (part 2)

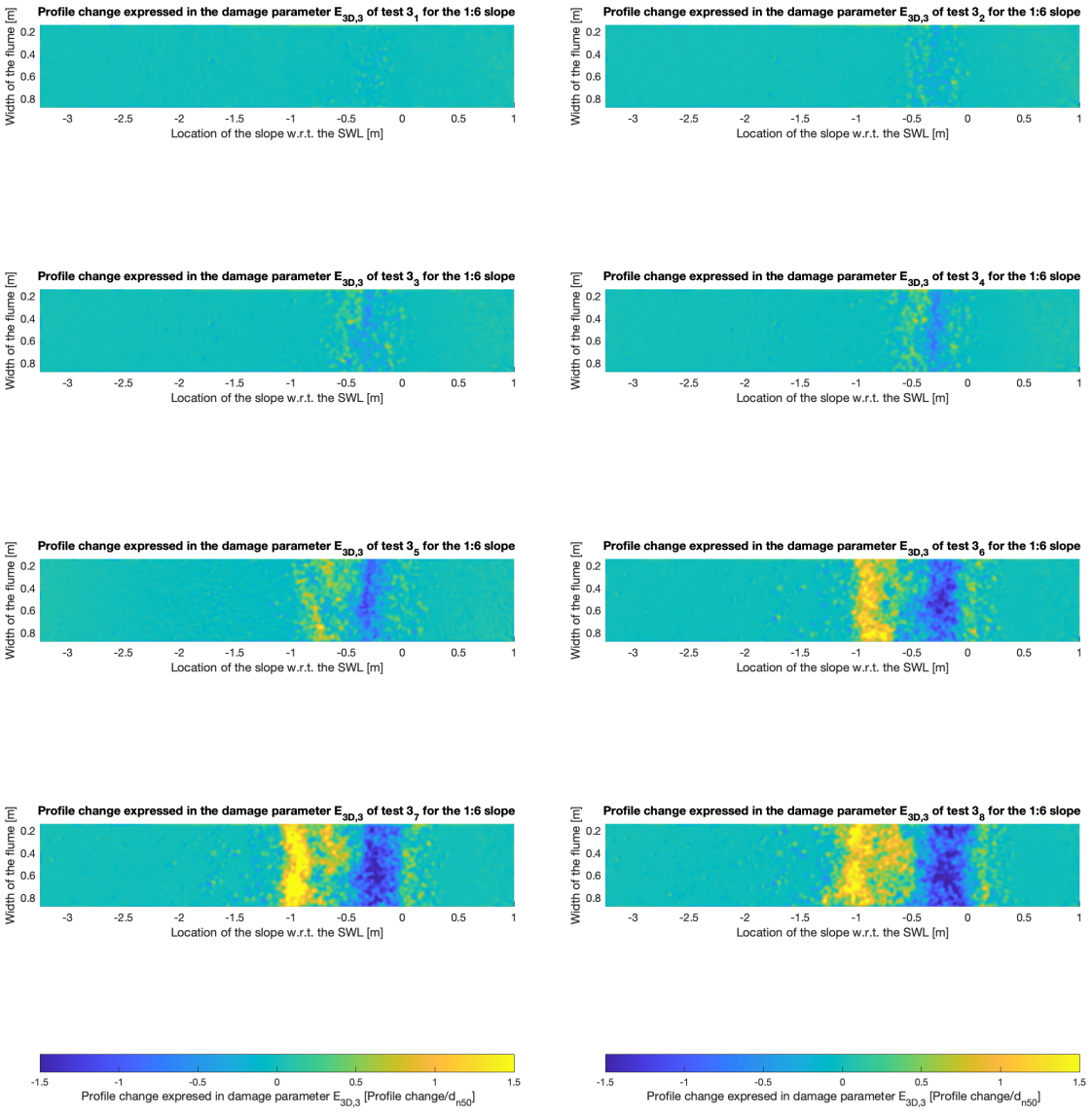

Figure M.4: Results 3D profiles for test 3

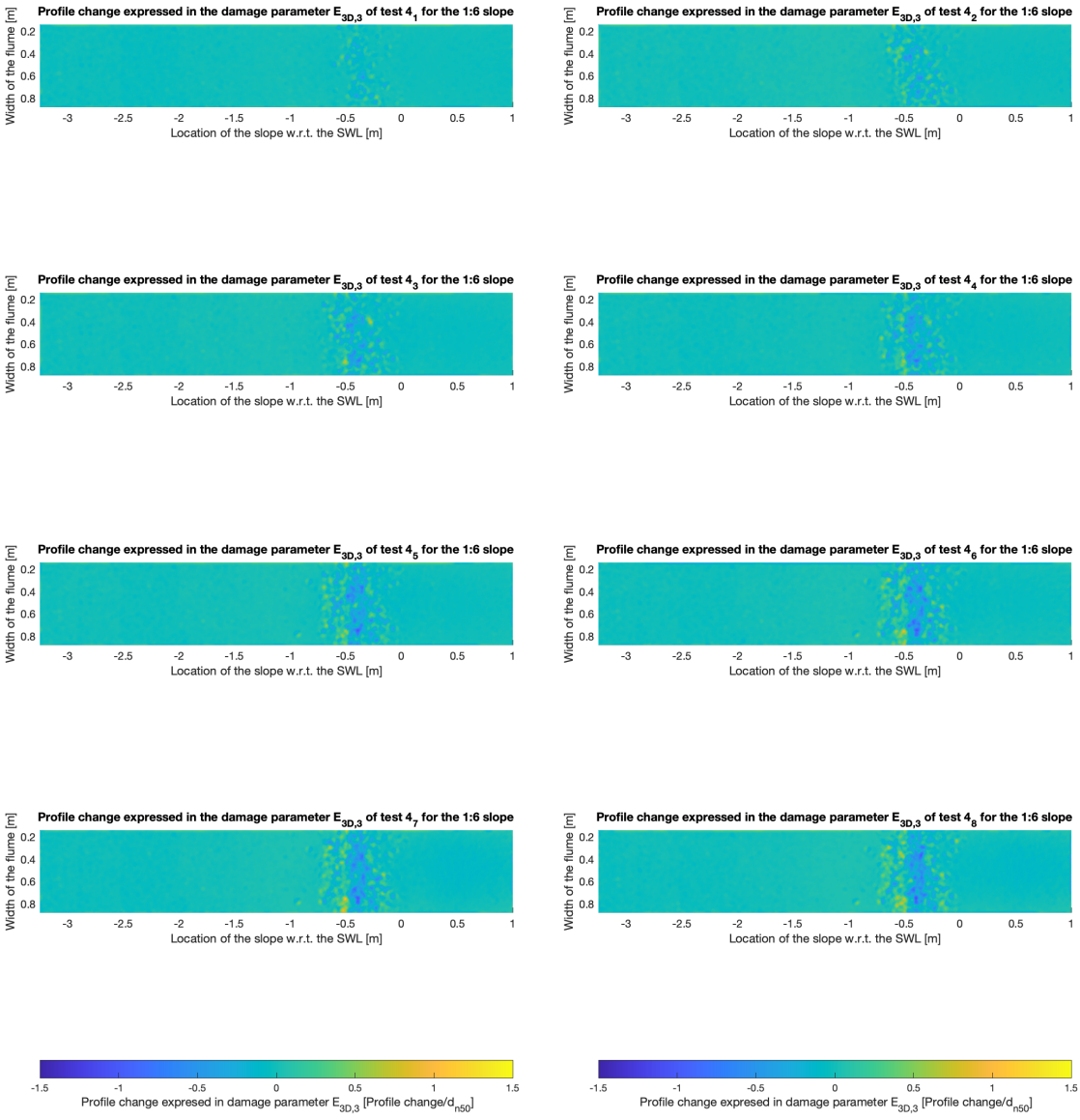

Figure M.5: Results 3D profiles for test 4

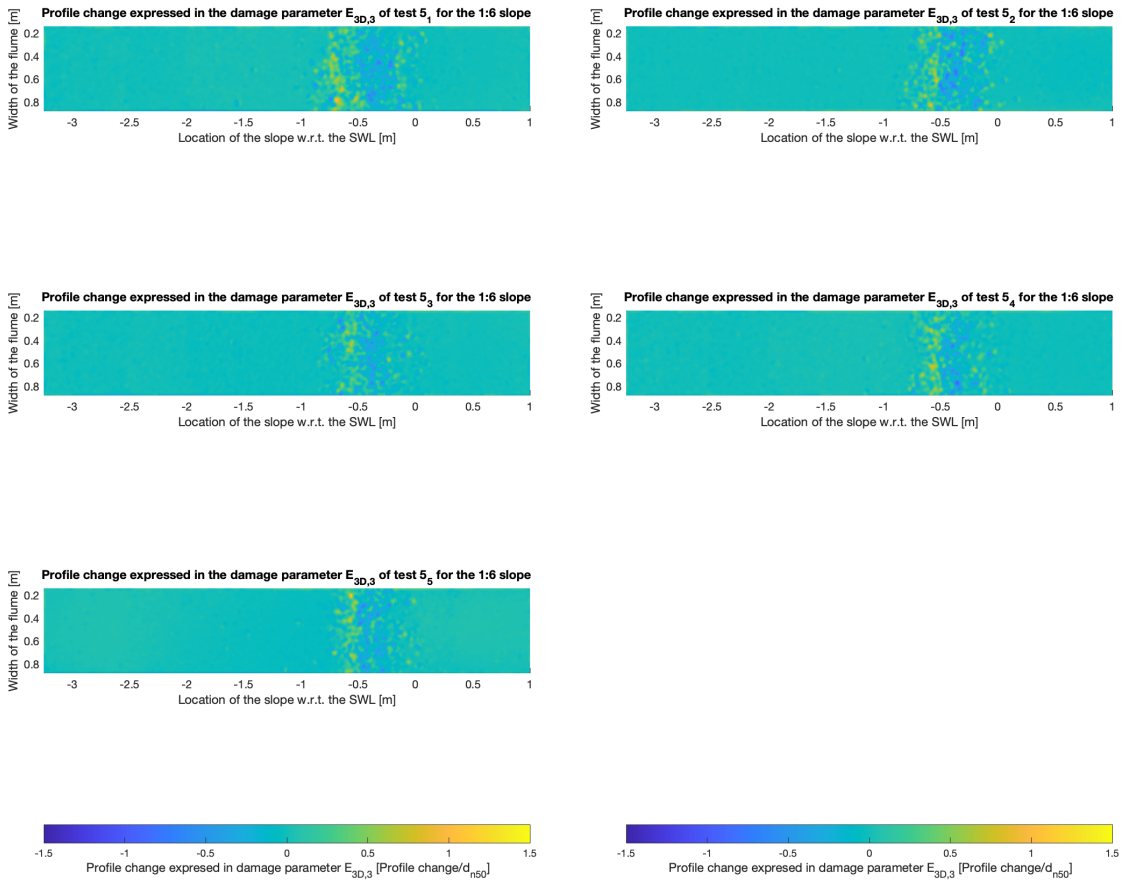

Figure M.6: Results 3D profiles for test 5

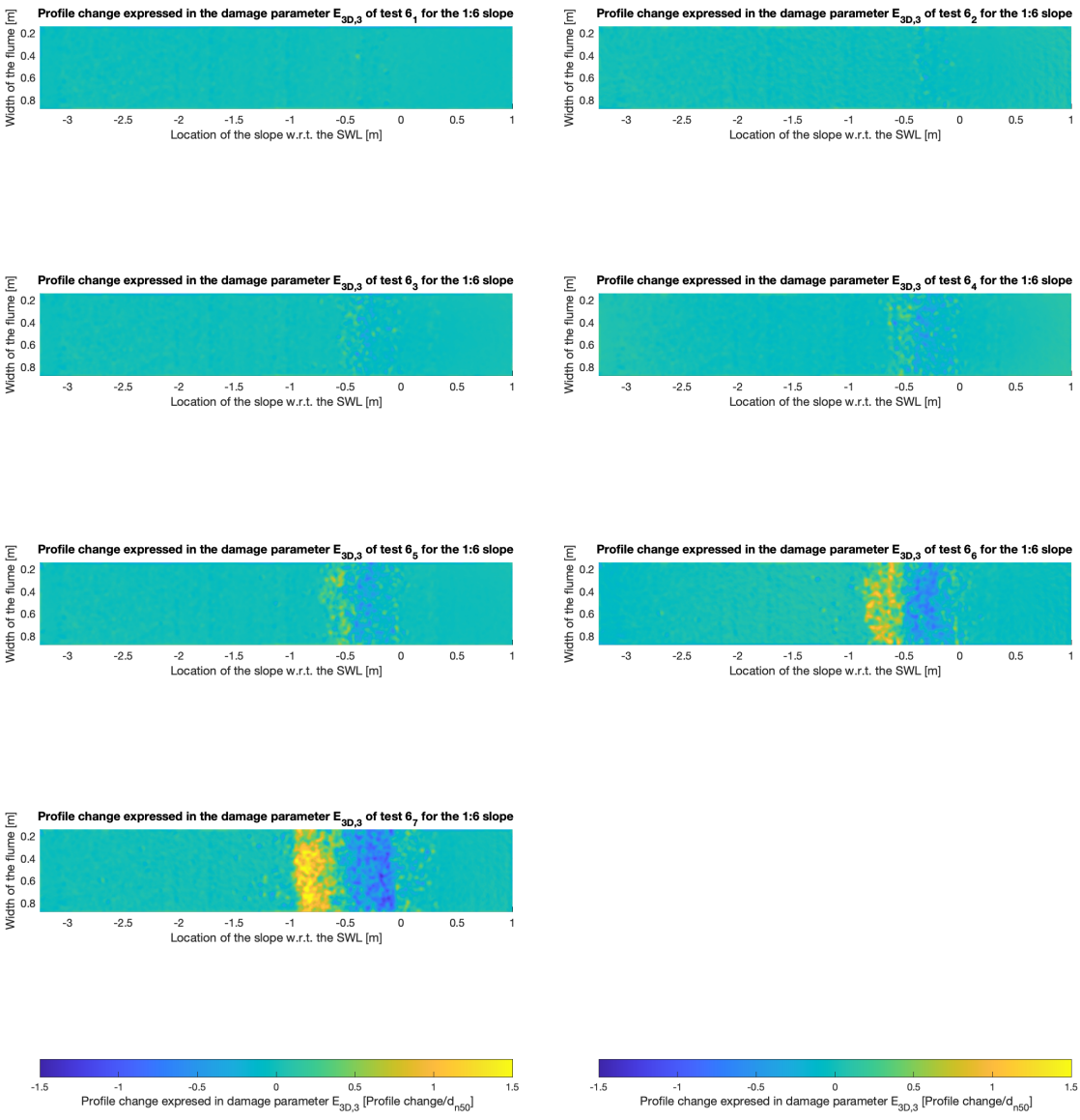

Figure M.7: Results 3D profiles for test 6

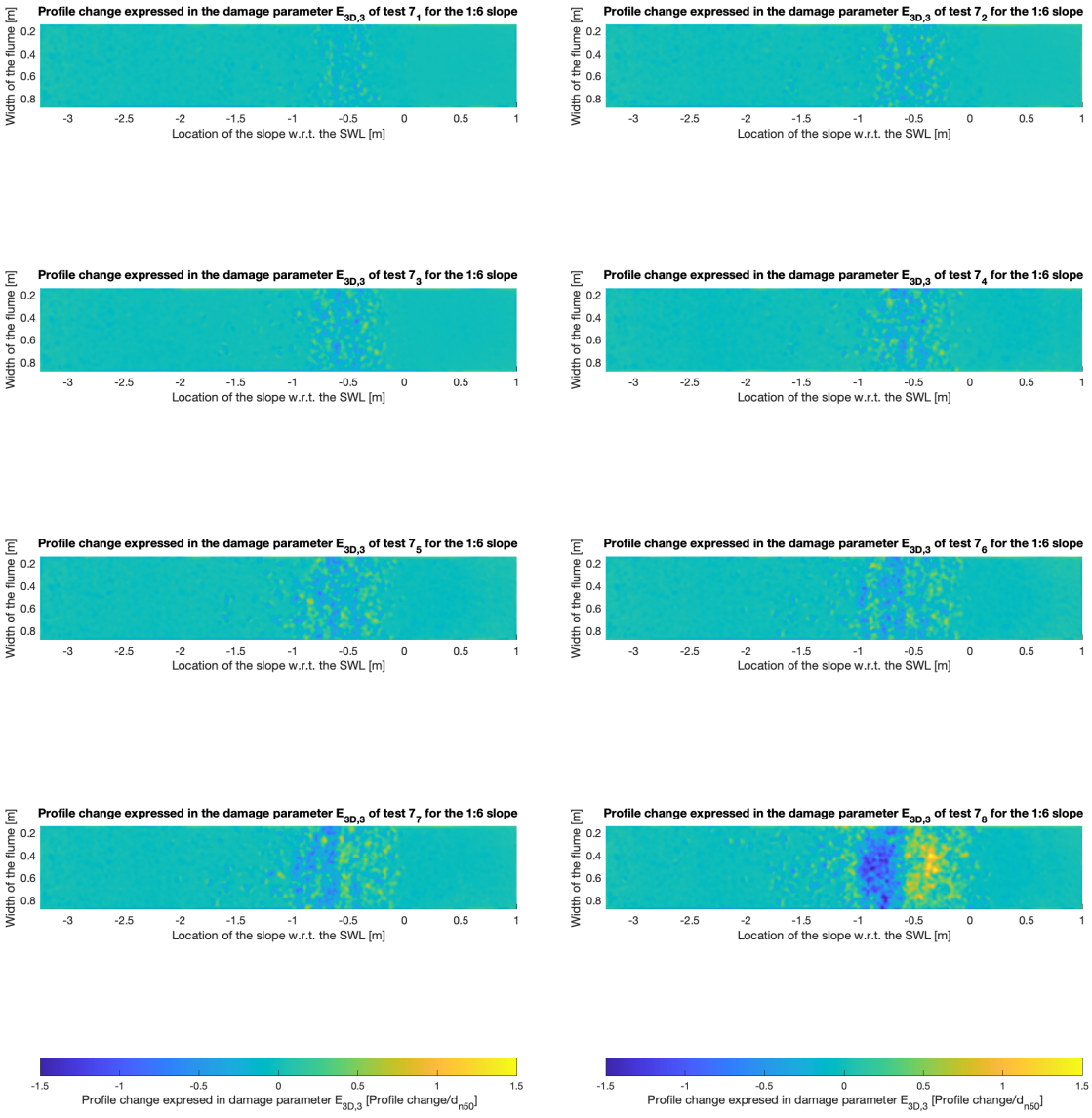

Figure M.8: Results 3D profiles for test 7 (part 1)

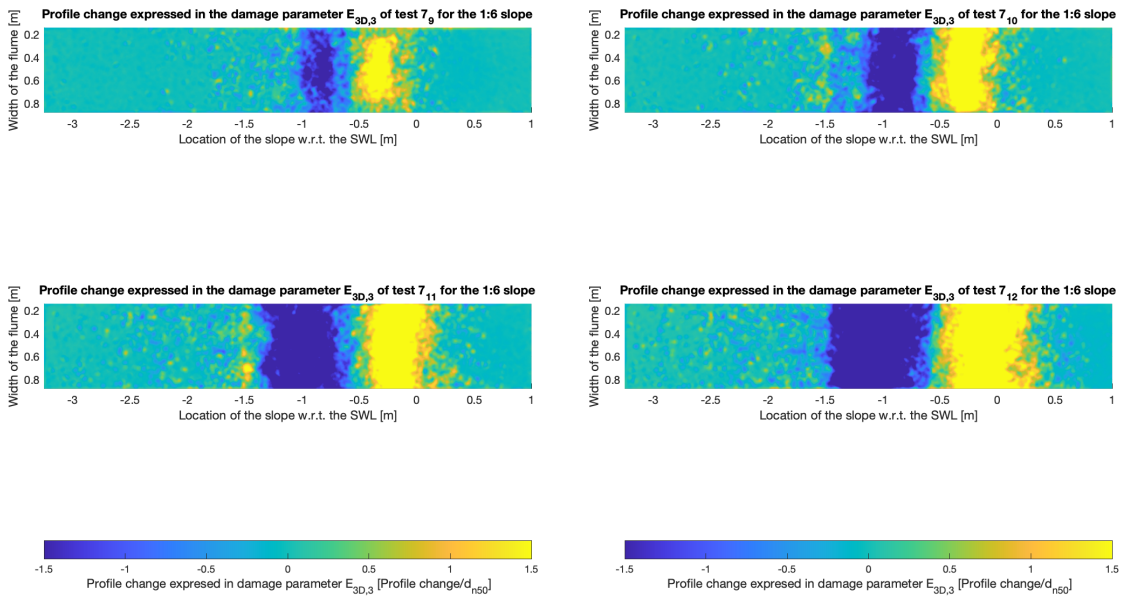

Figure M.9: Results 3D profiles for test 7 (part 2)

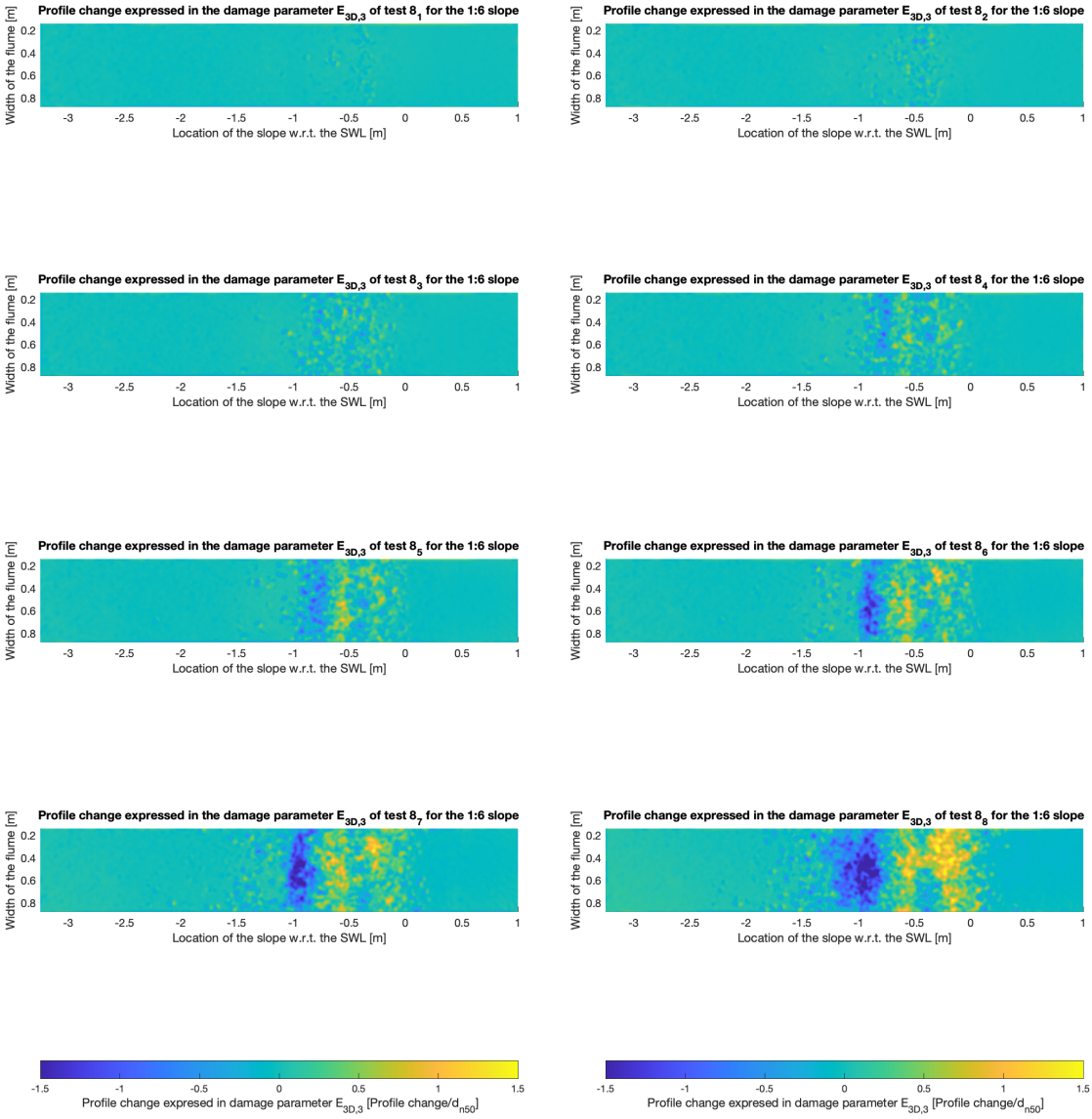

Figure M.10: Results 3D profiles for test 8 (part 1)

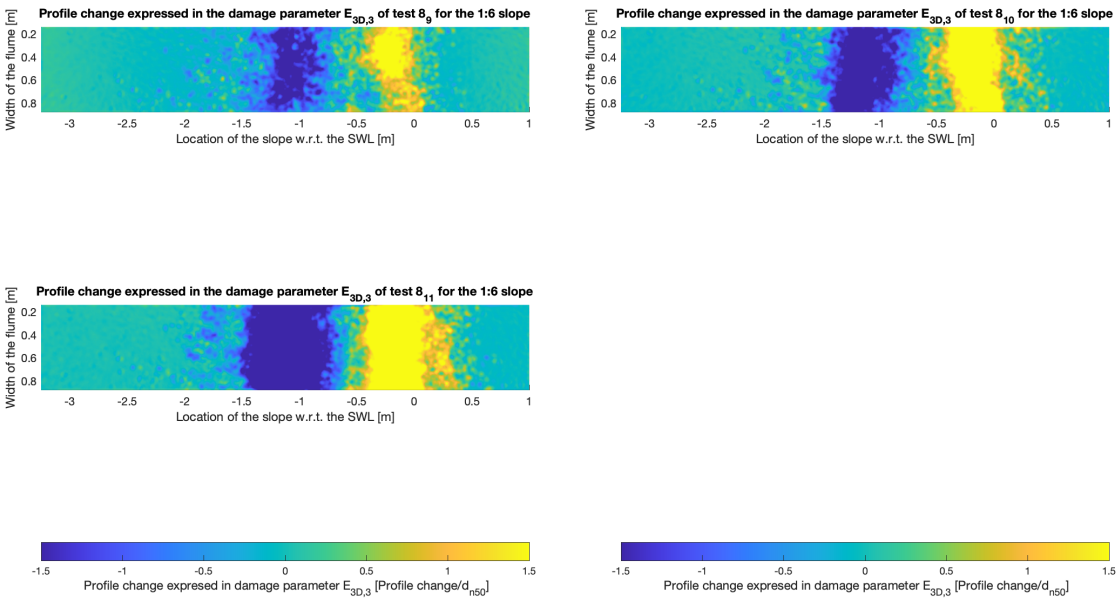

Figure M.11: Results 3D profiles for test 8 (part 2)

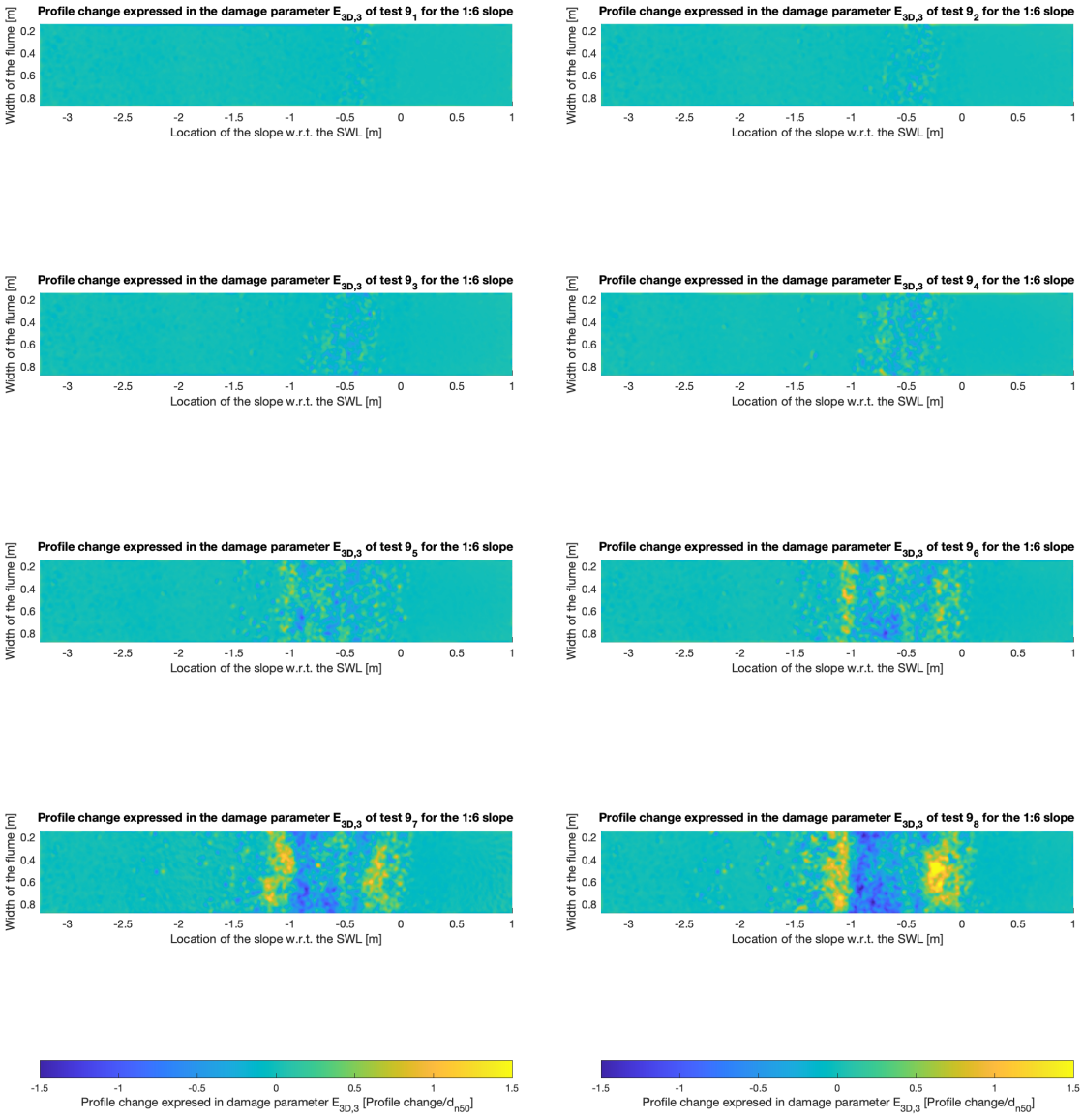

Figure M.12: Results 3D profiles for test 9 (part 1)

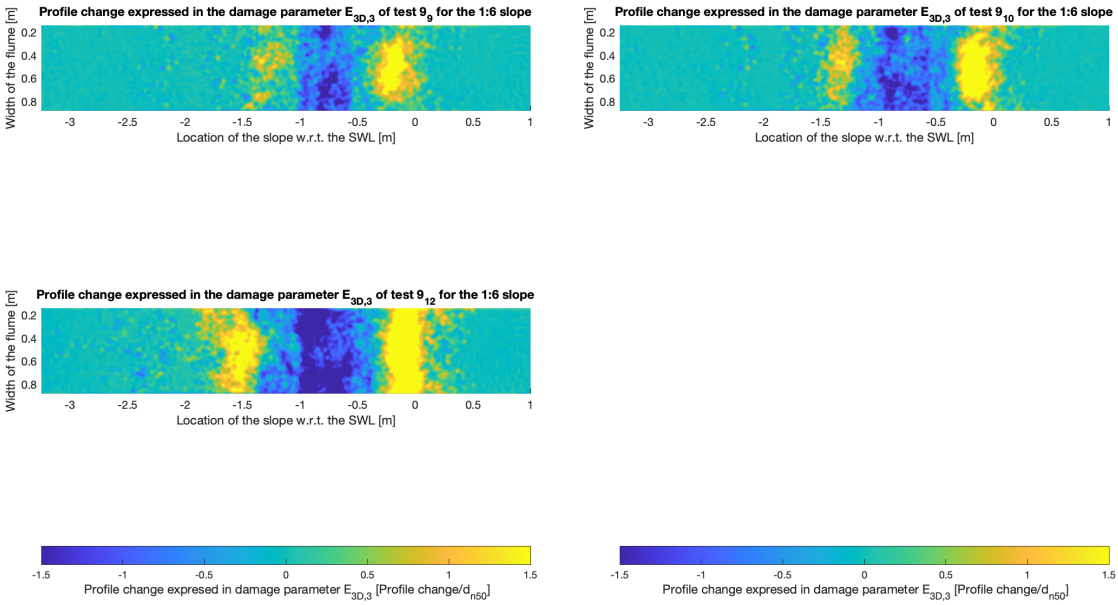

Figure M.13: Results 3D profiles for test 9 (part 2)

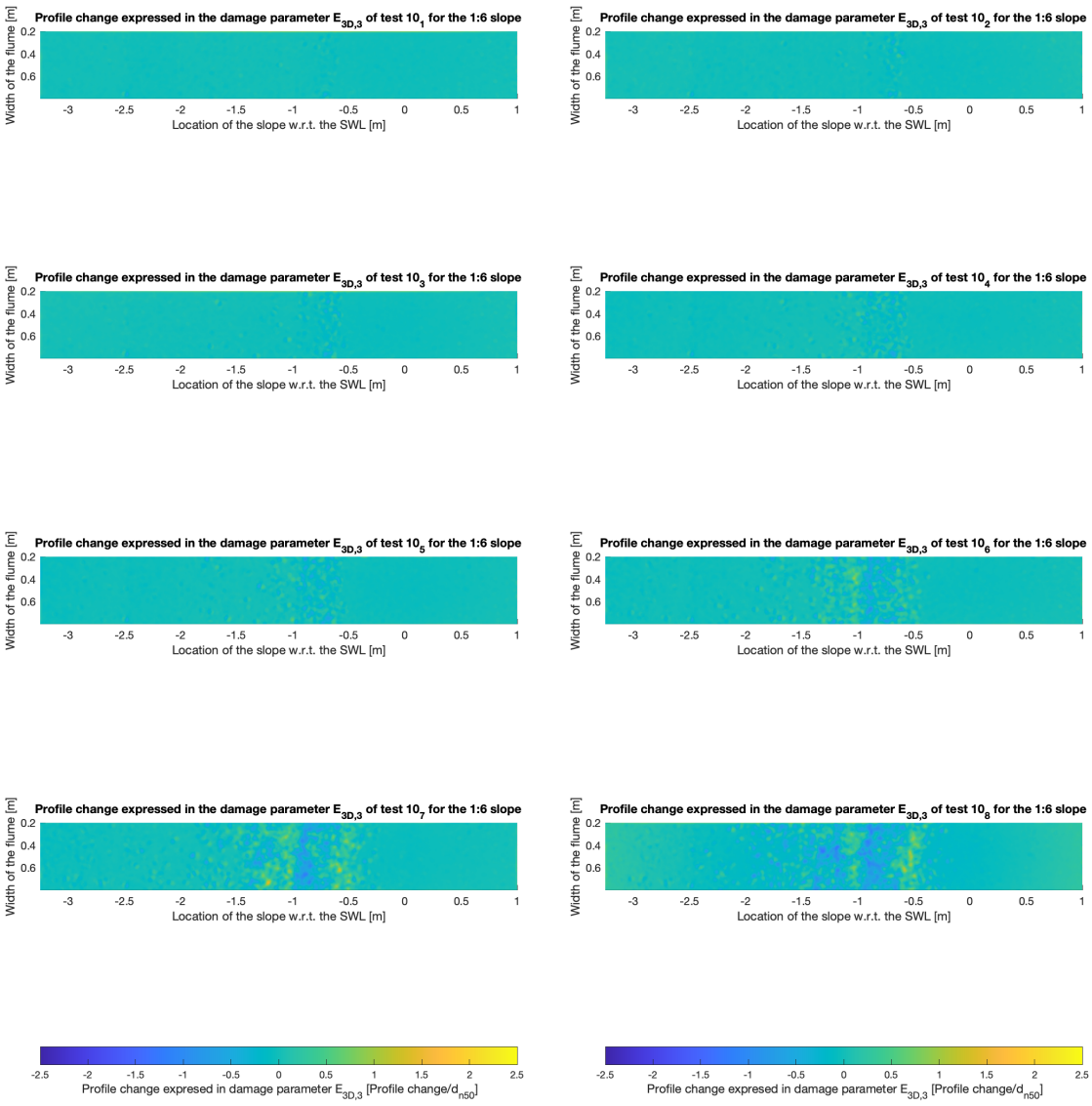

Figure M.14: Results 3D profiles for test 10 (part 1)

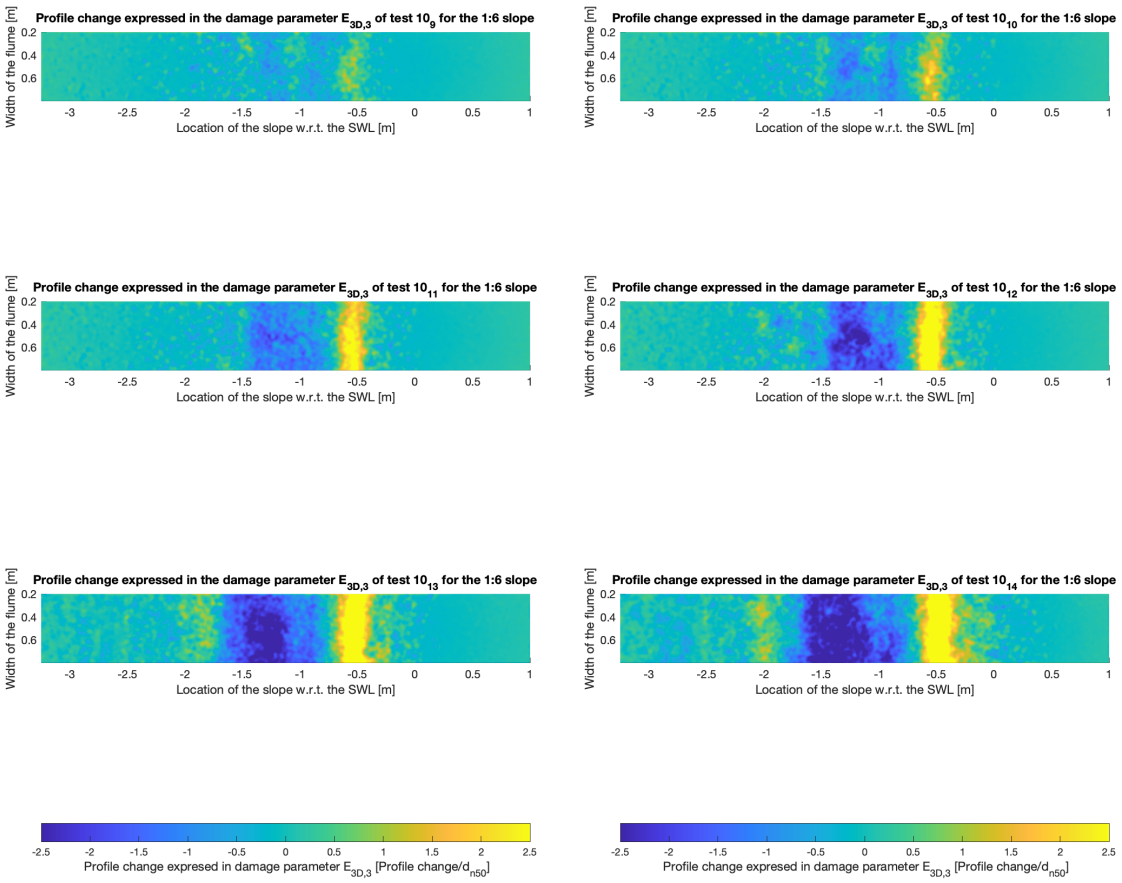

Figure M.15: Results 3D profiles for test 10 (part 2)

N
Test results slope 1:6 - 1:10

Test Information	H_s	N_s	$\xi_{m-1,0}$	N_{total}	S	$E_{3D,3}$	T	F_p	$N_{plunging}$
1_01	0.027	0.94	1.66	1013	0.00	0.25	2.5	1.00	1013
1_03	0.048	1.67	1.56	1124	2.95	0.77	2.5	1.00	1124
1_04	0.057	1.98	1.48	1215	2.32	0.84	2.5	1.00	1215
1_05	0.059	2.05	1.51	1208	2.77	1.08	2.5	1.00	1208
1_06	0.067	2.33	1.48	1154	13.74	1.05	2.5	1.00	1154
1_07	0.076	2.64	1.46	1172	13.80	1.40	2.5	1.00	1172
2_02	0.033	1.15	0.99	947	0.05	0.31	2.5	1.00	946
2_03	0.040	1.39	1.01	998	0.28	0.49	2.5	1.00	999
2_04	0.052	1.81	0.95	1018	0.61	0.60	2.5	0.99	1010
2_05	0.062	2.15	0.94	1072	1.80	0.84	2.5	0.99	1058
2_06	0.070	2.43	0.94	1072	3.03	0.76	2.5	0.99	1058
2_07	0.081	2.82	0.92	1078	4.64	1.20	2.5	0.98	1058
2_08	0.087	3.02	0.94	1048	6.81	1.07	2.5	0.99	1035
2_09	0.102	3.55	0.95	1082	9.20	1.41	2.5	0.99	1073
2_10	0.118	4.10	0.96	1091	15.67	1.36	2.5	0.99	1084
3_01	0.043	1.49	0.87	952	0.14	0.38	2.5	0.96	914
3_02	0.059	2.05	0.80	1105	1.36	0.54	2.5	0.92	1014
3_03	0.070	2.43	0.79	1039	2.35	0.73	2.5	0.91	941
3_04	0.078	2.71	0.79	1040	4.01	0.95	2.5	0.91	947
3_05	0.100	3.48	0.78	1116	9.45	1.32	2.5	0.90	1003
4_01	0.060	2.09	0.81	273	0.38	0.51	2.5	0.92	252
4_02	0.064	2.22	0.78	806	0.77	0.64	2.5	0.90	728
4_03	0.061	2.12	0.79	1848	1.41	0.66	2.5	0.91	1678
4_04	0.063	2.19	0.77	3987	1.94	0.67	2.5	0.89	3567
4_05	0.065	2.26	0.76	8219	2.94	0.81	2.5	0.89	7292
4_06	0.065	2.26	0.76	12650	3.17	0.95	2.5	0.89	11233
4_07	0.065	2.26	0.76	15262	3.20	0.93	2.5	0.89	13541
4_08	0.065	2.26	0.76	20482	3.43	1.02	2.5	0.89	18144
5_02	0.086	2.99	0.76	1085	2.78	0.71	2.5	0.88	958
5_04	0.085	2.95	0.76	1082	3.17	0.83	2.5	0.89	958
5_06	0.086	2.99	0.76	1093	1.64	0.68	2.5	0.88	967
5_08	0.084	2.92	0.76	1095	1.43	0.76	2.5	0.89	970
5_10	0.083	2.88	0.77	1080	2.27	0.76	2.5	0.90	967
6_01	0.039	1.36	0.83	1046	0.00	0.18	2.5	0.94	979
6_02	0.048	1.67	0.82	990	0.13	0.38	2.5	0.93	920
6_03	0.059	2.05	0.80	1101	0.74	0.58	2.5	0.92	1011
6_04	0.072	2.50	0.78	1038	2.80	0.71	2.5	0.90	933
6_05	0.078	2.71	0.79	1072	3.07	0.73	2.5	0.91	976
6_06	0.098	3.41	0.79	1131	7.39	0.91	2.5	0.91	1025
6_07	0.119	4.14	0.79	1118	14.10	1.33	2.5	0.91	1012

Figure N.1: Main test results slope 1:6 (part 1)

Test Information	H_s	N_s	$\xi_{m-1,0}$	N_{total}	S	$E_{3D,3}$	T	F_p	$N_{plunging}$
7_01	0.054	1.88	0.92	949	0.51	0.52	5	0.98	933
7_02	0.063	2.19	0.92	964	0.87	0.70	5	0.98	947
7_03A	0.069	2.40	0.95	1003	1.27	0.89	5	0.99	993
7_04	0.076	2.64	0.96	1020	1.38	0.84	5	0.99	1014
7_05A	0.082	2.85	0.97	1051	4.90	0.92	5	1.00	1046
7_06	0.105	3.65	0.94	1077	14.09	1.62	5	0.99	1065
8_01	0.026	0.90	1.66	1062	0.00	0.38	5	1.00	1062
8_02	0.036	1.25	1.63	1110	0.11	0.67	5	1.00	1110
8_03	0.049	1.70	1.52	1165	0.35	0.83	5	1.00	1165
8_04	0.057	1.98	1.47	1210	2.14	1.12	5	1.00	1210
8_05	0.062	2.15	1.48	1188	4.92	1.11	5	1.00	1188
8_06	0.066	2.29	1.50	1137	7.85	1.64	5	1.00	1137
8_07	0.076	2.64	1.47	1140	12.22	2.02	5	1.00	1140
8_08	0.084	2.92	1.47	1170	25.72	2.14	5	1.00	1170
9_01	0.050	1.74	0.80	954	0.36	0.38	5	0.92	876
9_02	0.063	2.19	0.78	1097	0.58	0.52	5	0.90	985
9_03	0.072	2.50	0.78	1028	1.10	0.73	5	0.90	925
9_04	0.079	2.75	0.79	1097	1.08	0.61	5	0.91	993
9_05	0.101	3.51	0.78	1116	1.57	1.10	5	0.90	1004
9_06	0.118	4.10	0.79	1098	4.50	1.27	5	0.91	997
9_07	0.130	4.52	0.78	1101	9.08	1.35	5	0.90	992
9_08	0.142	4.94	0.78	1081	15.92	1.51	5	0.90	973
9_09	0.151	5.25	0.78	1052	26.94	2.12	5	0.90	950
9_10	0.159	5.53	0.79	1078	38.42	2.16	5	0.91	978
10_01	0.042	1.46	0.80	1045	0.00	0.49	10	0.91	955
10_02	0.048	1.67	0.82	959	0.27	0.53	10	0.93	892
10_03	0.063	2.19	0.78	979	0.44	0.56	10	0.90	884
10_04	0.075	2.61	0.77	1353	0.38	0.57	10	0.89	1203
10_05	0.079	2.75	0.78	1094	0.40	0.72	10	0.90	990
10_06	0.099	3.44	0.79	1101	1.36	0.96	10	0.91	998
10_07	0.120	4.17	0.78	1111	5.40	1.17	10	0.90	1002
10_08	0.130	4.52	0.78	1100	7.23	1.34	10	0.90	994
10_09	0.142	4.94	0.78	1086	7.93	1.30	10	0.90	977
10_10	0.151	5.25	0.78	1045	27.55	1.73	10	0.90	944
10_11	0.163	5.67	0.78	1064	46.95	2.24	10	0.90	957
10_12	0.171	5.94	0.78	1066	72.98	3.32	10	0.90	961
10_13	0.192	6.67	0.77	1049	102.78	3.63	10	0.90	940
10_14	0.205	7.13	0.77	1057	127.07	3.76	10	0.90	947

Figure N.2: Main test results slope 1:6 (part 2)

Test Information	H_s	N_s	$\xi_{m-1,0}$	N_{total}	S	$E_{3D,3}$	T	F_p	$N_{plunging}$
1A	0.017	0.59	1.26	1114	0.00	0.18	2.5	1.00	1114
1B	0.024	0.83	1.28	1156	0.25	0.47	2.5	1.00	1156
1C	0.032	1.11	1.23	1183	0.22	0.43	2.5	1.00	1183
1D	0.042	1.46	1.16	1201	0.31	0.49	2.5	1.00	1201
1E	0.054	1.88	1.11	1272	0.54	0.66	2.5	1.00	1272
1F	0.065	2.26	1.14	1239	1.10	0.89	2.5	1.00	1239
1G	0.072	2.50	1.14	1173	3.00	0.81	2.5	1.00	1173
1H	0.081	2.82	1.14	1200	6.46	1.21	2.5	1.00	1200
2A	0.025	0.87	0.90	1083	0.05	0.34	2.5	0.97	1055
2B	0.036	1.25	0.85	1086	0.09	0.34	2.5	0.95	1031
2C	0.041	1.43	0.89	1110	0.12	0.34	2.5	0.97	1078
2E	0.068	2.36	0.86	1137	0.39	0.60	2.5	0.95	1085
2F	0.080	2.78	0.85	1106	0.47	0.58	2.5	0.95	1048
2G	0.087	3.02	0.86	1128	1.90	0.69	2.5	0.96	1078
2H	0.096	3.34	0.87	1101	1.45	1.00	2.5	0.96	1055
2I	0.110	3.82	0.81	1114	3.94	1.11	2.5	0.92	1029
3A	0.053	1.84	0.71	1180	0.17	0.28	2.5	0.83	985
3B	0.073	2.54	0.69	1181	0.38	0.44	2.5	0.81	960
3C	0.095	3.30	0.70	1227	1.88	0.80	2.5	0.83	1018
3D	0.119	4.14	0.72	1164	8.16	1.31	2.5	0.84	980
3NA	0.041	1.43	0.73	1037	0.00	0.26	2.5	0.85	885
3NB	0.055	1.91	0.68	1094	0.18	0.40	2.5	0.80	880
3NC	0.066	2.29	0.69	1131	0.29	0.47	2.5	0.81	916
3ND	0.081	2.82	0.67	1109	1.19	0.57	2.5	0.79	878
3NE	0.091	3.16	0.68	1154	0.52	0.81	2.5	0.80	925
3NF	0.105	3.65	0.67	1117	1.68	0.87	2.5	0.79	883
3NG	0.119	4.14	0.67	1125	1.79	0.89	2.5	0.79	888
4A	0.052	1.81	0.61	1047	0.00	0.22	2.5	0.71	746
4B	0.066	2.29	0.61	1036	0.00	0.44	2.5	0.71	740
4C	0.084	2.92	0.59	1101	0.60	0.61	2.5	0.69	763
4D	0.100	3.48	0.60	1104	1.22	0.57	2.5	0.71	779
4E	0.116	4.03	0.59	1105	2.89	0.73	2.5	0.69	767
4F	0.131	4.55	0.60	1091	1.28	1.14	2.5	0.70	761
4G	0.150	5.21	0.59	1114	2.46	0.77	2.5	0.69	764
4H	0.167	5.80	0.59	1110	4.00	1.23	2.5	0.68	760

Figure N.3: Main test results slope 1:8 (part 1)

Test Information	H_s	N_s	$\xi_{m-1,0}$	N_{total}	S	$E_{3D,3}$	T	F_p	$N_{plunging}$
5A	0.056	1.95	0.57	1079	0.05	0.40	2.5	0.67	719
5B	0.071	2.47	0.57	1060	0.23	0.30	2.5	0.66	702
5C	0.091	3.16	0.56	1107	0.46	0.48	2.5	0.65	716
5D	0.106	3.68	0.56	1127	1.19	0.80	2.5	0.65	730
5E	0.122	4.24	0.57	1132	2.08	0.86	2.5	0.65	740
5F	0.140	4.87	0.55	1108	2.57	0.81	2.5	0.63	694
5G	0.153	5.32	0.54	1088	2.95	1.00	2.5	0.62	674
5H	0.171	5.94	0.54	1113	5.82	1.23	2.5	0.61	680
6A	0.117	4.07	0.69	263	1.32	0.79	2.5	0.82	214
6B	0.117	4.07	0.68	531	2.06	0.99	2.5	0.81	430
6C	0.118	4.10	0.68	1087	2.72	0.86	2.5	0.81	877
6D	0.117	4.07	0.68	2199	5.89	0.93	2.5	0.80	1759
6E	0.118	4.10	0.67	4435	3.52	1.41	2.5	0.79	3524
6F	0.119	4.14	0.67	7789	7.46	1.10	2.5	0.79	6168
6G	0.119	4.14	0.67	11155	13.93	1.22	2.5	0.79	8828
6H	0.119	4.14	0.67	15603	20.45	1.45	2.5	0.79	12372
7A	0.055	1.91	0.68	1100	0.00	0.50	5	0.80	879
7B	0.067	2.33	0.68	1134	0.23	0.53	5	0.80	910
7C	0.080	2.78	0.67	1126	0.30	0.54	5	0.80	895
7D	0.092	3.20	0.67	1167	1.07	0.63	5	0.80	930
7E	0.106	3.68	0.67	1124	0.44	0.70	5	0.79	886
7F	0.120	4.17	0.66	1120	3.60	0.83	5	0.79	881
7G	0.132	4.59	0.67	1106	3.80	1.07	5	0.79	876
7H*	0.144	5.01	0.67	1084	7.27	1.76	5	0.80	863
7I	0.156	5.42	0.68	1073	35.34	2.01	5	0.80	860
8A	0.025	0.87	1.23	1186	0.12	0.23	5	1.00	1186
8B	0.035	1.22	1.17	1170	0.08	0.38	5	1.00	1170
8C	0.043	1.49	1.14	1223	0.24	0.61	5	1.00	1223
8D	0.052	1.81	1.13	1296	0.41	0.60	5	1.00	1296
8E	0.065	2.26	1.14	1236	3.01	1.08	5	1.00	1236
8F	0.073	2.54	1.12	1182	10.98	1.15	5	1.00	1182
8G	0.081	2.82	1.13	1192	26.80	1.90	5	1.00	1192
9A	0.120	4.17	0.66	1133	1.20	0.71	2.5	0.79	890
9B	0.120	4.17	0.67	1120	5.95	0.89	2.5	0.79	883
9C	0.119	4.14	0.67	1122	3.59	0.74	2.5	0.79	890
9D	0.119	4.14	0.67	1122	1.26	0.73	2.5	0.79	888
9E	0.119	4.14	0.67	1121	2.26	0.72	2.5	0.79	888

Figure N.4: Main test results slope 1:8 (part 2)

Test Information	H_s	N_s	$\xi_{m-1,0}$	N_{total}	S	$E_{3D,3}$	T	F_p	$N_{plunging}$
1a	0.062	2.15	0.94	1361	3.85	0.53	2.5	0.99	1346
1b	0.087	3.02	0.91	1332	3.07	0.80	2.5	0.98	1300
11a	0.066	2.29	0.91	1196	2.16	0.66	2.5	0.98	1171
11b	0.086	2.99	0.91	1216	5.36	1.18	2.5	0.98	1190
2a	0.089	3.09	0.53	837	2.13	0.47	2.5	0.61	508
2b	0.106	3.68	0.52	1241	2.22	0.47	2.5	0.58	721
2c	0.121	4.21	0.54	1211	4.96	0.88	2.5	0.62	754
2d	0.141	4.90	0.54	1277	5.77	1.05	2.5	0.61	785
2e	0.159	5.53	0.54	1253	13.50	1.31	2.5	0.61	769
2f	0.179	6.22	0.53	1254	20.51	1.18	2.5	0.61	761
2g	0.205	7.13	0.53	1246	27.41	1.37	2.5	0.59	737
3a	0.099	3.44	0.42	964	2.23	0.30	2.5	0.41	392
3b	0.116	4.03	0.42	1005	1.71	0.54	2.5	0.40	403
3c	0.134	4.66	0.42	1037	4.86	0.64	2.5	0.40	417
3d	0.148	5.14	0.43	1024	7.52	0.73	2.5	0.41	424
3e	0.165	5.73	0.43	1063	5.17	0.59	2.5	0.42	449
3f	0.183	6.36	0.44	1066	11.28	0.90	2.5	0.43	462
3g	0.203	7.06	0.44	1044	7.09	0.85	2.5	0.44	462
4a	0.076	2.64	0.64	1152	1.70	0.53	2.5	0.76	878
4b	0.094	3.27	0.65	1164	3.22	0.64	2.5	0.77	898
4c	0.114	3.96	0.67	1140	4.16	0.76	2.5	0.79	897
4d	0.134	4.66	0.65	1212	6.86	1.20	2.5	0.76	927
5a	0.101	3.51	0.47	928	4.88	0.44	2.5	0.51	469
5b	0.118	4.10	0.46	1103	2.21	0.55	2.5	0.49	538
5c	0.132	4.59	0.47	1063	3.62	0.66	2.5	0.50	527
5d	0.15	5.21	0.47	1093	4.57	0.70	2.5	0.50	543
5e	0.169	5.87	0.47	1076	4.98	0.73	2.5	0.50	541
5f	0.189	6.57	0.48	1053	11.09	0.76	2.5	0.51	535
5g	0.207	7.19	0.48	1048	16.43	1.05	2.5	0.51	538
6a	0.145	5.04	0.53	336	4.56	0.93	2.5	0.61	204
6b	0.143	4.97	0.53	1135	5.35	0.96	2.5	0.61	689
6c	0.141	4.90	0.54	2236	5.37	0.95	2.5	0.61	1374
6d	0.142	4.94	0.54	4298	13.00	1.07	2.5	0.61	2625
6e	0.143	4.97	0.53	7360	6.46	1.14	2.5	0.61	4454
6f	0.142	4.94	0.54	11456	11.02	1.03	2.5	0.61	6968
7a	0.109	3.80	0.90	1194	11.92	1.62	5	0.97	1161
7b	0.126	4.39	0.87	1292	29.43	1.99	5	0.96	1240
8a	0.161	5.61	0.53	1076	1.55	0.94	5	0.61	652
8b	0.184	6.41	0.53	1136	6.47	1.67	5	0.60	682
8c	0.203	7.07	0.53	1137	12.72	1.60	5	0.60	678

Figure N.5: Main test results slope 1:10

O

Test results of measurements slope 1:6

Test Information												
Test	**Steer file**	s_{0p} van H_{m0}	s_{0p} van $H_{1/3}$	s_{0p} van $H_{1/3}$ & $T_{m-1,0}$	N	$H_s/\Delta * d_{n50}$	ξ_p	$\xi_{m-1,0}$	H_{m0}	$H_{1/3}$	T_p	$T_{m-1,0}$
1_initial												
1_01	1_01	0.010	0.009	0.010	1013	0.94	1.78	1.78	0.029	0.027	1.394	1.299
1_02	1_02	0.010	0.009	0.011	1085	1.29	1.76	1.76	0.039	0.037	1.611	1.48
1_03	1_03	0.010	0.010	0.012	1124	1.67	1.72	1.72	0.051	0.048	1.79	1.628
1_04	1_04	0.010	0.010	0.013	1215	1.98	1.69	1.69	0.06	0.057	1.919	1.676
1_05	1_05	0.010	0.010	0.012	1208	2.05	1.71	1.71	0.063	0.059	1.976	1.742
1_06	1_06	0.011	0.010	0.013	1154	2.33	1.66	1.66	0.07	0.067	2.045	1.818
1_07	1_07	0.011	0.011	0.013	1172	2.64	1.61	1.61	0.079	0.076	2.117	1.919
1_08	1_08	0.010	0.010	0.013	1173	2.95	1.71	1.71	0.088	0.085	2.374	2.029
2_initial												
2_01	2_01	0.021	0.018	0.025	924	0.49	1.24	1.24	0.016	0.0140	0.7	0.601
2_02	2_02	0.027	0.024	0.029	947	1.15	1.08	1.08	0.036	0.0330	0.931	0.858
2_03	2_03	0.026	0.024	0.028	998	1.39	1.09	1.09	0.043	0.0400	1.037	0.964
2_04	2_04	0.029	0.027	0.031	1018	1.81	1.03	1.03	0.056	0.0520	1.113	1.034
2_05	2_05	0.030	0.028	0.032	1072	2.15	1.01	1.01	0.067	0.0620	1.199	1.109
2_06	2_06	0.028	0.026	0.032	1072	2.43	1.04	1.04	0.075	0.0700	1.312	1.18
2_07	2_07	0.027	0.026	0.033	1078	2.82	1.03	1.03	0.084	0.0810	1.4	1.246
2_07_H	X	X	X	X	X	X	X	X	X	X	X	X
2_08	2_08	0.029	0.027	0.032	1048	3.02	1.03	1.03	0.093	0.0870	1.443	1.317
2_09	2_09	0.027	0.025	0.031	1082	3.55	1.05	1.05	0.108	0.1020	1.602	1.449
2_10	2_10	0.026	0.025	0.031	1091	4.10	1.06	1.06	0.123	0.1180	1.729	1.57
2_11	2_11	0.027	0.026	0.032	1097	4.94	1.04	1.04	0.147	0.1420	1.866	1.675
3_initial		X	X									
3_01	3_01	0.038	0.035	0.037	952	1.49	0.89	0.89	0.046	0.0430	0.883	0.858
3_02	3_02	0.042	0.040	0.044	1105	2.05	0.84	0.84	0.063	0.0590	0.975	0.927
3_03	3_03	0.044	0.041	0.046	1039	2.43	0.83	0.83	0.075	0.0700	1.049	0.99
3_04	3_04	0.042	0.039	0.045	1040	2.71	0.85	0.85	0.083	0.0780	1.131	1.054
3_05	3_05	0.042	0.040	0.047	1116	3.48	0.84	0.84	0.105	0.1000	1.26	1.17
3_06	3_06	0.041	0.039	0.046	1106	4.17	0.85	0.85	0.126	0.1200	1.397	1.29
3_07	3_07	0.041	0.040	0.046	1103	4.48	0.84	0.84	0.132	0.129	1.444	1.339
3_08	3_08	0.041	0.040	0.046	1084	4.90	0.84	0.84	0.145	0.141	1.499	1.396
4_initial												
4_01	4_01	0.044	0.041	0.043	273	2.09	0.83	0.83	0.065	0.060	0.968	0.943
4_02	4_02	0.045	0.042	0.046	533	2.22	0.82	0.82	0.068	0.064	0.985	0.943
4_03	4_03	0.044	0.041	0.045	1042	2.12	0.83	0.83	0.065	0.061	0.978	0.928
4_04	4_04	0.044	0.042	0.047	2139	2.19	0.82	0.82	0.066	0.063	0.976	0.923
4_05	4_05	0.047	0.044	0.048	4232	2.26	0.80	0.80	0.069	0.065	0.974	0.927
4_06	4_06	0.047	0.044	0.048	4431	2.26	0.80	0.80	0.069	0.065	0.972	0.928
4_07	4_07	0.047	0.044	0.048	2612	2.26	0.80	0.80	0.069	0.065	0.974	0.927
4_08	4_08	0.047	0.044	0.049	5220	2.26	0.80	0.80	0.069	0.065	0.972	0.925

Figure O.1: Test results of measurements slope 1:6 (part 1)

Test Information												
Test	Steer file	s_{0p} van H_{m0}	s_{0p} van $H_{1/3}$	s_{0p} van $H_{1/3}$ & $T_{m-1,0}$	N	$H_s/\Delta * d_{n50}$	ξ_p	$\xi_{m-1,0}$	H_{m0}	$H_{1/3}$	T_p	$T_{m-1,0}$
5_01_ref		NON-CUMULATIVE										
5_02	5_01	0.047	0.044	0.049	1085	2.99	0.80	0.80	0.091	0.086	1.115	1.059
5_03_ref												
5_04	5_02	0.046	0.044	0.049	1082	2.95	0.81	0.81	0.089	0.085	1.119	1.057
5_05_ref												
5_06	5_03	0.043	0.044	0.049	1093	2.99	0.80	0.80	0.083	0.086	1.118	1.062
5_07_ref												
5_08	5_04	0.046	0.043	0.049	1095	2.92	0.81	0.81	0.089	0.084	1.115	1.052
5_09_ref												
5_10	5_05	0.045	0.043	0.047	1080	2.88	0.81	0.81	0.087	0.083	1.112	1.061
6_initial												
6_01	6_01	0.042	0.039	0.041	1046	1.36	0.85	0.85	0.042	0.0390	0.801	0.779
6_02	3_01	0.043	0.040	0.042	990	1.67	0.84	0.84	0.051	0.0480	0.873	0.854
6_03	3_02	0.043	0.040	0.044	1101	2.05	0.84	0.84	0.063	0.0590	0.974	0.928
6_04	3_03	0.043	0.041	0.047	1038	2.50	0.83	0.83	0.077	0.072	1.066	0.994
6_05	3_04	0.041	0.039	0.045	1072	2.71	0.85	0.85	0.082	0.0780	1.128	1.054
6_06	3_05	0.042	0.040	0.046	1131	3.41	0.84	0.84	0.103	0.0980	1.257	1.173
6_07	3_06	0.042	0.039	0.046	1118	4.14	0.85	0.85	0.126	0.119	1.395	1.291
7_initial												
7_01	2_04	0.030	0.028	0.033	949	1.88	1.01	1.01	0.058	0.054	1.114	1.021
7_02	2_05	0.029	0.027	0.033	964	2.19	1.02	1.02	0.067	0.063	1.216	1.101
7_03A	2_06	0.027	0.025	0.032	1003	2.40	1.06	1.06	0.074	0.069	1.326	1.182
7_04	2_07	0.027	0.025	0.030	1020	2.64	1.06	1.06	0.081	0.076	1.389	1.264
7_05A	2_08	0.027	0.025	0.030	1051	2.85	1.06	1.06	0.087	0.082	1.450	1.319
7_06	2_09	0.028	0.026	0.032	1077	3.65	1.04	1.04	0.110	0.105	1.599	1.455
7_07	2_10	0.026	0.025	0.031	1092	4.10	1.06	1.06	0.122	0.118	1.729	1.570
7_08	2_11	0.027	0.026	0.031	1096	4.76	1.04	1.04	0.142	0.137	1.832	1.687
7_09	7_09	0.027	0.026	0.034	1100	5.67	1.04	1.04	0.167	0.163	1.990	1.762
7_10	7_10	0.028	0.027	0.034	1113	6.33	1.03	1.03	0.190	0.182	2.084	1.843
8_initial												
8_01	1_01	0.010	0.009	0.010	1062	0.90	1.82	1.82	0.029	0.026	1.393	1.273
8_02	1_02	0.010	0.009	0.011	1110	1.25	1.78	1.78	0.039	0.036	1.605	1.474
8_03	1_03	0.010	0.010	0.012	1165	1.70	1.70	1.70	0.052	0.049	1.792	1.604
8_04	1_04	0.011	0.010	0.013	1210	1.98	1.68	1.68	0.060	0.057	1.912	1.675
8_05	1_05	0.011	0.010	0.013	1188	2.15	1.66	1.66	0.064	0.062	1.970	1.750
8_06	1_06	0.010	0.010	0.013	1137	2.29	1.68	1.68	0.068	0.066	2.059	1.829
8_07	1_07	0.011	0.011	0.013	1140	2.64	1.61	1.61	0.079	0.076	2.118	1.923
8_08	1_08	0.010	0.010	0.013	1170	2.92	1.72	1.72	0.086	0.084	2.375	2.021
8_09	8_09	0.011	0.010	0.014	1228	3.20	1.71	1.71	0.101	0.092	2.470	2.072
8_10	8_10	0.011	0.009	0.015	1285	3.30	1.77	1.77	0.112	0.095	2.590	2.013
8_11	8_11	0.011	0.009	0.018	1328	3.65	1.76	1.76	0.122	0.105	2.710	1.934

Figure O.2: Test results of measurements slope 1:6 (part 2)

Test Information												
Test	**Steer file**	s_{0p} van H_{m0}	s_{0p} van $H_{1/3}$	s_{0p} van $H_{1/3}$ & $T_{m-1,0}$	N	$H_s/\Delta * d_{n50}$	ξ_p	$\xi_{m-1,0}$	H_{m0}	$H_{1/3}$	T_p	$T_{m-1,0}$
9_initial												
9_01	9_01	0.043	0.040	0.044	954	1.74	0.84	0.84	0.054	0.050	0.897	0.854
9_02	3_02	0.046	0.043	0.047	1097	2.19	0.81	0.81	0.067	0.063	0.968	0.928
9_03	3_03	0.045	0.042	0.047	1028	2.50	0.82	0.82	0.077	0.072	1.053	0.995
9_04	3_04	0.043	0.041	0.046	1097	2.75	0.83	0.83	0.084	0.079	1.114	1.051
9_05	3_05	0.041	0.040	0.047	1116	3.51	0.84	0.84	0.105	0.101	1.274	1.178
9_06	3_06	0.040	0.039	0.045	1098	4.10	0.85	0.85	0.123	0.118	1.396	1.291
9_07	3_07	0.042	0.040	0.046	1101	4.52	0.84	0.84	0.135	0.130	1.443	1.339
9_08	3_08	0.041	0.040	0.047	1081	4.94	0.84	0.84	0.146	0.142	1.503	1.397
9_09	9_09	0.042	0.040	0.046	1052	5.25	0.84	0.84	0.16	0.151	1.562	1.449
9_10	9_10	0.042	0.040	0.046	1078	5.53	0.85	0.85	0.168	0.159	1.604	1.496
9_11	9_11	0.042	0.040	0.046	1066	5.94	0.84	0.84	0.179	0.171	1.655	1.538
9_12	9_12	0.043	0.041	0.046	1051	6.57	0.83	0.83	0.197	0.189	1.719	1.617
9_13	9_13	0.042	0.041	0.048	885	7.13	0.83	0.83	0.21	0.205	1.797	1.663
10_initial												
10_01	6_01	0.046	0.042	0.044	1045	1.46	0.82	0.82	0.045	0.042	0.796	0.778
10_02	3_01	0.042	0.038	0.042	959	1.67	0.86	0.86	0.052	0.048	0.894	0.855
10_03	3_02	0.046	0.043	0.046	979	2.19	0.81	0.81	0.067	0.063	0.968	0.936
10_04	3_03	0.046	0.043	0.048	1353	2.61	0.81	0.81	0.079	0.075	1.052	0.999
10_05	3_04	0.042	0.040	0.046	1094	2.75	0.84	0.84	0.083	0.079	1.123	1.05
10_06	3_05	0.042	0.040	0.046	1101	3.44	0.84	0.84	0.103	0.099	1.257	1.18
10_07	3_06	0.041	0.039	0.046	1111	4.17	0.85	0.85	0.125	0.120	1.396	1.289
10_08	3_07	0.041	0.040	0.046	1100	4.52	0.84	0.84	0.135	0.130	1.445	1.345
10_09	3_08	0.041	0.040	0.047	1086	4.94	0.84	0.84	0.146	0.142	1.506	1.397
10_10	9_09	0.042	0.040	0.046	1045	5.25	0.84	0.84	0.159	0.151	1.561	1.448
10_11	9_10	0.042	0.040	0.047	1064	5.67	0.84	0.84	0.171	0.163	1.607	1.495
10_12	9_11	0.041	0.040	0.046	1066	5.94	0.85	0.85	0.179	0.171	1.664	1.537
10_13	9_12	0.044	0.042	0.047	1049	6.67	0.82	0.82	0.2	0.192	1.713	1.616
10_14	9_13	0.042	0.040	0.047	1057	7.13	0.84	0.84	0.214	0.205	1.805	1.669

Figure O.3: Test results of measurements slope 1:6 (part 3)

P

Test results damage domains and locations for slope 1:6 - 1:10

	2D			E3Dm			E3Dm (27dn50)		
Test	S	Sall	E2D	m=1	m=3	m=5	m=1	m=3	m=5
1_initial									
1_01	0.00	0.00	0.00	0.88	0.28	0.15	0.86	0.25	0.15
1_02	5.37	3.14	0.07	1.60	0.67	0.47	1.24	0.67	0.47
1_03	2.95	3.97	0.23	1.54	0.77	0.71	1.34	0.77	0.71
1_04	2.32	2.83	0.20	1.44	0.84	0.60	1.37	0.84	0.60
1_05	2.77	5.43	0.21	2.07	1.08	0.72	1.72	1.08	0.70
1_06	13.74	8.96	0.43	1.80	1.15	0.85	1.79	1.05	0.85
1_07	13.80	14.02	0.51	2.34	1.40	1.17	2.34	1.40	1.17
1_08	33.42	33.68	1.61	2.98	2.50	2.43	2.91	2.50	2.43
2_initial									
2_01	0.00	0.00	0.00	0.85	0.17	0.07	0.50	0.11	0.06
2_02	0.05	0.11	0.00	1.18	0.34	0.13	0.85	0.31	0.12
2_03	0.28	0.24	0.02	1.31	0.56	0.27	1.25	0.49	0.27
2_04	0.61	0.66	0.09	1.56	0.65	0.41	1.56	0.60	0.41
2_05	1.80	1.20	0.22	1.68	0.84	0.58	1.21	0.84	0.58
2_06	3.03	2.00	0.27	1.53	0.88	0.62	1.52	0.76	0.60
2_07	4.64	2.85	0.38	1.86	1.20	0.83	1.86	1.20	0.83
2_07_H	4.71	2.93	0.39	1.91	1.20	0.83	1.86	1.21	0.83
2_08	6.81	3.97	0.51	1.92	1.13	0.84	1.71	1.07	0.78
2_09	9.20	6.60	0.70	1.98	1.44	1.19	1.98	1.41	1.16
2_10	15.67	7.58	0.76	2.08	1.41	1.16	2.08	1.36	1.08
2_11	24.21	10.89	0.88	2.25	1.62	1.43	2.25	1.43	1.28
3_initial									
3_01	0.14	0.44	0.06	1.24	0.38	0.16	1.23	0.38	0.16
3_02	1.36	1.61	0.15	1.25	0.54	0.36	1.13	0.54	0.36
3_03	2.35	2.66	0.29	1.35	0.73	0.58	1.17	0.73	0.58
3_04	4.01	4.44	0.50	1.64	0.95	0.76	1.64	0.95	0.75
3_05	9.45	10.05	0.80	1.85	1.32	1.19	1.85	1.32	1.19
3_06	18.13	18.48	0.97	2.19	1.72	1.45	2.19	1.72	1.45
3_07	23.22	23.31	1.19	2.30	1.76	1.66	2.30	1.76	1.66
3_08	27.69	27.89	1.20	2.38	1.99	1.71	2.27	1.99	1.71
4_initial									
4_01	0.38	0.56	0.07	1.28	0.51	0.32	1.28	0.51	0.32
4_02	0.77	0.94	0.11	1.29	0.64	0.48	1.29	0.64	0.48
4_03	1.41	1.83	0.21	1.36	0.76	0.52	1.36	0.66	0.52
4_04	1.94	2.53	0.24	1.45	0.89	0.52	1.36	0.67	0.49
4_05	2.94	3.11	0.27	1.51	1.06	0.69	1.59	0.81	0.58
4_06	3.17	3.26	0.34	1.55	1.03	0.77	1.55	0.95	0.74
4_07	3.20	4.40	0.32	1.59	1.00	0.70	1.52	0.93	0.64
4_08	3.43	4.25	0.37	1.89	1.09	0.68	1.54	1.02	0.68
5_01_ref									
5_02	2.78	2.94		1.5311	0.7136	0.54	1.53	0.71	0.54
5_03_ref									
5_04	3.17	3.19		1.5985	0.8349	0.61	1.47	0.83	0.61
5_05_ref									
5_06	1.64	2.02		1.737	0.7056	0.42	1.69	0.68	0.42
5_07_ref									
5_08	1.43	1.66		1.3543	0.9472	0.62	1.35	0.76	0.47
5_09_ref									
5_10	2.27	3.34		1.4137	0.7575	0.48	1.33	0.7575	0.47

Figure P.1: Test results of damage domains and locations for slope 1:6 (part 1)

	2D			E3Dm			E3Dm (27dn50)		
Test	S	Sall	E2D	m=1	m=3	m=5	m=1	m=3	m=5
6_initial									
6_01	0.00	0.00	0.03	0.98	0.19	0.15	0.80	0.18	0.14
6_02	0.13	0.40	0.05	0.86	0.38	0.20	0.77	0.38	0.20
6_03	0.74	1.34	0.11	1.12	0.57	0.32	1.08	0.58	0.32
6_04	2.80	3.97	0.19	1.26	0.71	0.50	1.26	0.71	0.50
6_05	3.07	3.10	0.27	1.18	0.76	0.57	1.15	0.73	0.49
6_06	7.39	8.12	0.46	1.49	0.91	0.75	1.49	0.91	0.75
6_07	14.10	14.44	0.67	1.87	1.33	1.07	1.87	1.33	1.04
7_initial									
7_01	0.51	1.26	0.13	1.38	0.52	0.25	1.14	0.48	0.24
7_02	0.87	2.01	0.18	1.43	0.70	0.40	1.14	0.48	0.24
7_03A	1.27	2.31	0.26	1.46	0.89	0.54	1.46	0.89	0.54
7_04	1.38	3.69	0.27	1.44	0.84	0.51	1.44	0.84	0.51
7_05A	4.90	5.28	0.40	1.68	0.92	0.69	1.68	0.92	0.66
7_06	14.09	15.66	0.80	2.20	1.62	1.33	2.20	1.62	1.26
7_07	31.50	31.99	1.60	3.05	2.56	2.33	3.05	2.56	2.33
7_08	64.76	51.10	2.41	3.91	3.08	2.96	3.91	3.08	2.96
7_09	95.51	60.06	2.92	4.14	3.38	3.35	4.06	3.68	3.35
7_10	146.17	69.09	3.66	5.12	4.78	4.60	5.12	4.78	4.60
8_initial									
8_01	0.00	0.02	0.03	1.51	0.38	0.16	1.19	0.35	0.15
8_02	0.11	0.19	0.05	1.40	0.67	0.41	1.27	0.50	0.22
8_03	0.35	0.60	0.11	1.47	0.83	0.41	1.45	0.77	0.40
8_04	2.14	3.40	0.29	1.61	1.12	0.69	1.61	1.12	0.66
8_05	4.92	5.64	0.43	1.58	1.11	0.79	1.58	1.11	0.79
8_06	7.85	10.04	0.83	2.33	1.64	1.49	2.33	1.64	1.49
8_07	12.22	14.76	1.04	2.78	2.02	1.78	2.78	2.02	1.78
8_08	25.72	30.30	1.16	2.63	2.14	1.86	2.63	2.14	1.86
8_09	60.86	56.18	1.79	3.42	2.69	2.50	3.42	2.69	2.50
8_10	78.36	79.65	2.46	3.73	3.33	3.16	3.73	3.33	3.16
8_11	143.50	140.65	3.83	4.87	4.25	4.36	4.87	4.53	4.36
9_initial									
9_01	0.36	0.76	0.06	1.38	0.38	0.19	0.76	0.23	0.15
9_02	0.58	0.88	0.07	1.20	0.52	0.40	0.98	0.50	0.28
9_03	1.10	2.70	0.14	1.81	0.73	0.35	1.60	0.73	0.34
9_04	1.08	1.74	0.15	1.51	0.61	0.40	1.16	0.61	0.38
9_05	1.57	4.07	0.22	1.46	1.10	0.73	1.33	1.10	0.73
9_06	4.50	7.19	0.29	2.09	1.27	0.96	1.60	0.96	0.75
9_07	9.08	12.80	0.61	1.78	1.35	1.03	1.76	1.35	1.03
9_08	15.92	18.73	0.78	1.99	1.51	1.25	1.94	1.48	1.25
9_09	26.94	27.27	1.23	2.72	2.12	1.92	2.72	2.12	1.92
9_10	38.42	38.62	1.29	2.88	2.16	1.92	2.79	2.16	1.80
9_11	50.66	51.50	1.83	3.25	2.60	2.36	3.06	2.57	2.23
9_12	65.29	65.92	1.91	3.42	3.02	2.79	2.98	2.45	2.25
9_13	90.90	91.47	2.02	3.27	2.77	2.54	3.12	2.62	2.46
10_initial									
10_01	0.00	0.00	0.03	1.48	0.49	0.21	1.028	0.1989	0.104
10_02	0.27	0.77	0.07	1.48	0.53	0.27	1.19	0.53012	0.2692
10_03	0.44	1.95	0.12	1.48	0.56	0.34	1.176	0.42074	0.2305
10_04	0.38	0.91	0.12	1.44	0.57	0.47	1.306	0.45465	0.2292
10_05	0.40	2.93	0.15	1.77	0.72	0.45	1.407	0.5711	0.2856
10_06	1.36	3.85	0.37	1.66	0.96	0.63	1.664	0.9613	0.6319
10_07	5.40	7.48	0.54	2.02	1.17	0.91	2.019	1.17102	0.9119
10_08	7.23	25.70	0.65	2.09	1.34	1.06	1.962	1.33564	1.0586
10_09	7.93	28.62	0.65	2.61	1.30	1.04	2.609	1.29874	1.0404
10_10	27.55	39.49	1.00	2.44	1.73	1.63	2.439	1.72507	1.6258
10_11	46.95	58.85	1.32	3.21	2.24	1.91	3.213	2.24229	1.9082
10_12	72.98	79.78	2.06	3.81	3.32	3.04	3.807	3.31985	3.0385
10_13	102.78	107.24	2.66	4.30	3.63	3.29	4.301	3.6265	3.2945
10_14	127.07	126.97	2.80	4.36	3.76	3.39	4.356	3.75737	3.3944

Figure P.2: Test results of damage domains and locations for slope 1:6 (part 2)

Test Information			Test conditions		Damage domain				Max damage location			
Series	Run	$s_{o,p}$	$H_{1/3}$	$\frac{Hs}{\Delta d_{n50}}$	Low	Mid-Low	Mid-High	High	2D max	$E_{3D,1}$ max	$E_{3D,3}$ max	$E_{3D,5}$ max
	A	0.009	0.017	0.59	-3.03	0.00	0.00	0.72	-	-3.01	-3.09	-3.20
	B	0.008	0.024	0.84	-2.14	-0.17	0.67	1.03	0.18	-0.13	0.26	0.18
	C	0.009	0.032	1.11	-3.09	-0.67	0.89	0.97	0.13	-0.10	0.14	0.14
1	D	0.009	0.042	1.46	-4.02	-1.82	0.68	0.74	-0.55	-1.50	-1.47	-1.53
	E	0.011	0.054	1.88	-4.63	-2.11	0.55	0.78	0.11	-1.17	-0.82	-0.42
	F	0.010	0.065	2.26	-3.85	-2.70	1.00	1.11	-1.89	-1.88	-1.10	-1.07
	G	0.010	0.072	2.51	-3.48	-2.54	1.09	1.25	-0.80	-1.72	-1.09	-1.08
	H	0.009	0.081	2.82	-4.57	-2.70	0.99	1.12	-1.08	-1.18	-1.17	-1.20
	A	0.016	0.025	0.87	-1.31	0.19	0.24	0.54	-	0.23	0.18	0.10
	B	0.020	0.036	1.25	-1.60	0.13	0.31	0.72	-	0.16	0.12	0.10
	C	0.017	0.041	1.43	-1.41	-1.13	0.64	0.64	0.09	0.27	0.26	0.32
	D*	[redacted]										
2	E	0.020	0.068	2.37	-2.60	-1.18	0.49	0.64	-0.33	-0.27	-0.28	-0.33
	F	0.020	0.08	2.79	-3.38	-1.11	0.54	0.58	-0.26	-0.24	0.12	0.12
	G	0.020	0.087	3.03	-3.11	-2.03	0.80	0.92	-0.25	-1.36	0.15	-0.45
	H	0.020	0.096	3.34	-3.04	-2.74	0.73	0.92	-0.81	-0.70	-0.72	-0.74
	I	0.019	0.110	3.83	-3.07	-2.50	0.82	1.00	-0.70	-0.96	-0.96	-0.98
	A	0.028	0.053	1.85	-1.89	-1.11	0.37	0.54	0.16	0.19	0.18	0.17
	B	0.026	0.073	2.54	-2.30	-0.88	0.55	0.55	-0.57	0.14	-0.52	-0.50
3	C	0.027	0.095	3.31	-3.57	-2.08	0.60	0.73	-0.23	-0.22	-0.23	-0.26
	D	0.026	0.119	4.14	-3.34	-2.48	0.88	0.99	-0.32	-0.39	-0.39	-0.32
	E	0.025	0.145	5.05	-2.74	-2.04	0.81	0.82	-0.29	-0.75	-0.72	-0.72
	A	0.026	0.041	1.43	-1.77	-0.34	0.27	0.79	-	0.24	-1.77	0.03
	B	0.030	0.055	1.92	-1.84	-1.05	0.59	0.75	0.32	-1.02	-1.05	-1.00
	C	0.029	0.066	2.30	-1.82	-1.73	0.62	0.79	0.05	-0.79	-0.77	0.14
	D	0.029	0.081	2.82	-1.48	-1.41	0.55	0.71	-0.24	-0.41	-0.41	-0.28
3N	E	0.028	0.091	3.17	-2.01	-1.99	0.59	0.75	-0.14	-0.57	-0.39	-0.38
	F	0.029	0.105	3.66	-3.06	-1.93	0.64	0.66	-0.69	-0.67	-0.67	-0.35
	G	0.029	0.119	4.14	-2.70	-1.89	0.68	0.69	-0.11	-0.48	-0.48	-0.32
	H	0.029	0.13	4.53	-3.06	-1.92	0.64	0.77	-0.37	-0.40	-0.39	-0.43
	I	0.030	0.145	5.05	-2.74	-2.23	0.72	0.73	-0.37	-0.42	-0.42	-0.42
	A	0.038	0.052	1.81	-1.11	-0.56	0.43	0.57	-	0.12	0.24	-0.02
	B	0.038	0.066	2.30	-3.37	-0.87	0.41	0.49	0.04	-0.21	-0.15	-0.15
	C	0.040	0.084	2.93	-2.65	-1.24	0.56	0.64	-0.17	-0.45	-0.16	-0.14
4	D	0.038	0.1	3.48	-2.08	-1.56	0.57	0.74	-0.13	0.18	-0.62	-0.63
	E	0.038	0.116	4.04	-3.36	-1.58	0.63	0.64	-0.36	-1.03	-0.11	-0.44
	F	0.038	0.131	4.56	-2.98	-2.00	0.64	0.69	-0.45	-0.51	-0.47	-0.47
	G	0.039	0.15	5.22	-2.60	-2.19	0.66	0.70	-0.57	-0.61	-0.61	-0.62
	H	0.040	0.167	5.82	-2.40	-1.97	0.62	0.63	-0.51	-0.58	-0.51	-0.52
	A	0.048	0.056	1.95	-1.03	-0.29	0.33	0.40	-	-0.27	-0.27	-0.23
	B	0.045	0.071	2.47	-2.49	-0.80	0.35	0.51	0.03	-0.30	0.00	0.02
	C	0.047	0.091	3.17	-3.20	-1.24	0.53	0.64	0.01	0.18	0.16	-0.19
	D	0.045	0.106	3.69	-2.75	-1.10	0.47	0.55	-0.22	0.15	-0.16	-0.17
5	E	0.043	0.122	4.25	-3.02	-1.46	0.49	0.51	-0.17	-1.44	-0.58	-0.59
	F	0.046	0.14	4.88	-2.64	-1.43	0.59	0.61	-0.11	0.02	-0.10	-0.55
	G	0.049	0.153	5.33	-2.46	-1.68	0.46	0.60	-0.09	-1.15	-0.51	-0.51
	H	0.050	0.171	5.96	-2.20	-1.92	0.53	0.60	-0.40	-0.41	-0.57	-0.42
	I	0.050	0.189	6.58	-2.05	-1.75	0.55	0.65	-0.41	-0.40	-0.41	-0.41
	A	0.028	0.117	4.07	-2.79	-1.80	0.66	0.68	-0.87	-0.77	-0.88	-0.87
	B	0.028	0.117	4.07	-2.79	-1.80	0.65	-0.40	-0.14	-0.13	-0.80	-0.80
	C	0.029	0.118	4.11	-2.77	-2.11	0.64	0.65	-0.61	-0.56	-0.60	-0.87
6	D	0.028	0.117	4.07	-2.79	-2.13	0.65	0.66	-0.32	-0.13	-0.10	-0.90
	E	0.029	0.118	4.11	-3.35	-3.13	0.70	0.86	-0.58	-0.38	-0.37	-0.36
	F	0.029	0.119	4.14	-3.35	-3.10	0.70	0.82	-0.41	-0.13	-0.66	-0.65
	G	0.029	0.119	4.14	-3.35	-3.10	0.77	0.87	-0.32	-0.12	-0.12	-0.37
	H	0.030	0.119	4.14	-3.35	-3.10	0.77	0.90	-0.20	-0.66	-0.24	-0.38
	A	0.030	0.055	1.92	-4.21	-0.76	0.47	0.70	-	-0.50	-0.50	-0.50
	B	0.029	0.067	2.33	-3.46	-0.86	0.61	0.65	0.14	-0.41	-0.41	-0.34
	C	0.028	0.08	2.79	-2.90	-0.93	0.60	0.65	-0.25	-0.12	-0.34	-0.28
	D	0.029	0.092	3.20	-2.52	-2.50	0.61	0.69	-0.55	-0.10	-0.10	-0.96
	E	0.030	0.106	3.69	-2.32	-2.19	0.66	0.76	-0.80	-0.20	-0.21	-1.13
7	F	0.029	0.12	4.18	-2.78	-1.93	0.73	0.79	-0.68	-1.04	-1.03	-0.98
	G	0.029	0.132	4.60	-2.71	-1.84	0.80	0.86	-0.63	-0.90	-0.90	-0.92
	H**	0.030	0.144	5.02	-2.49	-1.70	0.76	0.80	-0.57	-0.82	-0.85	-0.84
	I	0.028	0.156	5.43	-2.29	-2.15	0.83	0.90	-0.53	-0.84	-0.84	-0.81
	J	0.029	0.173	6.03	-2.07	-1.96	0.75	0.84	-0.44	-0.68	-0.68	-0.67
	K	0.029	0.189	6.58	-1.91	-1.89	0.82	0.82	-0.41	-0.59	-0.60	-0.59
	L	0.029	0.198	6.90	-1.82	-1.81	0.78	0.78	-0.41	-0.60	-0.59	-0.59
	A	0.008	0.025	0.87	-2.52	-1.77	0.38	0.63	0.23	-3.98	-4.05	-4.13
	B	0.010	0.035	1.22	-1.80	-0.69	0.56	0.70	0.00	-2.82	-2.86	-2.89
	C	0.010	0.043	1.50	-2.34	-1.99	0.69	0.95	0.41	-0.47	-0.48	-0.48
	D	0.010	0.052	1.81	-2.36	-2.32	0.81	1.00	-0.89	-2.04	-0.40	-0.40
	E	0.010	0.065	2.26	-3.68	-2.37	0.82	0.97	-1.12	-1.77	-1.77	-1.67
8	F	0.010	0.073	2.54	-3.58	-3.24	0.95	1.16	-1.00	-1.36	-1.57	-1.42
	G	0.009	0.081	2.82	-3.83	-3.20	1.18	1.20	-0.89	-1.41	-1.39	-1.38
	H	0.010	0.093	3.24	-3.61	-3.54	1.10	1.26	-0.91	-1.34	-1.33	-1.28
	I	0.011	0.101	3.52	-3.33	-3.26	1.17	1.28	-1.01	-1.32	-1.33	-1.34
	J	0.011	0.11	3.83	-3.23	-2.99	1.19	1.26	-0.98	-1.33	-1.31	-1.31
	K	0.010	0.118	4.11	-3.01	-2.79	1.10	1.17	-0.92	-1.17	-1.18	-1.22
	A	0.029	0.12	4.18	-2.72	-2.62	0.69	0.70	-0.23	-0.36	-0.35	-0.35
	B	0.029	0.12	4.18	-3.31	-2.25	0.64	0.84	-0.20	-0.19	-0.25	-0.27
9	C	0.029	0.119	4.14	-2.84	-2.31	0.67	0.81	-0.21	-0.22	-0.41	-0.73
	D	0.029	0.119	4.14	-2.83	-2.52	0.66	0.78	-0.21	-1.51	-0.65	-0.63
	E	0.029	0.119	4.14	-3.24	-1.98	0.65	0.75	-0.17	0.40	-0.70	-0.59

Figure P.3: Damage domains and locations for all tests of slope 1:8

Test Information		Test conditions			Damage domain				Max damage location			
Series	Run	$s_{o,p}$	$H_{1/3}$	Hs Δd_{n50}	Low	Mid-Low	Mid-High	High	2D max	$E_{3D,1}$ max	$E_{3D,3}$ max	$E_{3D,5}$ max
1	A	0.009	0.062	2.16	-4.15	-3.35	0.44	0.50	-0.34	-1.10	-1.10	-0.71
	B	0.010	0.087	3.03	-3.10	-3.00	0.47	0.59	-0.63	-1.66	-1.16	-1.16
	C	0.009	0.109	3.80	-2.48*	-2.47	0.53	0.82	-0.55	-1.04	-1.04	-1.03
11	A	0.009	0.066	2.30	-3.73	-2.48	0.23	0.29	0.17	-1.41	-1.42	-1.41
	B	0.010	0.086	3.00	-3.14	-3.13	0.49	0.63	-0.61	0.08	-1.19	-1.20
	C	0.010	0.11	3.83	-2.45	-2.45	0.38	0.49	-0.82	-1.24	-1.24	-1.25
	D	0.010	0.126	4.39	-2.14*	-2.14	0.69	0.71	-0.64	-1.12	-1.12	-1.10
2	A	0.030	0.089	3.10	-2.19	-1.85	0.19	0.36	-0.09	-0.40	-0.56	-0.57
	B	0.031	0.106	3.69	-2.48	-2.28	0.17	0.47	-0.03	-0.16	-0.16	-0.48
	C	0.027	0.121	4.21	-2.23	-2.17	0.40	0.54	-0.44	-0.82	-0.83	-0.81
	D	0.029	0.141	4.91	-1.91*	-1.87	0.35	0.45	-0.36	-0.83	-0.83	-0.82
	E	0.028	0.159	5.54	-1.70*	-1.70*	0.49	0.50	-0.18	-1.42	-1.02	-0.80
	F	0.028	0.179	6.23	-1.51*	-1.51*	0.44	0.53	-0.32	-0.49	-0.53	-0.53
	G	0.030	0.205	7.14	-1.32*	-1.32*	0.56	0.56	-0.26	-0.51	-0.71	-0.79
	H	0.031	0.225	7.84	-1.20*	-1.20*	0.50	0.51	-0.34	-0.58	-0.56	-0.56
	I	0.029	0.245	8.53	-1.10*	-1.10*	0.46*	0.47*	-0.22	-0.83	-0.84	-0.84
3	A	0.052	0.099	3.45	-2.64	-1.70	0.05	0.31	0.00	-0.18	-0.18	-0.18
	B	0.052	0.116	4.04	-2.25	-1.04	0.10	0.27	-0.06	-0.54	-0.55	-0.44
	C	0.051	0.134	4.67	-1.95	-1.14	0.19	0.23	0.21	-0.55	-0.76	-0.75
	D	0.050	0.148	5.15	-1.79	-1.76	0.19	0.34	-0.17	-0.55	-0.55	-0.55
	E	0.048	0.165	5.75	-1.61	-1.58	0.38	0.39	-0.14	-0.57	-0.54	-0.76
	F	0.044	0.183	6.37	-1.45	-1.42	0.39	0.42	-0.25	-0.48	-0.79	-0.79
	G	0.045	0.203	7.07	-1.33	-1.33	0.40	0.41	-0.23	-0.84	0.02	0.02
4	A	0.018	0.076	2.65	-1.96	-1.76	0.25	0.29	-0.20	-1.49	-0.76	-0.76
	B	0.019	0.094	3.27	-2.48	-2.01	0.43	0.46	-0.04	-0.48	-0.97	-0.96
	C	0.017	0.114	3.97	-2.37	-2.36	0.39	0.57	-0.82	-0.87	-1.46	-1.29
	D	0.019	0.134	4.67	-2.01*	-2.01	0.46	0.56	-0.58	-0.97	-0.97	-0.97
	E	0.019	0.157	5.47	-1.72*	-1.72*	0.57	0.67	-0.50	-1.37	-0.89	-0.89
	F	0.020	0.174	6.06	-1.55*	-1.55*	0.51	0.67	-0.40	-0.78	-0.76	-0.78
5	A	0.038	0.101	3.52	-1.78	-1.31	0.07	0.08	-0.31	-0.08	-0.37	-0.37
	B	0.039	0.118	4.11	-2.29	-1.20	0.22	0.24	-0.24	-0.33	-0.31	-0.62
	C	0.039	0.132	4.60	-2.05*	-1.36	0.22	0.33	-0.33	-1.24	-0.28	-0.55
	D	0.036	0.15	5.22	-1.80*	-1.77	0.31	0.35	-0.31	0.25	-0.61	-0.61
	E	0.037	0.169	5.89	-1.60*	-1.60	0.41	0.41	-0.17	-0.43	-0.75	-0.75
	F	0.038	0.189	6.58	-1.43*	-1.43	0.41	0.42	-0.39	-0.55	-0.56	-0.41
	G	0.036	0.207	7.21	-1.30*	-1.30	0.57	0.57	-0.23	-0.54	-0.73	-0.53
6	A	0.029	0.145	5.05	-1.83	-1.79	0.34	0.46	-0.42	-0.77	-0.77	-0.77
	B	0.029	0.143	4.98	-1.89*	-1.82	0.34	0.46	-0.68	-0.74	-1.30	-0.99
	C	0.028	0.141	4.91	-1.91*	-1.84	0.35	0.47	0.07	-0.63	-0.93	-0.94
	D	0.029	0.142	4.95	-1.90*	-1.87	0.46	0.58	-0.73	0.39	-1.06	-1.04
	E	0.029	0.143	4.98	-1.89*	-1.85	0.46	0.58	-0.73	-1.11	-0.91	-0.91
	F	0.029	0.142	4.95	-1.90*	-1.87	0.46	0.58	-0.52	-0.87	-0.87	-0.93
7	A	0.009	0.109	3.80	-2.12*	-2.12*	0.51	0.72	-0.73	-1.46	-1.47	-1.46
	B	0.010	0.126	4.39	-1.83*	-1.83*	0.56	0.63	-0.66	-1.26	-1.27	-1.36
	C	0.010	0.137	4.77	-1.69*	-1.69*	0.82	0.90	-0.58	-1.34	-1.28	-1.25
8	A	0.028	0.161	5.61	-1.43*	-1.43*	0.41	0.43	-0.69	-1.76	-1.38	-1.38
	B	0.028	0.184	6.41	-1.26*	-1.26*	0.36	0.41	-0.59	-1.01	-1.01	-1.01
	C	0.029	0.203	7.07	-1.14*	-1.14*	0.48	0.63	-0.52	-1.25	-1.24	-1.24
				Average values	-2.4	-1.9	0.4	0.5	-0.4	-0.8	-0.8	-0.8

* These tests are considered to be unreliable, because the damage location is expected to be outside the measured area.

Figure P.4: Damage domains and locations for all tests of slope 1:10

Q
Accuracy 3D parameters

To give a reliable range of 3D damage numbers, the initial profile has been shifted with the accuracy limit of +/- 0.5 mm obtained from the check tests. Figure Q.1 shows the damage profile calculated following the method described in section 3.2.5.

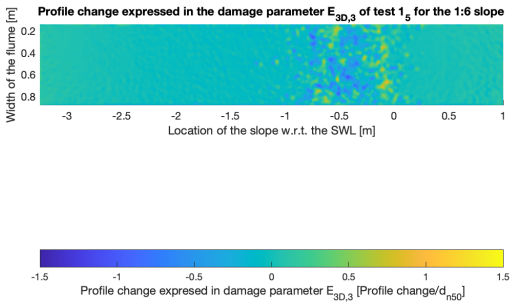

Figure Q.1: 3D damage profile

Figure Q.2 shows the damage profile with a translated initial profile of 0.5 mm.

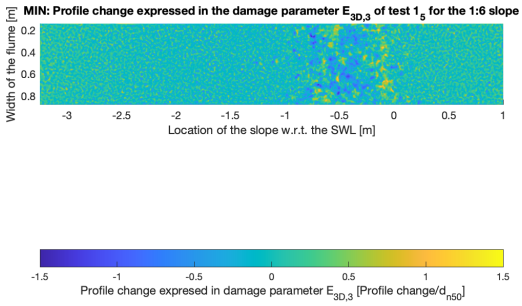

Figure Q.2: 3D damage profile combined with minus accuracy limit of 0.5 mm on initial profile

Figure Q.2 shows the damage profile with a translated initial profile of 0.5 mm.

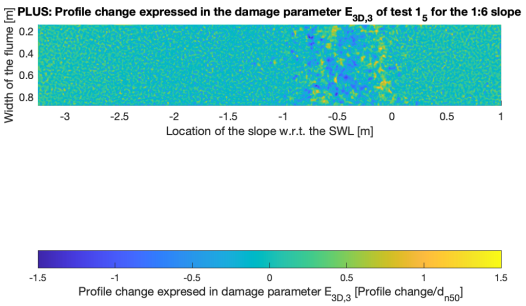

Figure Q.3: 3D damage profile combined with plus accuracy limit of 0.5 mm on initial profile

R

Quantification of 2D damage parameters

R.1 Damage parameter S

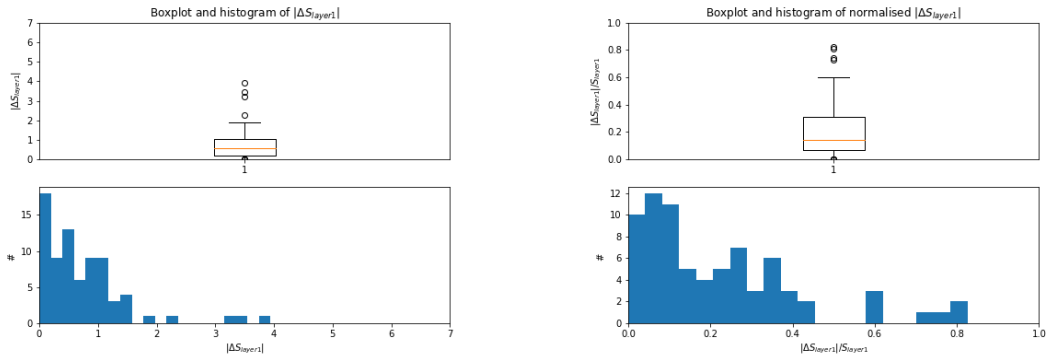

(a) Absolute difference

(b) Normalised difference

Figure R.1: a) Absolute and b) normalised difference of damage parameter S for layer 1 ($2.5 * d_{n50}$) compared with +/- threshold situations

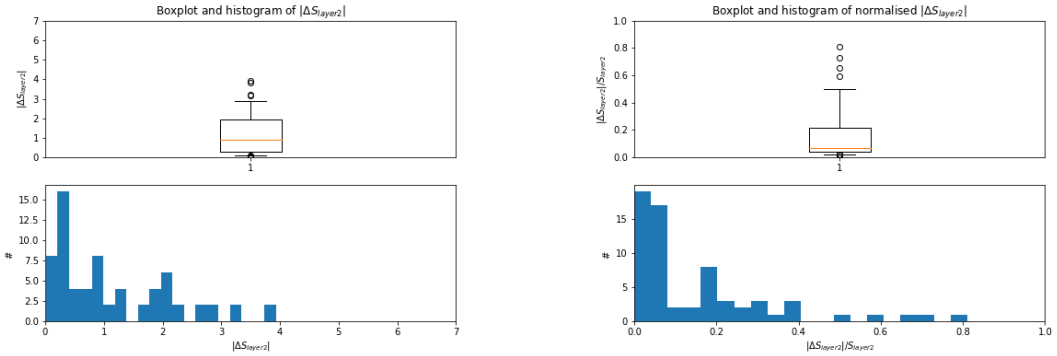

(a) Absolute difference (b) Normalised difference

Figure R.2: a) Absolute and b) normalised difference of damage parameter S for layer 2 ($5 * d_{n50}$) compared with +/- threshold situations

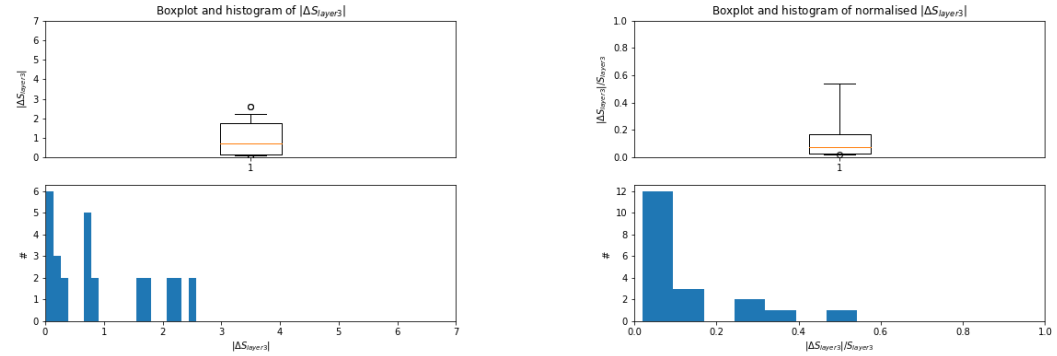

(a) Absolute difference (b) Normalised difference

Figure R.3: a) Absolute and b) normalised difference of damage parameter S for layer 3 ($10 * d_{n50}$) compared with +/- threshold situations

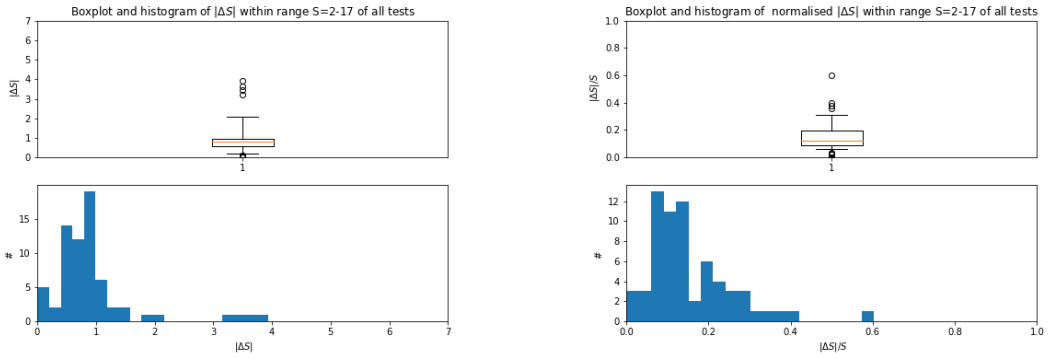

(a) Absolute difference (b) Normalised difference

Figure R.4: a) Absolute and b) normalised difference of damage parameter S for range $S = 2 - 17$ compared with +/- threshold situations

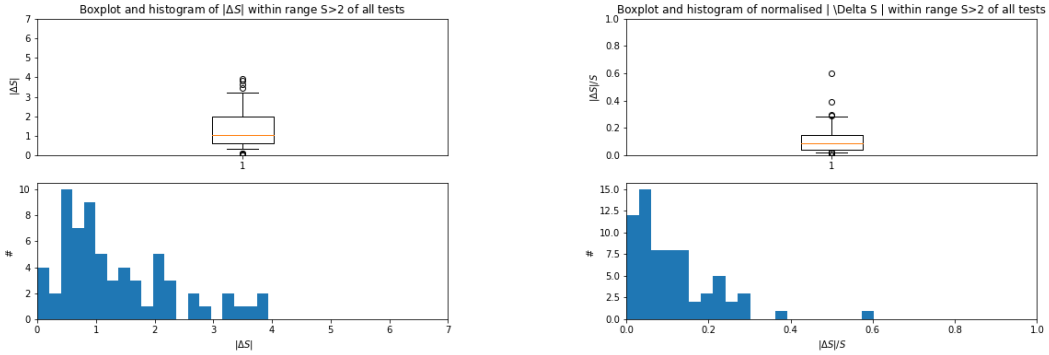

(a) Absolute difference (b) Normalised difference

Figure R.5: a) Absolute and b) normalised difference of damage parameter S for range $S > 2$ compared with +/- threshold situations

R.2 Damage parameter S_{all}

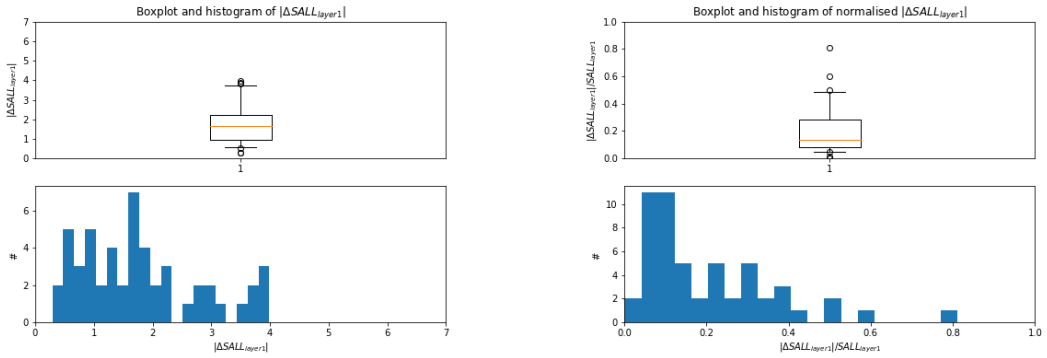

(a) Absolute difference (b) Normalised difference

Figure R.6: a) Absolute and b) normalised difference of damage parameter S_{all} for layer 1 ($2.5 * d_{n50}$) compared with +/- threshold situations

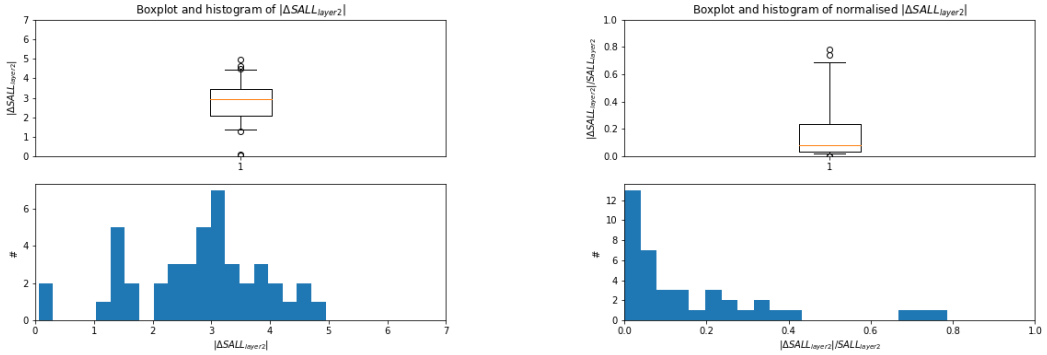

(a) Absolute difference (b) Normalised difference

Figure R.7: a) Absolute and b) normalised difference of damage parameter S_{all} for layer 2 ($5 * d_{n50}$) compared with +/- threshold situations

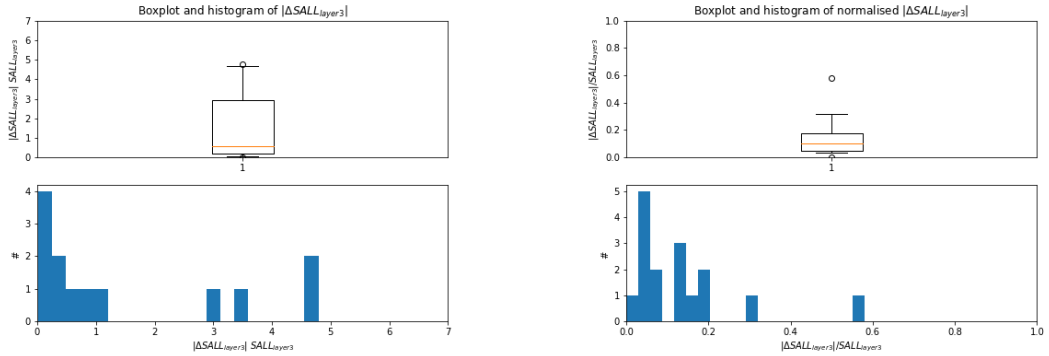

(a) Absolute difference (b) Normalised difference

Figure R.8: a) Absolute and b) normalised difference of damage parameter S_{all} for layer 3 ($10 * d_{n50}$) compared with +/- threshold situations

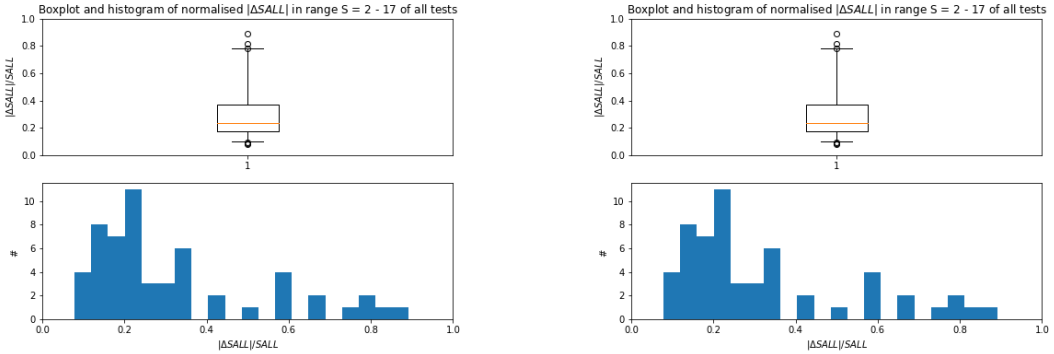

(a) Absolute difference (b) Normalised difference

Figure R.9: a) Absolute and b) normalised difference of damage parameter S_{all} for range $S = 2 - 17$ compared with +/- threshold situations

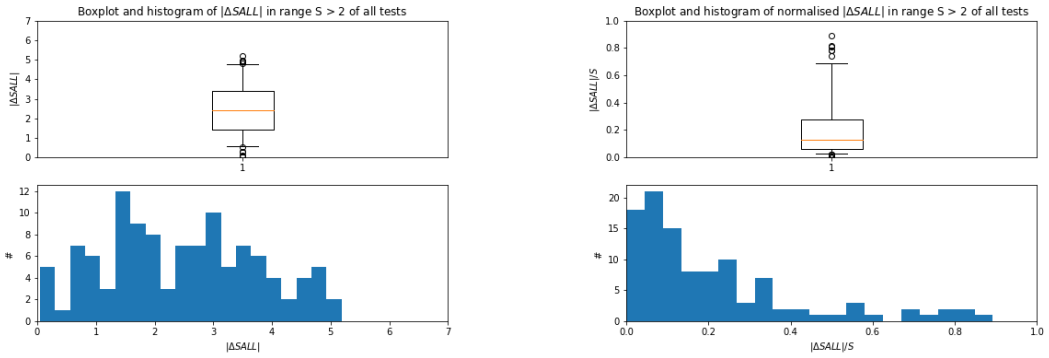

(a) Absolute difference

(b) Normalised difference

Figure R.10: a) Absolute and b) normalised difference of damage parameter S_{all} for range $S > 2$ compared with +/- threshold situations

S

Quantification of 3D damage parameters

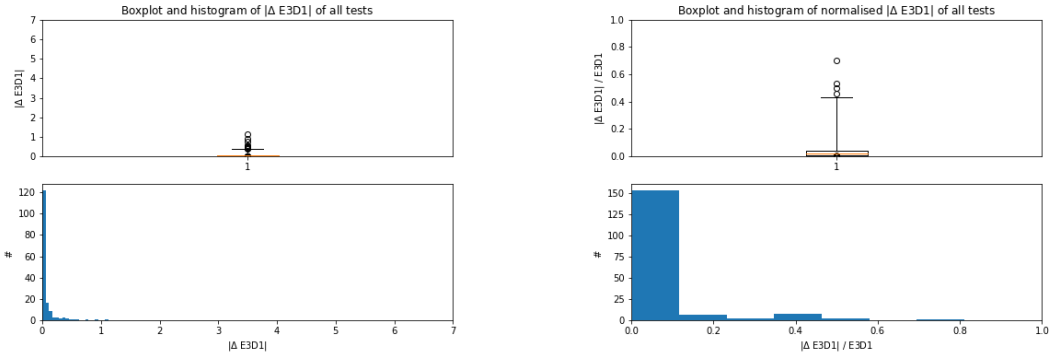

(a) Absolute difference

(b) Normalised difference

Figure S.1: a) Absolute and b) normalised difference of damage parameter E_{3D1} compared with +/- threshold situations

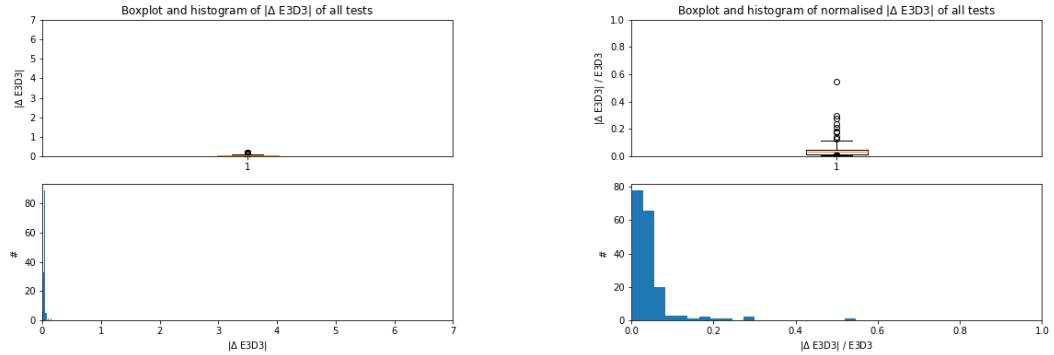

(a) Absolute difference

(b) Normalised difference

Figure S.2: a) Absolute and b) normalised difference of damage parameter E_{3D3} compared with +/- threshold situations

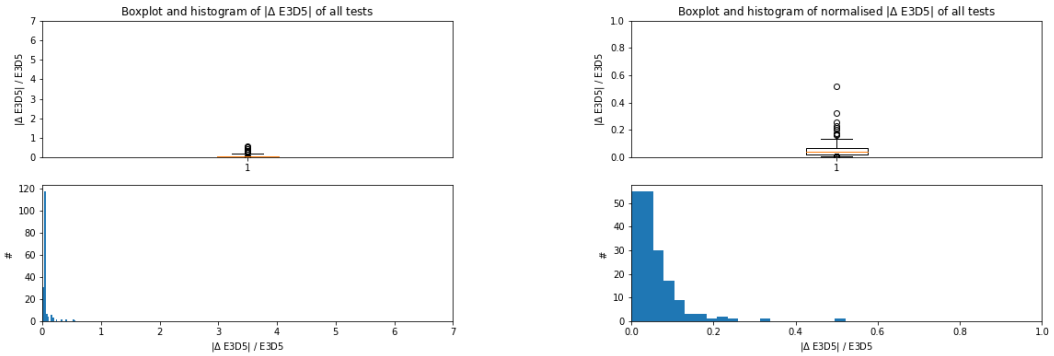

(a) Absolute difference

(b) Normalised difference

Figure S.3: a) Absolute and b) normalised difference of damage parameter E_{3D5} compared with +/- threshold situations

T

Comparison method of Eldrup and formula of Van der Meer plunging

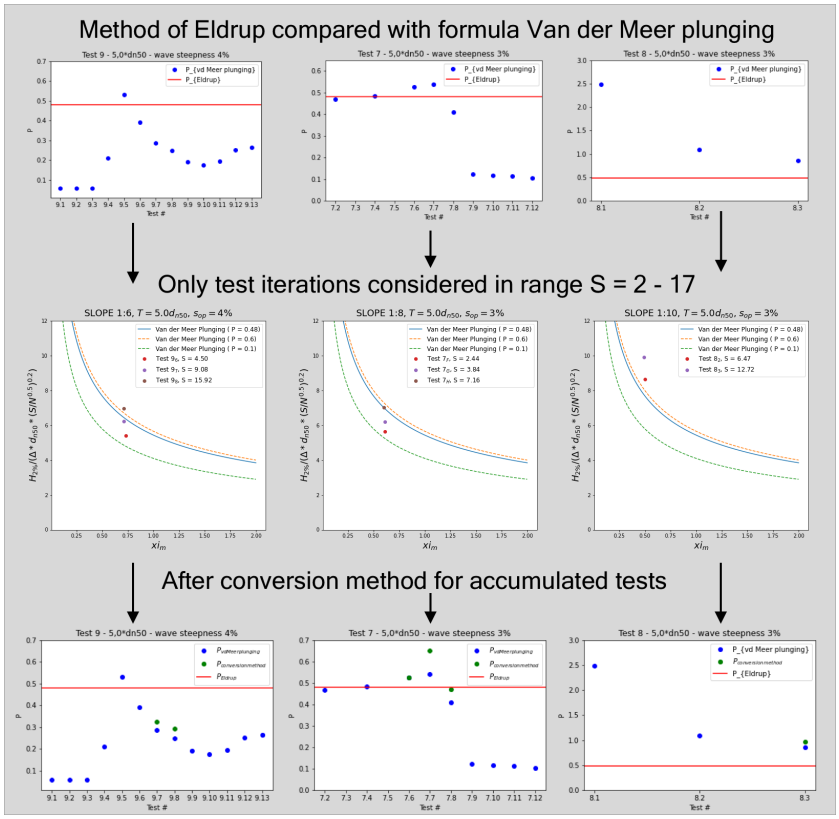

Figure T.1: Comparison method Eldrup and Van der Meer for results for slope 1:6, 1:8 and 1:10

U
Change of colour band width

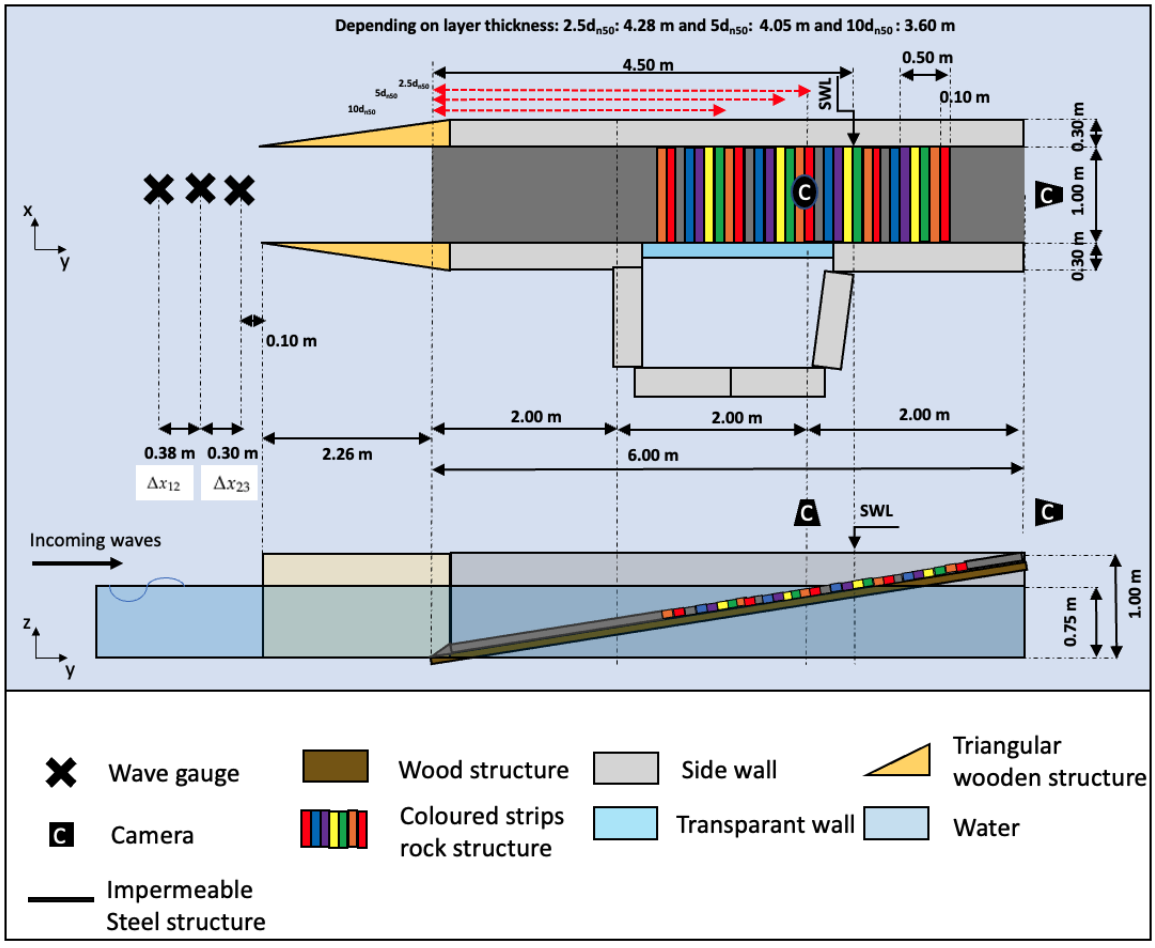

Figure U.1: Top view test set-up with colour band w = 0.1 m for slope 1:6 based on experiment of Van Wijland (2020) and Mossinkoff (2019)

Table U.1: Results damage numbers based on displacements slope 1:6

Test number	Analyzed w [m]	N_{od}	S_{od}
Test 6_{01}	0.1	-	-
	0.5	-	-
Test 6_{02}	0.1	-	-
	0.5	-	-
Test 6_{03}	0.1	0.06	0.10
	0.5	0.04	0.08
Test 6_{04}	0.1	0.15	0.25
	0.5	0.09	0.15
Test 6_{05}	0.1	0.47	0.79
	0.5	0.30	0.49
Test 6_{06}	0.1	1.70	2.84
	0.5	1.39	2.32
Test 6_{07}	0.1	3.48	5.80
	0.5	1.55	2.59

V
Damage limits

Slope	Damage limit	S_{mean}	$S_{95\%}$	$E3D3_{mean}$	$E3D3_{95\%}$
1:6	start	0.17	0.34	0.40	0.49
	intermediate	2.04	2.80	0.67	0.73
	failure	17.95	19.84	1.48	1.68
1:8	start	0.17	0.34	0.43	0.36
	intermediate	1.65	4.72	0.67	0.85
	failure	20.45	20.45	1.45	1.45
1:10	start	3.08	4.62	0.41	0.47
	intermediate	2.4	4.55	0.64	0.76
	failure	21.45	26.72	1.28	1.36

The used profiles are as following:

- Slope 1:6, start of damage: Test 2.02, 3.01, 4.01, 6.02, 8.01 and 9.01.
- Slope 1:6, intermediate damage: Test 3.02, 3.03, 4.03, 4.04, 5.02, 5.06, 6.04, 7.02, 8.02 and 9.03
- Slope 1:6, failure damage: Test 1.07, 2.11, 2.10 and 3.06
- Slope 1:8, start of damage: Test 2B, 2C, 3A, 3B, 3NB, 5A and 5B.
- Slope 1:8, intermediate damage: Test 1E, 1F, 2E, 2F, 2G, 3C, 3ND, 3NE, 4C and 4D.
- Slope 1:8, failure damage: Test 6H
- Slope 1:10, start of damage: Test 3a, 5a, 2a.
- Slope 1:10, intermediate damage: Test 1b, 3c, 4a, 5b, 5c and 11a.
- Slope 1:10, failure damage: Test 2f, 2g and 7b.

  Test considered as failure damage are tests where the bottom becomes visible. Sometimes the area where the bottom is visible is slightly larger than for other test, therefore it is important to use a conservative value as a damage limit for failure.

  For the tests with layer thickness $5d_{n50}$, only the impermeable layer became visible for slope 1:6 and wave steepness 1%. Therefore the failure limit according to the definition of failure can not be determined for this test series.